CHROMIUM DEPORTMENT IN COPPER MATTE EQUILIBRATED WITH Cr_xO-CONTAINING SLAG

by

Munyaradzi Kwatara

Thesis Presented in partial fulfilment of the requirements for the degree of Master of Science in Engineering (Extractive Metallurgical Engineering) in the Department of Process Engineering at the University of Stellenbosch

April 2006

Supervisors : Dr J J Eksteen

Prof L Lorenzen

DECLARATION

I, the Undersigned, hereby declare that the work contained in this thesis is my own original work and has not previously, in part or in its entirety, been submitted at any university for a degree.

_____ 12 January 2006

Munyaradzi Kwatara

ABSTRACT

An understanding of the behaviour of chromium in mattes equilibrated with chrome-saturated slags is essential for the prediction and control of chromium deportment in these melts. The main ore reserves of South Africa's platinum group metals (PGM) are associated with the Merensky and UG2 reefs of the Bushveld Complex. The gradual depletion of the pyroxenitic Merensky reef over the years has necessitated the PGM industry to exploit the underlying chromite-rich UG2 reef.

The problem with UG2 reef is that it contains significant amounts of chromium, this being typically 5% (reported as Cr_2O_3) against <1% for the Merensky reef (in concentrates). Chromium has a number of deleterious effects on base-metal smelting processes. Under given conditions, it forms chromite spinels, which can accumulate and, over a period of time, form undesirable build-ups resulting in reduced furnace operational volume. The chromite spinels also tend to increase slag viscosity, thereby impacting negatively on the slag/matte separation, which leads to matte entrainment in slag. Moreover, high viscosities lead to problems with tapping of the furnace melts. Finally it can be said that chromium that deports to the matte during smelting will normally tend to precipitate as spinels during subsequent converting, and lead to the formation of very stable and unwanted slag foams in the converter.

In literature, there exists very little published work on the behaviour of chromium in sulphur-saturated systems such as matte-smelting furnaces. The few publications that exist in this area do not cover the effect of controlling all the pertinent variables simultaneously on the behaviour of chromium in mattes in equilibrium with chromium-containing slags. Hence the main focus of the present study was to investigate the effect of temperature and of sulphur and

oxygen fugacities on the mineralogical and deportment behaviour of chromium in a matte-slag system.

All the three variables (temperature, oxygen fugacity (pO_2), and sulphur fugacity (pS_2)) were investigated at three levels. Temperatures studied were 1300˚C, 1400˚C, and 1500˚C. Oxygen and sulphur fugacities were established by controlling the mix-ratios of purified carbon dioxide, carbon monoxide, sulphur dioxide, and argon. Oxygen fugacities were maintained at 10^{-10}atm, 10^{-8}atm, and 10^{-6}atm; whereas sulphur fugacities were maintained at 10^{-6}atm, 10^{-4}atm, and 10^{-2}atm. In order to investigate the effect of each of these three variables (temperature, pS_2, and pO_2) at different levels of the other variables, a completely randomised 3^3 full factorial experimental design was adopted.

The study revealed that chromium is generally present in matte as both dissolved CrS and as precipitated oxidic and sulphidic chromium spinel phases. It was shown that as the conditions become more oxidising ($pO_2 = 10^{-6}$atm), CrS (which is soluble in matte) becomes a predominant phase, and as the conditions become more reducing ($pO_2 = 10^{-10}$atm), the sulphospinel, daubreelite ($FeCr_2S_4$), becomes a more predominant phase. Oxidic chromium spinels were found to be present in matte under the more oxidising conditions (pO_2 of 10^{-6}atm) of this investigation. The presence of the above-mentioned phases was confirmed using X-ray diffraction.

Subject to the experimental conditions employed in this research, chromium was found to partition the least to matte under the conditions of; low temperature, high pO_2, and low pS_2. Conversely, chromium was found to partition the most to matte under the conditions of; high temperature, low pO_2, and high pS_2.

The partitioning of chromium between slag and matte was fitted to the following statistical models;

$$Log\,CPC = -0.818 + \frac{3.033\,x\,10^{3}}{T} - 0.019\,log\left(pS_2\right) + 0.012\,log\left(pO_2\right)$$

with a Pearson correlation coefficient of 0.9207,

and, including the second order main effects;

$$Log\,CPC = 9.459 - \frac{32.93\,x\,10^{3}}{T} - 18.71\,x\,10^{-3}\,log\left(pS_2\right) + \left(\frac{31.32\,x\,10^{6}}{T} - 110.2\,x\,10^{-3}\right) log\left(pO_2\right) + -\frac{204.3}{T^{2}}$$

with a Pearson Correlation coefficient of 0.966; where CPC is the chromium partition coefficient between slag and matte [%Cr_{slag}] / [%Cr_{matte}].

A response surface analysis of the experimental data showed that there is a direct proportionality between the logarithms of Chromium Partitioning Coefficient (CPC) and pO_2, and an inverse proportionality between the logarithms of CPC and pS_2 for all the temperature regimes employed in this investigation (1300°C, 1400°C, and 1500°C).

The industrial significance of the research findings is that larger amounts of chromium will dissolve in matte in the newer high temperature electrical furnaces (which are operated under much more reducing conditions than the flash furnaces and reverberatory furnaces). While the higher operating temperatures would favour more fluid slags during smelting, the higher chrome deportment to matte might lead to increased operating (foaming and tapping) problems in the subsequent converting step where the conditions are more oxidising and temperatures are lower. It is expected that these converting conditions will lead to increased precipitation of the oxidic chromium spinel minerals in the matte which will tend to associate with the injected bubbles and transfer to the converter slag by flotation.

OPSOMMING

‘n Begrip van die gedrag van chroom in swawelmetaal (mat) in ewewig gebring met chroom-bevattende slakke is van belang vir die voorspelling en beheer van die chroom verspreiding tussen hierdie smelte. Die hooftipe ertsreserwes van Suid Afrika se platinum groep metale (PGM’s) is geassosieer met die Merensky en UG2 riwwe van die Bosveldstollingskompleks. Die geleidelike opverbruik van die piroksenitiese Merensky-rif oor jare het noodgedwonge gelei tot verhoging in die ekstraksie en verwerking van die chromiet-ryke UG2-rif deur die PGM industrie.

Die probleem met die UG2 rif is dat dit beduidende hoeveelhede chroom bevat, tipies in die orde van 5% (gerapporteer as Cr_2O_3) teenoor die Merensky rif wat minder as 1% chroom bevat in flotasiekonsentrate. Chromiet het ‘n aantal nadelige gevolge op die smelting van basis-metaal minerale. Onder sekere toestande vorm die chromiet spinelle wat kan akkumuleer en, oor ‘n periode van tyd, ongewensde neerslae in oonde kan vorm wat lei tot ‘n vermindering in die bedryfsvolume van die oond. Verder lei dit tot ‘n verhoging van die waargenome slak viskositeit, en vervolgens tot swakker skeiding van die mat en slak smelte, groter mat-meesleuring in slak en ‘n swak tapbaarheid van die smelte. Ten slotte kan gesê word dat chroom oordrag na die mat (in opgeloste vorm) tydens smelting sal lei tot chroom spinel presipitasie tydens die daaropvolgende omsetting van die mat en lei tot die vorming van ongewensde baie stabiele slak-skuime in die omsetter.

Min inligting is beskikbaar in die literatuur oor die gedrag van chroom in mat-slak sisteme. Die weinige manuskripte wat wel gepubliseer is, gee nie voldoende inligting oor die berdyfsbereik van die hoofveranderlikes van belang nie. Verder is die studies normaalweg beperk tot chroombevattende slakke en was chroom-

bevattende matte selde gedek. Die hooffokus van die hierdie studie is dus om die effek van temperatuur asook die effekte van swawel (pS_2) en suursof fugasiteite (pO_2) te bepaal op die mineralogiese- en ewewigsgedrag van chroom is mat-slak sisteme. Die effekte van al drie hierdie veranderlikes (temperatuur, asook suurstof en swawel gas fugasiteite) is bestudeer op drie vlakke. Die gekose temperature was 1300°C, 1400°C, en 1500°C. Die suurstof en swawel fugasiteite was bepaal deur die beheer van die mengverhoudings van koolstofmonoksied, koolstofdioksied, swaweldioksied en argon. Die suurstoffugasiteite was gehandhaaf op 10^{-10}atm, 10^{-8}atm, en 10^{-6}atm, terwyl die swawelfugasiteite gehandhaaf was op 10^{-6}atm, 10^{-4} atm, en 10^{-2}atm. ‘n Volledige 3^3 faktoriaalontwerp is gedoen vir die drie veranderlikes wat ondersoek was op 3 vlakke.

Die studie het getoon dat chroom normaalweg teenwoordig is in mat as opgeloste CrS asook gepresipiteerde oksidiese en sulfiediese spinelle. Soos die toestande meer oksiderend word (by $pO_2=10^{-6}$atm) was gevind dat die opgeloste Cr meestal voorkom as CrS, maar dat, soos die toestande meer reduserend van aard word, die sulfospinel fase naamlik daubreeliet ($FeCr_2S_4$), dominant word. Oksidiese chroom spinelle was altyd gevind onder die meer oksiderende toestande. Die teenwoordigheid van die genoemde fases was ook bevestig deur X-straaldiffraksie.

Onderhewig aand die toestdande gebruik in die navorsing was gevind dat chroom verdeling na die mat geminimeer word by toestande van: lae temperatuur, hoë pO_2 , en lae pSO_2. Omgekeerd, die chroom verdeling na die mat word gemaksimeer onder toestdande van hoë temperatuur, lae pO_2 , en hoë pSO_2.

Die verdeling van chroom tussen slak en mat was gepas deur die volgende regressiemodel:

$$Log\,CPC = -0.818 + \frac{3.033\,x\,10^{3}}{T} - 0.019\,log\left(pS_2\right) + 0.012\,log\left(pO_2\right)$$

met ‘n Pearson korrelasie koëffisiënt van 0.9207;

of, indien tweede orde effekte in ag geneem word:

$$Log\,CPC = 9.459 - \frac{32.93\,x\,10^{3}}{T} - 18.71\,x\,10^{-3}\,log\left(pS_2\right) + \left(\frac{31.32\,x\,10^{6}}{T} - 110.2\,x\,10^{-3}\right) log\left(pO_2\right) + -\frac{204.3}{T^{2}}$$

met ‘n Pearson korrelasie koëffisiënt van 0.9660; waar CPC die chroom partisie koëffisiënt is tussen slak en mat $[\%Cr_{slak}]/[\%Cr_{mat}]$.

‘n Respons-oppervlakanalise van die eksperimentele data het getoon dat daar ‘n direkte eweredigheid bestaan tussen die logaritmes van die chroom van die CPC en pO_2 en ‘n omgekeerde eweredigheid tussen die logaritmes van die CPC en pS_2 vir alle temperatuurgebiede wat beskou was.

Die industriële belang van die bogenoemde gevolgtrekkinge is dat groter hoeveelhede chroom sal oplos in mat in die nuwer hoë temperatuur elektriese oonde (wat ook bedryf word onder meer reduserende toestande as die flitssmeltings- en rewerbereeroonde). Terwyl die hoër bedryfstemperature wel sal lei tot meer vloeibare slakke, sal die chroom-oordrag na die mat waarskynlik lei tot meer bedryfsprobleme (weens skuiming en tapprobleme) in die daaropvolgende omsettingstap, waar kondisies meer oksiderend en temperature laer is. Dit word verwag dat hierdie omsettingskondisies sal lei tot verhoogde presipitasie van oksidiese chroom spinelle in die mat wat sal neig om te assosieer met die blaaslug en floteer na die slak.

ACKNOWLEDGEMENTS

My profound gratitude is hereby extended to the following persons:

- Dr Eksteen, for his valuable contributions, guidance, and unwavering support throughout the duration of this research.
- Professor Lorenzen, for his valuable guidance.
- Dr Bucher for assisting with the XRD analyses in Karlsruhe, Germany.
- Ms Esme Spicer, for orienting me on the use of the Scanning Electron Microscope.
- Dr Gardner (Department of Statistics and Actuarial Science, University of Stellenbosch), for introducing me to the concepts of Design and Analysis of Experiments.
- Professor Le Roux (Department of Statistics and Actuarial Science, University of Stellenbosch), for his valuable critique of the data analysis techniques adopted in this research.
- Mr Jannie Banard and his workshop team, Department of Process Engineering (University of Stellenbosch), for their professional workmanship in all the fabrication work for which I sought their assistance.
- Department of Process Engineering, University of Stellenbosch, who funded this research.
- My family members for their support and encouragement.
- Last, but not least, my fiancée, Chesner, for her support, encouragement, and assistance with some of the reprographics.

GLOSSARY

Below is a list of the acronyms used in this thesis, arranged alphabetically, and the meanings thereof;

- Ar : Argon
- CO : Carbon monoxide
- CO_2 : Carbon dioxide
- CPC : Chromium Partition Coefficient
- Coplot : Conditioning Plot
- EDS : Energy-Dispersive Spectroscopy
- Eq : Equation
- Fig : Figure
- ICP : Induction Coupled Plasma
- LOI : Loss On Ignition
- MFC : Mass Flow Controller
- MIR : More Information Required
- NID : Normally and Independently Distributed
- PID : Proportional-Integral-Derivative
- PGM : Platinum Group Metals
- pO_2 : Oxygen partial pressure
- pS_2 : Sulphur partial pressure
- SEM : Scanning Electron Microscope
- Temp.Inverse : The inverse of Temperature. Sometimes written as $(\text{Temperature})^{-1}$ or $\frac{1}{T}$
- UG2 : Upper Group 2 (which is a chromitite reef)
- XRD : X-Ray Diffraction

DEDICATION

This thesis Dedicated to My Loving Mum and Grandmother, by whose prayers and support I am what I am today…….

TABLE OF CONTENTS

CHAPTER 1

INTRODUCTION

The main ore resource of South-Africa's Platinum Group Metal (PGM) Industry lies in the Bushveld Complex (BC), which contains the world's largest Platinum Group metals reserve (Vermaak, 1985). The BIC consists of the Merensky, Upper Group-2 (UG2), and Plat reefs. The preference by the platinum industry has been to exploit the Merensky reef over the other two. Consequently, there has been a gradual depletion of the Merensky reef over the years, thereby necessitating a strategic move by the industry towards increased beneficiation of the UG2 seam, which in-fact contains a significant amount of chromium (in its oxidic form).

The main constituent of the UG2 reef is chromite $[(Fe.Mg)^{2+}O.(Cr.Fe.Al)^{3+}O_3]$ which has a chromium-to-iron ratio of approximately 1.35. Comparatively, Merensky ore consists mainly of sulphides, these being pyrrhotite (45%), pentlandite (32%), chalcopyrite (16%), pyrite (2-4%) and minor amounts of other sulphides (Liddell *et al.*, 1986).

Typical chemical compositions for UG2 and Merensky are shown below.

Table 1.1 : Typical run of mine ore composition (Bartie, 2004)

ROM	PGM (g/t)	Ni (wt%)	Cu (wt%)	Cr_2O_3 (wt%)
Merensky	4-8	0.16-0.20	0.10-0.16	0.1
UG2	4.6-7.3	0.0010-0.029	0.004-0.012	27-34

Table 1.2 : Typical concentrate feed composition (Liddell *et al.*, 1986)

ROM	PGM (g/t)	Ni (wt%)	Cu (wt%)	S (wt%)	Cr_2O_3 (wt%)
Merensky	150-250	3.2	2.1	9.0	0.3
UG2	300-600	1.7	0.75	3.6	2.9

As can be seen from tables 1.1 and 1.2, UG2 ore contains a significant amount of chromium (in its oxidic state) relative to Merensky ore. However, the presence of chromium in PGM smelting processes is highly undesirable due to the numerous operational challenges that it presents.

1.1 EFFECT OF CHROME ON BASE-METAL SMELTERS

Chromium has a tendency to form spinels under normal smelting conditions. These are refractory complexes that can accumulate in the furnace. Over a period of time, these can form undesirable accretions that reduce furnace operational volume, thereby impacting negatively on throughput levels.

1.2 RESEARCH QUESTIONS & RESEARCH OUTLINE

The objectives of the current study are encompassed in the following research questions:

A. How does chromium partition between slags and mattes that are commonly encountered in Industry?
B. In what mineral form does chromium occur in matte under different conditions?
C. What are the effects of the following variables on the partitioning characteristics and mineralization of chromium in matte and slag?
    i. Temperature
    ii. Oxygen Partial pressure
    iii. Sulphur Partial Pressure

The hypotheses associated with the above research questions were drawn from the literature survey and have been presented in chapter 2

The experimental technique employed in this study is the classical three-phase equilibrium method comprising of a gas, matte, and a slag phase. A drop quench technique was used to investigate the phase equilibria of the slag/matte system. The techniques are discussed in detail in chapter 3.

The experimental design employed was a completely randomised 3^3 full factorial design with two replicates. This design enables an analysis of the effect of one factor on the response at different levels of the other factors. The experimental variables employed in this work were temperature, oxygen partial pressure (pO_2), and sulphur partial pressure (pS_2). Each of these factors was analysed at

three different levels, the response variable being the partition coefficient of chromium between slag and matte.

Partition coefficients in this research are defined by the following relation

$$CPC = \frac{[\%Cr]_{Slag}}{[\%Cr]_{Matte}} \qquad \text{……..} \qquad \text{Eq 1.1}$$

Where CPC = Partition coefficient of chromium between slag and matte;

$[\%Cr]_{Slag}$ = wt% chromium in the slag phase;

$[\%Cr]_{Matte}$ = wt% chromium in the matte phase.

It should be noted that a number of authors tend to define partition coefficients as a ratio of chromium in matte versus chromium in slag (which is an inverse of the definition selected in this work). In comparing the results of these workers with those obtained in this research, one should bear in mind this inverse attribute. The definition in Eq. 1.1 ensures that the values for CPC are greater than unity, making it easier for one to observe the trends in CPC as the different factors are varied.

At a given slag and matte composition, the partition coefficient is an indication of the affinity of chromium for the slag relative to the matte (McKenzie and Nell, 1994). According to equation 1.1, the greater the numeric value of the partition coefficient, the more strongly the chromium is partitioned into the slag

The quantitative data generated was analysed using the relevant statistical techniques applicable for this type of experimental design. These included an

analysis of variance (ANOVA) for the response variable (partition coefficients), regression analysis, and a response surface analysis.

It should be noted that the slag-matte system chosen for this research was a Cu-Fe-Cr-S matte equilibrated with an MgO-Fe-Al_2O_3-Cr_2O_3-SiO_2 slag. Nickel was not used in this study, but will be added in future research. In comparison to iron and copper, nickel is intermediate in its thermodynamic behaviour with regard to sulphur and oxygen (iron having the largest affinity for oxygen and copper the largest affinity for sulphur). In subsequent research, Calcium (as CaO) will also be added to the slag. This research was performed as part of a larger experimental programme which will eventually cover the whole Fe-Cu-Ni-Co-Cr-S system.

˚CHAPTER 2

LITERATURE SURVEY

2.1 INTRODUCTION

In the geological and material science literature, there exist a large amount of data pertaining to the solubility of chromium and sulphur in both natural and synthetic silicate melts. There is, however, very little published work on the solubility of chromium in sulphur-rich melts such as found in matte-smelting furnaces – which in fact is the primary focus of this research. Added to this, the phase diagrams for spinel stability are not well defined for the conditions prevailing in the matte smelting environment (McKenzie and Nell, 1994).

2.2 FOCUS OF THE LITERATURE REVIEW

The first section of this literature review focuses on the few previous investigations on the solubility and partitioning of chromium between matte and slag under controlled gas composition environments. The knowledge gaps identified will help focus the current research in a certain direction.

The second part of this review investigates the work that has been done on the mineralogy of chromium in the slag phase only. A significant amount of literature exists for chromium behaviour in slag, but only those publications that have a bearing on the scope of the current research will be discussed.

The third part is a review of other literature that provide guidelines on the most appropriate experimental parameters (such as ranges for gas partial pressures, and sample weights) to be adapted in the current investigation. This literature pertains to slag/matte equilibria investigations that have been conducted under conditions extrapolated from matte-smelting industry practice, even though they did not specifically include chromium as an element of interest. The presentation of this part differs from others in this review in that more emphasis is placed on discussing the conditions under which these experiments were conducted, rather than the results obtained.

The fourth section gives a brief insight into the phase equilibria of the slag and matte system adapted in this work.

A brief survey of the thermodynamic concepts of slag and matte is presented in the fifth part of this chapter.

The sixth and seventh sections give the summary of the literature survey and the hypotheses drawn from the literature respectively.

2.3 PARTITIONING OF CHROMIUM BETWEEN MATTE AND SLAG

2.3.1 Partitioning Under an Inert Atmosphere

McKenzie and Nell (1994) investigated the partitioning of chrome between slag and matte under an argon atmosphere at 1500˚C in a muffle furnace. Samples consisting of 100g of Merensky concentrate and slag were equilibrated at this temperature for one hour in recrystallised alumina crucibles and quenched in

water. During experiments the redox state was controlled by the initial additions of carbon or ferrosilicon to the charge.

Chromium spinels were found to occur in all matte samples generated, and were heterogeneously distributed in this phase. Based on the observed textures, the authors suggested that spinel was a primary phase in all of the matte samples, indicating that the experiments were saturated with respect to spinel in the matte. Slag samples were also found to contain abundant exsolved sulphide droplets.

They found that there is a strong correlation between the partitioning of iron and chromium into the matte, as shown in Fig 2.1.

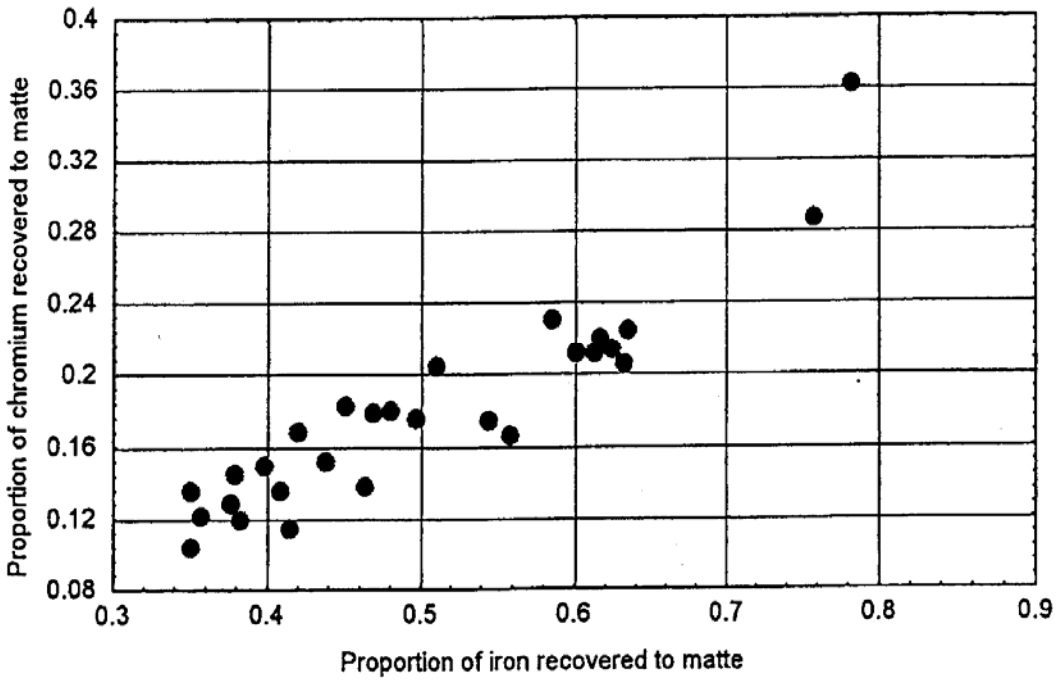

Fig 2.1 : Plot of the proportion of chromium recovered to matte versus the proportion of iron recovered to the matte (McKenzie and Nell, 1994)

This trend was explained using the reaction equations below, and was said to hold for chromium partitioning as well.

$$FeO + \tfrac{1}{2}S_2 \Leftrightarrow FeS + \tfrac{1}{2}O_2 \qquad \text{Eq 2.1}$$

However, even though Mackenzie and Nell (1994) did not explicitly give a similar reaction for chromium, it was implied in their discussion of the results shown in Fig 2.1. The implied reaction is shown below;

$$CrO + \tfrac{1}{2}S_2 \Leftrightarrow CrS + \tfrac{1}{2}O_2 \qquad \text{Eq 2.2}$$

It can be seen from reactions in Eq 2.1 and 2.2 that under reducing conditions, both reactions will shift to the right. This could explain why there is a direct relationship between chromium and iron partitioning to the matte as shown in Fig 2.1.

2.3.2 Partitioning Under Controlled pO_2 and pSO_2

De Villiers and Kleyenstüber (1993) investigated the partitioning of chromium between sulphide and silicate melts at 1500°C. Synthetic slags with different quantities of Fe_2O_3 and four natural rock compositions were equilibrated under a controlled partial pressure of oxygen and sulphur. A mixture of carbon monoxide, carbon dioxide, and sulphur dioxide was used to attain gas partial pressures of $10^{-10.5}$ to $10^{-0.5}$atm for oxygen and $10^{-3.7}$ to $10^{-1.2}$atm for sulphur. Most of the samples were equilibrated at the experimental temperature for 24 hours. Since the silicate samples were placed in platinum loops in the furnace, the resulting loss of iron from the charges to the loops was compensated for by haematite additions to the slag of 8% and 20%, respectively.

The resultant partition coefficients were plotted as a function of pO_2 as shown in Fig 2.2.

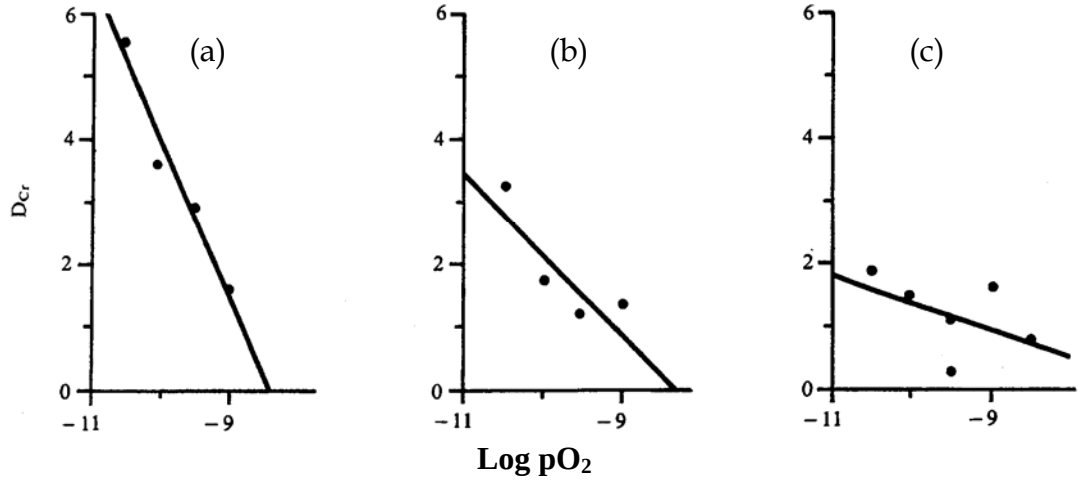

Fig 2.2: Chromium partition coefficients as a function of oxygen partial pressure
(a) samples with an Fe_2O_3 addition of 20%
(b) samples with an Fe_2O_3 addition of 8%, and
(c) runs using electroplated platinum-wire loops
(De Villiers and Kleyenstüber, 1993)

The largest error observed was the inhomogeneous nature of the sulphides, which showed an incipient exsolution of an oxide phase in many samples. This oxide phase was identified as a chromium-rich spinel. The general trend noted was that the partitioning of chromium into the sulphide melt increases with a decrease in the partial pressure of oxygen.

2.4 BEHAVIOUR OF CHROMIUM IN SLAG

Pretorius and Muan (1989) determined the solubility and activity-composition relations of chromium oxide in melts of the systems $CaO\text{-}CrO_x\text{-}SiO_2$ and $CaO\text{-}Al_2O_3\text{-}CrO_x\text{-}SiO_2$ at 1500°C by equilibrating melts with Pt-Cr alloys at known oxygen pressures. It was shown that the increase in the concentration of the

divalent chromium ions with a decrease in the oxygen pressure and melt basicity, resulted in a dramatic increase in the solubility of chromium oxide in the liquid phase.

Roeder and Reynolds (1991) investigated the solubility of chromium in basaltic melts using the drop-quench technique in a vertical tube furnace. This research is of interest because basaltic melts resemble industrial slags to a large extent, as can be noted in Table 2.1, which lists a typical composition of one of the rock samples used in their work (compare with Table 3.2).

Table 2.1: Typical basaltic rock composition (Roeder and Reynolds, 1991)

	SiO_2	TiO_2	Al_2O_3	Fe_2O_3	MnO	MgO	CaO	Na_2O	K_2O	P_2O_5	LOI
%	45.50	0.58	10.24	14.02	0.30	16.43	9.81	1.02	0.12	0.06	4.00

They saturated the rock powders with chromite (0.05-1.4wt% Cr_2O_3) and allowed the system to equilibrate at 1300°C. Required gas fugacities (*f*) were attained using a CO_2, H_2 and air mixture, with log fO_2 ranging from –3 to –12.8.
They found that chromium solubility in the melt decreased with increasing oxygen fugacity, as shown in Fig 2.3. This is in agreement with the findings of Pretorius and Muan (1993) for CaO-CrO_x-SiO_2 and CaO-Al_2O_3-CrO_x-SiO_2 slag systems.

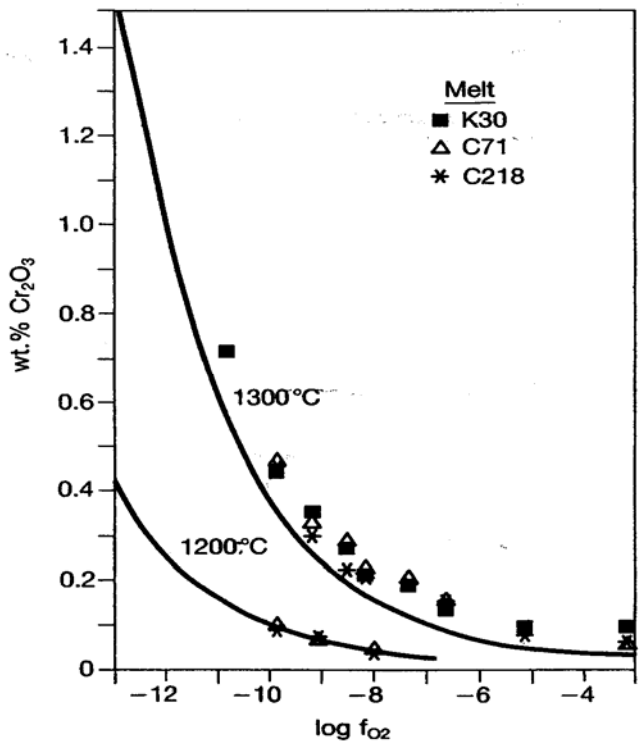

Fig 2.3 : Plot of total Cr as wt.% Cr_2O_3 vs log *f*O2 for the samples used (Roeder and Reynolds, 1991)

They also determined the ratio of the different oxidation states of chromium and iron in the equilibrium melt, and part of their results are shown in Fig 2.4.

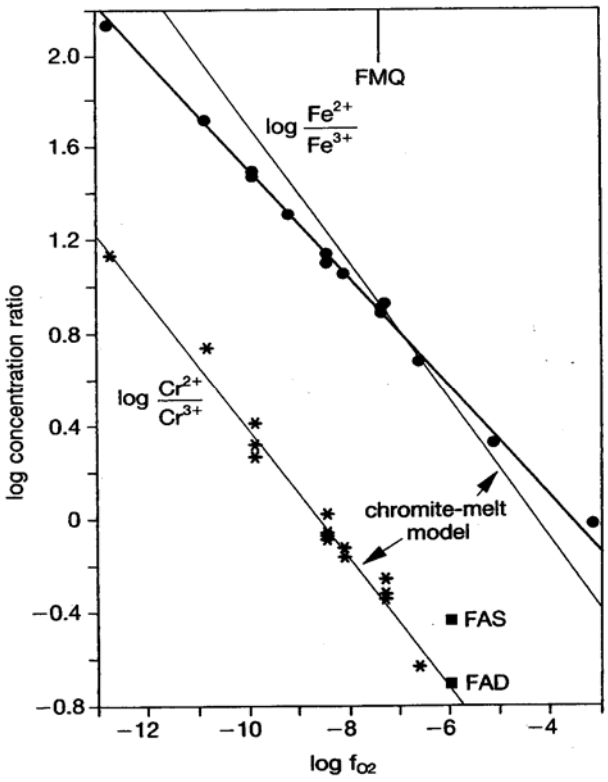

Fig 2.4 : Logarithmic plot of Fe^{2+}/Fe^{3+} and Cr^{2+}/Cr^{3+} in melts as determined by Roeder and Reynolds (1991)

The plot of chromite in Fig 2.4 was made using a thermodynamic model because they claimed that no known method exists to measure the oxidation state of chromium in melts containing Fe. It was also noted in their work that the Cr_2O_3 dissolved in the silicate melt at 1200˚C is a third of that dissolved at 1300˚C, implying a significant increase in Cr_2O_3 solubility in slag with temperature.

Fahey *et al.* (2004) studied the solubility of Cr_2O_3 in calcium ferrite slags at 1573 K using the drop quench technique. A high oxygen partial pressure of 3.7 x 10^{-4}atm was used in order to simulate converting conditions. This is somewhat higher than the pressures employed in this research where the focus was on the smelting. However, their results are still of interest as the behaviour of chromium

is reported for conditions which are more oxidizing. Some of their findings of particular interest to this work are shown in Fig 2.5.

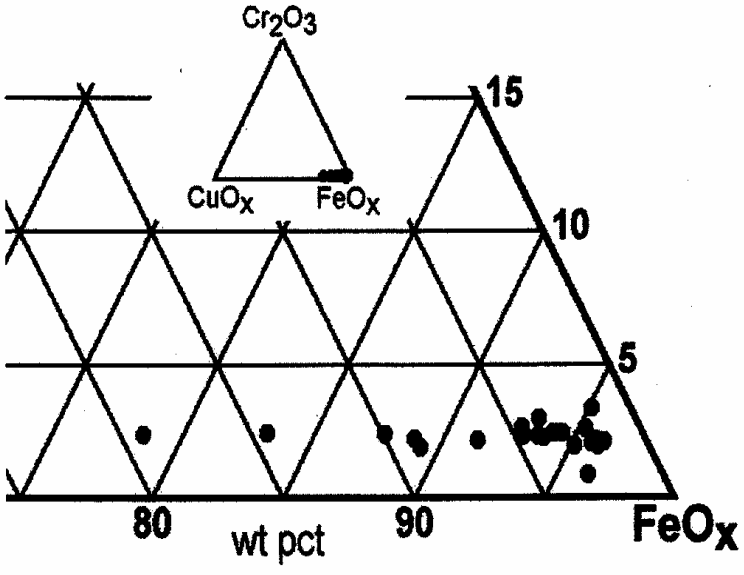

Fig 2.5 : The Cr_2O_3 content of the liquid in equilibrium with solid phases as a function of the CuO_x content at 1573K (Fahey *et al.*, 2004)

It was found that approximately 2wt % of Cr_2O_3 can dissolve into calcium ferrite slag under their experimental conditions.

In his study of the effect of temperature, slag chemistry, and oxygen partial pressure on the behaviour of chromium oxide in melter slags, Bartie (2004) reported similar results as mentioned for the other authors above. His study revealed that chromium oxide partitions very strongly into the spinel phase relative to the liquid phase, especially at lower temperatures, and higher oxygen partial pressures and bulk chromium oxide content. He also reported that the solubility of chromium oxide in the liquid phase increased with increasing temperature and decreasing oxygen partial pressure. This is in agreement with the findings of Pretorius and Muan (1989). They studied the phase equilibria by

means of drop-quench experiments using synthetic slags with bulk FeOx/MgO ratios of 0.6-1.9, and bulk chromium oxide contents of 1.2-1.7%. Temperatures investigated were 1400˚C, 1500˚C, and 1600˚C, with pO_2 ranges of $6.8x10^{-10}$ – $8.3x10^{-5}$atm.

2.5 OTHER SLAG /MATTE EQUILIBRIA

As has already been mentioned above (Section 2.1), the review presented in this section focuses on the experimental technique and conditions in that no discussion of the results is mentioned. This is because this literature was used only as a benchmark for experimental parameters applied in this research. These parameters include ranges for gas partial pressures, size of sample most suitable for a drop quench and equilibration experiments, temperature ranges, and so on. Therefore, only the parameters applied to the different slag/matte systems will be highlighted. In most cases, the system studied is similar to the one for the current investigation, except that most of them did not include chromium as a component.

Wang *et al.* (1973) used a sample size of 4g (2g of copper alloy and 2g of fayalite slag to investigate the distribution of copper-nickel and copper-cobalt alloys and silica saturated fayalite slags. The three-phase equilibrium experiments were conducted at pO_2 of 10^{-10} – 10^{-6} atm in the temperature range 1250˚C – 1350˚C. Of particular interest are the gas pressure ranges and temperatures, as these are similar to industry practice. Even though their results are not of interest to this research, they observed that at constant pO_2 and temperature, the metal solubility increased with the metal activity in the alloy phase.

Choi and Cho (1997) investigated the distribution behaviour of cobalt, selenium and tellurium between nickel-copper-iron matte and silica saturated iron silicate slag. Alumina crucibles were used to equilibrate 5g of slag and 5g of matte. The sample size used in this work was identical to that adopted by these authors.

Rhogani *et al.* (2000) used a sample weight of 16g (8g slag and 8g matte) with pSO_2 of 10.1, 50.7, and 103kPa, pS_2 10^{-5} – 10^{-2}, at 1573K to investigate the phase equilibria and minor element distribution between slag and a copper matte. The copper and sulphur solubilities in the slag were found to be independent of pSO_2 when the matte grade was specified, and this behaviour was ascribed to the constancy of (pO_2/pS_2) against pSO_2 at a given matte grade. Of interest to this research were the pS_2 range and the sample sizes which they used in their work.

Tavera and Bedolla (1990) studied the phase equilibrium between matte and fayalite slag phases at pSO_2 1.6 x 10^{-7} to 0.4atm and pO_2 of 3.16x10^{-13}atm to 10^{-6}atm at 1473 – 1573K. They noted that the concentrations of copper in their experimental slags were lower than 1% as long as the matte grade was kept below 65%Cu. Even though no mention was made of the sample size used, the experimental parameters which they adopted (temperature and gas partial pressures are particular of interest to the current research.

Tavera and Davenport (1979) studied the phase equilibria between matte and fayalite slag at pSO_2 0.1 – 1.0 atm and temperature 1423 – 1573K. Their work showed that whereas FeS has a high solubility for oxygen and is itself soluble in slag under oxidizing conditions, Cu_2S and slag are almost completely immiscible. The temperature range and gas partial pressure which they used are important benchmarks for this work. However, the sample size which they used for their equilibration experiments was not mentioned.

Font *et al.* (1998) analysed the phase equilibrium and minor elements distribution between iron silicate base slag and nickel-copper-iron matte at 1573 K. A sample size of 6g matte and 6g slag was used in the investigation. The temperature and sample size were of interest to the current research. Their study found that at a given matte grade, the solubility of copper in slag was independent of pSO_2, while the solubility of nickel was dependent on pSO_2.

Luraschi and Elliot (1980) investigated the thermodynamic behaviour of oxygen and sulphur at $10^{-10} \leq pO_2 \leq 10^{-9}$atm and $10^{-4} \leq pS_2 \leq 10^{-2}$atm at 1473K. A sample of 10g was melted in an alumina crucible. Their research resulted in a model to predict the oxygen content of matte as a function of pO_2, pS_2, and iron content. In as far as this research is concerned, a useful benchmark from the work of Luraschi and Elliot is the pO_2, pS_2 and temperature ranges which they applied.

Itagaki (2003) studied the distribution of minor elements in sulphide smelting by equilibrating different types of slag at pSO_2 0.1, 0.5, and 1.0 atm. The investigation showed that the dependency of the distribution ratios of some minor elements between matte and slag on the matte grade, pSO_2, and slag basicity can be explained reasonably well on the basis of thermodynamics.

Nagamori *et al.* (1975) investigated impurity distribution between slag and copper at $10^{-11} \leq pO_2 \leq 10^{-6}$atm. The range of pO_2 which they used is closely similar to that used by Wang *et al.* (1973), and is of particular interest to the current research. Even though their results are not of any interest to this work, they found out that the dissolution of Bi, Sb, and As in the slag was independent of the oxygen potential, suggesting atomic rather than oxidic dissolution.

2.6 PHASE EQUILIBRIA

This subsection gives some details on the phase diagrams of particular interest to this research. As will be noted in chapter 3, the selection of experimental compositions for the slag and matte used in this research was done in consultation with published phase diagrams and industry practices. The systems presented are Fe-Cr, Cr-S, Cu-Fe-S, FeO_x-MgO-SiO_2.

2.6.1 Fe-Cr System

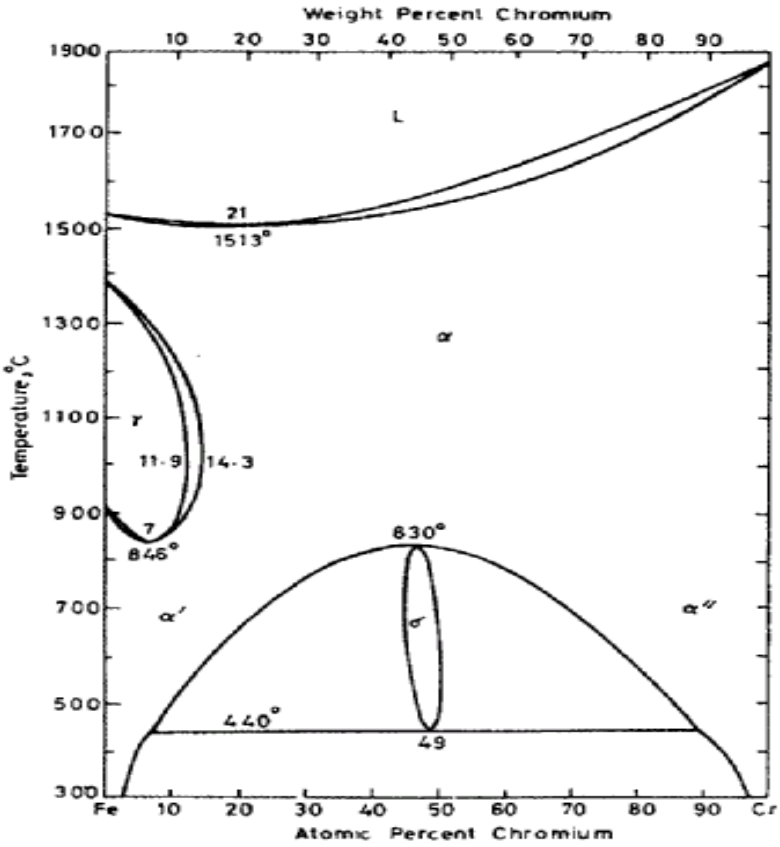

Fig 2.6 : Fe-Cr Phase Diagram (Kubashcewski, 1982)

The Fe-Cr phase diagram reviewed by Kubashcewski (1982) is shown in Fig 2.6. Fe-Cr alloys solidify as a continuous series of body centered cubic (bcc) solid

solutions (α), with a minimum in the liquidus at 1513°C and 21 at% (19.8wt%) Cr. A minimum in the γ loop occurs at 846°C and 7at.% (6.5wt.%) Cr. The σ phase forms congruently from α at 830°C and 47at.%(45.2wt.%) Cr. It decomposes eutectoidally at 440°C to the iron-rich α′ and the chromium rich α″ phases.

2.6.2 Cr-S_X System

An understanding of the Cr-S_x system is considered pertinent to the understanding of the behaviour of chromium in matte systems. In this section, literature on the different forms of Cr-S compounds and conditions under which they form will be explored.

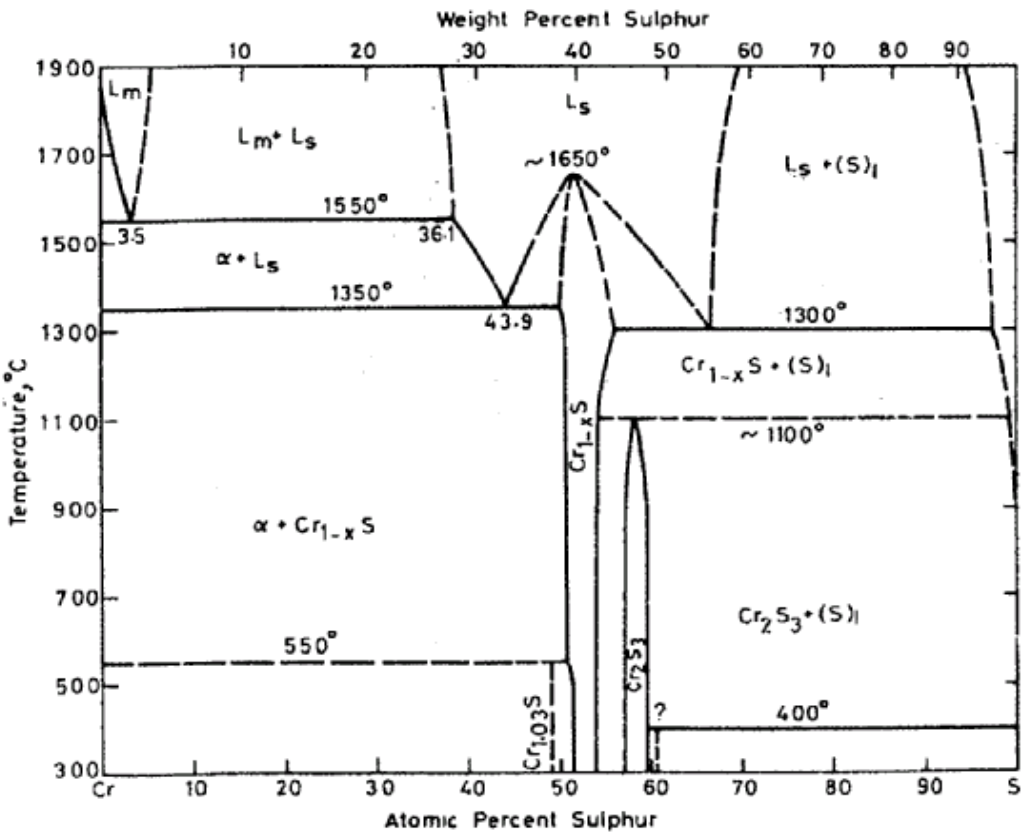

Fig 2.7 : Cr-S Phase Diagram (El Goresy and Kullerud,1969)

The Cr-S phase diagram determined by El Goresy and Kullerud (1969) is shown in Fig 2.7. They used the data of Vogel and Reinbasch (1938) for the solidification range. There are two regions of liquid immiscibility : one between liquid chromium L_m and the sulphide liquid L_s, and the other between L_s and a sulphur-rich liquid $(S)_1$. The corresponding monotectic reactions are at 1550 and 1300°C. A eutectic reaction at 1350°C and 43.9at.%(32.5wt.%) S yields α (Cr-S solid solution) and $Cr_{1-x}S$. According to Jellinek (1957), several intermediate compounds exist between the compositions CrS and Cr_2S_3. These are CrS, Cr_7S_8, Cr_5S_6, Cr_3S_4, and at least two modifications of Cr_2S_3 (trigonal and rhombohedral). X-ray investigations showed that Cr_3S_4 and Cr_7S_8 exhibit rather broad homogeneity ranges, while the others do not (Jellinek, 1957). Additional confirmatory work and a study of the properties of these Cr-S_x intermediate compounds were conducted by other researchers (Dwight *et al.*, 1962; Bouchard and Wold, 1966; Van Laar, 1967; Popma and Van Bruggen, 1969; Igaki *et al.*, 1971; Mikami *et al.*, 1972; Anzai and Hamaguchi, 1975; Rau, 1977) At 1100°C and at the nominal composition of Cr_2S_3, a rhombohedral structure forms through a peritectic reaction.

2.6.3 Cr-Fe-S System

The ternary phase diagram of the system Cr-Fe-S is shown in Fig 2.8. At temperatures above 700°C, $Fe_{1-x}S$ and $Cr_{1-x}S$ form a series of solid solutions (Vogel and Reinbasch, 1938; Kaneko *et al.*, 1963), denoted by λ in Fig 2.8. This solid solution splits into an iron-rich and chromium-rich sulphide at lower temperatures (Vogel and Reinbasch, 1938; El Goresy and Kullerud, 1969).

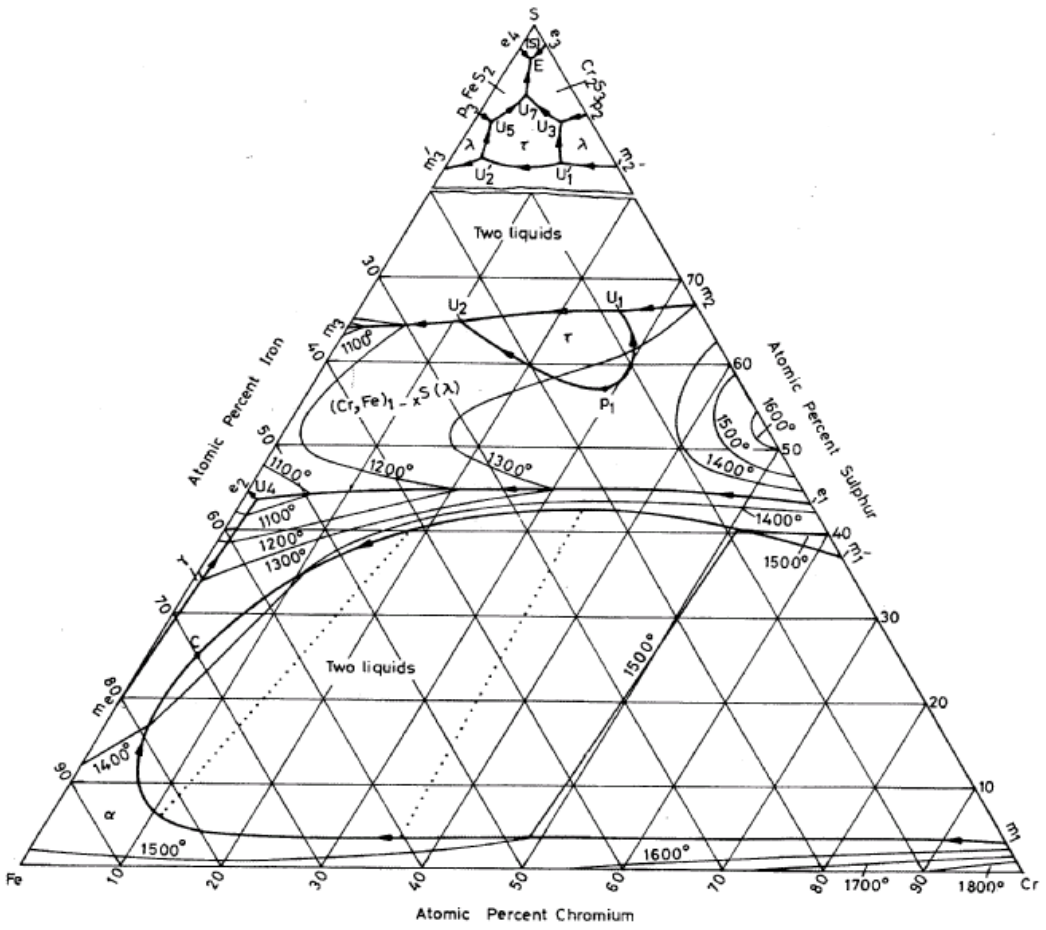

Fig 2.8 : Cr-Fe-S System (Raghavan, 1988)

A ternary compound called daubreelite with a fixed composition Cr_2FeS_4 (denoted by τ) also forms in this system, as reported by Bouchard *et al.* (1965), Shick and Von Neida (1969), and Watanabe (1972). It is stable at ambient pressures up to 1350˚C (El Goresy and Kullerud, 1969), and has the normal spinel structure (Lutz *et al.*, 1983). Its hypothetical liquidus projection is shown in fig 2.8. Daubreelite is taken to form peritectically. The monotectic univariant line arising from the miscibility gap in sulphur-rich alloys of the Cr-S system m_2 is assumed to undergo two transition reactions U_1 and U_2, before it reaches the monotectic point m_3 on the Fe-S side. A study of Fig 2.8 reveals that $(Cr,Fe)_{1-x}S(\lambda)$

is the most predominant phase for melts containing ± 40-65% S. In the lower sulphur (0-40%) regions, two liquids form; a $(Cr,Fe)_{1-x}S$ liquid in equilibrium with a low sulphur alloy melt which forms the α-alloy. Lutz *et al.* (1983) also confirmed the stability region of daubreelite, and his results are shown in Fig 2.9 below.

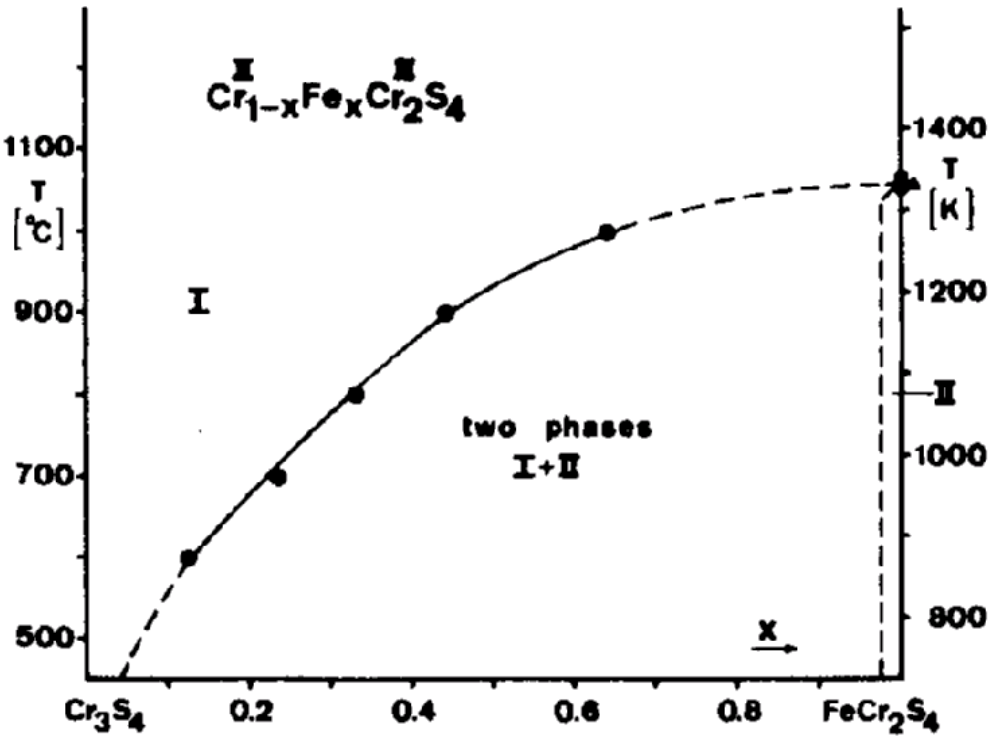

Fig 2.9 : Phase Diagram of the System Cr_3S_4-$FeCr_2S_4$. [I represents Cr_3S_4 and II represents $FeCr_2S_4$ (Lutz *et al.*, 1983)

2.6.4 Slag System

The slag systems that will be considered are FeO_x-Cr_2O_3-SiO_2 and MgO-Cr_2O_3-SiO_2. This is because of their relevance to this study, as can be noted from the compositions in Table 3.2. The system FeO_x-MgO-Cr_2O_3-SiO_2 combining all the four components will also be discussed.

2.6.4.1 FeO_x-Cr_2O_3-SiO_2 System

Muan and Somiya (1960) studied the phase equilibria in the system FeO_x-Cr_2O_3 in air, a scenario which represents an oxygen isobaric section (pO_2 = 0.21 atm) through the quartenary system Fe-Cr-Si-O, at a total pressure of 1 atm. The diagram in Fig 2.10 represents the liquidus projection of this system as per their findings. An enlarged picture of the region adjacent to the SiO_2 apex is inserted in a separate sketch in the upper right-hand corner of the figure. They reported that the lowest temperature in this system is 1455°C, and is a eutectic temperature where tridymite, magnetite, and liquid coexist in equilibrium.

As can be seen from the diagram, Muan and Somiya (1960) reported that there are three isobaric invariant points in the system. The phase assemblages present at these invariant points are as follows : At 1710°C, cristobalite, spinel (ss) (50wt% iron oxide, 50wt% Cr_2O_3), sesquioxide(ss) (29wt% iron oxide, 71wt% Cr_2O_3), liquid (91wt% SiO_2, 6wt% iron oxide, 3wt% Cr_2O_3), and gas (pO_2 = 0.21atm.) coexist in equilibrium. Spinel (ss) (43wt% iron oxide, 57wt% Cr_2O_3), sesquioxide(ss) (18wt% iron oxide, 82 wt% Cr_2O_3), two liquids (89wt% SiO_2, 5wt% iron oxide, 6wt% Cr_2O_3 and 31wt% SiO_2, 46wt% iron oxide, 23wt% Cr_2O_3, respectively), and gas (pO_2 = 0.21 atm.) are present together in equilibrium at approximately 1850°C. At 1700°C, cristobalite, spinel (ss) (69wt% iron oxide, 31wt% Cr_2O_3), and two liquids (83wt% SiO_2, 15wt% iron oxide, 2wt% Cr_2O_3 and 34wt% SiO_2, 56wt% iron oxide, 10wt% Cr_2O_3, respectively) coexist with gas (pO_2 = 0.21 atm.) in stable equilibrium.

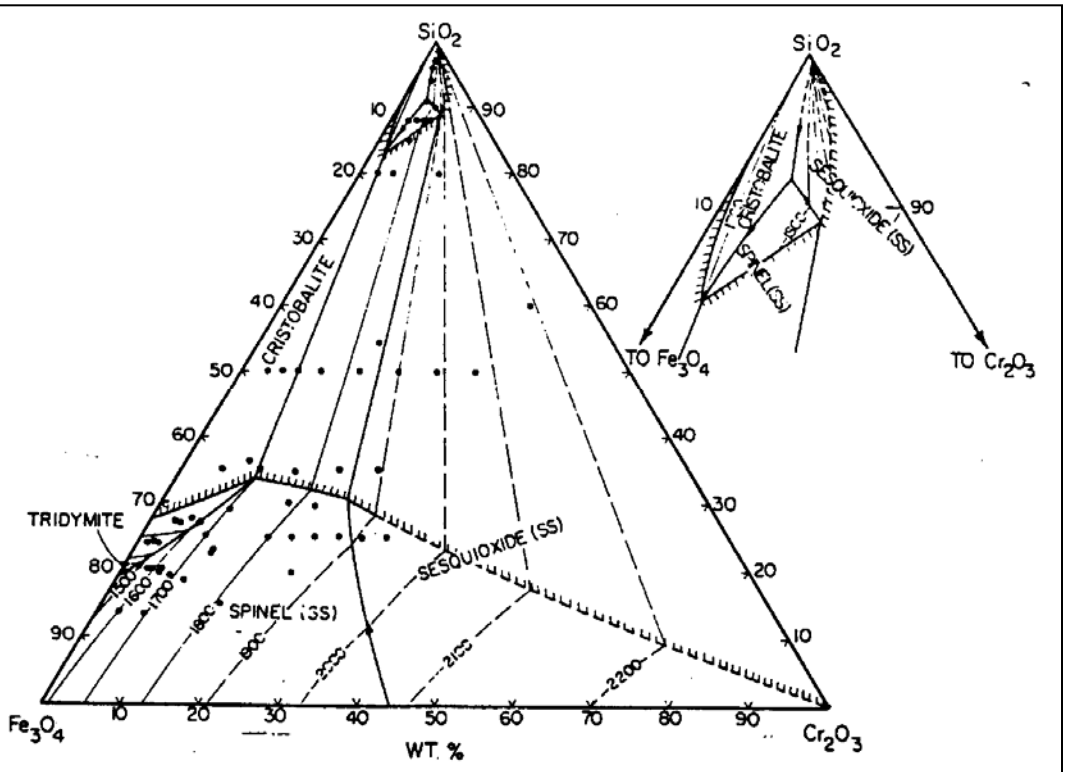

Fig 2.10 : Projection of Fe_3O_4-Cr_2O_3-SiO_2 liquidus surface in the system Iron oxide-Cr_2O_3-SiO_2 in air (Muan and Somiya, 1960)

Their research also clearly showed the effect of Cr_2O_3 on slag liquidus temperatures.

2.6.4.2 Effect of Cr_2O_3 on Slag Liquidus Temperatures

In studying the system FeOx-Cr_2O_3-SiO_2, Muan and Somiya (1960) noted that as Cr_2O_3 was added to iron oxide-SiO_2 mixtures, liquidus temperatures increased rapidly along the boundary curve where silica (tridymite or cristobalite, depending on temperature), spinel ($FeO \cdot Fe_2O_3$-$FeO \cdot Cr_2O_3$) solid solution (SS), and liquid are present together in equilibrium. Liquidus temperatures continued to rise as more Cr_2O_3 was added, first along the spinel (ss) liquidus surface

through the two-liquid region and subsequently along the sesquioxide(ss) (Fe_2O_3-Cr_2O_3 solid solution) liquidus surface.

2.6.4.3 MgO-Iron Oxide-Cr_2O_3-SiO_2

The phase diagram of this system is shown in Fig 2.11. The left part of Fig 2.11 (Keith (1954)), is the very narrow primary phase fields of olivine and pyroxene, amounting to a maximum of only about 2wt% Cr_2O_3 in the liquid. Arculus *et al.* (1974) reported that the maximum Cr_2O_3 contents of olivine and pyroxene in equilibrium with liquid in this system are approximately 0.5 and 0.3wt% respectively. He noted that there is no significant solid solution in the sesquioxide phase or cristobalite, but there is extensive solid solution of Cr_2O_3 in periclase.

The spinel phase is picrochromite ($MgCr_2O_4$), which melts congruently at approximately 2350˚C and exhibits a small amount of solid solution toward both Cr_2O_3 and MgO. The large spinel field dominates the left face (fig 2.11) and also extends as a narrow region nearly to the SiO_2 apex. The hatched curve is the outer, or low-silica, boundary of the two-liquid region.

The right face of fig 2.11 represents the system iron oxide-Cr_2O_3-SiO_2 in air at 1 atm, after Muan and Somiya (1960). This has been discussed in section 2.6.4.1.

The base of Fig 2.11 is the system MgO-iron oxide-SiO_2 in air, after Muan and Osborn (1956). Spinels on this join belong to the magnesio-ferrite-magnetite solid solution series. The $MgFe_2O_4$ end of the series contains 33wt% Fe_3O_4 and melts incongruently to magnesiowustite and liquid at 1713˚C, whereas the iron oxide

end melts incongruently at 1591˚C to a magnetite-haematite solid solution and liquid.

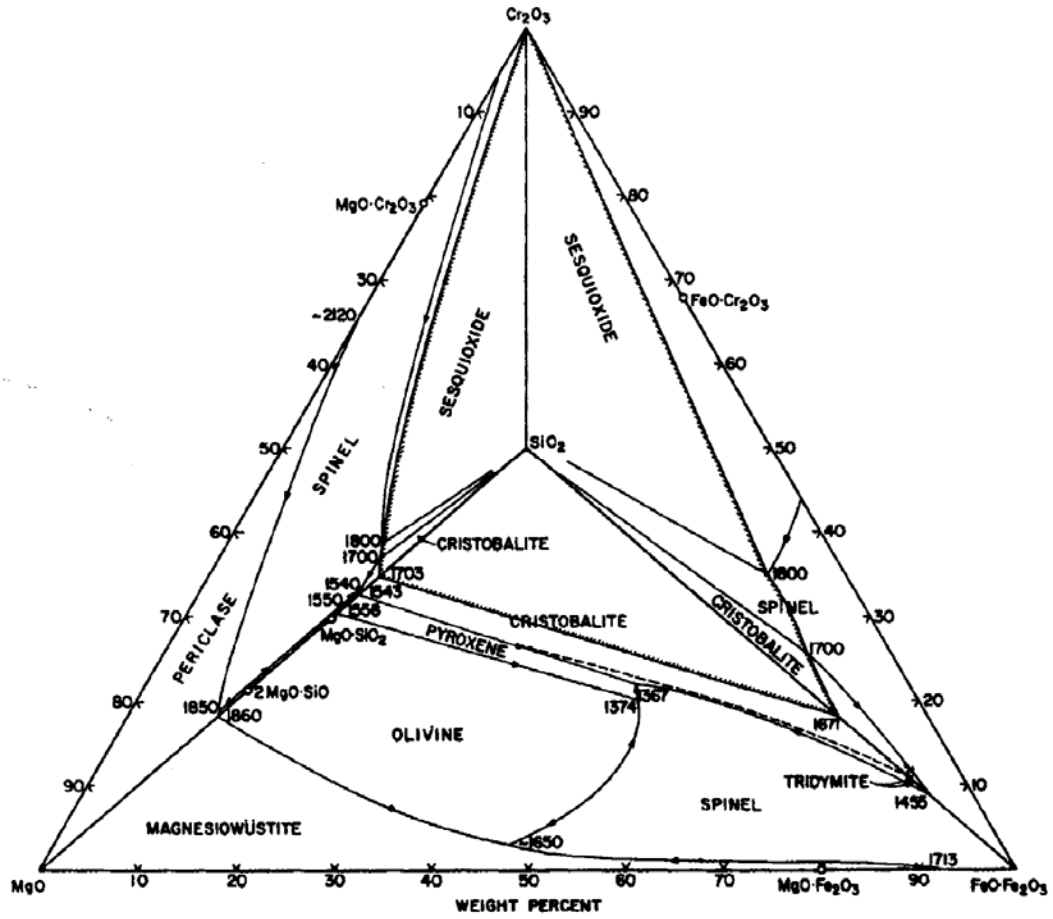

Fig 2.11 : MgO-Iron Oxide-Cr_2O_3-SiO_2 in air at 1atm. For plotting purposes, all iron oxide calculated as Fe_3O_4. Left face after Keith (1954), right face after Muan and Somiya (1960); base after Muan and Osborn (1956)

The pyroxene and olivine phases occupy large fields on the base of fig 2.11, as compared with the left face, and both exhibit significant amounts of solid solution toward their respective iron-bearing end-members.

2.7 THERMODYNAMICS OF CHROMIUM IN SLAGS AND MATTES

2.7.1 Thermodynamic Relations in Slag

Pretorius and Muan (1989) determined the thermodynamic parameters for chromium partitioning in slags by equilibrating a silicate melt with a Pt-Cr alloy at 1500˚C. The pertinent reactions considered are as follows;

$$[Cr]_{alloy} + 3/4O_2 = (CrO_{1.5})_{melt} \qquad \text{Eq 2.3}$$

$$K_1 = \frac{a_{CrO_{1.5}}}{a_{Cr}.(pO_2)^{\frac{3}{4}}} = e^{-\left(\frac{\Delta G_1^o}{RT}\right)} \qquad \text{Eq 2.4}$$

and

$$[Cr]_{alloy} + 1/2O_2 = (CrO)_{melt} \qquad \text{Eq 2.5}$$

$$K_2 = \frac{a_{CrO}}{a_{Cr}.(pO_2)^{\frac{1}{2}}} = e^{-\left(\frac{\Delta G_2^o}{RT}\right)} \qquad \text{Eq 2.6}$$

where (a) with appropriate subscripts are activities of the various species, K_1 and K_2 are equilibrium constants, ΔG_i^o is the standard free energy of reaction I, and pO_2 is the oxygen partial pressure. The value of K_1 ($10^{9.269}$) was calculated from the free energy of formation of Cr_2O_3 ($\Delta G^o_{Cr_2O_3} = -1092.383 + 237.93T\ kJ\ mole^{-1}$) and the enthalpy of fusion of Cr_2O_3 ($\Delta G^o_{fus} = 129.69\ kJ\ mole^{-1}$, $T_{fus} = 2603K$), with the value of K_2 being $10^{6.513}$.

Combining equations (2.3) and (2.5)

$$CrO_{1.5} = CrO + \tfrac{1}{4}O_2 \qquad \text{Eq 2.7}$$

for which

$$K_3 = \frac{a_{CrO} \cdot (pO_2)^{\frac{1}{4}}}{a_{CrO_{1.5}}} = 10^{-2.754} \qquad \text{Eq 2.8}$$

Pretorius and Muan (1989) suggested that, from the above relationships, and for a given oxygen pressure, if either a_{CrO} or $a_{CrO_{1.5}}$ is know, then the activity of the other oxide can be determined. However, this may be difficult if Fe^{2+} and Fe^{3+} are present. Moreover, the activity coefficient models are not defined

2.7.2 Thermodynamic Relations in Matte

McKenzie and Nell (1994) have mentioned that the following equation holds for the dissolution of chromium in mattes.

$$CrO + \tfrac{1}{2}S_2 = CrS + \tfrac{1}{2}O_2 \qquad \text{Eq 2.9}$$

$$K = \frac{a_{CrS} \cdot (pO_2)^{\frac{1}{2}}}{a_{CrO} \cdot (pS_2)^{\frac{1}{2}}} \qquad \text{Eq 2.10}$$

However, there is no published literature on the activity coefficients of CrS and CrO in matte.

2.8 SUMMARY OF LITERATURE REVIEW

The following list is a summary of the findings that were made from the survey:

- There exists a very limited amount of literature on the behaviour of chromium in slag/matte systems under controlled gas environments of sulphur and oxygen. Among these is the work by De Villiers and Kleyenstüber (1993), in which the temperature was fixed at 1500˚C. Their focus was on the partitioning of chromium in the bulk phases (sulphide and silicate), without much attention on the associated phase equilibria. This study will include temperature as a variable, and the range will also include 1500˚C, which was studied by De Villiers and Kleyenstüber (1993) using natural geological rock samples. An analysis of the phase equilibria will also be conducted in order to understand the phases to which chromium partitions in base metal slags and mattes under the different conditions of temperature and gas partial pressures. Similarly, McKenzie and Nell (1994) studied the behaviour of chromium in matte/slag systems at 1500˚C, but without necessarily controlling the partial pressure of oxygen and sulphur.

- There is no published literature on this subject (slag/matte equilibration under controlled gas environments) involving an analysis of the effect of one variable on chromium distribution at different levels of other factors. In fact, no mention is made of the experimental strategy undertaken (e.g., one-factor-at-a-time approach, best-guess approach, or factorial approach (Montgomery, 2005). A clear definition of the experimental strategy adopted will have a serious bearing on the manner in which the results obtained from any investigation are interpreted. This study will adopt a completely randomized full factorial approach whereby the main effects and the interaction effects for all factor-combinations will be explored systematically. The factors (variables)

to be investigated are temperature, partial pressure of sulphur and oxygen, the ranges of which are listed in table 3.4

2.9 HYPOTHESES DRAWN FROM LITERATURE SURVEY

From the literature survey findings, the following hypotheses are proposed;

- The variables; temperature, oxygen partial pressure, and sulphur partial pressure have an effect on the equilibrium chemistry of the slag and matte phases. A variation in these variables is likely to affect and determine the predominant phases.
- Chromium spinels can be found in mattes equilibrated with slags under certain conditions, though these conditions are not yet explicitly defined in literature.
- The partitioning of chromium to slag and matte is affected by temperature and the partial pressures of oxygen and sulphur.

CHAPTER 3

EXPERIMENTAL PROCEDURES

This chapter describes the experimental techniques and procedures used to study the behaviour of chromium in Fe-Cu-S mattes equilibrated with chrome-saturated melter slags under varying temperatures and controlled partial pressures of sulphur and oxygen. The first section gives some details of the equipment and materials used to conduct this research. This is followed by a system definition and a description of the experimental methods used. Discussions on the analytical procedures adopted, gas partial pressure validation experiments also follow, including the determination of the time required for equilibration in the experiments.

3.1 EQUIPMENT

3.1.1 Furnace

The furnace employed was a Carbolite six-element vertical tube furnace with a maximum temperature limit of 1800˚C. A schematic diagram of the furnace is shown in fig 3.1.

Temperature regulation and control was modulated by a Eurotherm 2416CC (utilizing Proportional-Integral-Derivative control philosophy) controller within which a 2132 overtemperature safety device was imbedded.

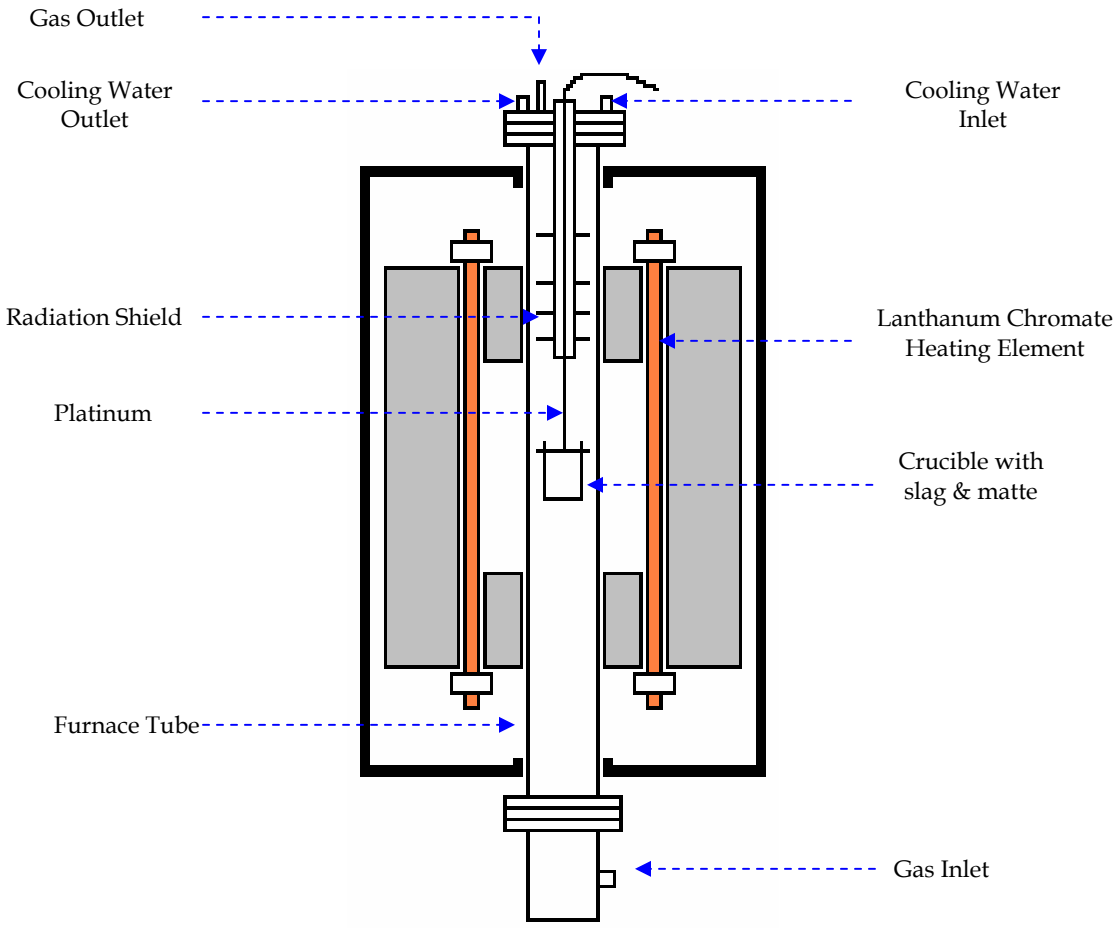

Fig 3.1 : Vertical Tube Furnace

The reaction chamber consisted of a recrystallized alumina tube (85mm OD, 75mm ID, 1200mm length) held in vertical posture by a manifold of adjustable clamping mechanism.

Fitted to the top of the tube was a set of water cooled stainless steel flanges, coupled to the tube by means of rubber "O"-rings. This top end was also fitted with a ceramic radiation shield for maximum heating of the hot zone.

The crucible was suspended in the hot zone by supporting it on the same recrystallised alumina tubing on which the radiation shield "fins" were fitted.

The tube was firmly secure to the top flange by means of rubber "O"-rings and brass fittings.

The bottom of the tube was fitted with a stainless steel extension, custom-designed to facilitate a bottom-up gas injection configuration into the furnace chamber.

3.1.1.1 Temperature Measurement Equipment

A dual temperature measurement approach was adopted, this being;

i. Measurement by means of the furnace in-built thermocouple, this being displayed on the digital interface on the Programmable Eurotherm Controller box.
ii. Measurement by means of a Pt/Pt – 6% Rh thermocouple encapsulated in a recrystallised alumina sheath. It should be noted that the thermocouple was not inserted into the furnace for the duration of all the runs, otherwise it would have been difficult to maintain a closed furnace environment. Hence it was only randomly and intermittently inserted mainly as a control to check the accuracy of the controller readings.

3.1.1.2 Thermocouple Calibration

The method used was adopted from Bartie *et al.* (2004). The thermocouples used in this study (type-B) were calibrated against the melting temperature of copper (1083˚C). High purity copper turnings were melted in a graphite crucible to just below 1120˚C. The programmable controller of the tube furnace was

programmed to hold the temperature at 1118˚C for one hour, and to switch off immediately after that. A cooling curve (shown in fig 3.2) was then plotted by noting the rate of change of the melt temperature with time measured at 30-second intervals.

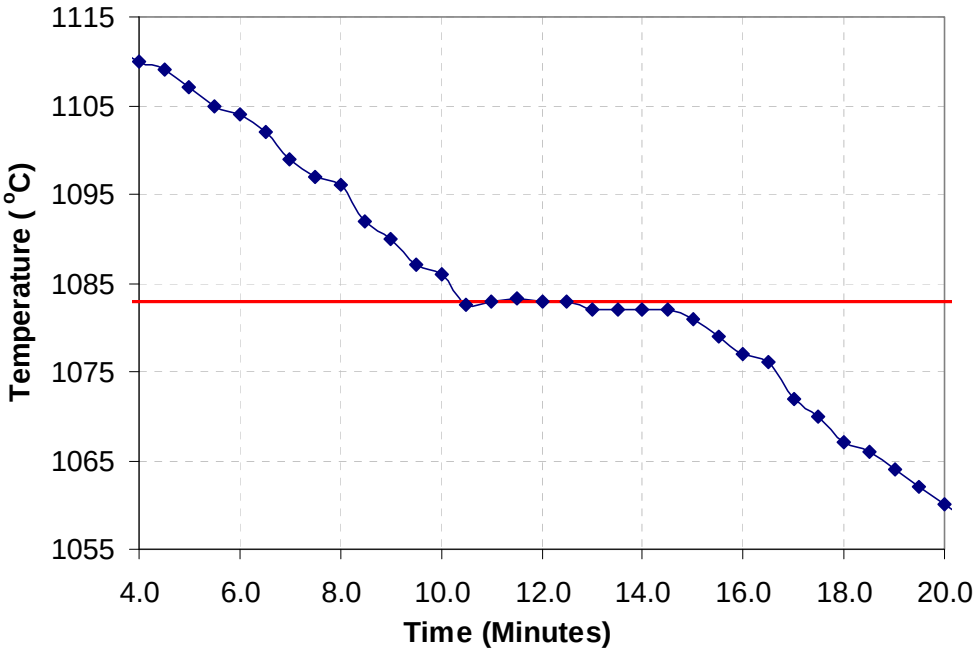

Fig 3.2: Cooling Curve for Thermocouple calibration

It can be noted from Fig 3.2 that the temperature remained constant between 1083˚C and 1082˚C for 4 minutes. It was noted that before attaining the temperature of 1083˚C, the temperature first dropped to slightly below 1083˚C before rising again to 1083˚C and further cooling thereafter. This is because in pure metals, at solidification point, insufficient energy is released by the heat of fusion to create a stable boundary, and hence some undercooling is always necessary to form stable nuclei (Porter and Easterling, 1981). The horizontal line on the cooling curve gives the solidification (or melting) temperature of copper (Avner, 1974).

It can be clearly seen that temperatures were measured accurately and no corrections to thermocouple readings were required.

3.1.1.3 Establishment of a Closed Environment

To ensure a completely closed set-up, a piece of rubber tubing was fitted on top of the recrystallised alumina tube which supported the radiation shield. After suspending the sample in the hot zone, the tubing was then clamped to ensure a gas-tight environment in the furnace heating chamber.

The bottom part of the tube was closed with a thin plastic film that was tightly secured in place by means of an elastic rubber banding.

3.1.1.4 Determination of the Furnace Hot zone

This was achieved by traversing a thermocouple across the length of the furnace tube and noting the equilibrium temperature. The thermocouple was moved in steps of 5cm and allowed to equilibrate for about 10minutes before the temperature was recorded. This exercise was conducted for two different furnace temperature settings, this being at 1473K and 1673K, and the temperature profiles obtained are shown in fig 3.3.

Following this exercise, the position of the hotzone was clearly marked on the surface of the furnace, and all samples were positioned in such a way that they would be in the middle of this 10cm heating bandwidth.

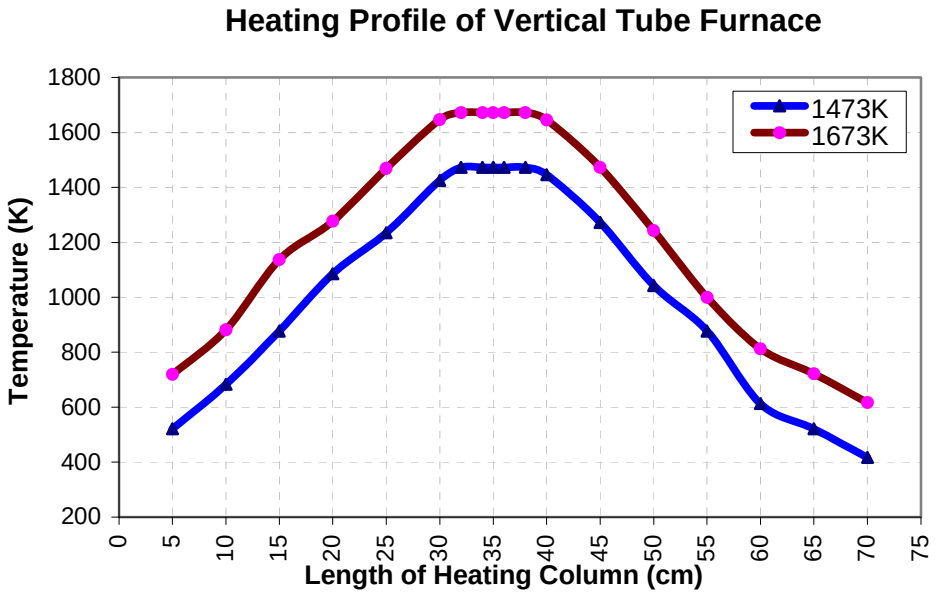

Fig 3.3 : Tube Furnace temperature profile

3.1.2 Gas Handling System

The gas flow configuration employed in the experimental work is as shown in *Fig 3.4*.

This consisted of the following sub-units;

i. Gas supply
ii. Control and Measurement
iii. Gas cleaning
iv. Gas mixture homogenisation facility

3.1.2.1 Gas supply

Four gas cylinders containing argon, carbon monoxide, carbon dioxide, and sulphur dioxide were arranged in a parallel ringmain configuration as shown in *Fig 3.4*. The purity of all the gases was at least 99.9%.

3.1.2.2 Gas Cleaning

Silica gel was utilised to remove any traces of moisture/water vapour in the gas streams, this being applied to the carbon dioxide, carbon monoxide, and argon streams. The carbon monoxide and argon streams were subsequently passed over anhydrous soda-lime granules to remove any carbon dioxide that could have been present in these gas streams.

The gas mixture was then passed through a deoxidising furnace containing copper turnings at about 500˚C. The deoxidising furnace consisted of a steel tube fitted in an alumina sleeve.

3.1.2.3 Gas Measurement and Control

This was achieved by means of four differently sized Celerity Instruments UNIT Mass Flow Controllers (hereafter referred to as MFCs), each MFC handling one gas at a time, and fitted with an in-built non-return valve. Each MFC could be configured to handle any of the gases used in this investigation (in-fact, each is compatible to adapt to over 50 different types of gas) by means of a software package called Multiflo Configurator. All valves were completely digitally controlled with accurate control from 1% to 99% of the fully open position. The setting of required flow parameters and the control of gas flow were effected by means of another software package called Multiflo Virtual Interface, this being interlinked to Multiflo Configurator.

3.1.2.4 Gas-mix Homogenisation

In order to ensure a uniformly mixed gas train, the inlet stream into the furnace was passed through a cylinder of glass beads as shown in Fig. 3.4.

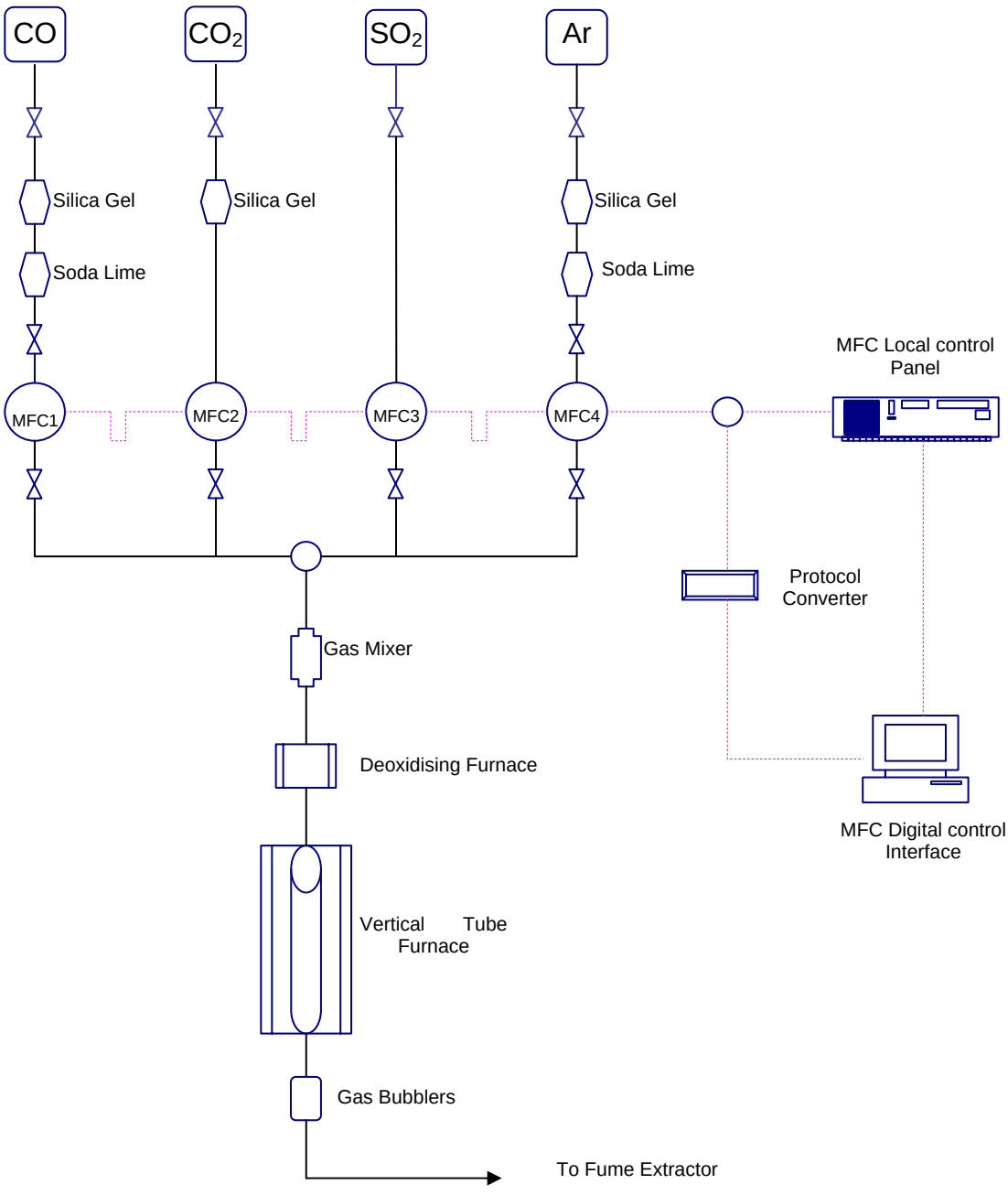

Fig 3.4 : Schematic of Gas Cleaning and Control System

3.2 MATERIALS

3.2.1 Matte and Slag

The materials used to prepare the equivalent matte and slag were selected based on industry practice, but with only a few components. This was so in order to keep the system as simple as possible, and yet large enough to allow meaningful deductions to be made. The other reason was also to safeguard against "noise" effects of other components.

Samples for each experimental run were made by mixing appropriate quantities of the relevant powders. Details for the powders used are outlined in Tables 3.1 and 3.2.

Also shown in these two tables (3.1 and 3.2) is the composition for the matte and slags used in this work. These compositions were selected based on typical industrial compositions. These benchmarking compositions are also shown in the tables.

Table 3.1 : Raw materials for the basic matte

Matte Components	**Composition (wt %)**	
	Experimental	**Industry**
Cu_2S	36	10
FeS	64	64
Other (e.g Ni, PGMs)	-	26

Table 3.2 : Raw materials for the master slag

Slag Components	Composition (wt %)	
	Experimental	**Industry**
FeO	15	8
SiO_2	55	48
MgO	25	24
Cr_2O_3	5	3.5
Other (e.g CaO, Al_2O_3)	-	16.5

3.2.2 Preparation of Wustite

Wustite (FeO) was prepared by mixing stoichiometric amounts of ferric (Fe_2O_3) and iron powder (Fe) according to the reaction;

$$Fe + Fe_2O_3 = 3FeO \qquad \text{Eq 3.1}$$

The method was adopted from Nzontta *et al.* (1999). The mixture was pressed with a 5 metric ton load using a hydraulic press to produce a pellet that was then heated in a tube furnace at 900˚C for 12hrs in an Argon atmosphere. The final product was a dark metallic grey pellet, which was then ground into a powder in a ring mill and stored under absolute alcohol in a dessicator. This was done in order to avoid reoxidation of the ferrous oxide to ferric oxide (a reddish colour). This exercise was performed in duplicate, and the XRD spectra obtained are shown in Figs D21 and D22 in Appendix D.

The spectra in Figs D21 and D22 show that almost all the ferric was reduced to wustite.

3.2.3 Crucibles

"The principal obstacle to successful experimentation with sulphide systems is the container. Ideally, it should remain completely inert but with sufficient strength for use at high pressures and temperatures" (Barnes, 1971). It is with this motivation that the crucible materials used in this work were selected. The materials adopted by the researchers in section 2.5 have also been taken as a benchmark.

The details of the crucibles used in all experiments are shown in Table 3.3. As can be noted, these were all made from recrystallised alumina, except for those used for pO2 validation (section 3.6.1).

Table 3.3 : Crucible details

Experiment	**Material**
Equilibration	Recrystallised Alumina
Drop Quench	Recrystallised Alumina
pO_2 Validation	Iron
pS_2 Validation	Recrystallised Alumina

3.2.4 Gases

The gases used (Carbon dioxide, carbon monoxide, argon, and sulphur dioxide) were supplied by BOC Gases Ltd, with a minimum purity of 99.9%. The gases were dried cleaned prior to use, as mentioned earlier on (section 3.1.2.2).

The gas mix ratios used to attain the required partial pressures were calculated using Factsage Thermochemical Software version 5.3.1 (developed by Bale *et al.*, 2002), and the flows used for the experiments are shown in Appendix A.

3.3 SYSTEM DEFINITION

In this section, the system employed in this study is defined in full perspective in table 3.4.

Table 3.4 : System Definition

System	:	*Fe-Cu-S-Cr-Mg-Al-Si-O (Al as Al_2O_3 entrained from crucible material)*
No. of Components	:	*8*
No. of Phases	:	*5 [Al_2O_3 (at saturation); Cr_2O_3 (at saturation in slag); two liquids (slag and matte); one gas]*
Degrees of Freedom	:	*5 , [calculated from Gibbs Phase Rule, i.e. (P + F = C + 2) (Gaskell, 1973)], where P = No. of phases, F = No. of Degrees of Freedom, C = No. of components*
This means that five independent variables need to be specified to define completely the state of the system		
Independent Variables	:	*Temperature; Sulphur partial pressure (pS_2); Oxygen partial pressure (pO_2); Matte composition; Slag composition*
Temperature	:	*1300˚C, 1400˚C, 1500˚C*
Gas Partial Pressure	:	*Calculated with Factsage Thermochemical Software V. 5.3.1(developed by Bale et al., 2002)*
pO_2	:	*10^{-10}atm, 10^{-8}atm, 10^{-6}atm*
pS_2	:	*10^{-6}atm, 10^{-4}atm, 10^{-2}atm*
Initial Matte Composition	:	*Listed in table 3.1*
Initial Slag Composition	:	*Listed in table 3.2*

This definition is fundamental to the understanding of the system at hand, and it forms a crucial part of the basis upon which the experimental planning and design was conducted (see section 3.4.1).

The selection of the experimental parameters in table 3.1 was based on industry practice and reports made by other researchers (section 2.5).

3.4 METHOD

3.4.1 Experimental Design

The experimental design employed was a completely randomised 3^3 full factorial design with two replicates. This design enables an analysis of the effect of each factor on the response at different levels of other factors. The experimental variables (or factors) are temperature, partial pressure of oxygen (pO_2), and partial pressure of sulphur (pS_2). Each of these factors was analysed at three levels, the response variable of concern being the partition coefficient of chromium between slag and matte.

Fig 3.7 is a graphical representation of the treatment combinations employed in this research. A treatment is synonymous to a factor level, for example, temperature is a factor with three levels or three treatments. The factors in Fig 3.7 have been coded, with a low represented by (-1), medium by (0), and high by (+1). Each treatment combination is represented by 3 digits, where the first digit indicates the level of pO_2, the second digit indicates the level of pS_2, and the third digit the level of temperature. For example, (-1 0 +1) denotes the treatment

combination corresponding to pO_2 at low level (10^{-10}atm), pS_2 at medium level (10^{-4}atm), and temperature at high level (1500˚C).

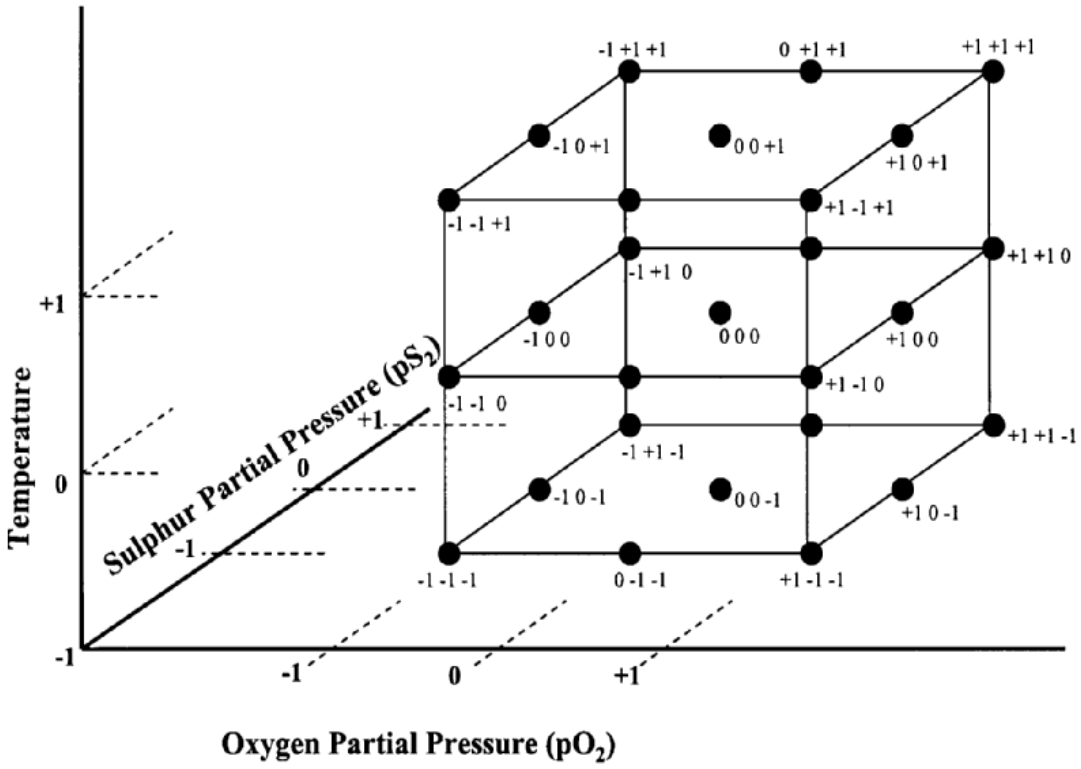

Fig 3.7 : Treatment combinations in the 3^3 full factorial experimental design employed in this study for each replicate

Key of Coded Variables			
	-1	0	+1
Temp	1300°C	1400°C	1500°C
pO_2	10^{-10}atm	10^{-8}atm	10^{-6}atm
pS_2	10^{-6}atm	10^{-4}atm	10^{-2}atm

The experimental runs in each replicate were randomized in order to minimize the effects of any extraneous factors that could have been present.

3.4.2 Pre-Experimental Scanning

The ranges of some of the parameters in table 3.4 (temperature, pS_2 and pO_2) were modelled out using Factsage Thermochemical Software version 5.3.1 (developed by Bale *et al.*, 2002). The primary aim of undertaking this exercise was to identify the dominant phases in the system under the selected operating ranges.

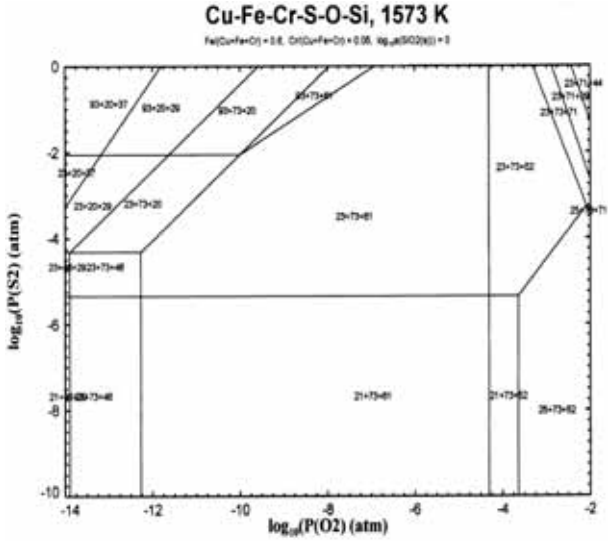

Fig 3.8 : Predominance Diagram at 1300°C

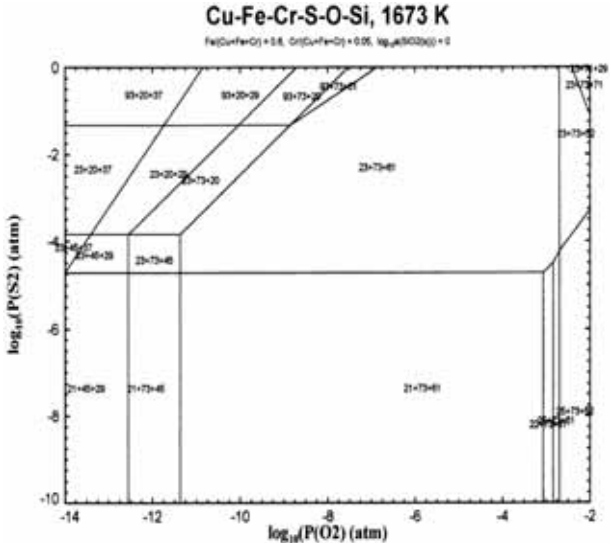

Fig 3.9 : Predominance Diagram at 1400°C

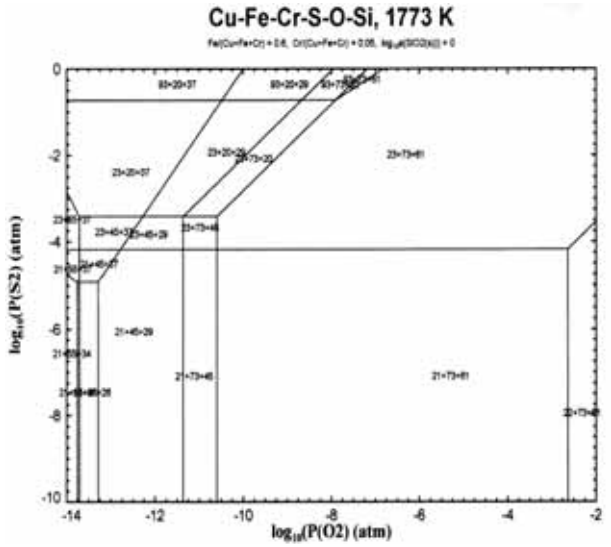

Fig 3.10 : Predominance Diagram at 1500°C

No	Component		No	Component
20	FeS (L)		45	Fe (S)
21	Cu (L)		46	Fe (S2)
22	Cu_2O (L)		52	Fe_3O_4 (S)
23	Cu_2S (L)		55	FeSi (S)
25	$(Cu_2O)(Fe_2O_3)$		61	$2FeO{\cdot}SiO_2$ (S)
29	Cr_2O_3 (S)		65	FeS (S)
34	Cr_3Si (S)		71	$FeSO_4$ (S)
37	CrS (S)		73	$FeCr_2O_4$ (S)
44	$Cr_2(SO_4)_3$ (S)		93	Cu_5FeS_4 (S)

Table 3.4 : Key to some Phases in the Predominance Diagrams

A "step-by-step" procedure for the construction of predominance diagrams has been provided by Pelton (2001) and Bale *et al.* (1986).

From the predominance diagrams in figs. 3.8-3.10, the main phases present in the system bounded by the parameters in table 3.4 are liquid copper (Cu (L)), chalcocite (Cu_2S (L)), fayalite ($2FeO{\cdot}SiO_2$) and spinel ($FeCr_2O_4$). This shows that the ranges are feasible, as some of the phases are in agreement with the findings of the workers in section 2.5. The software used to calculate the predominance diagrams could only handle a maximum of three metallic elements, hence the exclusion of aluminium and magnesium (see system in table 3.4). But since this preliminary modeling exercise was meant to give a rough idea of the possible dominant phases prior to experimentation, the exclusion of these two elements was not considered to be completely misleading for the purposes of this exercise.

3.4.3 Drop-quench experiments

The drop-quench technique was used as a means to identify the different forms in which Chromium exists at the temperatures and gas partial pressures investigated. The assumption of this technique is that if the quenching is effective, the phases formed at elevated temperatures are preserved at room temperature (Kullerud, 1971).

The experiments involved suspending alumina crucibles containing 0.4g of slag and matte powders (with a slag/matte weight ratio of 1:1) onto a platinum wire. One end of the wire was secured onto the water-cooled end of the furnace. The furnace tube was then purged for 30 minutes with the appropriate gas mixture, after which the samples were then lowered into the hot zone of the furnace and equilibrated for 8 hours (see section 3.7).

Upon attainment of equilibrium, the platinum wire suspending the crucibles was then released, allowing the samples to drop through the plastic sheath on the bottom of the furnace, into a water/ice bath beneath the furnace. The bath consisted of 10 litres of pre-refrigerated water in equilibrium with a thin layer of finely crushed ice.

Prior to the experiments the position of the constant temperature zone of the furnace was determined by use of a thermocouple (see section 3.1.1.5). The flowrates of the gases used to achieve the required gas atmosphere were controlled by a set of pre-calibrated mass flow controllers (section 3.1.2.3).

3.4.4 Slag-matte-gas equilibrium experiments

The three-phase equilibration technique was used to determine the bulk distribution profiles of Chromium in slag and matte.

The experimental procedure adopted was similar to the one used for the drop-quench experiments, except for two aspects. First, the mass of the slag and matte powders used was 5g each. Secondly, the quenching method applied was different from the drop-quenched experiments. The samples were cooled by lowering them into the cold zone of the furnace without initially piercing through the plastic sheath at the bottom furnace end-cap. This was achieved by attaching an additional 1.5m platinum wire to the upper end of the wire suspending the samples, and slowly lowering down at a rate which was aimed at preventing any turbulent movement of the molten phases. The crucibles were then held in this position for two hours, and then lowered further down into an empty stainless steel bath underneath the furnace. The gas flows were not adjusted during the whole cooling cycle.

3.5 ANALYTICAL PROCEDURES

3.5.1 SEM – EDS

Imaging of the drop-quench samples and analysis of the phase compositions was accomplished using a Leo® 1430VP Scanning Electron Microscope. Prior to imaging or analysis the samples were sectioned, polished and sputter-coated with carbon to enhance surface conductivity. Phases were identified with backscattered electron (BSE) and/or Secondary electron images, and phase compositions quantified by EDS analysis using an Oxford Instruments® 133KeV detector and Oxford INCA software. Beam conditions during the quantitative analyses were 20 KV and approximately 1.5nA, with a working distance of 13 mm and a specimen beam current of -3.92nA. Despite the relatively low energy of the beam, X-ray counts with the set-up used were typically ~ 5000cps. The counting time was 50 seconds live-time.

At least three points were analysed for each sub-phase identified on the SEM, and a statistical mean was then computed.

3.5.2 X-Ray Diffraction

This technique was used for phase-identification in the drop-quench samples. Use was made of a Bruker AXS D8 Advance X-ray machine with a 1.5406Å Kα1 radiation. The time/step was varied from 300 – 4300 seconds with a stepsize of 0.026^{o}. All the analyses were done using a Vantec 1 detector at the Bruker AXS Laboratories in Karlsruhe (Germany).

3.5.3 ICP - AES

Slag and matte samples from the equilibration experiments were dissolved in aqua regia (mixture of 1 part HNO_3 and 3 parts HCl) and analysed with a Liberty Series II radial emission inductively coupled plasma atomic emission spectrometer.

3.5.4 Titrametric Analysis

This technique was applied to determine the ferrous and ferric content in the slag samples obtained from the oxidation partial pressure validation experiments.

The samples were analysed for calcium, ferrous iron, and total iron. Calcium was determined by spectrophotometric titration with ethylene-diamine-tetra-acetic acid di-sodium salt as the titrant and copper ammonium complex as indicator. Ferrous was determined volumetrically with $K_2Cr_2O_7$ as the titrant and 4-diphenylaminesulphonic acid sodium salt as the indicator. For an analysis of total iron, iron was pre-reduced with $SnCl_2$, and ferric was calculated as the difference between total iron and ferrous iron (Harris and Kratochvil, 1974).

3.6 VERIFICATION OF GAS PARTIAL PRESSURE

As has been noted in table 3.4, the gas mix ratios necessary to achieve the required gas partial pressures of oxygen and sulphur were calculated using Factsage Thermochemical Software version 5.3.1 (developed by Bale *et al.*, 2002). The MFC's were then set at appropriate setpoints in order deliver the calculated gas flows. It was therefore necessary to verify that the mass flow controllers delivered the intended flows to achieve the required partial pressure in the vertical tube furnace. This was done by conducting two independent experimental checks for the partial pressures of oxygen and sulphur.

3.6.1 Validation of Oxygen Partial Pressure

These were checked using a method adopted from Takeda *et al.* (1980) and Yazawa *et al.* (1981). A master sample was made by mixing 20g (total mass of initial mix) of CaO and Fe_2O_3, premelting the mixture in an iron crucible for 1 hr in an inert atmosphere, crushing and homogenizing using the technique suggested by Wills (1997). For each experimental run to verify the oxygen partial pressure, a 3g sample was weighed from the master and equilibrated for 30 hours in an iron crucible in the appropriate gas atmosphere. The exercise was conducted for all the oxygen partial pressures employed in this work (10^{-10}, 10^{-8}, and 10^{-6}atm). According to Yazawa *et al.* (1981), the oxygen partial pressure in this slag-gas system can be calculated using the relation.

$$\log pO_2 = 5.88\log\left(\frac{Fe^{3+}}{Fe^{2+}}\right) - 0.106(\%CaO) - \frac{32400}{T} + 14.82 \qquad \text{Eq 3.2}$$

Upon attaining the equilibrium time, the samples were quenched in a similar manner to the equilibration experiments in section 3.4.4, and prepared for analysis.

Ferrous and ferric contents of the equilibrium slag were determined titrimetrically as detailed in section 3.5.3. Calcium oxide was determined using ICP (section 3.5.2) (analysed as calcium and converted to CaO). These were then substituted into Eq 3.2. Table 3.5 gives a comparison of the results obtained with the ones calculated using Factsage Thermochemical Software version 5.3.1 (Bale *et al.*, 2002)

Table 3.5 : Verification of oxygen partial pressure

Run No.	Log pO_2		Standard Deviation (%)
	Factsage Calculation	Verification Test	
1	-10	-9.831	1.72
2	-8	-7.852	1.88
3	-6	-5.908	1.56

As can be seen, the actual flow as determined experimentally was higher than the set-value (Factsage calculation) by an average of 1.72% for all the three runs. If need be, this correction factor may be applied to the flowrates calculated by Factsage (in section 3.2) for improved precision.

3.6.2 Validation of Sulphur Partial Pressure

The method used by Mishra and Pruseth (1994) to determine sulphur partial pressures was employed using pyrrhotite ($Fe_{1-x}S$). A 1 gram sample of pyrrhotite was placed in the tube furnace at a temperature of 1 000K. This temperature was chosen because it was the highest that could be found in literature to benchmark with. Since the aim was to verify that the mass flow controllers were delivering

the correct flow as calculated using Factsage, the verification was ultimately done at this temperature, despite it being lower that the minimum temperature employed in this work. This also meant that the verification for the MFC flowrates were done at a slightly lower flow than the one actually employed in this research. The experiments were conducted at the three partial pressures of sulphur employed in this research (10^{-6}, 10^{-4}, and 10^{-2}atm) by manipulating the mix ratios of the SO_2-CO_2-CO-Ar gas system, as calculated using Factsage.

After quenching of the pyrrhotite, smears were made for XRD analysis. Ni-filtered CuK_α X-ray was used with a scanning speed of 0.01˚ 2θ/sec and a chart speed of 50mm/2θ using a Philips PW 1710 XRD. The (111) reflection of metallic Si (d = 3.135Å) was used as an internal standard. The Fe content of the pyrrhotite N_{FeS}^{P} was calculated from the d_{102} spacing according to the procedure of Yund and Hall (1969). The partial pressure of sulphur was then calculated at 1000K using the thermochemical data in the Fe-S system (Toulmin and Barton, 1964). Table 3.6 shows the results obtained and these may be compared to the flowrates as determined by Factsage

Table 3.6 : Verification of sulphur partial pressure

Run No.	Log pS_2		Standard Deviation (%)
	Factsage Calculation	Verification Test	
1	-8	-7.869	1.66
2	-6	-5.898	1.73
3	-4	-3.925	1.91

As can be seen from table 3.6, the same trend obtained in the oxygen partial pressure experiments was noted for the sulphur experiments. The flowmeters were under-reading by an average of 1.77%. For greater precision, the partial pressures obtained from the verification experiments may be used as the actual

sulphur partial pressures. However, for the purposes of the discussion in this and other sections, the sulphur partial pressures will be quoted without applying the correction factor (i.e., as 10^{-6}, 10^{-4}, 10^{-2} atm).

An alternative technique for pS_2 Validation has been presented in Appendix E.

3.7 DETERMINATION OF EQUILIBRATION TIME

In this section, the experiments to determine the time required for the slag/matte system to attain equilibrium are discussed.

Slag and matte powder of equal weight and composition were heated in alumina crucibles for increasing time intervals. Equilibration times considered were 2, 4, 8, 12, 16 and 24 hrs. The composition and weight of the samples was similar to the ones employed in the 3-phase equilibration experiments in Section 3.4.4. All experiments were conducted at 1300˚C, this being the lowest temperature employed in this research. The gas atmosphere was controlled to give an oxygen partial pressure of 10^{-8} atm and pS_2 of 10^{-4}atm for one set of experiments. This has been quoted in literature as being representative of industry practice (Kongoli and Yazawa, 2001; Rosenqvist, 1974; also see section 2.5), and is the median level of the gas partial pressures employed in this work. The second set of experiments were performed at the least levels of all the parameters (temperature = 1300˚C, $pO_2 = 10^{-10}$atm, $pS_2 = 10^{-6}$atm. The assumption in this case is that if the equilibration time is determined at the lowest of the three temperatures, then this time should be more than enough for higher temperature. This is because at higher temperatures, reaction kinetics and mass transfer rates tend to be faster than at lower temperatures.

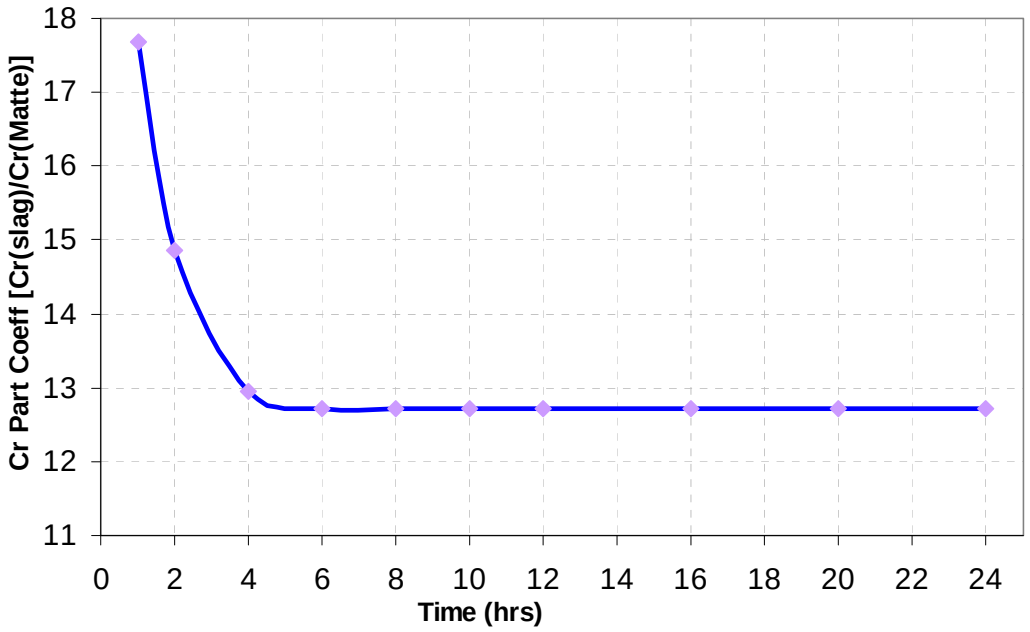

Fig 3.11: Chromium Distribution vs Time : $pO_2 = 10^{-8}$atm, $pS_2 = 10^{-4}$ atm

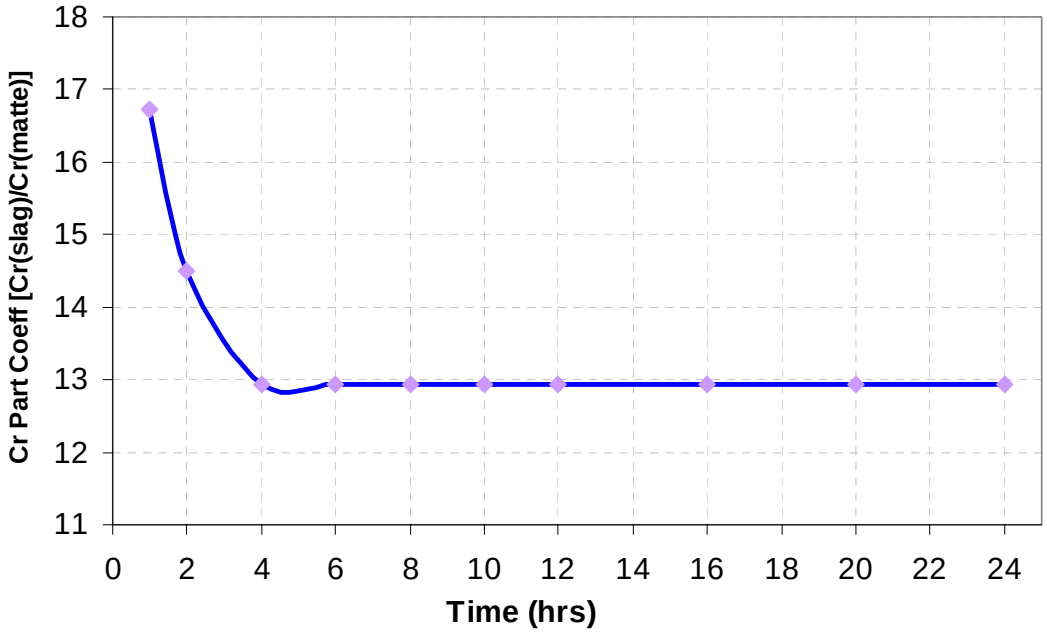

Fig 3.12: Cr Distribution vs Time : $pO_2 = 10^{-10}$atm, $pS_2 = 10^{-6}$atm

It can be seen from figs 3.11 and 3.12 that the distribution ratio of Chromium between the matte and the slag, defined by equation 1.1, remain constant after about 6 hours in both cases.

Run times of 8hrs were then selected as a prudent measure, even though the results show that equilibrium was attained in about 6 hours. This equilibrium time was employed even for the higher temperature experiments, though it is anticipated that equilibrium was attained even earlier due to increased kinetics.

CHAPTER 4

PRESENTATION OF SUMMARISED RESULTS

This section presents the results of the drop quench experiments and the three-phase equilibration experiments.

4.1 EQUILIBRATION EXPERIMENTS

The three-phase equilibration experimental results are ICP results showing the bulk distribution of chromium in mattes and slags for each of the factor combinations investigated. These are presented in Tables 4.1 and 4.2 (for the two replicates), which also include values for the chromium partition coefficient as calculated using the formula in Eq 1.1.

4.2 DROP-QUENCH EXPERIMENTS

The drop-quench experimental results are SEM analyses of the composition of the slag and matte constituent phases. Table 4.3 is a summary of these results. As mentioned in section 3.5, at least three points were analysed for each sub-phase identified on the SEM, and a statistical mean was then computed. Hence table 4.3 is a summary of the means for each of the sub-phases in the matte and slag phases. The original analyses from which these means were computed are presented in Appendix B.

The micrograph images that were generated on the SEM for the drop-quench experiments are presented in Appendix C. Phases identification was done using XRD technique, and the spectra obtained is presented in Appendix D, and in the last part of this chapter. A discussion of these results is presented in chapter 5.

Table 4.1 : Three –phase Equilibration Experiments : Replicate No.1

Temp (°C)	Phase	$pS_2 = 10^{-6}$ atm			$pS_2 = 10^{-4}$ atm			$pS_2 = 10^{-2}$ atm		
		$pO_2 = 10^{-10}$ atm	$pO_2 = 10^{-8}$ atm	$pO_2 = 10^{-6}$ atm	$pO_2 = 10^{-10}$ atm	$pO_2 = 10^{-8}$ atm	$pO_2 = 10^{-6}$ atm	$pO_2 = 10^{-10}$ atm	$pO_2 = 10^{-8}$ atm	$pO_2 = 10^{-6}$ atm
1300	Matte	0.336	0.329	0.298	0.360	0.347	0.329	0.439	0.385	0.345
	Slag	4.353	4.360	4.391	4.345	4.358	4.376	4.254	4.308	4.348
	Partition Coefficient	*12.955*	*13.252*	*14.735*	*12.069*	*12.559*	*13.301*	*9.690*	*11.190*	*12.603*
1400	Matte	0.462	0.440	0.447	0.525	0.499	0.471	0.561	0.548	0.484
	Slag	4.227	4.249	4.242	4.180	4.206	4.234	4.132	4.145	4.209
	Partition Coefficient	*9.149*	*9.657*	*9.490*	*7.962*	*8.429*	*8.989*	*7.365*	*7.564*	*8.696*
1500	Matte	0.497	0.521	0.504	0.571	0.541	0.526	0.596	0.571	0.557
	Slag	4.192	4.168	4.185	4.134	4.164	4.179	4.097	4.122	4.136
	Partition Coefficient	*8.435*	*8.000*	*8.304*	*7.240*	*7.697*	*7.945*	*6.874*	*7.219*	*7.425*

Key of Coded Variables			
	-1	0	+1
Temperature	1300°C	1400°C	1500°C
pO_2	10^{-10} atm	10^{-8} atm	10^{-6} atm
pS_2	10^{-6} atm	10^{-4} atm	10^{-2} atm

Table 4.2 : Three –phase Equilibration Experiments : Replicate No.2

Temp (°C)	Phase	$pS_2 = 10^{-6}$ atm			$pS_2 = 10^{-4}$ atm			$pS_2 = 10^{-2}$ atm		
		$pO_2 = 10^{-10}$ atm	$pO_2 = 10^{-8}$ atm	$pO_2 = 10^{-6}$ atm	$pO_2 = 10^{-10}$ atm	$pO_2 = 10^{-8}$ atm	$pO_2 = 10^{-6}$ atm	$pO_2 = 10^{-10}$ atm	$pO_2 = 10^{-8}$ atm	$pO_2 = 10^{-6}$ atm
1300	Matte	0.324	0.340	0.287	0.372	0.352	0.317	0.426	0.353	0.334
	Slag	4.396	4.380	4.433	4.349	4.369	4.404	4.291	4.364	4.383
	Partition Coefficient	*13.568*	*12.882*	*15.446*	*11.691*	*12.412*	*13.893*	*10.073*	*12.363*	*13.123*
1400	Matte	0.474	0.451	0.392	0.491	0.503	0.439	0.497	0.511	0.468
	Slag	4.246	4.269	4.328	4.230	4.218	4.282	4.220	4.206	4.249
	Partition Coefficient	*8.958*	*9.466*	*11.041*	*8.615*	*8.386*	*9.754*	*8.491*	*8.231*	*9.079*
1500	Matte	0.483	0.497	0.511	0.564	0.536	0.548	0.634	0.588	0.572
	Slag	4.237	4.223	4.209	4.157	4.185	4.173	4.083	4.129	4.145
	Partition Coefficient	*8.772*	*8.497*	*8.237*	*7.371*	*7.808*	*7.615*	*6.440*	*7.022*	*7.247*

Key of Coded Variables			
	-1	0	+1
Temperature	1300°C	1400°C	1500°C
pO_2	10^{-10} atm	10^{-8} atm	10^{-6} atm
pS_2	10^{-6} atm	10^{-4} atm	10^{-2} atm

Table 4.3 : Drop Quench Experiments

Run No	Temp (°C)	Log pO_2 (atm)	Log pS_2 (atm)	Phase	Subphases	% O	% Si	% Mg	%Al	%Cr	%S	% Fe	% Cu	Total
34	1300	-10	-6	Matte	Cu-rich Glass	0.01	0.00	0.00	0.00	0.09	4.15	4.92	92.24	101.42
				Slag	Glass	37.17	18.16	4.83	3.85	0.16	0.00	19.65	17.00	100.82
					Olivine	41.06	21.97	13.32	0.13	0.52	0.02	22.05	0.07	99.13
					Spinel	29.11	1.30	4.79	3.09	31.63	0.00	25.27	5.71	100.91
32	1300	-8	-6	Matte	Fe-rich sulphide	0.51	0.00	0.01	0.14	0.19	25.49	20.54	53.88	100.77
					Cu	0.72	0.00	0.00	0.14	0.01	2.03	7.41	89.78	100.09
					Cu-rich Glass	0.61	0.00	0.04	0.13	0.02	24.12	18.40	57.23	100.55
				Slag	Glass	37.39	18.77	4.28	3.20	0.24	0.15	36.76	0.11	100.89
					Olivine	41.10	23.86	12.80	0.14	0.41	0.10	21.51	0.13	100.03
					Spinel	28.54	0.07	2.09	1.80	38.54	0.00	28.75	0.00	99.80
29	1300	-6	-6	Matte	Cu-rich Glass	0.03	0.00	0.01	0.09	0.10	19.60	6.43	74.22	100.48
					Cu	0.54	0.00	0.00	0.20	0.01	0.14	1.02	99.18	101.08
				Slag	Glass	37.01	16.22	4.64	4.70	0.13	0.49	37.73	0.13	101.05
					Olivine	38.09	16.99	15.12	0.13	0.50	0.02	29.85	0.06	100.76
					Spinel	27.63	0.18	2.57	2.42	33.62	0.01	34.20	0.04	100.67
36	1300	-10	-4	Matte	Cu-rich Glass	0.00	0.00	0.00	0.00	0.00	27.44	21.05	52.25	100.74
					Fe-rich sulphide	0.80	0.00	0.00	0.00	0.12	24.56	32.25	42.96	100.68
				Slag	Glass	39.05	23.05	8.25	2.21	0.48	0.39	26.16	0.30	99.88
					Olivine	42.86	25.53	12.65	0.23	0.73	0.06	18.87	0.08	101.02
					Spinel	30.48	0.72	3.01	2.62	38.76	0.13	24.79	0.14	100.65
25	1300	-8	-4	Matte	Cu-rich Glass	1.56	0.00	0.04	0.14	0.01	25.26	12.05	62.10	101.16
					Cu	0.83	0.00	0.00	0.23	0.00	0.08	1.60	96.88	99.61
					Fe-rich sulphide	13.21	0.20	0.04	0.14	0.16	14.16	36.39	36.39	100.69
				Slag	Glass	34.95	15.08	7.34	2.46	0.20	0.31	39.89	0.17	100.40
					Olivine	36.40	15.75	15.28	0.15	0.84	0.07	32.45	0.05	101.00
					Spinel	28.19	0.12	2.16	0.71	39.92	0.01	29.05	0.01	100.18
28	1300	-6	-4	Matte	Cu-rich Glass	0.28	0.00	0.00	0.13	0.11	21.22	5.59	73.90	101.23
				Slag	Glass	36.87	18.95	1.20	7.42	0.20	0.29	35.67	0.28	100.88
					Olivine	41.63	24.90	13.24	0.18	0.80	0.03	20.26	0.08	101.13
					Spinel	29.17	0.70	2.48	0.43	39.83	0.07	27.14	0.00	99.82
37	1300	-10	-2	Matte	Cu-rich Glass	0.00	0.00	0.00	0.00	0.00	26.69	21.54	51.79	100.02
					Fe-rich sulphide	0.68	0.00	0.03	0.01	0.22	24.91	34.12	40.12	100.08
				Slag	Glass	40.78	21.90	2.62	7.54	0.32	0.62	26.95	0.26	100.99
					Olivine	43.27	25.26	12.47	0.22	0.59	0.07	19.12	0.06	101.06
					Spinel	29.27	0.13	2.43	1.79	41.47	0.03	24.85	0.00	99.97
38	1300	-8	-2	Matte	Cu-rich Glass	0.35	0.01	0.00	0.03	0.08	24.63	22.70	52.27	100.08
					Fe-rich sulphide	1.62	0.01	0.13	0.11	0.27	22.01	34.07	41.15	99.37
				Slag	Glass	37.89	6.04	7.67	16.65	0.55	0.41	30.96	0.25	100.41
27	1300	-6	-2	Matte	Cu-rich Glass	0.34	0.00	0.04	0.13	0.03	27.79	20.68	51.58	100.59
					Cu	0.78	0.00	0.19	0.00	0.02	7.33	8.09	84.63	101.03
					Fe-rich sulphide	17.49	0.53	0.16	0.15	0.62	11.44	46.15	24.23	100.77
				Slag	Glass	39.68	22.18	1.91	7.51	0.51	0.34	28.60	0.15	100.90
					Olivine	41.32	24.46	11.85	0.22	0.68	0.04	21.01	0.05	99.62
					Spinel	30.73	0.12	2.88	1.69	41.03	0.03	23.95	0.01	100.42

Table 4.3 (continued)

Run No	Temp	Log pO_2 (atm)	Log pS_2 (atm)	Phase	Subphases	% O	% Si	% Mg	%Al	%Cr	%S	% Fe	% Cu	Total
44	1400	-10	-6	Matte	Cu-rich Glass	0.52	0.00	0.06	0.11	0.03	25.27	22.27	52.16	100.41
					Fe-rich sulphide	0.23	0.00	0.00	0.07	0.29	32.26	56.05	11.74	100.63
					Spinel	22.56	0.26	1.39	0.24	30.70	6.00	27.20	12.58	100.94
				Slag	Glass	40.80	8.91	7.09	20.10	0.68	0.30	21.12	0.14	99.13
43	1400	-8	-6	Matte	Cu-rich Glass	0.15	0.01	0.04	0.11	0.02	26.62	23.20	50.66	100.80
					Fe-rich sulphide	0.61	0.05	0.07	0.07	0.79	31.11	59.53	8.98	101.20
				Slag	Glass	38.69	20.96	7.06	2.30	0.54	0.41	30.77	0.15	100.89
					Olivine	39.26	18.14	24.25	0.14	0.28	0.04	18.68	0.14	100.93
					Spinel	32.81	1.36	5.33	0.33	39.02	0.01	21.55	0.03	100.43
41	1400	-6	-6	Matte	Cu-rich Glass	0.39	0.00	0.01	0.09	0.31	22.50	7.58	69.50	100.38
					Cu	0.49	0.00	0.00	0.16	0.00	0.88	0.45	98.54	100.53
				Slag	Glass	36.75	15.08	6.00	6.95	0.07	0.17	35.11	0.24	100.37
					Olivine	39.38	23.15	12.80	0.91	0.81	0.04	22.10	0.04	99.22
					Spinel	32.03	0.00	4.78	5.02	36.82	0.01	23.07	0.06	101.79
45	1400	-10	-4	Matte	Cu-rich Glass	0.32	0.02	0.03	0.10	0.01	25.69	21.14	53.21	100.52
					Fe-rich sulphide	0.30	0.00	0.02	0.08	0.93	33.56	55.11	11.74	101.75
				Slag	Glass	41.36	9.45	6.73	20.59	0.64	0.34	20.72	0.19	100.03
42	1400	-8	-4	Matte	Cu-rich Glass	0.32	0.00	0.03	0.08	0.02	25.27	22.59	52.57	100.87
					Fe-rich sulphide	0.49	0.00	0.00	0.08	0.82	30.63	59.79	8.71	100.52
				Slag	Glass	37.47	21.56	6.73	2.39	0.60	0.39	31.06	0.30	100.50
					Olivine	38.63	17.24	23.30	0.11	0.42	0.02	20.92	0.03	100.67
					Spinel	31.11	1.96	5.06	0.35	39.96	0.13	22.32	0.13	101.03
40	1400	-6	-4	Matte	Cu-rich Glass	0.40	0.01	0.00	0.12	0.00	22.04	6.94	70.99	100.49
					Cu	0.12	0.00	0.00	0.12	0.01	0.02	0.49	98.68	99.43
					Fe-rich sulphide	1.67	0.00	0.22	0.13	0.76	20.54	41.35	36.11	100.78
				Slag	Glass	37.07	15.42	5.76	7.10	0.08	0.20	34.85	0.29	100.77
					Olivine	37.44	0.18	7.83	25.28	7.77	0.01	22.19	0.00	100.69
					Spinel	31.57	0.14	3.79	3.03	40.22	0.01	22.78	0.03	101.57
46	1400	-10	-2	Matte	Cu-rich Glass	0.43	0.01	0.05	0.14	0.03	25.55	21.97	52.56	100.74
					Fe-rich sulphide	0.35	0.04	0.12	0.05	1.01	32.14	58.93	8.53	101.17
					Spinel	28.81	0.44	0.59	0.18	27.05	7.82	25.49	9.93	100.30
				Slag	Glass	40.07	19.25	7.05	8.68	1.21	0.45	22.95	0.28	99.94
39	1400	-8	-2	Matte	Cu-rich Glass	0.50	0.00	0.02	0.09	0.66	25.53	23.37	50.09	100.27
					Cu	0.40	0.00	0.00	0.13	0.01	11.81	12.38	76.20	100.93
				Slag	Glass	38.40	7.79	7.86	17.71	0.51	0.27	27.31	0.19	100.05
					Olivine	39.26	8.64	7.61	19.21	1.53	0.43	22.06	0.18	98.93
					Spinel	32.37	1.88	6.48	0.35	36.96	0.13	22.76	0.07	101.00
47	1400	-6	-2	Matte	Cu-rich Glass	0.30	0.01	0.03	0.07	0.04	25.07	20.95	53.17	99.65
					Fe-rich sulphide	0.32	0.00	0.03	0.04	0.92	33.14	59.51	7.79	101.74
					Spinel	27.92	0.10	1.67	0.66	32.75	0.01	36.68	0.04	99.82
				Slag	Glass	39.74	20.00	8.68	7.89	0.57	0.43	21.51	0.15	98.97

Table 4.3 (continued)

Run No	Temp	Log pO_2 (atm)	Log pS_2 (atm)	Phase	Subphases	% O	% Si	% Mg	%Al	%Cr	%S	% Fe	% Cu	Total
52	1500	-10	-6	Matte	Cu-rich Glass	0.34	0.00	0.06	0.06	0.02	25.85	23.54	50.39	100.26
					Fe-rich sulphide	0.44	0.02	0.04	0.11	0.87	32.04	56.22	11.77	101.52
				Slag	Glass	41.66	17.23	6.32	12.10	0.31	0.33	22.38	0.29	100.60
					Olivine	40.83	0.15	9.24	33.65	0.49	0.00	15.21	0.00	99.56
					Spinel	32.63	0.15	4.85	5.19	40.36	0.01	18.33	0.03	101.54
55	1500	-8	-6	Matte	Cu-rich Glass	0.35	0.00	0.00	0.12	0.00	26.85	22.42	51.61	101.36
					Fe-rich sulphide	0.24	0.01	0.04	0.13	0.97	29.30	51.46	19.36	101.51
				Slag	Glass	36.79	16.03	5.88	9.84	2.39	0.31	26.80	0.17	98.21
					Olivine	37.72	0.25	7.78	25.52	11.16	0.01	17.19	0.02	99.65
					Spinel	30.37	0.11	4.21	5.79	39.32	0.55	18.94	0.41	99.69
50	1500	-6	-6	Matte	Cu-rich Glass	0.81	0.00	0.00	0.18	0.03	19.64	0.54	77.54	98.74
					Fe-rich sulphide	1.03	0.00	0.02	0.12	0.93	14.80	51.56	32.01	100.46
				Slag	Glass	36.54	4.81	11.02	14.53	0.13	0.08	29.74	1.66	98.52
					Olivine	35.84	6.91	26.76	0.14	7.39	0.01	21.76	0.10	98.91
					Spinel	31.49	0.20	5.15	4.36	39.63	0.01	19.83	0.01	100.70
57	1500	-10	-4	Matte	Cu-rich Glass	0.61	0.00	0.07	0.10	0.09	24.50	17.21	58.02	100.60
					Fe-rich sulphide	1.57	0.01	0.07	0.06	1.09	32.07	47.60	18.51	100.98
					Spinel	27.88	0.13	0.44	0.07	37.29	2.17	29.93	2.78	100.70
				Slag	Glass	42.74	19.28	8.49	10.93	3.42	0.25	15.29	0.15	100.54
54	1500	-8	-4	Matte	Cu-rich Glass	0.37	0.02	0.06	0.07	0.13	27.24	23.05	50.16	101.09
					Fe-rich sulphide	0.53	0.02	0.14	0.04	0.96	28.58	51.04	20.17	101.48
				Slag	Glass	38.44	16.08	6.42	11.24	3.37	0.35	24.42	0.34	100.66
49	1500	-6	-4	Matte	Cu-rich Glass	0.98	0.00	0.00	0.15	0.00	20.32	0.57	77.65	99.67
					Cu	0.66	0.00	0.00	0.21	0.05	0.20	0.08	97.41	98.61
					Fe-rich sulphide	19.19	0.11	0.00	0.13	0.93	7.36	28.50	44.02	100.24
				Slag	Glass	39.18	15.62	4.26	12.03	0.02	0.05	28.51	1.65	101.31
					Alumina-rich	44.29	2.21	4.25	40.59	0.00	0.13	6.77	1.36	99.61
					Olivine	37.65	6.82	28.86	0.11	5.23	0.03	21.27	0.07	100.06
					Spinel	29.74	0.23	7.25	5.04	38.17	0.01	20.10	0.01	100.55
56	1500	-10	-2	Matte	Cu-rich Glass	0.34	0.00	0.01	0.10	0.07	26.06	16.10	57.82	100.49
					Fe-rich sulphide	1.41	0.01	0.01	0.08	0.86	32.76	59.96	6.19	101.29
					Spinel	26.47	0.13	0.22	0.06	41.02	2.62	28.36	1.44	100.31
				Slag	Glass	40.50	18.19	7.96	10.44	7.36	0.19	14.94	0.06	99.63
					Olivine	42.01	23.17	6.63	11.60	1.21	0.23	14.43	0.01	99.28
53	1500	-8	-2	Matte	Cu-rich Glass	0.45	0.02	0.04	0.08	0.13	25.51	24.73	48.57	99.54
					Fe-rich sulphide	0.31	0.02	0.05	0.04	0.89	30.50	55.88	13.87	101.54
					Spinel	25.47	0.13	1.08	0.04	37.85	1.26	32.95	0.92	99.70
				Slag	Glass	41.08	16.64	5.76	12.99	0.23	0.32	21.28	0.25	98.55
					Alumina-rich	40.17	0.17	9.01	33.21	0.63	0.02	15.51	0.00	98.71
					Spinel	31.25	0.16	4.12	3.89	42.52	0.00	18.41	0.03	100.38
48	1500	-6	-2	Matte	Cu-rich Glass	0.94	0.00	0.00	0.21	0.69	20.06	0.56	76.39	98.84
					Cu	0.70	0.00	0.00	0.23	0.00	0.29	0.09	97.12	98.42
				Slag	Glass	37.11	15.56	5.05	11.91	0.10	0.08	29.68	1.40	100.88
					Alumina-rich	39.83	0.14	7.78	29.82	0.06	0.03	21.77	0.11	99.54
					Olivine	38.12	7.27	28.54	0.13	4.14	0.02	20.96	0.08	99.25

Micrograph 4.1 : Typical Cr Distribution in Matte (1400°C)

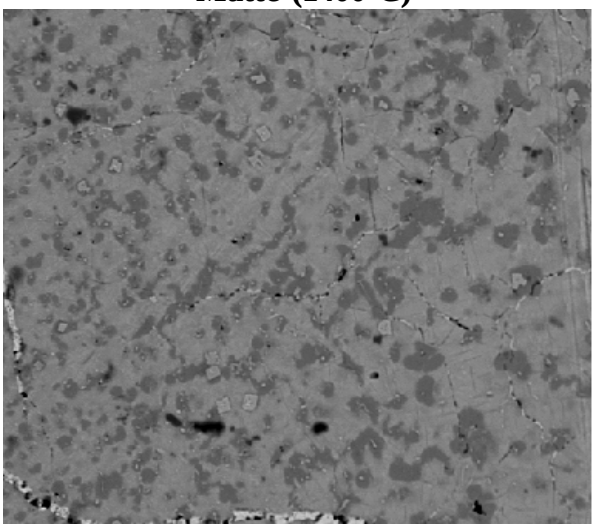

Micrograph 4.2 : Cr Distribution in Micrograph A

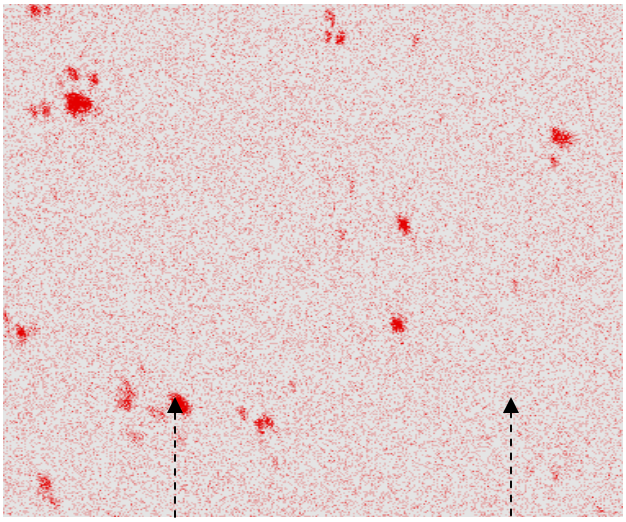

Undissolved Chromium(spinel) *Dissolved Chromium*

Micrograph 4.3 : Superimposition of Micrograph 4.2 on 4.1

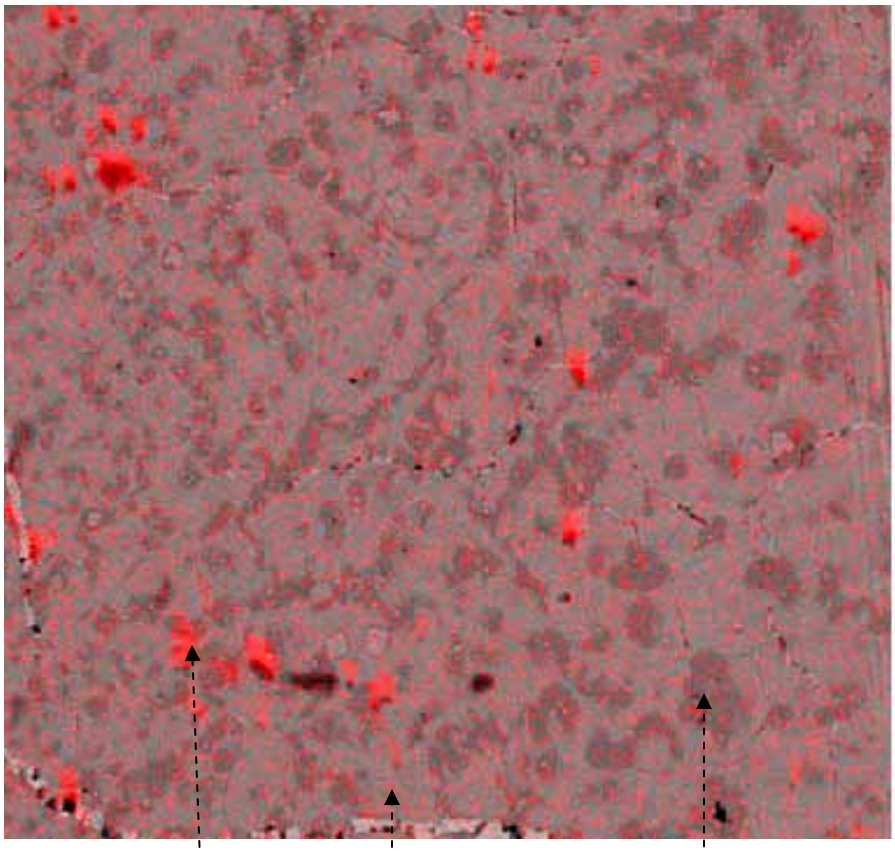

Spinel *Cu-rich Glass* *Fe-rich sulphide*

Micrograph 4.4 : Typical Cr Distribution in Matte (1500°C)

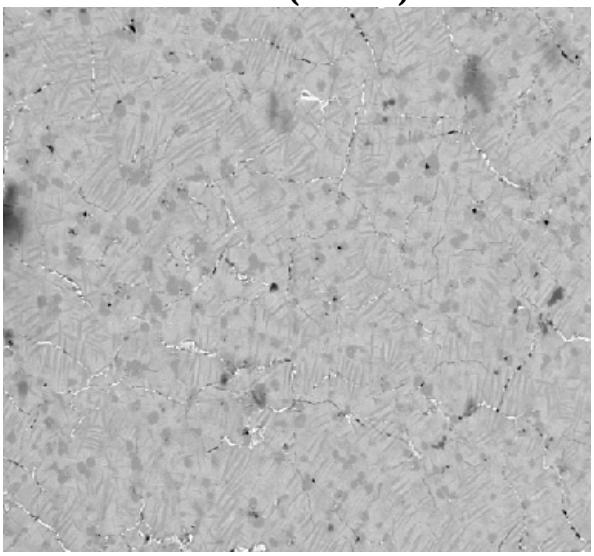

Micrograph 4.5 : Cr Distribution in Micrograph D

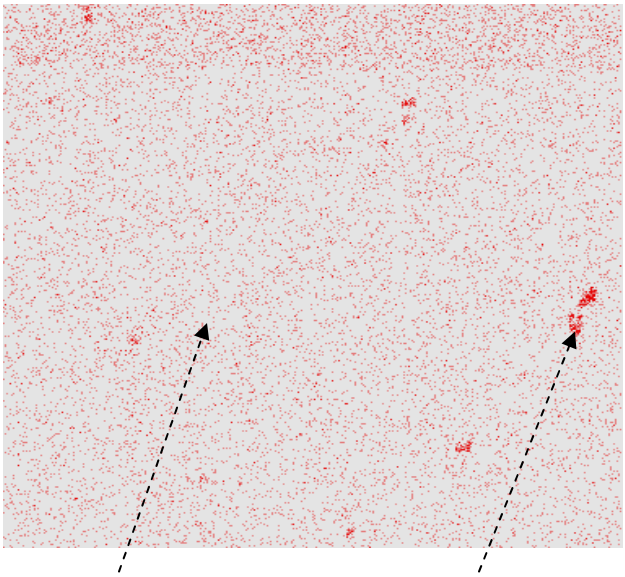

Micrograph 4.6 : Superimposition of Micrograph 4.5 on 4.4

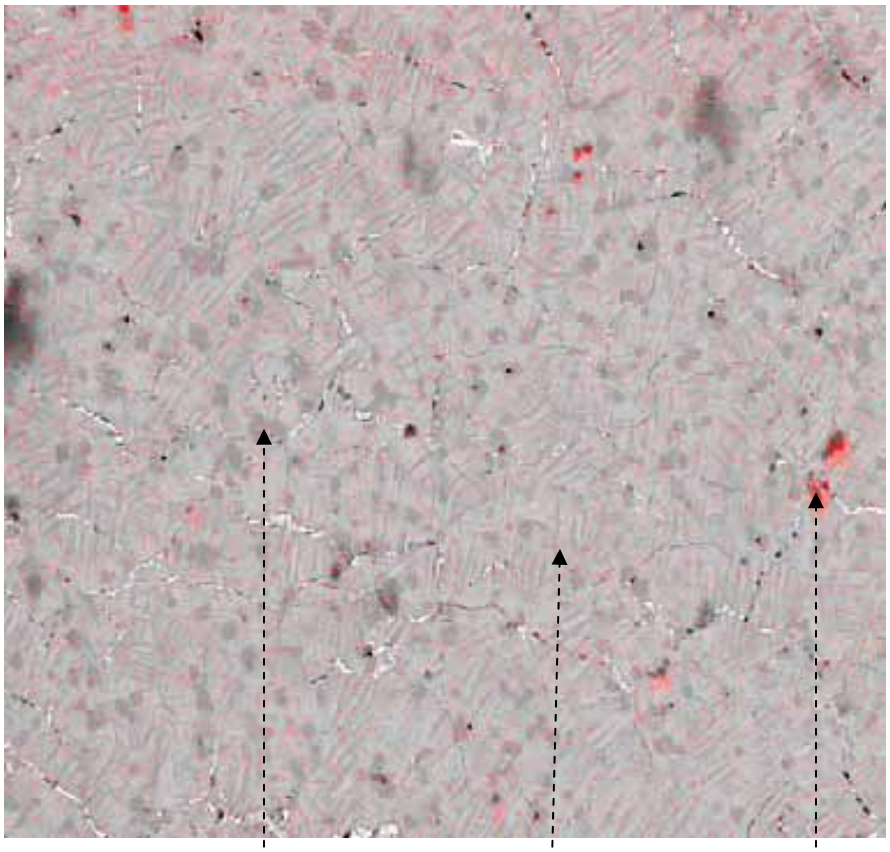

Micrograph 4.7 : **Phase Distribution in a Typical Slag**

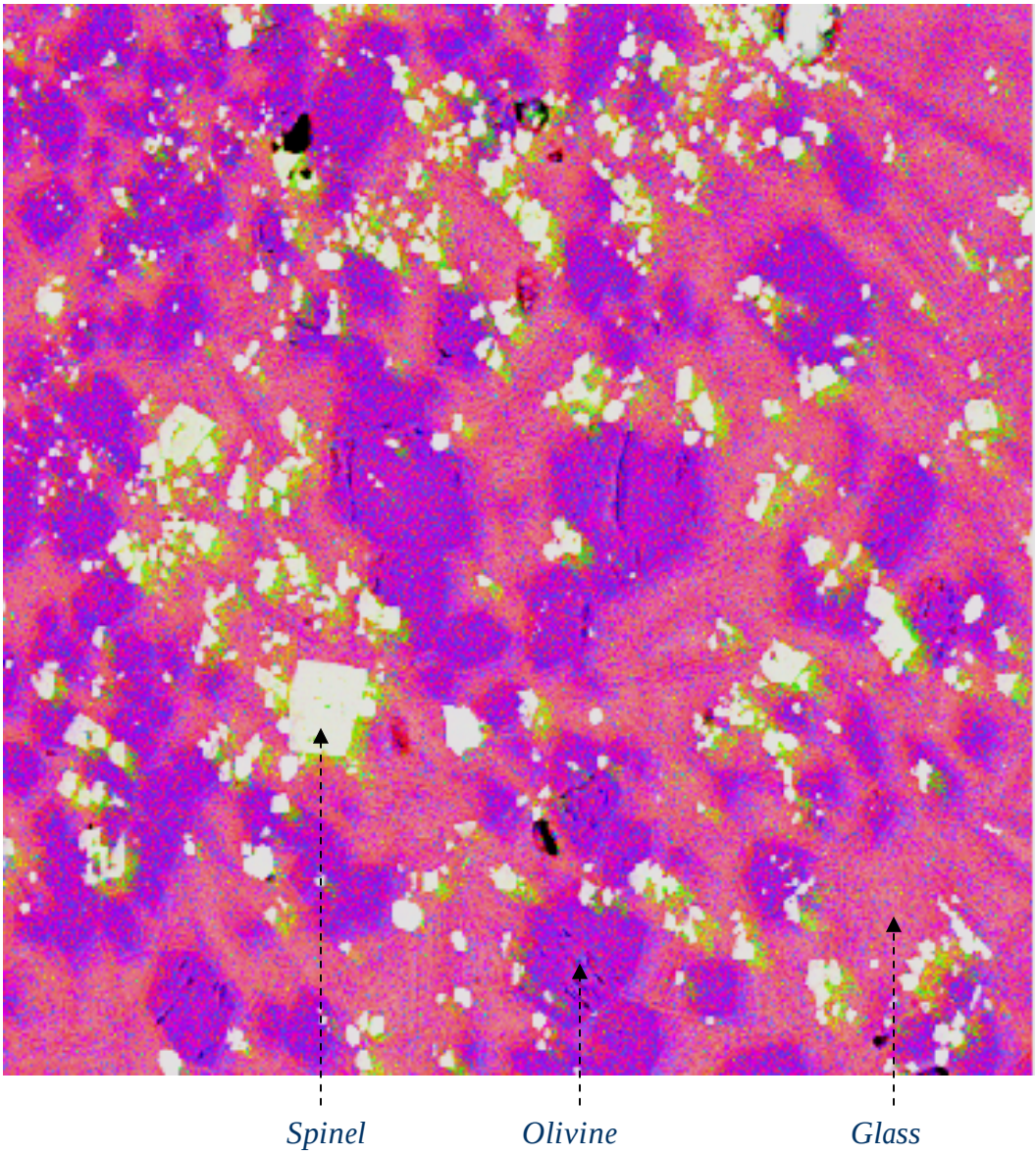

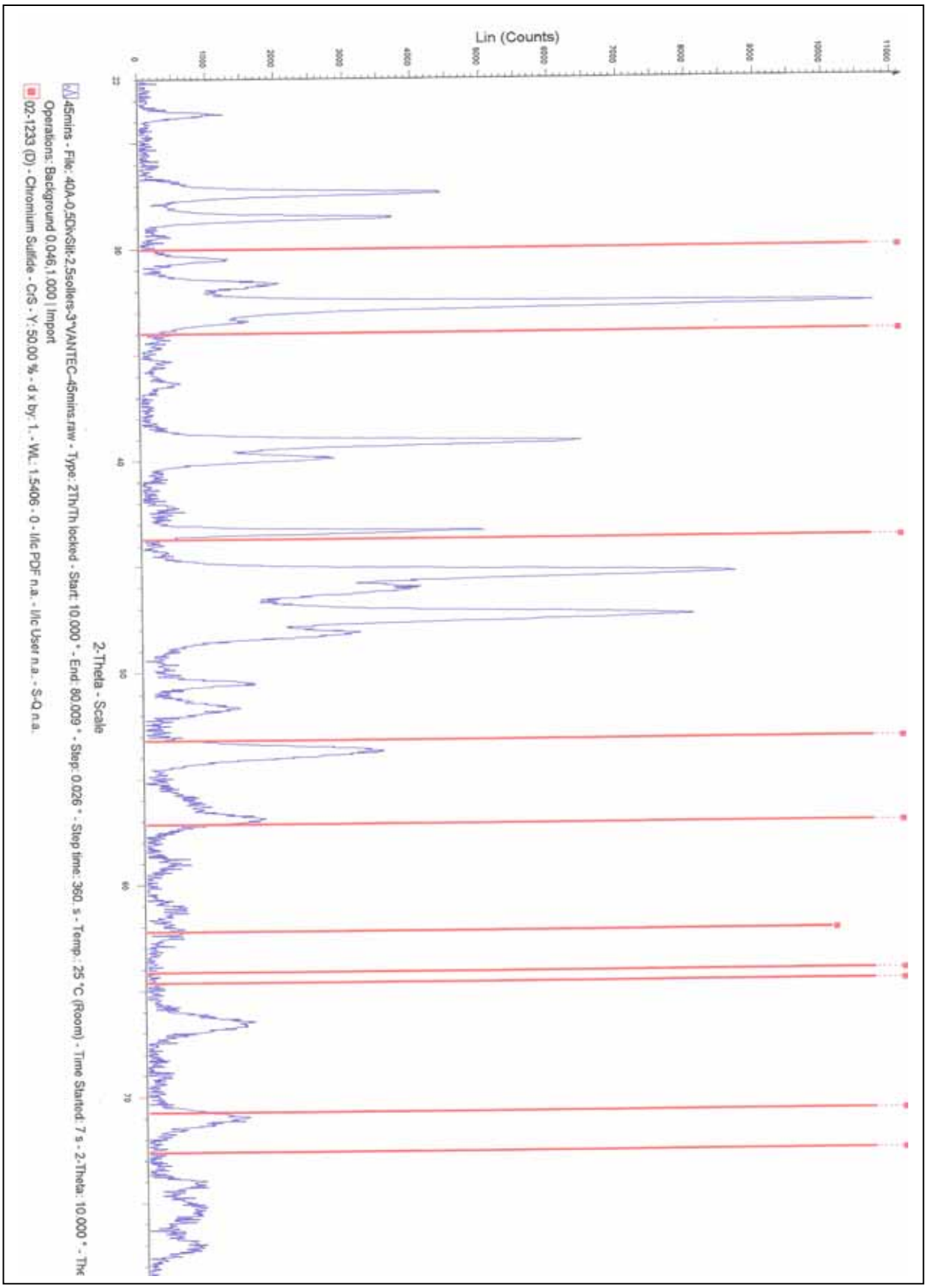

Fig 4.1 : XRD Profile for Chromium Sulphide (CrS) in Matte (Temperature = 1400°C, $pO_2 = 10^{-4}$ atm, $pS_2 = 10^{-4}$ atm)

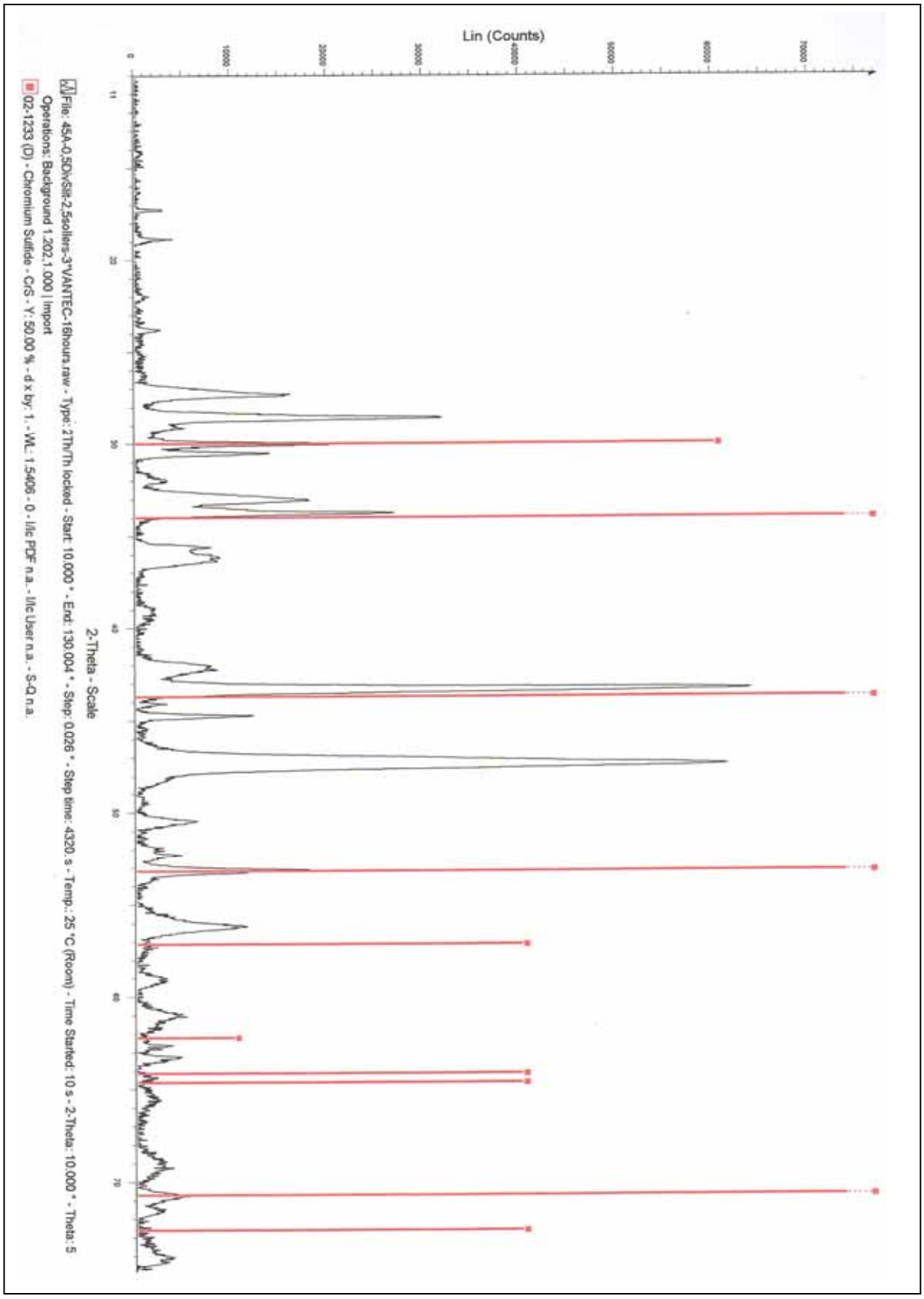

Fig 4.2 : XRD Profile for Chromium Sulphide (CrS) in Matte (Temperature = 1400°C, $pO_2 = 10^{-9}$ atm, $pS_2 = 10^{-4}$ atm)

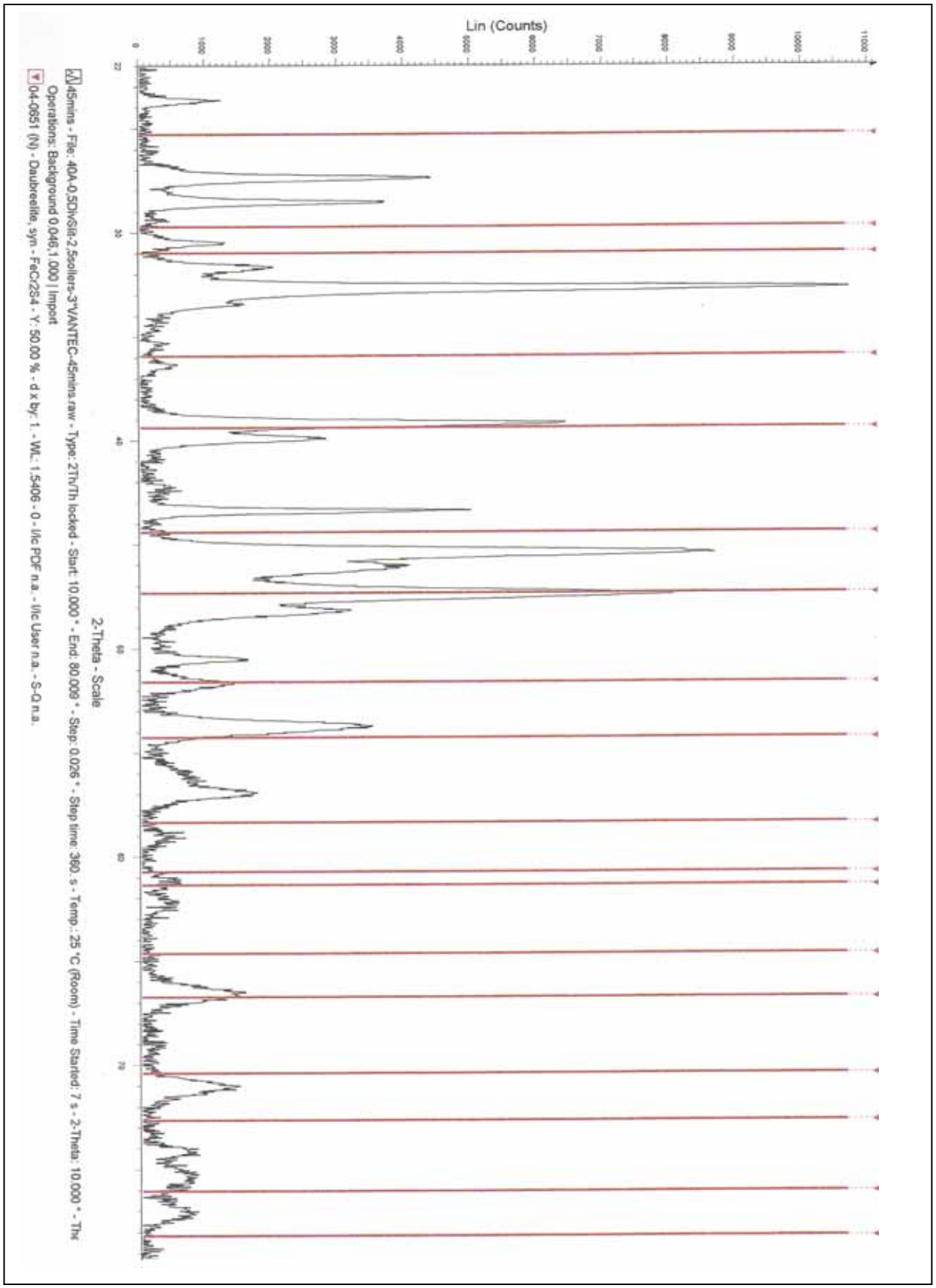

Fig 4.3 : XRD Profile for Daubreelite ($FeCr_2S_4$) in Matte (Temperature = 1400°C, pO_2 = 10^{-4} atm, pS_2 = 10^{-4} atm)

CHAPTER 5

ANALYSIS AND DISCUSSION OF RESULTS

5.1 OVERVIEW OF RESULTS ANALYSIS AND DISCUSSION

The results shown in chapter 4 are analysed and interpreted in this section. As mentioned in section 3.3, the experimental design employed in this work was a completely randomized 3^3 full factorial design, and hence the results generated were analysed within that context using R statistical software version 2.0.1 (Developed by the R Development Core Team, 2004).

The first section discusses the X-ray diffraction results obtained for the drop-quench samples. The XRD analyses were aimed at identifying the predominant phases in the system studied in this work.

The micrographs obtained from the scanning electron microscope for the drop-quench experiments are discussed in the second part.

A number of graphical representations of the data obtained from the three-phase equilibration experiments and the discussion thereof are presented in the third section of this chapter. The purpose of the graphs is to give a visual display of the effect of the experimental variables on chromium distribution in the matte and slag phases; and these include a scatter plot, interaction plots, and conditioning plots of the data.

The fourth part presents a statistical modeling exercise of the experimental data. This includes an analysis of variance, regression analysis, response surface analysis, and a plot of equilibrium contours of chromium partitioning in the slag and matte phases.

The final section of this chapter discusses the diagnostic tests that were conducted on the statistical models which were generated for the data.

5.2 ANALYSIS OF PHASE EQUILIBRIA

In this section, some discussion on the results of the drop-quench experiments is presented. It should be noted that the XRD analyses presented in this work are only indicative of the phases which might be present in the matte, and not necessarily conclusive. However further analytical techniques, such as the Rietveld refinement software (Nell, 2006) would be required to explicitly determine the phases present in the system.

The initial XRD phase analysis of the matte at a local laboratory (in South-Africa) did not yield very good results because only a few peaks were obtained for all the mattes. Subsequent analysis conducted at the Bruker AXS Laboratories in Karlsruhe (Germany) gave satisfactory results, and these have been presented in Figs 4.1-4.3 and Figs D1-D17 (in Appendix D). However, the only setback is that not all samples could be analysed. The few that were analysed will be discussed and observations made will be compared to the SEM results (phase chemistry and micrographs) for the other samples which were not analysed by XRD. Based on this comparison, the phases in the samples which were not analysed by XRD will then be predicted. A recommendation with regards to the adequacy of this predictive technique for the phases has been presented in chapter 6.

In the following discussion, a "matching" peak for a phase under investigation implies that the confidence level of the presence of that phase is relatively high. However, one can conclusively decipher the presence of a given phase if a number of matching peaks are obtained – a generally accepted number being at least three (Bucher, 2005).

The main focus of the XRD analysis was on phase identification in the matte. Bartie (2004) has studied in detail the phase equilibria in similar slag systems containing chromium as a component. The main phases identified in the matte are shown in Table 5.1, which also gives a summary of the observations made in the matte samples that were analysed. The main phases identified, as can be seen in Table 5.1 are bornite, chromium sulphides, daubreelite, and spinel

Table 5.1 : XRD results for mattes

Compound		**Lattice**	**Matte No.**	**2θ value at Matching Peaks**	**Decision– Presence?**	**Reference**
Bornite	$FeCu_5S_4$	Face Centred Cubic	40	27.3°, 32.7°, 36.2°, 47.2°	Yes	Fig D1
			45	27.2°, 36.2°, 47.2°, 65.8°	Yes	Fig D2
			57	22.0°, 27.2°, 47.2°	Yes	Fig D3
Chromium Sulphides	CrS	Hexagonal	40	No matching peaks	No	Fig 4.1
			45	30.0°, 53.1°, 70.7°	Yes	Fig 4.2
	Cr_2S_3	Rhombohedral	40	No matching peaks	No	Fig D4
			45	44.8°	No	Fig D5
			57	44.8°	No	Fig D6
	Cr_3S_4 (Brezinaite)	Monoclinic	40	27.2°	No	Fig D7
			45	27.2°, 30.0°, 44.4°	Possibly	Fig D8
			57	27.2°, 30.0°, 44.8°, 71.2°	Possibly	Fig D9
	Cr_5S_6	Hexagonal	40	57.0°, 58.8°, 70.9°	Possibly	Fig D10
			45	18.9°, 33.8°	*MIR	Fig D11
			57	18.9°, 33.8°	*MIR	Fig D12
	Cr_7S_8	Hexagonal	40	56.9°	No	Fig D13
			45	33.8°, 70.7°	*MIR	Fig D14
			57	33.8°, 70.7°	*MIR	Fig D15
Daubreelite	$FeCr_2S_4$	Face Centred Cubic	40	44.2°, 47.3°, 51.5°	Yes	Fig 4.3
			45	47.3°	No	Fig D16
			57	47.3°	No	Fig D17

Spinel	Mg(Cr, Fe,Al)$_2O_4$	Face Centred Cubic	40	36.5°, 77.1°, (ferrian); 30.5°, 43.5°,47.5°, 53.9° (Mg_2CrO_4)	Yes	Fig D18
			45	18.9°, 64.2°, (ferrian); 35.8°, 47.5° (Mg_2CrO_4)	*MIR	Fig D19
			57	35.8°, 43.5°, 47.5° (Mg_2CrO_4)	Yes	Fig D20

*MIR – More Information required

Table 5.2 : Experimental conditions for the mattes shown in Table 5.1

Matte No.	40	45	57
Temperature (°C)	1400	1400	1500
pO_2 (atm)	10^{-6}	10^{-10}	10^{-10}
pS_2 (atm)	10^{-4}	10^{-4}	10^{-4}

The matte number is the sample number which is similar to the "run number" in Table 4.3, which gives the experimental conditions under which these mattes were generated. However, these experimental conditions have been extrapolated from Table 4.3 and summarized in Table 5.2. The "reference" column in Table 5.1 refers to the figure showing the XRD spectrum of the phase in question. For example, the XRD spectrum for bornite in matte number 40 is shown in Fig D1 in Appendix D (as shown in the "reference" column of Table 5.1). Matte 40 was analysed for 45minutes using a stepsize of 0.026° and steptime of 360 seconds, whereas the run time for matte 45 was 16 hours with a stepsize of 0.026° and steptime 4320 seconds. Similar parameters for matte 57 were 9.4 hours for the run time, with a stepsize and steptime of 0.026° and 4320 seconds respectively.

In essence, Table 5.1 collates the relevant information from all the spectra of the mattes analysed by XRD which are presented in Appendix D. Of major interest is the number of matching peaks, whose 2θ values are shown in Table 5.1. Based on the number of matching peaks obtained, a decision was then made to predict the

presence or absence of a given phase, and this is also shown in Table 5.1 under the column "Decision-Presence?".

For some of the phases, their presence was an outright "Yes" (implying that they were present), or "No" (implying their absence). However, for some, whose decision was "MIR" (more information required), about two matching peaks were obtained. An examination of these "MIR" cases would generally seem to indicate that with longer scanning times focused at specific 2θ regions, more information could still be obtained to conclusively decipher the presence or absence of the phase in question. For some of the phases, the decision made about their presence was "Possibly", these being cases in which the phases in question were identified by XRD. However, an examination of the phase diagrams of these "Possibly" cases often seemed to raise questions about whether they were actually present at the equilibrium high temperature, or could have been a result of exsolution due to possible inefficient cooling. More information will be given under the discussion of each of the concerned phases.

The following passages give a brief discussion of the phases shown in table 5.1

5.2.1 Bornite

Excellent peaks were obtained for the face-centred cubic bornite structure, as can be seen in Table 5.1. The presence of bornite was highly evident in all the mattes analysed as shown in Table 5.1. This is in agreement with the phase diagram shown in Fig 5.1

5.2.2 Chromium Sulphide (CrS)

Matte 40 did not give any matching peaks whereas matte 45 gave three excellent matching peaks for CrS, as shown in Table 5.1. This shows that CrS was present at

lower oxygen partial pressures of 10^{-10}atm, and absent at higher oxygen partial pressure of 10^{-6}atm. This observation will be collated with, and further discussed in the light of, the ICP results plotted in section 5.5.2

5.2.3 Other Cr-S_x compounds

The discussion in this subsection focuses on the other Cr-S_x compounds, except CrS. Before a discussion of the XRD spectra that were obtained for these other Cr-S_x compounds, a brief background of their presence in matte is presented briefly.

As has been mentioned in section 2.6.2, several intermediate compounds exist between the compositions CrS and Cr_2S_3. These are CrS, Cr_7S_8, Cr_5S_6, Cr_3S_4, and at least two modifications of Cr_2S_3 (trigonal and rhombohedral) (Jellinek, 1957). These compounds are shown in the Cr-S phase diagram in Fig 2.7. This diagram suggests that these intermediate CrS_x compounds form as exsolution compounds, particularly at temperatures below 1300°C. The concept of exsolution has been discussed extensively by Bret (1964). This means that an identification of the intermediate CrS_x compounds by XRD could possibly indicate that the quenching of these samples was not fast enough, hence their exsolution from the matte system.

Figs D7-D9 show the XRD spectra obtained for brezinaite (Cr_3S_4) for mattes 40, 45 and 57 respectively. Matte 40 (shown in Fig D7) gave only one closely matching peak at 27.2°, indicating that brezinaite was not present in the matte quenched from 1400°C at a pO_2 of 10^{-6}atm. Matte 45 (shown in Fig D8) gave three excellent matching peaks at 2θ values of 27.2°, 30.0°, and 44.4°, as outlined in Table 5.1, while the 57.0° – 67.0° region shows that more information could be obtained with longer scan times in this range. This strongly suggests the possible presence of a brezinaite structure in the matte under a more reducing environment relative to matte 40. Matte 57 gave a profile which is almost similar to that of matte 45, with the strongest peaks at 2θ values of 27.2°, 30.0°, 44.8°, and 71.2°. This suggests the presence of brezinaite in matte, subject to the conditions under which matte 57 was generated (Table 5.2). The presence of brezinaite was noted for a pO_2 of 10^{-10}atm, at both temperatures of 1400°C and 1500°C. This may seem to suggest that if it is

assumed that brezinaite is not formed by exsolution, then the effect of oxygen partial pressure is stronger than the effect of temperature (in the temperature region 1400˚C-1500˚C) in determining the presence of brezinaite in matte, subject to the experimental conditions applied in this research.

One of the intermediate CrS_x compounds is Cr_2S_3, whose XRD profiles for mattes 40, 45, and 57 are shown in Figs D4-D6, respectively (Appendix D). Matte 40 did not give any matching peaks, as shown in Fig D4, implying the absence of Cr_2S_3 in this matte sample. Matte 45 showed only one matching peak at 44.8˚ 2θ, with matte 57 showing a similar profile, as shown in Figs D5 and D6. From these observations, it can be seen that the Cr_2S_3 structure was not evident in the mattes investigated.

The spectra shown in Figs D10-D12 were obtained by testing for the presence of the hexagonal Cr_5S_6 in matte. Matte 40, as shown in Fig D10, gave three strong peaks at 57.0˚, 58.8˚ and 71.0˚ 2θ, suggesting the possibility of Cr_5S_6 in this matte. An examination of the region $61.0^\circ<2\theta<63.0^\circ$ seems to suggest that further evidence pointing to the possible presence of Cr_5S_6 in this matte could be obtained with longer scan times in this region. Matte 45 (shown in Fig D11) gave only one matching peak at 33.7˚ 2θ, indicating the absence of Cr_5S_6 in this matte. Two good peaks were obtained for matte 57 at 18.8˚ and 33.8˚ (Fig D12), making it difficult to conclusively predict the presence on Cr_5S_6 in this matte.

The presence of Cr_7S_8 in matte was also investigated and the spectra obtained are shown in Figs D13-D15. Matte 40 gave only one matching peak at 56.9° 2θ, indicating the absence of this CrS_x species in matte quenched at 1400°C with pO_2 of 10^{-10}atm and pS_2 of 10^{-6} and pS_2 of 10^{-4}atm. Comparatively, two peaks were obtained for matte 45 (Fig D14), thereby suggesting that the presence of Cr_7S_8 could not be conclusively predicted in this matte. Similarly, matte 57 also gave two matching peaks at 33.8˚ and 70.8˚ 2θ, resulting in the same conclusion as that for the presence of Cr_6S_7 in matte 45.

5.2.4 Daubreelite

At higher oxygen partial pressure, daubreelite seems to be the more predominant phase instead. As can be seen from Table 5.1, daubreelite was more dominant in matte 40 ($pO_2 = 10^{-6}$ atm, $pS_2 = 10^{-4}$atm, temperature = 1400°C), and was absent in the other mattes analysed. This shows that as the conditions become more oxidizing, the "dissolved" chromium (in the form of CrS) forms a Cr-Fe-S spinel called daubreelite.

5.2.5 Spinel

As can be seen in Fig D18-D20 in Appendix D, spinel was analysed in two forms ; ferrian [$Mg(Al,Fe)_2O_4$ and Mg-Cr spinel ($MgCr_2O_4$). This was primarily because these are the only spinels for which the XRD machine had standards. Matte 40 gave two matching peaks for ferrian (2θ of 36.5°, 77.1°) and four matching peaks for Mg-Cr spinel (2θ of 30.5°, 43.5°,47.5°, 53.9°). In Table 5.1, these peaks are lumped together as for one compound, and the conclusion is that spinel is definitely present in the matte generated at 1400°C at pO_2 of 10^{-6}atm and pS_2 of 10^{-4}atm.

Matte 45 gave two matching peaks at 18.9° and 64.2°. Similarly, two matching peaks were obtained for $MgCr_2O_4$ at 35.8° and 47.5°. This suggests that spinel was either absent completely, or that it could have been present in very low quantities., hence the "MIR" decision about its possible presence in this matte (45). However, relative to matte 40, this observation in matte 45 seems to suggests that the presence in matte is more explicitly pronounced under an oxidising atmosphere, all the other conditions being maintained equal.

Matte 57 gave three matching peaks for $MgCr_2O_4$, suggesting that spinel was present under the conditions at which this matte was generated (see Table 5.2)

These observations generally confirm that the spinel-shaped phases present in some of the mattes in Appendix C were indeed spinel.

5.3 DROP-QUENCH EXPERIMENTS

The XRD analyses in section 5.2 were to identify the phases in the drop-quench samples. Some of the phases were identified with a significantly high confidence level, for example, bornite (Cu_5FeS_4). The identification of some of the phases was not completely explicit, as they gave a few matching peaks and some which were not that explicit. Hence, for the purposes of this discussion, the major phases observed in the matte will be referred to as Fe-rich or Cu-rich sulphide phases as shown in the micrographs in Appendix C. These micrographs will simply be referred to by the Micrograph number, which is on the top-left corner of each micrograph. The number on the top right of each micrograph refers to the experimental run number. Therefore, to find out the conditions under which each sample was run, the run number on the top right is referenced to Table 4.3. For a more detailed analysis of the phases, the run number can be referenced to Appendix B.

5.3.1 Drop-Quench Samples at 1300°C

These are shown in micrographs 1-18 in Appendix C.

5.3.1.1 Matte Samples at 1300°C

An analysis of the matte micrographs at this temperature show that there were some samples which represented a complete liquid solubility at this temperature and were observed as homogeneous phases. This is typical of the mattes in

micrographs 1 and 11, for runs number 34 and 28, respectively (refer to table 4.3 for the gas environment under which they were run). The chromium content for these mattes is very low, being 0.09 and 0.11wt% respectively. Because these are predominantly copper, iron, and sulphur, use can be made of the Cu-Fe-S phases diagram in the pseudo-binary phase diagram shown below in Fig 5.1;

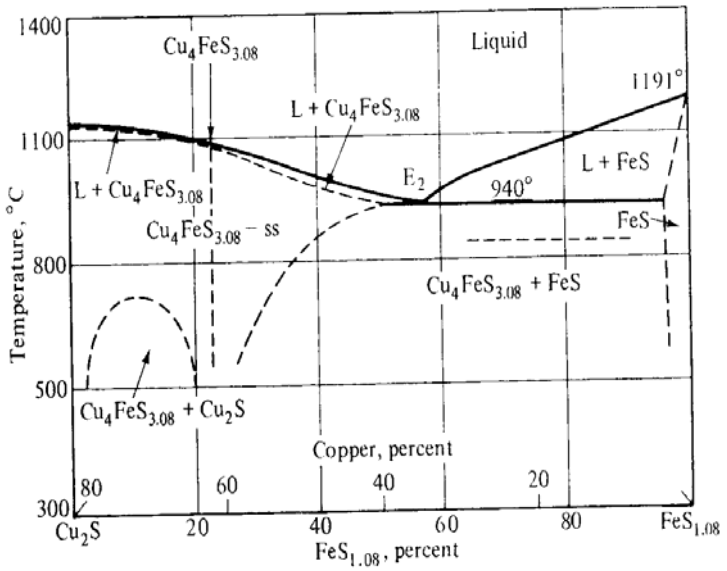

Fig 5.1 : Binary Cu_2S-$FeS_{1.08}$ System
(after Rosenqvist, 1974)

At the temperature of interest, the predominant liquid phase is rich in copper with a bornite matrix, as shown in Fig 5.1.

The rest of the mattes contained basically the Cu-rich sulphide liquid phase with a primary Fe-rich sulphide. Generally chromium contents of the Fe-rich sulphides were significantly higher than that of the Cu-rich sulphide phases. This is in line with the complete miscibility of iron and chromium and their respective sulphides depicted in the phase diagrams in Figs 2.6 and 2.8 in the temperature and composition range of interest.

5.3.1.2 Slag Samples at 1300°C

Generally these showed 3 main phases: olivine, glass and spinel. This is in agreement with the findings of Bartie *et al.* (2004). This was the general trend except for a few slags, such as the one shown in micrograph 16, which gave a glass structure and was run at a pO_2 of 10^{-8}atm and a high pS_2 of 10^{-2}atm. The spinels were generally Chrome-spinels with Cr contents of up to 41% (as in micrographs 14 and 18). Generally, more chromium reported to the olivine than to the glass phase. This is also in agreement with the findings of Bartie *et al.* (2004).

5.3.2 Drop-Quench Samples at 1400°C

These are shown in micrographs 19-36 in Appendix C.

5.3.2.1 Matte Samples at 1400°C

All the mattes at this temperature showed at least two phases, the general ones being Cu-rich liquid and Fe-rich sulphides. As in the 1300°C mattes, chromium distribution in the Fe-rich sulphide phases was higher in all cases than in the Cu-rich sulphide phases. The same explanation of complete liquid solubility between the two applies in this case as well. The presence of the primary Fe-rich phase may be viewed in the light of the Cr-Fe-S diagram in Fig 2.8.

A notable feature of these mattes is the presence of chromium spinels in some. This was particularly evident in micrographs 19, 31, and 35, where the spinel can be identified as angular particles of small size (< 10μm) embedded in the Fe-rich sulphide. An inspection of the gas conditions under which they were run shows it was an oxidizing environment in all cases. This seems to suggest that the presence of spinel occurs when furnace conditions are more oxidizing with regard to the conditions investigated in this work.

5.3.2.2 Slag Samples at 1400˚C

As for the 1300˚C slags, the slags at this temperature also generally consisted of three phases, chromium-rich spinels, olivine, and the glass phase, as observed by Bartie *et al*. (2004). However, there were more slags at this temperature with dominant glass proportions than at 1300˚C. These are shown in micrographs 20, 26, 32, and 36. This is to be expected as quenching was done at a higher temperature.

5.3.3 Drop-Quench Samples at 1500˚C

These are shown in micrographs 37-54 in Appendix C.

5.3.3.1 Matte Samples at 1500˚C

These also generally consisted of Cu-rich liquid with Fe-rich primary, though in some cases a copper primary phase was observed, as in micrographs 47 and 53. The same trend for the distribution of chromium in the Fe-rich sulphide phase relative to the Cu-rich sulphide phase applies as for 1300˚C and 1400˚C mattes.

Spinel presence in the matte was noted for the mattes in micrographs 43, 49, and 51, representing mattes from samples 57, 56, and 53 respectively, as shown in Appendix C. All these mattes were generated at oxygen partial pressures of 10^{-6} and 10^{-8}atm. No spinels were identified in the mattes generated at oxygen partial pressures of 10^{-10}atm, this being in agreement with the observations made for the mattes generated at 1400˚C.

5.3.3.2 Slag Samples at 1500˚C

The same scenario as the one for the slags in 1400˚C applies, except that the number of slag samples with glass phases was higher than for the 1300˚C and 1400˚C.

The spinel phases present were not as distinct in terms of crystal shape as those in 1300˚C and 1400˚C slags.

5.4 Presence of Dissolved and "Undissolved" Chromium in Matte

This section seeks to integrate the observations noted with the concepts that have been developed in sections 5.2 and 5.3.

It was seen from the XRD analyses that some of the Cr-S_x compounds were present in their different forms. Elemental maps of chromium in matte were generated using SEM/EDS in order investigate the distribution profiles of chromium across the matte matrix. In this case, all the chromium-bearing points were shaded pink. It can be seen from the phase maps in Micrographs 4.2 and 4.5 that chromium was present not only as spinel (the "undissolved" phase), but also as dissolved chromium, as depicted by the finely disseminated phase tinted in pink colour. Micrograph 4.2 is a chromium map for the matte in micrograph 4.1. Micrograph 4.3 is simply a superimposition of micrograph 4.2 onto 4.1. It is suggested that the spinels noted in the phase maps are in two forms, these being: a chromium-sulphidic spinel such as daubreelite ($FeCr_2S_4$) (for the more oxidizing conditions), or possibly Cr_3S_4 (under more reducing conditions (refer to section 5.2)); and also that some of the spinel is oxidic in nature [$Mg(Cr,Fe,Al)_2O_4$].

The presence of chromium-sulphur spinels was highly evident in some of the mattes, as discussed in section 5.2. It was noted in section 3.5 that the SEM analyses were conducted on at least three random points of a detected phase and a mean for each phase calculated in the table shown in Appendix B. This implies that there are chances that some of the phases identified as a spinel could have been missed out in the analysis. For example, micrograph 4.2 contains more than ten spinel points. If only three were identified, as was the case in these analyses, it means that a number of other "undissolved" similar phases would be missed out, especially given that the spinels in the mattes did not, in some cases, have the distinctive "spinel shape and appearance" as the ones in slags (compare with spinels in micrograph 4.7 or micrograph 31 in Appendix C).

In view of the above-mentioned observations, it is suggested that chromium oxidic spinels are present in matte as a result of either chemical reaction or physical entrainment in matte. The assumption that spinel presence could be due to a chemical reaction could be further advanced by the observations made for the drop-quench experiments in section 5.3. It was noted in section 5.4 that these oxidic spinels were generally present in mattes generated under the more oxidizing conditions of this research ($pO_2 = 10^{-6}$atm). As for the chromium sulphidic spinels, it is suggested that they could have been a result of exsolution (refer to Bret (1964), for a detailed discussion of exsolution) thereby implying inefficient cooling of the drop-quench samples, or they could have been present in the high temperature systems. The premise of sulphidic spinel presence in matte at high temperature is more substantial for daubreelite, as can be seen from the phase diagram in Fig 2.9, which shows that daubreelite is stable at high temperatures, such as those employed in this work.

Micrograph 4.5 is also a chromium map of the matte in micrograph 4.4, and micrograph 4.6 is a superimposition of the two. A close comparison of the two shows that there is a greater amount of chromium spinels for the low temperature

matte than for the higher temperature one. These two mattes were subjected to similar gas partial pressures, the only difference being temperature. The matte in Micrograph 4.2 was generated at 1400˚C, whereas the matte in Micrograph 4.5 was generated at 1500˚C. This shows that at equal gas partial pressures, there is more chromium present as spinel at lower temperature than at higher temperature.

These findings are in agreement with the work done by McKenzie and Nell (1994), who found that spinel crystals were present in all their experiments. However, this comparison should be made while bearing in mind that their work was conducted in an inert atmosphere at 1500˚C.

5.5 EQUILIBRATION EXPERIMENTS

This section discusses the results obtained for the equilibration experiments. It is important to re-emphasise that the drop quench experiments and these equilibration experiments should not be viewed as disjointed. This is because the aim of the equilibration experiments was to study the behaviour distribution characteristics of chromium in the bulk phases, i.e., matte and slag phases. On the other hand, the drop quench experiments were performed under identical conditions as the equilibration experiments, the primary aim being to study the phase equilibria of chromium distribution in the sub-phases of the matte and slag phases. Examples of the sub-phases of slag include spinel and olivine; while those of matte include bornite, daubreelite and CrS_x compounds. Hence these two sets of experiments should be rightly treated as complementary of each other.

The equilibration experiments formed the quantitative part of the experiments, where chromium partition coefficients were determined. The effect of the

experimental variables (temperature, pO_2, and pS_2) on the partitioning of chromium between slag and matte is assessed.

The first part of this section gives the scatter plot of chromium partition coefficients as a function of temperature and oxygen and sulphur partial pressures, followed by an assessment of interaction effects of these variables on chromium partitioning. The effect of these variables on the response variable (chromium partitioning) is then explored using conditioning plots.

The partitioning of chromium is then statistically modeled as a function of the experimental variables in the second part of this section. A response surface analysis is presented together with the contour plots of chromium distribution. The model validation techniques applied to the statistical model are also outlined.

The last part gives the results of a post-experimental system modeling exercise performed with Factsage Thermochemical Software version 5.3.1 (developed by Bale *et al.*, 2002).

5.5.1 Scatter Plot of Experimental Variables

A scatter plot for the chromium partitioning data was generated in order to visualise the relationships between the variables (Fig 5.2). In this discussion, reference to the panels is made by column and row, as is the convention on graph coordinates. Thus the lower left panel is (1,1), and the one to its right is (2,1). Panel (2,4) is a plot of Chromium partition coefficients (as defined by Equation 1.1) against the inverse of temperature (Temp.Inverse, which is the same as $\left(\frac{1}{T}\right)$). The general trend is an increase of the partitioning coefficient with an increase in Temp.Inverse (i.e., CPC is increasing with a decrease in temperature), implying that chromium partitions to the matte more strongly at higher temperatures. Panel

(3,4) gives a plot of the partition coefficient as a function of pS_2. The trend indicates a decrease of partition coefficients with an increase in pS_2. The plot of the response variable with pO_2 shown in panel (4,4) shows an increase of the partition coefficient with an increase in pO_2. These trends and their implications will be discussed further in section 5.5.2.

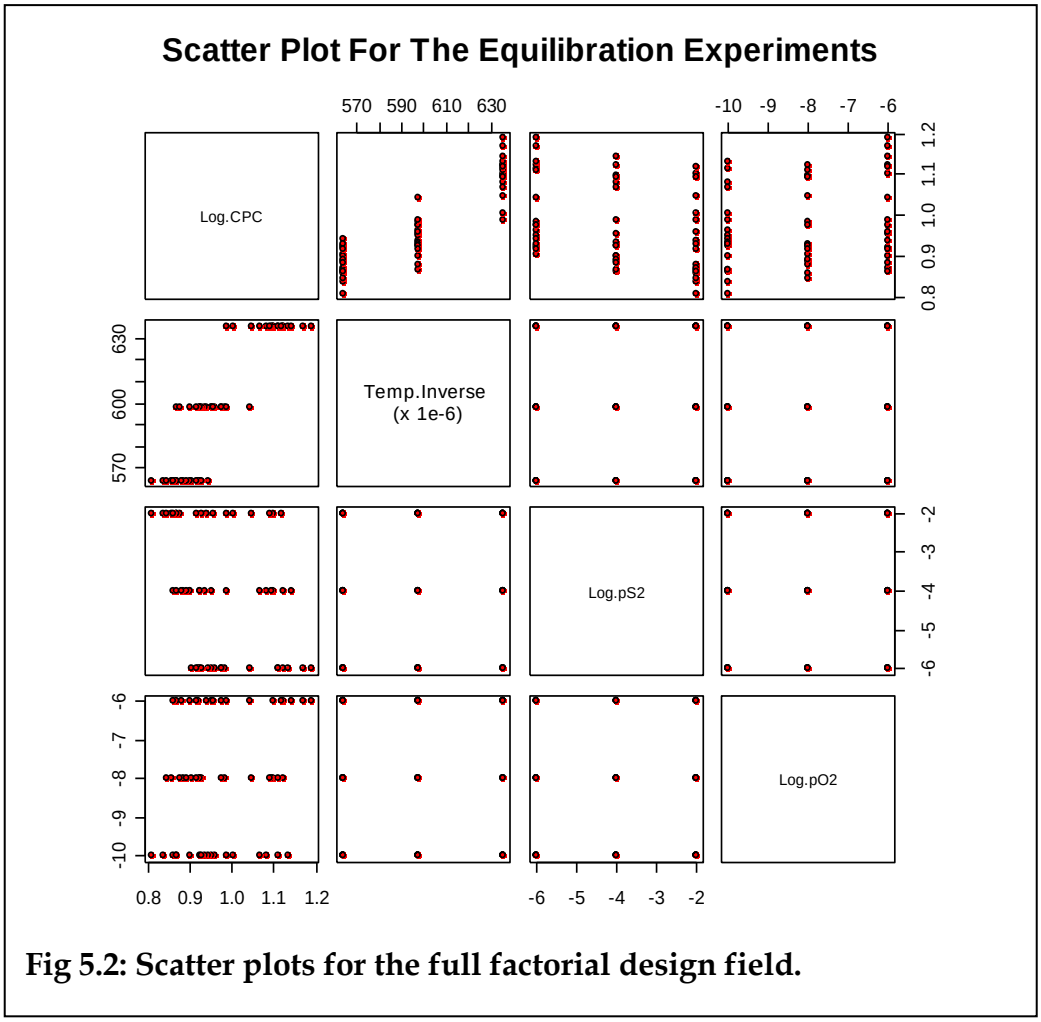

Fig 5.2: Scatter plots for the full factorial design field.

This representation of data as a scatter plot is useful in giving a "rough idea" of the relationships between the variables at a glance. Much information can then be obtained by plotting the distribution of chromium as a function of any one of the factors at the different levels of the other two factors. This representation is shown below in the form of conditioning plots.

5.5.2 Coplots of Experimental Factors

A Conditioning plot, or coplot, is a graphical method which shows how a response depends on a factor given different levels of the other factors (Chambers and Hastie, 1993). This plotting technique was adopted because it is a suitable representation of data generated within a factorial experimental design framework. The technique enables one to easily visulalise the general trends in the variation of one parameter against the other two (simultaneously), and to identify the conditions for minimum and maximum deportment of chromium in slag and matte.

5.5.2.1 Chromium Distribution vs pO_2 given $(Temperature)^{-1}$ and pS_2

The dependence panels are the 3 x 3 array of square panels and one "given panel" is on top and the other at the right hand side of the plot.

Chromium Partition coefficient is plotted against pO_2 in Fig 5.3 for those observations whose values of pS_2 and temperature lie in an interval. The intervals are shown on the "given" panels.

The panels will be referred to by column and row, numbering as we would on a graph; thus the lower left panel is (1,1), and the one to the right of it is (2,1). The co-ordinates of the end-panels have been labelled as an aid to the interpretation of this nomenclature.

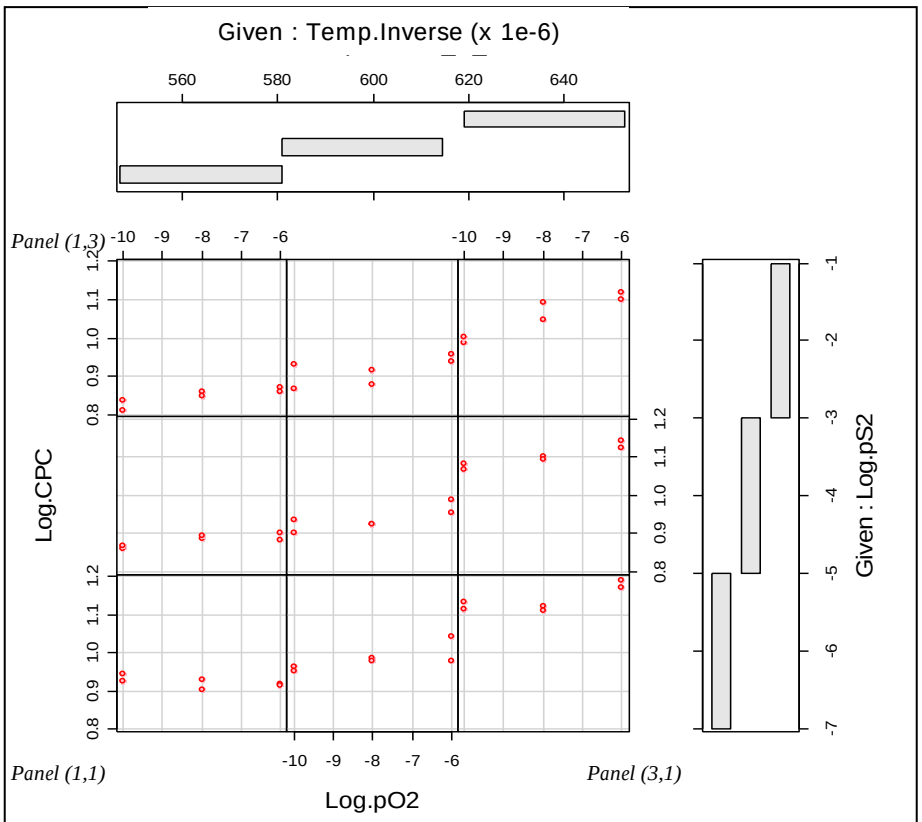

Fig 5.3 : Coplot of CPC vs pO_2 given (Temperature)$^{-1}$ and pS_2

It can be seen from Fig 5.3 that the general trend is that CPC increases with an increase in pO_2. According to the definition of CPC in Eq 1.1, this means that as conditions become more oxidising, more chromium tends to deport to the slag and less to the matte. Conversely, as conditions become more reducing, more chromium tends to partition to the matte and less to the slag. In other words, the trends obtained suggest that CPC (as defined by Eq. 1.1) is directly proportional to pO_2.

From Fig 5.3, it can also be noted that chromium tends to partition the least into the slag phase (i.e. when CPC is at its minimum) under the conditions of high temperature (1500˚C (i.e., $\frac{1}{T}$ = 564.016x10^{-6}K^{-1}), low pO_2 (10^{-10}atm), and high pS_2 (10^{-2}atm) as compared to the other factor combinations. This is represented by panel (1,3). Under these conditions (panel (1,3)), chromium tends to partition the most to the matte phase, which is an undesirable scenario for base metal smelters.

Referring back to the definition of Chromium Partition Coefficient (CPC) in Eq 1.1, the ideal situation for base metal smelters would be to maximise CPC. This implies maximising chromium partitioning to the slag and minimising its partitioning to the matte. The conditions which fit this requirement are depicted in the plot in panel (3,1) of Fig 5.3. This represents conditions of low temperature (1300˚C, or $\frac{1}{T}$ = 635.728x10^{-6}K^{-1}), high pO_2 (10^{-6}atm), and low pS_2 (10^{-6}atm).

The requirement for high partial pressure of oxygen atmosphere as a precursor to achieving minimal chromium partitioning to the matte has been reported by De Villiers and Kleyenstüber (1993), as mentioned in section 2.3.2. Even though in their work the sulphur partial pressure was not strictly controlled, they noted that chromium in sulphide melts increases with a decrease in pO_2, and their results are a useful benchmark to these experimental observations, as they are consistent with the trends in Fig 5.3.

Even though a high oxygen partial pressure is one of the conditions that facilitate low chromium partitioning to the matte, care should be taken to avoid conditions which promote excessive chrome-spinel formation in the slag fraction. It was observed in the micrographs discussed in section 5.2 that chrome-spinel formation in slag was more prevalent at high oxygen partial pressures. The formation of spinel in slags is a scenario which is undesirable in smelting furnaces due to its deleterious effects as detailed in chapter 1.

5.5.2.2 Chromium Distribution vs pS_2 given (Temperature)$^{-1}$ and pO_2

The coplot in Fig 5.4 suggests that CPC decreases with an increase in pS_2, with temperature and oxygen varying as shown. This means that as pS_2 increases, more Cr is deported to the matte, and less to the slag. Conversely, as pS_2 decreases, more Cr is deported to the slag and less to the matte. This observation could be the

reason why the soluble chromium was identified by XRD (section 5.2) to occur as CrS, an observation made for the samples that were run under high sulphur partial pressures.

The lowest partitioning of chromium to matte (obtainable by maximising equation 1.1, resulting in the highest CPC) is obtainable in panel (3,3). This represents conditions of low temperature (1300˚C, or $\frac{1}{T}$ = 635.728x10^{-6}K^{-1}), high pO_2 (10^{-6}atm), and low pS_2 (10^{-6}atm). This is a re-emphasis of what has been discussed in section 5.5.2.1 from a different perspective.

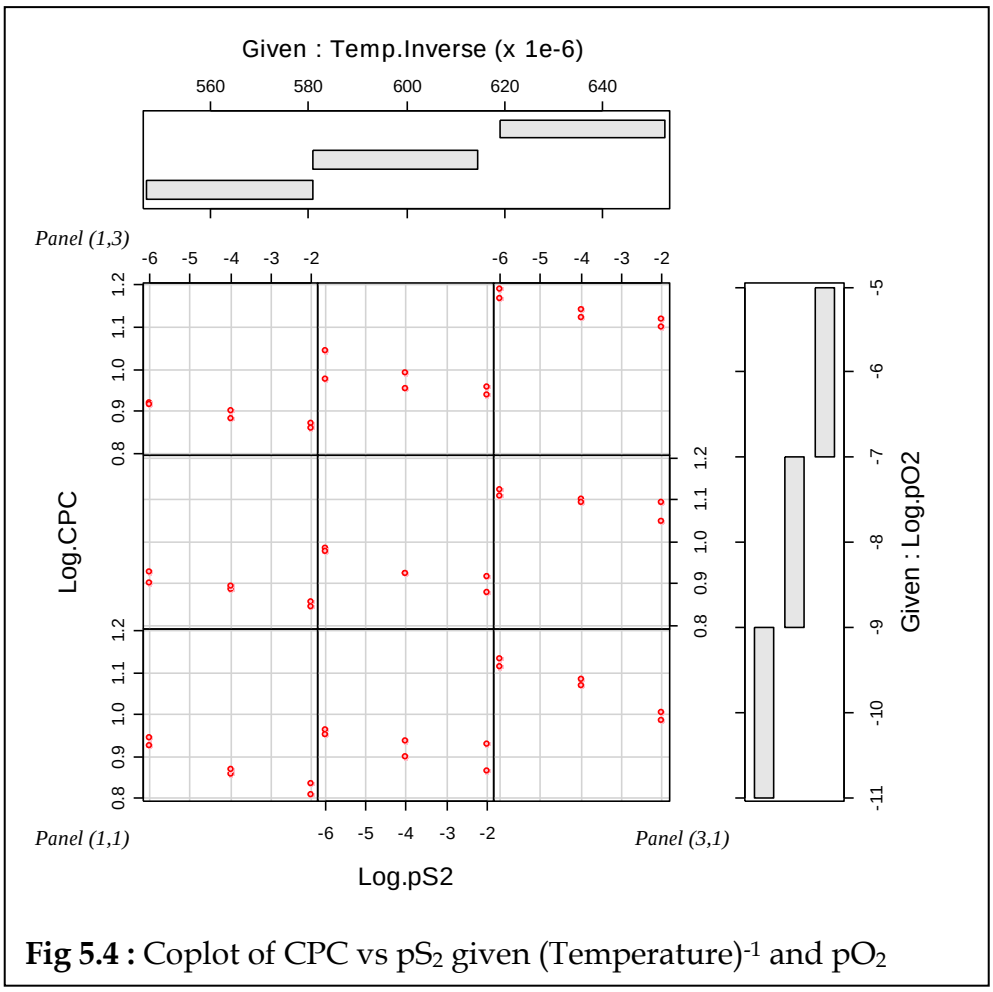

Fig 5.4 : Coplot of CPC vs pS_2 given (Temperature)$^{-1}$ and pO_2

The highest partitioning of chromium to matte (obtainable by minimising equation 1.1) is noted in panel and (1,1). This represents conditions of high temperature (1500˚C (i.e., $\frac{1}{T}$ = 564.016x10^{-6}K^{-1}), low pO_2 (10^{-10}atm), and high pS_2 (10^{-2}atm).

5.5.2.3 Chromium Distribution vs (Temperature)$^{-1}$ given pS_2 and pO_2

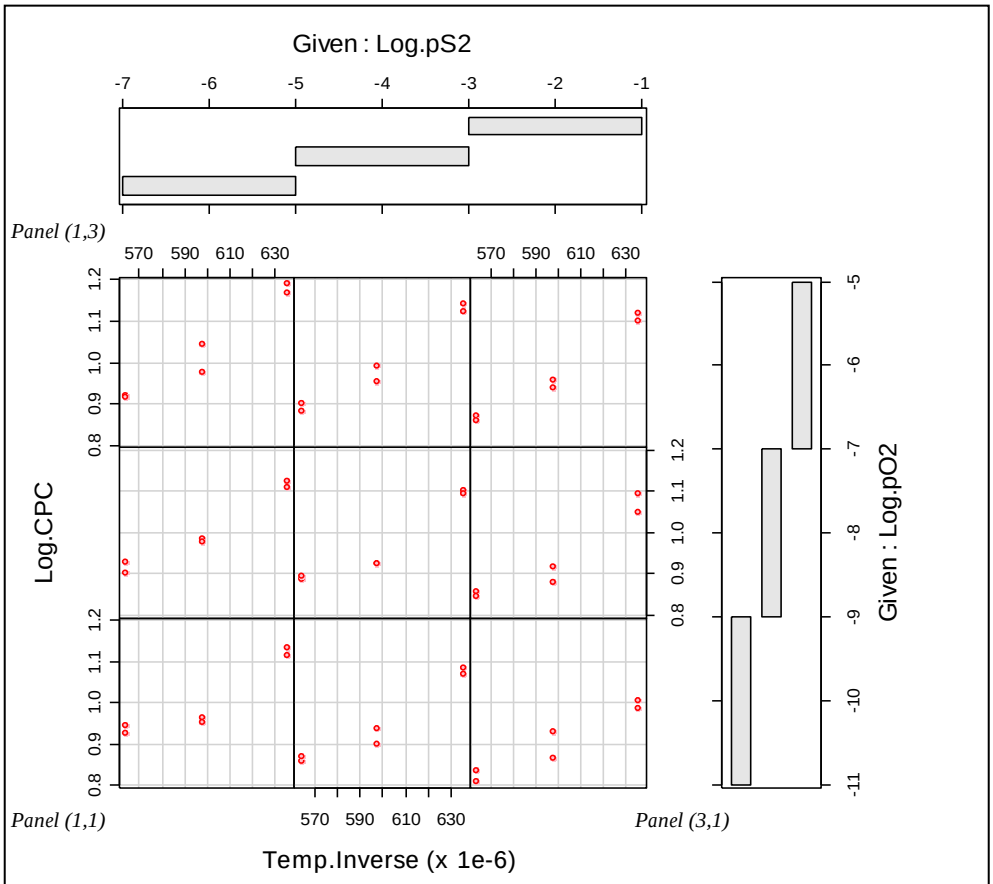

Fig 5.5 : Coplot of CPC vs (Temperature)$^{-1}$ given pO_2 and pS_2

Fig 5.5 shows the variation of Log CPC with the inverse of temperature in kelvin. As has already been noted in the preceding coplots, chromium partitions least to the matte phase by maximising equation 1.1, implying a the low level of temperature (1300˚C, or $\frac{1}{T}$ = 635.728x10^{-6}K^{-1}), low pS_2 (10^{-6}atm), and high pO_2(10^{-6}atm). This scenario is shown in panel (1,3), and is in line with the findings of De Villiers and Kleyenstüber (1993).

Even though a lower temperature seems to result in low chromium partitioning to the matte (at appropriate partial pressures of oxygen and sulphur), the tendency to form chrome spinels in the slag fraction is higher, as noted in section 5.2. This

observation was also reported by Bartie *et al.*(2004). Therefore, the challenge for base metal smelters would be to attain a compromise between a temperature which is low enough to ensure that Cr to the matte is minimal, yet high enough to ensure that spinel formation in the slag is minimised to avoid the problems associated with spinel formation, as discussed in chapter 1.

5.5.2.4 Summary : effects of experimental variables on Cr Partitioning

Table 5.3 gives a brief summary of the observations made in section 5.5.2.1-3 concerning the conditions which promote high or low partitioning of chromium to matte

Table 5.3 : Summary of Conditions for Cr Maximisation/Minimisation in Matte

	Least Chromium Partitioning to Matte	**Highest Chromium Partitioning to Matte**
CPC (as defined by Eq 1.1)	Maximised	Minimised
Temperature	Low (1300˚C (i.e., $\frac{1}{T}$ = 635.728x10^{-6}K^{-1}))	High (1500˚C (i.e., $\frac{1}{T}$ = 564.016x10^{-6}K^{-1}))
Oxygen partial pressure	High (10^{-6}atm)	Low (10^{-10}atm)
Sulphur partial pressure	Low (10^{-6}atm)	High (10^{-2}atm)

The experimental conditions outlined in the second column are those that were found to promote the lowest chromium partitioning to the matte in this investigation. This represents the set of conditions which are desirable and ideal for smelting processes. The third column of Table 5.3 consists of a summary of those conditions which were found to promote the highest chromium partitioning to matte, a scenario which is not recommendable to smelting processes.

5.5.3 Interaction Plots

These are a useful tool in identifying the nature of interaction between factors in a factorial design in as far as their effect on the response variable is concerned. If a plot of two factors gives straight and parallel lines, then there would be no interaction. Conversely, if the interaction plots are not parallel, or if they intersect, this will indicate some presence of interaction (Montgomery, 2005). An initial idea of the relative strength and nature of the interactions that exist between the experimental factors is vital especially if their effect on the response variable (Log.CPC, in this case) is to be modeled out (as will be done in section 5.3.4). The interaction plots for the three variables are shown in figs. 5.6-5.8.

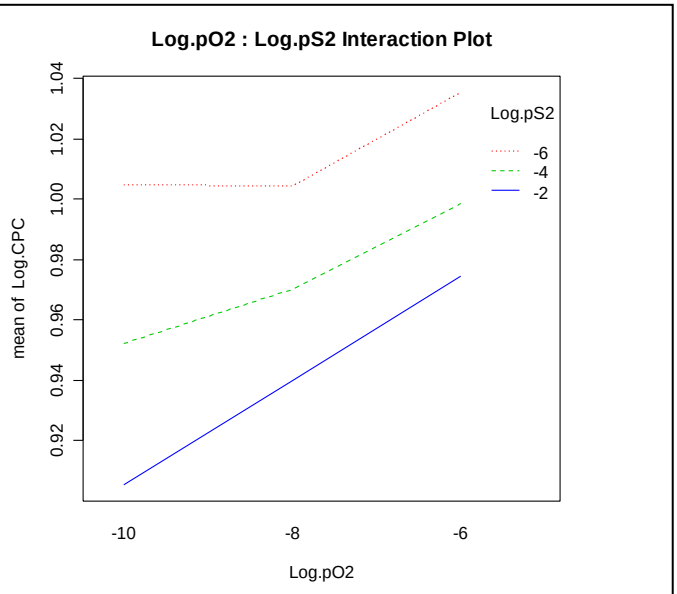

Fig 5.6

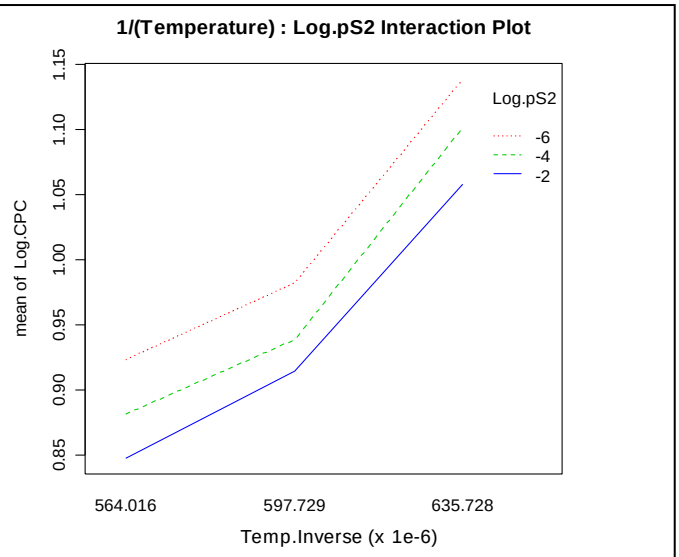

Fig 5.7

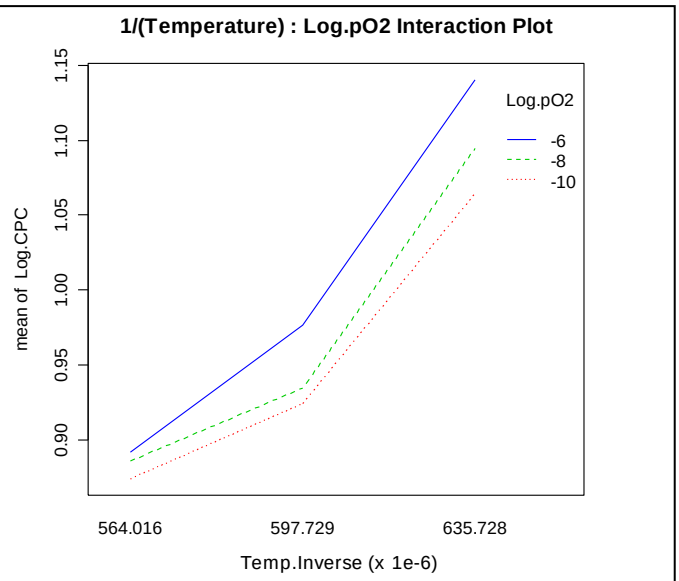

Fig 5.8

It can be seen that it is only in Fig 5.8 where the interaction plots tend to diverge towards each other, at lower values of $\frac{1}{T}$, showing that the effect of temperature on chromium partition coefficient in slag/matte systems varies significantly at different levels of oxygen partial pressures. These interactions will be further investigated and quantified in section 5.5.4.

5.5.4 Statistical Analysis

Statistical analysis of the data was conducted using a statistical software package called R. A regression model for the data was then fitted in order to define the dependence of chromium partition coefficient on the experimental factors investigated. An analysis of variance was applied according to Montgomery (2005) in order to test the significance of the model parameters. An analysis of the error terms (residuals) was also conducted as a diagnostic check for the fitted model.

5.5.4.1 Analysis of Variance (ANOVA)

Table 5.4 shows the analysis of variance of the data.

Table 5.4 : Analysis of variance for drop quench experiments

Source of Variation	Sum of Squares	Deg of Freedom	Mean Square	F_o	P - Value	Decision
A. $\frac{1}{T}$	445.49x10^{-3}	2	222.74x10^{-3}	635.45	<2.20x10^{-16}	Significant
B. $log(pS_2)$	50.59x10^{-3}	2	25.29x10^{-3}	72.16	1.47x10^{-11}	Significant
C. $log(pO_2)$	21.99x10^{-3}	2	11.00x10^{-3}	31.37	9.08x10^{-8}	Significant
A:B	0.62x10^{-3}	4	0.15x10^{-3}	0.44	0.78	Not Significant
A:C	6.06x10^{-3}	4	1.52x10^{-3}	4.32	7.86x10^{-3}	Significant
B:C	2.76x10^{-3}	4	0.69x10^{-3}	1.97	0.13	Not Significant
A:B:C	3.96x10^{-3}	8	0.49x10^{-3}	1.41	0.24	Not Significant
Residuals	9.46x10^{-3}	27	0.35x10^{-3}			
Total	540.93x10^{-3}	53				

The three factors [A = Temperature (represented by $\frac{1}{T}$), B = Sulphur partial pressure (represented by $log(pS_2)$), and C = Oxygen partial pressure (represented

by $log(pO_2)$)], are each at three levels arranged in a 3^3 factorial experimental design. The 27 treatment combinations have 26 degrees of freedom. Each main effect (A, B, and C) has 2 degrees of freedom, each two-factor interaction term (A:B, A:C, and B:C) has 4 degrees of freedom, and the three-factor interaction term has 8 degrees of freedom. Since there are two replicates, there are ($2 \times 3^3 - 1$) total degrees of freedom and $3^3(2 - 1)$ degrees of freedom for error (or residuals).

Using a 5% significance level, a model parameter is considered significant if the p-value (significance probability value) is less than 0.05 (Montgomery, 2005). Based on this preamble, a decision was then made as to whether a main effect or its interaction with other factors was significant or not and this shown in the last column of Table 5.4. From the table (5.4), it can be noted that all the three main effects (temperature, sulphur partial pressure and oxygen partial pressure) are statistically significant. Of the higher order interactions, only the temperature : oxygen partial pressure two-factor interaction effects (A:C) are significant. This observation can also be confirmed by an inspection of the interaction plot in Fig 5.7.

5.5.4.2 Regression Analysis

A regression analysis was performed in order to investigate the relationship between the experimental factors. The process of generating the model involved a step-wise variable reduction, and dropping out any statistically insignificant factor combinations from the ANOVA table of each model. Since the three factor interaction effects were shown to be insignificant (see Table 5.4), they were excluded from the model. The temperature : sulphur partial pressure and the sulphur partial pressure : oxygen partial pressure two-factor interaction effects were also omitted from the model.

5.5.4.2.1 Model with First Order Main Effects

The initial approach adopted was to derive a model containing first order main effects only. Table 5.5 gives the coefficients and the p-values of each of the main effects.

Table 5.5 : Regression coefficients for first order model

	Coefficient	**p-value**	**Decision**
Intercept	- 0.818	4.67×10^{-13}	Significant
T^{-1}	3.033×10^{3}	2.00×10^{-16}	Significant
$log(pS_2)$	-0.019	5.47×10^{-10}	Significant
$log(pO_2)$	- 0.012	7.53×10^{-6}	Significant
Pearson Correlation	0.9207		

Using the coefficients in Table 5.5, the regression equation for the first order main effects can be written as;

$$Log\,CPC = -0.818 + \frac{3.033 \times 10^{3}}{T} - 0.019\,log(pS_2) + 0.012\,log(pO_2) \quad \ldots \quad \text{Eq 5.1}$$

where CPC is the chromium partition coefficient as calculated by equation 1.1, and T is the temperature in Kelvin.

The advantage with the above representation is that is quite simple as it only contains linear effects. Even though a Pearson correlation coefficient of 92.07% for this model may be considered satisfactory, an inspection of Table 5.4 shows that there exists an opportunity to improve the accuracy of the model by incorporating the temperature : oxygen partial pressure two factor interaction effects.

5.5.4.2.2 Model with Second Order Main Effects

An analysis of variance was also conducted with the second order main effects included, and the results are shown in Table 5.6.

Table 5.6 : ANOVA with quadratic interaction effects of the main factors

Source of Variation	Sum of Squares	Deg of Freedom	Mean Square	F_o	P – Value	Decision
$\frac{1}{T}$	426.2×10^{-3}	1	426.2×10^{-3}	1107.37	$<2.20\times10^{-16}$	Significant
$log(pS_2)$	50.42×10^{-3}	1	50.42×10^{-3}	131.02	4.67×10^{-15}	Significant
$log(pO_2)$	21.42×10^{-3}	1	21.42×10^{-3}	55.65	1.87×10^{-9}	Significant
$(\frac{1}{T})^2$	19.29×10^{-3}	1	19.29×10^{-3}	50.13	6.91×10^{-9}	Significant
$[log(pS_2)]^2$	0.17×10^{-3}	1	0.17×10^{-3}	0.43	0.52	Not Significant
$[log(pO_2)]^2$	0.58×10^{-3}	1	0.58×10^{-3}	1.50	0.23	Not Significant
$\frac{1}{T}$ x $log(pO_2)$	5.16×10^{-3}	1	5.16×10^{-3}	13.39	6.48×10^{-4}	Significant
Residuals	17.70×10^{-3}	46	0.38×10^{-3}			
Total	540.94×10^{-3}	53				

It can be seen from Table 5.6 that the quadratic effects of temperature and pS_2 are not significant (by looking at their p-values). Excluding these two yields the following regression coefficients;

Table 5.7 : Regression coefficients for second order model

	Coefficient	p-value	Decision
Intercept	9.459	3.99×10^{-7}	Significant
$\frac{1}{T}$	-32.93×10^{3}	1.32×10^{-7}	Significant
$log(pS_2)$	-18.71×10^{-3}	2.47×10^{-15}	Significant
$log(pO_2)$	-110.2×10^{-3}	1.862×10^{-3}	Significant
$\frac{1}{T}$ x $log(pO_2)$	31.32×10^{6}	5.44×10^{-9}	Significant
$(\frac{1}{T})^2$	204.3	6.22×10^{-4}	Significant
Pearson Correlation	0.966		

The Pearson correlation coefficient in this case is higher (0.966) as shown in Table 5.7, implying that this quadratic model (with respect to temperature) is a better fit of the equilibration experiments data than the first order one. The equation may be written as;

$$Log CPC = 9.459 - \frac{32.93 x 10^3}{T} - 18.71 x 10^{-3} log\left(pS_2\right) + \left(\frac{31.32\ x 10^6}{T} - 110.2\ x 10^{-3}\right) log\left(pO_2\right) + - \frac{204.3}{T^2}$$

... Eq 5.2

Response surfaces and contour plots of chromium partitioning between slag and matte were then plotted using the model in Eq 5.2.

5.5.4.3 Response Surface Analysis of Chromium Distribution

The model generated in the above section was used to plot the response surfaces of the response variable (chromium partitioning coefficient) as a function of the three experimental factors (temperature, pO_2 and pS_2). Temperature was fixed at the three levels investigated (1300˚C, 1400˚C, and 1500˚C). The plots are shown below;

The diagrams in Figs 5.9-5.14 show the linearised relationships between chromium partition coefficient with pS_2 and pO_2 at the different temperatures employed in this work. The response surfaces in Figs 5.9, 5.11, and 5.13 clearly show the variation of Log.CPC as defined by the model in Eq 5.2. It can be seen from the response surfaces that Log.CPC is directly proportional to pO_2 and inversely proportional to pS_2 at a given temperature, within the temperature domain investigated in this work. This is in agreement with the observations noted when the data was plotted using conditioning plots in section 5.5.2. The contour plots in Figs 5.10, 5.12, and 5.13 give a profile of ranges of pS_2 and pO_2 over which the chromium partition coefficients are equal, subject to the experimental parameters applied in this investigation.

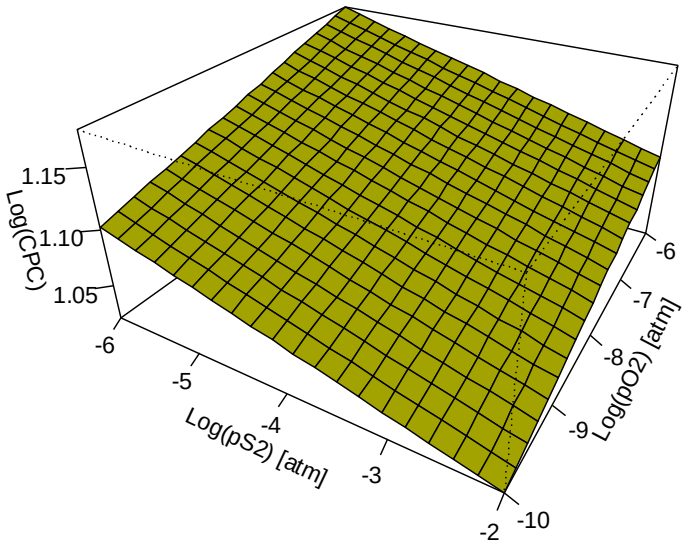

Fig 5.9: CPC Response Surface at 1300˚C

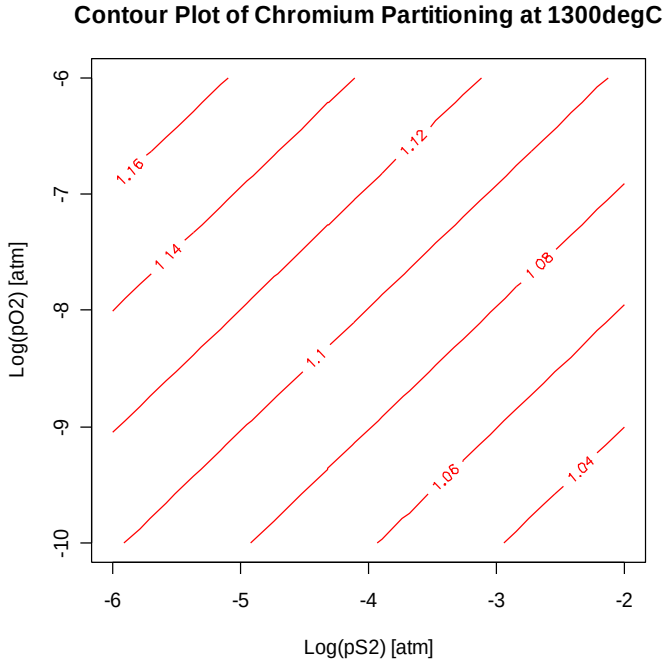

Fig 5.10: : CPC Contour Plot at 1300˚C

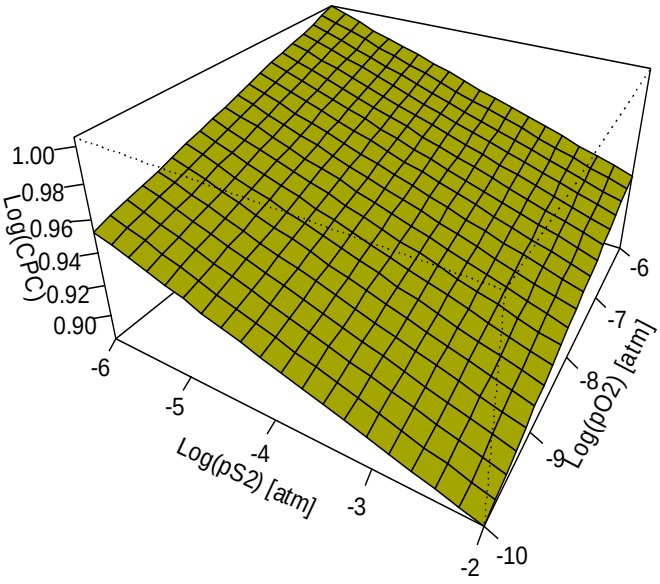

Fig 5.11: CPC Response Surface at 1400˚C

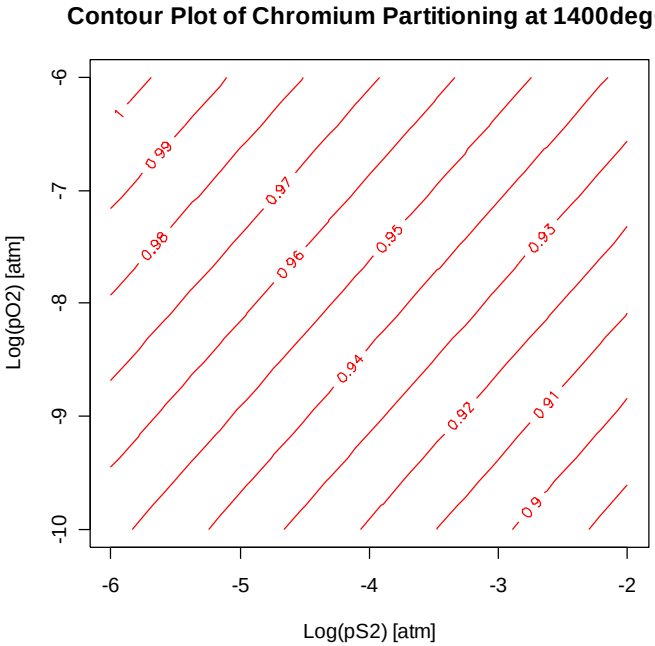

Fig 5.12: CPC Contour Plot at 1400˚C

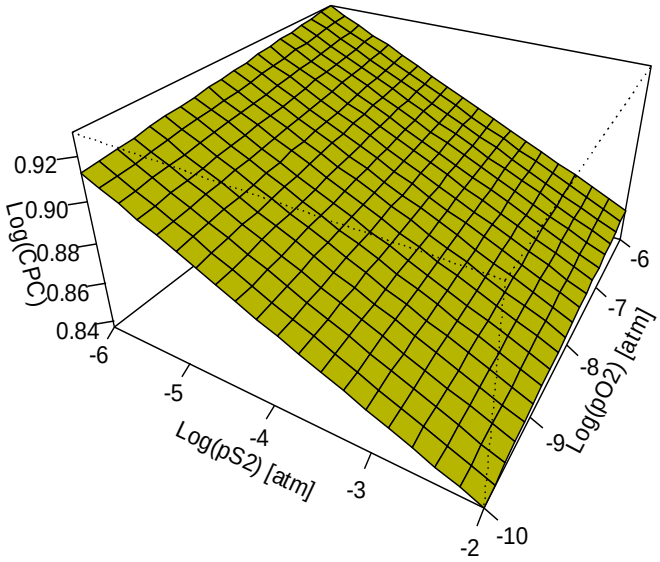

Fig 5.13: CPC Response Surface at 1500˚C

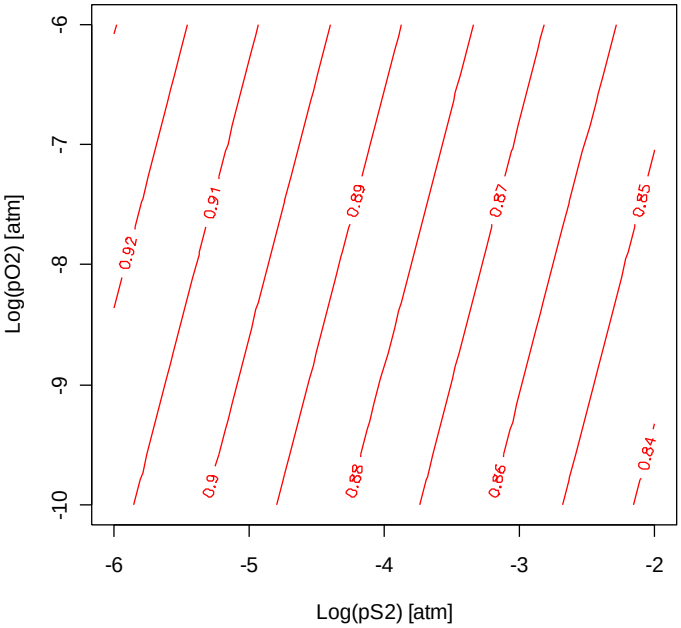

Fig 5.14: CPC Contour Plot at 1500˚C

5.5.4.4 Model Diagnostic Checks

5.5.4.4.1 Normality Assumption

A check of the normality assumption was made by plotting histogram of the residuals. If the NID(0, σ^2) assumption is satisfied, this plot should look like a sample from a normal distribution centred at zero.

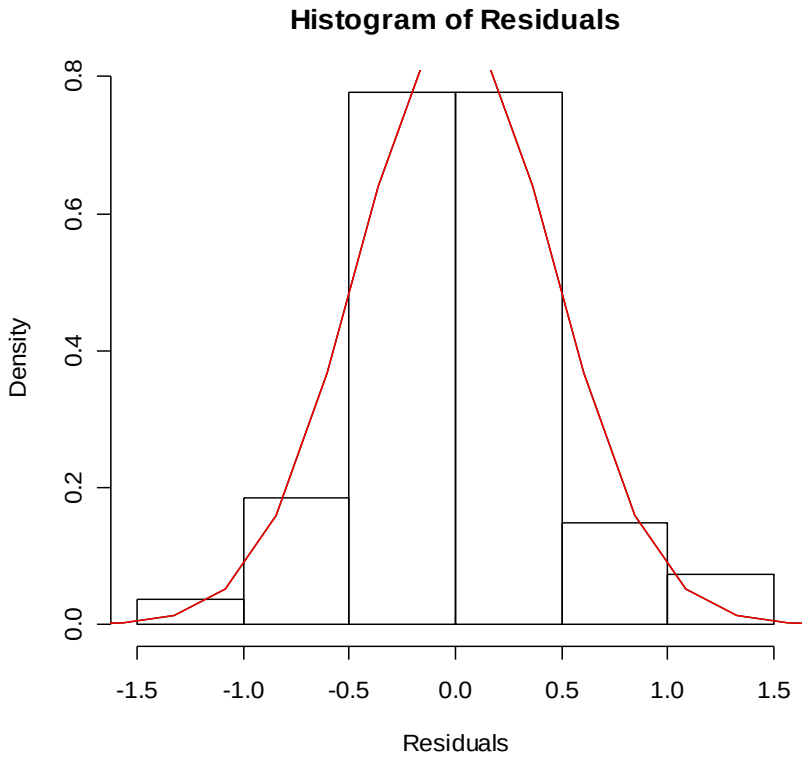

Fig 5.15: Histogram and probability density functions of residuals

As can be seen from Fig 5.15, the histogram does not give a perfect shape of a normal distribution as the corresponding negative and positive bars do not have the same height. This is particularly so for the (-1.0 to –0.5) and (0.5 – 1.0) bars. This distortion will become less apparent if the experimental runs were more than those considered in this investigation.

5.5.4.4.2 Normal Probability Plot for the Residuals

A normal Probability plot was constructed as an enhancement check for the assumption of normality for the error distribution of chromium distribution in the slag and matte phases. This plot was also generated using R;

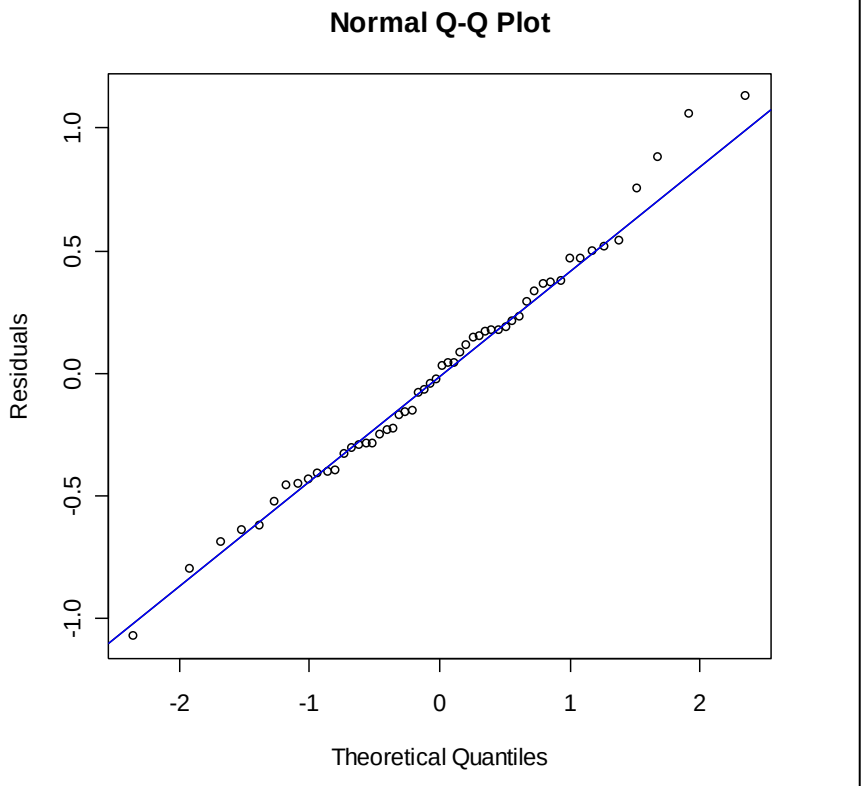

Fig 5.16: Quantile plot

Fig 5.16 shows the normal probability plot (Q-Q) plot of the residuals with a line passing through the upper and lower quartiles. The general impression from examining this display is that the error distribution is approximately normal. The tendency of the normal probability plot to bend down slightly on the left side and upward slightly on the right side implies that the tails of the error distribution are somewhat "thinner" than would be anticipated in a normal distribution: that is, the largest residuals are not quite as large (in absolute value) as expected
Since generally the plot resembles a straight line, it can be assumed that the error distribution in the chromium partitioning between slag and matte is a normal gaussian distribution.

The above two plots (the histogram and the normal probability plot in Fig 5.15 and 5.16 respectively) imply that the analysis of variance (ANOVA) shown in section 5.5.4.1 is robust to the normality assumption.

5.6 EXPERIMENTAL CONCERNS

This subsection discusses a few experimental concerns that could possibly have an effect on the interpretation of the results discussed in this chapter.

Even though all the necessary precautions were taken to ensure that the furnace was gas tight, there could have been some air ingress into the furnace via the surface of the plastic sheeting that was used to cover the bottom part of the furnace tube. A Molybdenum oxidation test could have been a good way of checking gas-tightness (Nell, 2006). However, this check was not conducted because information regarding the possibility of air ingress through the plastic sheeting became available after all the experiments had been executed.

CHAPTER 6

CONCLUSIONS AND RECOMMENDATIONS

This chapter gives a summary of the major findings of the research which have been discussed in chapter 5.

The first part of this chapter gives a summary of the findings from this work, and the second consists of recommendations for future work that have arisen from this research

6.1 CONCLUSIONS

The main findings from this study are listed below:

- From the XRD analyses, bornite is a distinct phase in the matte smelting process. Chromium sulphide compounds are present in matte in their different forms depending on temperature and gas environment.
- Chromium is present in matte generally as a dissolved and a spinel phase. The dissolved matte is present as Chromium sulphide (CrS), and is a more predominant phase under the most reducing conditions investigated in this work (pO_2 of 10^{-10}atm).

  Chemical mapping using the scanning electron microscope is a useful tool in graphically identifying the extent of chromium dissolution or entrainment in the matte. The dissolved matte is present as a finely disseminated and homogeneous phase right across the matte matrix. The chromium spinel phase in matte appears on a phase map as chromium "pockets" in the matte matrix, and is present in two forms. One form is as chromium-sulphidic spinels daubreelite ($FeCr_2S_4$). The second form is the chromium-oxidic spinel ($[(Fe,Mg)(Cr,Al)]_2O_4$). As conditions become more oxidising ($pO_2=10^{-6}$ atm), the soluble CrS becomes a predominant phase in matte. However, as the conditions become more reducing ($pO_2 = 10^{-10}$atm), the sulphidic spinel, daubreelite

($FeCr_2S_4$) becomes a predominant phase in the matte. Oxidic spinels were found to be present in matte under the more oxidising conditions. This was an indication that the oxidic spinel's presence in matte could possibly be due to chemical a reaction. However, in some cases this chrome oxidic spinel was found to be concentrated around the slag/matte interface, possibly due to its high specific gravity, and it was assumed that its presence was also partly due to physical entrainment. As can be noted, the mechanism by which chromium is present in matte is an area that requires a dedicated investigation.

- For equal gas partial pressures, there is less chromium present in matte in the form of oxidic spinel at higher temperatures than at lower temperatures. This was observed in for example, the mattes in micrographs 4.2 and 4.5. This further strengthens the need for further work in the area of characterising the mechanism of spinel presence in mattes under different conditions
- Chromium partitions very strongly to the spinel phase in slags, relative to the other sub-phases present in slag
- In the matte, chromium partitions more into the Fe-rich sulphide phase than into the copper rich phase. This is likely to be due to the complete miscibility of chromium and iron in the temperature ranges investigated in this research.
- From the equilibration experiments data analysis, it was observed that chromium partitions least to matte under the following conditions: low temperature (1300˚C (or $\frac{1}{T}$ = 635.728x10^{-6}K^{-1})); high pO_2 (10^{-6}atm), and low pS_2 (10^{-6}atm).

Conversely, chromium was found to partition the most to matte (a situation which is undesirable for base-metal smelters), under the following conditions: high temperature (1500˚C (i.e., $\frac{1}{T}$ = 564.016x10^{-6}K^{-1}), low pO_2 (10^{-10}atm), and high pS_2 (10^{-2}atm).

- The partitioning of chromium between matte and chrome saturated slags investigated in this work can be predicted by the following statistical models:

$$Log\,CPC = -0.818 + \frac{3.033\,x\,10^3}{T} - 0.019\,log\left(pS_2\right) + 0.012\,log\left(pO_2\right)$$

with a Pearson correlation coefficient of 0.9207,

or, including second order main effects;

$$LogCPC = 9.459 - \frac{32.93x10^{3}}{T} - 18.71x10^{-3}\log(pS_2) + \left(\frac{31.32\ x\ 10^{6}}{T} - 110.2\ x\ 10^{-3}\right)\log(pO_2) + -\frac{204.3}{T^{2}}$$

with a Pearson Correlation coefficient of 0.966

- A response surface generated from the above second order model clearly shows that, there is a direct proportionality between the logarithms of CPC and pO_2, and an inverse proportionality between the logarithms of CPC and pS_2 for all the temperature regimes employed in this investigation (1300°C, 1400°C, and 1500°C)
- The industrial significance of the conclusions above is that larger amounts of chromium will dissolve in matte in the newer high temperature electrical furnaces (which are also operate under much more reducing conditions than the flash furnaces and reverberatory furnaces). While the higher operating temperatures would favour more fluid slags during smelting, the higher chrome deportment to matte might lead to increased operating (foaming and tapping) problems in the subsequent converting step where the conditions are more oxidising and temperatures are lower. The converting conditions will lead to increased precipitation of the chromium spinel minerals which tends to associate with the injected bubbles and transfer to the slag by flotation.

6.2 RECOMMENDATIONS

The following is a list of recommendations that ensued from this work:

- Even though the number of samples analysed for XRD phase identification managed to give a fair indication of the phases present in the matte, a greater number of the samples generated in this work needs to be subjected to a similar analysis in order to obtain a more definitive identification of the phases predominant under each set of factorial conditions that were investigated in this research. The technology relevant to analyse the type of mattes in this work was only available in Germany, and there was a limitation on the number of samples that could be analysed. However, within the constraints encountered, the samples analysed for phase identification managed to give a fair indication of the phases predominant in the matte. It is postulated that the

phases identified in the samples that were analysed will still be present in the other samples that were not analysed for XRD phase identification, though in varying proportions, depending on the prevailing pSO_2, pO_2, and temperature regimes (as investigated in this work). This premise is confirmed by an analysis of the SEM results for both the samples that were analysed for XRD phase identification and those that were not (as shown in Table 4.3).

- It has been assumed that the chrome-spinel present in the matte was partly due to physical entrainment due to the heavy SG of spinel. However, the possibility of chemical entrainment cannot be overlooked. This is more so given that spinel presence in matte was noted to be higher in the more oxidising conditions as can be seen in for example, micrograph 35 in Appendix C with pO_2 of 10^{-6}atm and pS_2 of 10^{-2}atm. The mechanisms by which spinel is present in matte needs to be investigated further. This need for a further investigation is exacerbated by the fact that in some cases, slag glass phases (without spinel) were found to be in equilibrium with spinel-containing mattes, making it difficult to solely ascribe the presence of spinel to physical entrainment. This was noted in, for example micrographs 19 / 20, 31 / 32, 35 / 36 and 43 / 44 in Appendix C
- Conditions under which chrome deportment to the matte is minimal can be further investigated by using a Central Composite Design in the direction of steepest ascent, as identified from the response surface analysis (Montgomery, 2005). This tool will be quite useful for optimising operating conditions that minimise chrome deportment to the matte, and maximise its deportment to the slag. The conditions established in this work for chrome minimisation to matte (i.e., low temperature (1300°C (or $\frac{1}{T}$ = $635.728 \times 10^{-6} K^{-1}$)); high pO_2 (10^{-6}atm), and low pS_2 (10^{-6}atm)) could be taken as a useful starting point for designing the optimisation experiments.

CHAPTER 7

REFERENCES

The references are first listed alphabetically according to the surnames of authors, and subsequently according to the date of publication.

- Anzai S, Hamaguchi Y, "Thermal Expansion Behaviour through the Magnetic Transition in Cr_5S_6", Journal of the Physical Society of Japan, Vol 38, No.2, pp. 400-403, February 1975
- Arculus RJ, Gillberg ME, Osborn EF, "The System MgO-Iron Oxide-Cr_2O_3-SiO_2 : Phase Relations amoung Olivine, Pyroxene, Silica and Spinel in air at 1 atm", Carnegie Institution of Washington Year Book, 73, pp. 317-322, 1974
- Avner SH, "Introduction to Physical Metallurgy", 2nd Edition, McGraw-Hill Book Company, pp. 147-224, 1974
- Bale CW, Pelton AD, Thompson WT, "An Efficient Procedure for Computing Isothermal Predominance Diagrams", Canadian Metallurgical Quarterly, Vol. 25, pp. 107-112, 1986
- Bale CW, Chartrand P, Degterov SA, Eriksson G, Hack K, Ben Mahfoud R, Melançon J, Pelton AD, Petersen S, "Factsage Thermochemical Software and Databases", Calphad, 26(2), pp. 189-228, 2002
- Barnes HL, "Investigations in Hydrothermal Sulphide Systems", In : Ulmer GC (Ed.), "Research Techniques for High Pressure and High Temperature", Springer-Verlag, New York, pp. 289-316, 1971
- Barrentine LB, "An introduction to the Design of Experiments: A simplified Approach", ASQ Quality Press, 1999

- Bartie NJ, "The Effect of Temperature, Slag Chemistry, and Oxygen Partial Pressure on the Behaviour of Chromium Oxide in Melter Slags", MSc Thesis, University of Stellenbosch, Department of Process Engineering, 2004
- Biswas AK, Davenport WG, "Extractive Metallurgy of Copper", Pergamon Press, 1976
- Bouchard RJ, Russo PA, Wold A, "Preparation and Electrical Properties of some Thiospinels", Inorganic Chemistry, Vol. 4(5), pp. 685-688, 1965
- Bouchard RJ, Wold A, "Structural and Electrical Properties of some Monoclinic Ternary Sulphides", Journal of Physics and Chemistry of Solids, Vol. 27, pp. 591-595, 1966
- Bret R, "Experimental Data from the System Cu-Fe-S and their bearing on Exsolution Textures in Ores", Economic Geology, Vol. 59, pp. 1241-1269, 1964
- Bucher R, Private communication, Ithemba Labs, RSA, 2005
- Cawthorn RG, "The Platinum and Palladium Resources of the Bushveld Complex", South African Journal of Science 95, November / December 1999
- Chambers JM, Hastie TJ, "Statistical Models in S", Chapman & Hall, 1993
- Choi N, Cho WD, "Distribution Behavoiur of Cobalt, Selenium, and Tellurium between Nickel-Copper-Iron Matte and Silica-Saturated Iron Silicate Slag", Metallurgical and Materials Transactions B, Vol. 28B, pp. 429-438, 1997
- De Villiers JPR, and Kleyenstüber ASE, "The partitioning of chromium between sulphide and silica melts at controlled partial pressures of oxygen and sulphur". Mintek Report No. M139D, 21 December 1984(Reissued October 1993)
- De Villiers JPR, Mathias J, Muan A, "Phase Relations in the System CaO-Cr_xO-SiO_2 in Air and Solid-Solution Relations along the Ca_2SiO_4 –$Ca_3(CrO_4)_2$ join", Transactions of the Institution of Mining and Metallurgy (Section C: Mineral Processing and Extractive Metallurgy), pp. C55-C62, 1987

- De Villiers JPR, Muan A, "Liquidus-Solidus Phase Relations in the System CrO-Cr_2O_3-SiO_2-CaO", Journal of the American Ceramic Society, 75 (6), pp. 1333-1341, 1992
- Dwight K, Germann RW, Menyuk N, Wold A, "Magnetic properties of Cr_5S_6 in Chromium Sulphides", Journal of Applied Physics, Supplement to Vol.33, No.3, pp. 1341-1342, 1962
- El Goresy A, Kullerud G, "Cr-S and Fe-Cr-S Systems", Carnegie Institution of Washington Yearbook, 67, pp. 182-187, 1969
- Fahey NP, Swinbourne DR, Yan S, Osborn JM, "The solubility of Cr_2O_3 in calcium Ferrite Slags at 1573 K", Metallurgical and Materials Transactions B, 35B, pp. 197-202, April 2004
- Font J, M Hino, and K Itagaki, "Minor Elements Distribution between Iron-Silicate Base Slag and Ni_3S_2-Fe_S Matte under High Partial Pressures of SO_2" Materials Transactions, 39(8), pp. 834-840, 1998a
- Font JM, M Hino, and K Itagaki, "Phase Equilibrium and Minor Element Distribution between Iron-Silicate Base Slag and Nickel-Copper-Iron Matte at 1573 K under High Partial Pressures of SO_2". Materials Transactions, 40(1), pp. 20-26, 1999
- Font JM, Roghani G, Hino M, Itagaki K, "Solubility of Copper or Nickel in Iron Silicate Base Slag Equilibrated with Cu_2S-FeS or Ni_3S_2-FeS Matte under High Partial Pressures of SO_2", Metallurgical Review of the MMIJ, 15 (1), pp. 75-86, 1998c
- Font JM, Takeda Y, Itagaki K, "Phase Equilibrium between Iron Silicate Based Slag and Nickel-Iron Matte at 1573 K under High Partial Pressures of SO_2", Materials Transactions, JIM, 39 (6), pp. 652-657, 1998
- Gaskell DR, "Introduction to Metallurgical Thermodynamics", McGraw-Hill Kogakusha Ltd, 1973

- Harris WE, Kratochvil B, "Chemical Separations and measurements – background and procedures for modern analysis", Saunders golden series, W. B Saunders Company, London, pp. 77-81, 1974
- Igaki K, Ohashi N, Mikami M, "Phase Relations of Non-Stoichiometric Chromium Sulphide CrS_x in the Range of $1.200 \leq x \leq 1.480$", Journal of the Physical Society of Japan, Vol. 31, No.5, pp. 1424-1430, November 1971
- Itagaki K, "Distribution of Minor Elements in Sulphide Smelting", Yazawa International Symposium Vol. 1 : Materials Processing Fundamentals and New Technologies, TMS (The Minerals, Metals, and Materials Society), 2003
- Jellinek F, "The structures of the Chromium Sulphides", Acta Crystallographica, Vol. 10, pp. 620-628, 1957
- Jones RT, "JOM World Non-ferrous Smelter Survey, Part II: Platinum Group Metals", JOM, pp. 59-63, Dec 2004
- Jones RT, "Platinum Smelting in South Africa", South African Journal of Science 95, pp. 525-534, November / December 1999
- Kaneko H, Nishizawa T, Tamaki K, "Study of Phase Diagrams of Sulphides in Steels", Nippon Kinzoku Gakkai-Si, Vol. 27(7), pp.312-318, 1963
- Keith ML, "Phase Equilibria in the System $MgO\text{-}Cr_2O_3\text{-}SiO_2$", Journal of the American Ceramic Society, Vol. 37, No. 10, pp. 490-496, 1954
- Kim HG, Sohn HY, "Effects of CaO, Al_2O_3, and MgO Additions on the Copper Solubility, Ferric / Ferrous Ratio, and Minor Element Behaviour of Iron Silicate Slags", Metallurgical and Materials Transactions B, 29B, pp. 583-590, June 1998
- Kissin SA, Scott SD, "Device for measurement of sulphur fugacity mountable on the precession camera", American Mineralogist, Vol. 64, pp. 1306-1310, 1979
- Kongoli F, Yazawa A, "Liquidus Surface of $FeO\text{-}Fe_2O_3\text{-}SiO_2\text{-}CaO$ Slag Containing Al_2O_3, MgO, and Cu_2O at intermediate Oxygen Partial Pressures", Metallurgical and Materials Transactions B, Vol. 32B, pp. 583-592, 2001

- Kubaschewski O, "Iron-Chromium", Iron-Binary Phase Diagrams, Springer-Verlag, Berlin, pp. 31-34, 1982
- Kullerud G, "Experimental techniques in Dry Sulphide Research", In : Ulmer GC (Ed.), "Research Techniques for High Pressure and High Temperature", Springer-Verlag, New York, pp. 289-316, 1971
- Larrain JM, Lee S, "Thermodynamic Properties of Copper-Nickel-Sulphur Melts", Canadian Metallurgical Quarterly, 19, pp. 183-190, 1980
- Levenspiel O, "Chemical Reaction Engineering", 3rd Edition, John Wiley and Sons, New York, 1999
- Liddell KS, McRae LB, Dunne RC, "Process routes for beneficiation of noble metals from Merensky and UG2 ores", Pg 33 – 44, Mintek Review, No. 4, 1986
- Luraschi A, Elliot JF, "Thermodynamic Behaviour of Oxygen and Sulphur in Copper-Iron-Sulphur-Oxygen Mattes at 1200°C", Transactions of the Institute of Mining and Metallurgy, pp. C14-C25, 1979
- Lusk J, "An electrochemical method for determining equilibration temperatures for sulphide minerals", Economic Geology, Vol. 84, pp. 1663-1670, 1989
- Lusk J and Bray DM, "Phase relations and the electrochemical determination of sulphur fugacity for selected reactions in the Cu-Fe-S and Fe-S systems at 1 bar and temperatures between 185 and 460°C", Chemical Geology, Vol. 192, pp. 227-248, 2002
- Lutz HD, Koch U, Siwert H, "Phase Relationships of the Ternary Chromium Sulphides $Cr^{II}_{1-x}M_xCr^{III}_2S_4$ $(M = Mn, Fe, Co)$ with Cr_3S_4 and Spinel Structure", Materials Research Bulletin, Vol. 18, pp. 1383-1389, 1983
- McKenzie AD and Nell J, "Partitioning of solubility of chromium during the matte-smelting of chromium-bearing sulphide concentrates." Mintek Technical Memorandum No. 14574, 31 March 1994

- Mikami M, Igaki K, Ohashi N, "Electrical and Magnetic Properties of the Chromium Sulphide with Deviation from Stoichiometric Composition Cr_2S_3", Journal of the Physical Society of Japan, Vol. 32, No.5, pp. 1217-1221, May 1972
- Mishra B, Pruseth KL, "Phase Equilibrium study in the system Cu_2S-PbS-Sb_2S_3 : non-stoichiometry in sulfosalts and isothermal variation in sulfur fugacity", Contributions to Mineral Petrology, Vol. 118, pp. 92-98, 1994
- Montgomery DC, "Design and Analysis of Experiments", John Wiley & Sons Inc, 2005
- Muan A, Osborn EF, "Phase Equilibria at Liquidus Temperatures in the System MgO-FeO-Fe_2O_3-SiO_2", Journal of the American Ceramic Society, Vol. 39. No. 4, pp. 121-140, 1956
- Muan A, Somiya S, "Phase Equilibria in the System Iron Oxide-Cr_2O_3-SiO_2 in air", Journal of the American Ceramic Society, Vol. 43, No. 10, pp. 531-542, 1960
- Muan A, "Phase Relations in Chromium Oxide-Containing Systems at Elevated Temperatures", Geochimica et Cosmochimica Acta, 39, pp. 791-802, 1974
- Muan A, "Slag-Metal Equilibria involving Chromium as a Component", Mintek 50, pp. 897-904, 1992
- Muan A, Somiya S, "Phase Equilibrium Studies in the System Fe_xO-Al_2O_3-Cr_2O_3", Journal of the American Ceramic Society, 42 (12), pp. 603-613, 1959.
- Nagamori N, Mackey PJ, Tarassoff P, "Copper Solubility in FeO-Fe_2O_3-SiO_2-Al_2O_3 Slag and Distribution Equilibria of Pb, Bi, Sb, and As Between Slag and Metallic Copper", Metallurgical Transactions B, Vol. 6B, pp. 295-301, 1975
- Nell J, De Villiers JPR, " T-P_{O_2} Topological Analysis of Phase Relations in the System CaO-CrO-Cr_2O_3-SiO_2", Journal of the American Ceramic Society, 76 (9), pp. 2193-2200, 1993

- Nzontta MM, Sichen D, Seetharaman, "A study of Sulphide Capacities of Iron-Oxide Containing Slags", Metallurgical and Materials Transactions B, Vol. 30B, pp. 909-920, 1999
- Pei W, Wijk O, " Experimental study on the activity of chromium oxide in the CaO-SiO_2-Al_2O_3-MgOsat-CrO_x Slag", Scandinavian Journal of Metallurgy, Vol. 23, pp. 228-235, 1994
- Pelton AD, "Thermodynamics and Phase Diagrams of Materials", In : Kostorz G (Ed.) , "Phase Transformations in Materials", John Wiley-VCH, pp. 1-80, 2001
- Popma TJA, Van Bruggen F, "Structural and Magnetic Phase Transitions of Chromium Sulphides $Cr_{1-x}S$ with $0 \le x \le 0.12$ ", Journal of Inorganic and Nuclear Chemistry, Vol. 31, pp. 73-80, 1969
- Porter DA, Easterling KE, "Phase Transformations in Metals and Alloys" Van Nostrand Reinhold Company, USA, pp. 110-262, 1981
- Pretorius EB, Muan A, "Activity-Composition relations of chromium oxide in silicate melts", PhD Thesis, The Pennsylvania State University, 1989
- Pretorius EB, Snellgrove R, Muan A, "Oxidation State of Chromium in CaO-Al_2O_3-CrO_x-SiO_2 Melts under Strongly Reducing Conditions at 1500ºC", Journal of the American Ceramic Society, 75 (6), 1378-1381, 1992
- R Development Core Team. "R: A language and environment for statistical computing". R Foundation for Statistical Computing, Vienna, Austria. ISBN 3-900051-07-0, URL http://www.R-project.org., 2004
- Raghavan V, "Phase Diagrams of Ternary Iron Alloys", Vol. 2, pp. 107-120, The Indian Institute of Metals, Calcutta, 1988
- Rankin WJ, Biswas AK, "Oxidation States of Chromium in Slag and Chromium Distribution in Slag-Metal Systems at 1600ºC", Institution of Mining and Metallurgy, Section C, March, pp. C60-C70, 1978

- Rau H, “The Chromium-Sulphur System between 873 K and 1364 K”, Journal of the Less Common Metals, 55, pp 205-211, 1977
- Reddy RG, Healy GW, “Distribution of Cobalt Between Liquid Copper and Copper Silicate Slag at 1523 K”, Metallurgical and Materials Transactions B, 12B, pp. 509-516, 1981a
- Reddy RG, Healy GW, “The Solubility of Cobalt in Cu_2O-CoO-SiO_2 Slags in Equilibrium with Liquid Cu-Co Alloys”, Canadian Metallurgical Quarterly, 20(2), pp. 135-143, 1981b
- Rhines FN, “Phase Diagrams in Metallurgy”, McGraw-Hill Book Company, 1956
- Richardson FD, Jeffes JHE, “The thermodynamics of substances of interesting iron and steelmaking : III . Sulfides”. Journal of Iron and Steel Institute, Vol. 171, pp. 165-175, 1952
- Roeder PL, Reynolds I, “Crystallization of Chromite and Chromium Solubility in Basaltic Melts”, Journal of Petrology, Vol. 32, pp. 909-934, 1991
- Roghani G, Takeda Y, Itagaki K, “Phase Equilibrium and Minor Element Distribution between FeO_x-SiO_2-MgO-Based Slag and Cu_2S-FeS Matte at 1573K under High Partial Pressures of SO_2”, Metallurgical and Materials Transactions B, Vol. 31B, pp. 705-714, 2000
- Rosenqvist T, “Principles of Extractive Metallurgy”, McGraw-Hill, pp. 354-368, 1974
- Sano N, Lu W, Riboud PV, Maeda M, "Advanced Physical Chemistry for Process Metallurgy", Academic Press, London, pp. 5 - 117, 1997
- Sato M, “Electrochemical Measurements and Control of Oxygen Fugacity and other Gaseous Fugacities with Solid Electrolyte Systems”. In : Ulmer GC (Ed.), “Research Techniques for High Pressure and High Temperature”, Springer-Verlag, New York, 1971

- Schneeberg EP, "Sulfur Fugacity Measurements with the Electrochemical Cell $Ag|AgI_{(s)}|Ag_{2+x(s)}, f_{S_2}$", Economic Geology, Vol. 68, pp. 507-517, 1973
- Shick LK, Von Neida AR, "Single Crystal Growth of $CoCr_2S_4$ and $FeCr_2S_4$", J. Crys. Growth. 5(4), pp. 313-314, 1969
- Shridhar, S., Toguri, J.M., Simeonov, S., "Copper Losses and Thermodynamic Considerations in Copper Smelting", Metallurgical and Materials Transactions B, 28B, April, pp.191-200, 1997
- Smithells, "Smithells Metals Reference Book", Butterworth-Heineman, London, 1976
- Spiegel MR, "Shaum's Outline of Theory and Problems of Statistics", 2nd Ed, McGraw Hill Inc, 1988
- Stander F, "The effect of limited carbon addition on the smelting of PGM-Concentrates", South African Institute of Mining and Metallurgy Colloquium, April 1997
- Takeda Y, Nakazawa S, Yazawa A, "Thermodynamics of Calcium Ferrite Slags at 1200 and 1300°C", Canadian Metallurgical Quarterly, Vol. 19, pp. 297-305, 1980
- Tavera FJ, Davenport WG, "Equilibrations of Copper Matte and Fayalite Slag under Controlled Partial Pressures of SO_2", Metallurgical Transactions, Vol. 10B, pp. 237-241, 1979
- Tavera FJ, Bedolla E, "Distribution of Cu, S, O, and Minor Elements between Silica-saturated Slag, Matte, and Copper – Experimental Measurements", International Journal of Mineral Processing, Vol. 29, pp. 289-309, 1990
- Toulmin (III) P, Barton (Jr) PB, "A thermodynamic study of pyrite and pyrrhotite", Geochimica et Cosmochimica Acta, Vol. 28, pp. 641-671, 1964
- Ulmer GC (Ed.), "Research Techniques for High Pressure and High Temperature", Springer-Verlag, New York, 1971

- Van Laar B, "The Magnetic Structure of Trigonal Cr_2S_3", Physics Letters, Vol. 25A, No.1, pp. 27-29, 1967
- Van Laar B. "Ferrimagnetic and Antiferrimagnetic Structures of Cr_5S_6", Physical Review, Vol. 156, No. 2, pp. 654-662, 1967
- Verein Deutscher Eisenhuttenleute, "Slag Atlas", 2nd Edition, Verlag Stahleisen, Dusseldorf, 1995
- Vermaak CF, "The Platinum-Group Metals – A Global Perspective" Pg 1 – 92, A Mintek publication, 1995
- Vogel R, Reinbasch R, "The System Iron-Chromium-Chromium Sulphide-Iron Sulphide", Arch. Eisenhuttenwes., 11(9), 457-462, 1938
- Wang SS, Kurtis AJ, Toguri JM, "Distribution of Copper-Nickel and Copper-Cobalt Alloys and Silica-Saturated Fayalite Slags", Canadian Metallurgical Quarterly Vol. 12, No. 4, pp. 383-390, 1973
- Watanabe T, "Growth of $CoCr_2S_4$ and $FeCr_2S_4$ Single Crystals by Chemical Vapour Transport", Journal of the Physical Society of Japan, Vol 32, No.5, pp. 1443, 1972
- West DRF, "Ternary Equilibrium Diagrams", 2nd Edition, Chapman and Hall, 1982
- Wills, B.A., "Mineral Processing Technology", 6th Edition, Butterworth-Heinemann, Oxford, pp. 84-90, 1997
- Yazawa A, Takeda Y, Waseda Y, "Thermodynamic Properties and Structure of Ferrite Slags and their Process Implications", Canadian Metallurgical Quarterly, Vol. 20, pp. 129-134, 1981
- Yund RA, Hall HT, "Hexagonal and Monoclinic Pyrrhotites", Economic Geology, Vol. 64, pp. 420-423, 1969

Appendix A : Experimental Gas Flows

Temp (°C) ↓	**Log pS_2** →	**- 6**			**- 4**			**- 2**		
	Log pO_2 →	**- 10**	**- 8**	**- 6**	**- 10**	**- 8**	**- 6**	**- 10**	**- 8**	**- 6**
1300	CO_2 flow (cm^3min^{-1})	161	352	332	170	347	386	167	293	116
	CO flow (cm^3min^{-1})	235	48	5	230	47	2	228	40	1
	Ar flow (cm^3min^{-1})	203	199	168	199	196	4	198	166	12
	SO_2 flow (cm^3min^{-1})	1	1	95	1	10	208	7	101	471
	Total flow (cm^3min^{-1})	600	600	600	600	600	600	600	600	600
1400	CO_2 flow (cm^3min^{-1})	68	269	370	67	268	265	67	258	104
	CO flow (cm^3min^{-1})	332	131	18	331	132	13	329	126	1
	Ar flow (cm^3min^{-1})	199	199	193	200	198	140	198	192	42
	SO_2 flow (cm^3min^{-1})	1	1	19	2	2	182	6	24	453
	Total flow (cm^3min^{-1})	600	600	600	600	600	600	600	600	600
1500	CO_2 flow (cm^3min^{-1})	26	160	345	24	158	323	25	157	99
	CO flow (cm^3min^{-1})	373	241	52	374	240	49	371	237	22
	Ar flow (cm^3min^{-1})	200	198	199	200	200	186	198	196	57
	SO_2 flow (cm^3min^{-1})	1	1	4	2	2	42	6	10	422
	Total flow (cm^3min^{-1})	600	600	600	600	600	600	600	600	600

Appendix B : Full SEM Results

Run No	Temp (oC)	Log pO2	Log pS2	Phase	Subphase	Assay Point	% O	% Si	% Mg	%Al	%Cr	%S	% Fe	% Cu	Total
34	1300	-10	-6	Matte	Cu-rich Glass	Cu-rich_1	0.02	0.00	0.00	0.01	0.11	3.46	4.76	93.21	101.58
						Cu-rich_2	0.01	0.00	0.00	0.00	0.10	4.02	5.10	92.78	102.01
						Cu-rich_3	0.00	0.00	0.00	0.00	0.07	4.97	4.90	90.73	100.67
						Mean	**0.01**	**0.00**	**0.00**	**0.00**	**0.09**	**4.15**	**4.92**	**92.24**	**101.42**
				Slag	Glass	Glass_1	37.84	18.33	4.93	3.89	0.14	0.00	19.31	16.77	101.21
						Glass_2	37.17	18.26	4.92	3.74	0.16	0.00	19.49	17.95	101.70
						Glass_3	36.50	17.87	4.63	3.92	0.17	0.00	20.15	16.29	99.54
						Mean	**37.17**	**18.16**	**4.83**	**3.85**	**0.16**	**0.00**	**19.65**	**17.00**	**100.82**
					Olivine	Olivine_1	41.18	21.51	13.33	0.13	0.56	0.03	22.09	0.07	98.90
						Olivine_2	41.02	20.98	12.88	0.12	0.48	0.02	21.63	0.08	97.22
						Olivine_3	40.98	23.42	13.74	0.13	0.51	0.02	22.41	0.06	101.27
						Mean	**41.06**	**21.97**	**13.32**	**0.13**	**0.52**	**0.02**	**22.05**	**0.07**	**99.13**
					Spinel	Spinel_1	30.09	1.43	4.95	3.18	31.91	0.00	24.24	5.78	101.59
						Spinel_2	29.74	1.29	4.82	3.11	31.03	0.00	25.53	5.62	101.15
						Spinel_3	27.49	1.17	4.61	2.99	31.96	0.00	26.03	5.73	99.98
						Mean	**29.11**	**1.30**	**4.79**	**3.09**	**31.63**	**0.00**	**25.27**	**5.71**	**100.91**
32	1300	-8	-6	Matte	Fe-rich sulphide	Fe-rich_1	0.51	0.00	0.00	0.16	0.22	25.32	20.46	53.52	100.19
						Fe-rich_2	0.46	0.00	0.00	0.18	0.19	25.51	20.88	53.98	101.19
						Fe-rich_3	0.57	0.00	0.04	0.09	0.17	25.65	20.28	54.14	100.94
						Mean	**0.51**	**0.00**	**0.01**	**0.14**	**0.19**	**25.49**	**20.54**	**53.88**	**100.77**
					Cu-rich Glass	Cu-rich_1	0.56	0.00	0.00	0.16	0.04	23.90	19.39	56.52	100.56
						Cu-rich_2	0.64	0.00	0.02	0.11	0.00	23.40	18.41	57.01	99.60
						Cu-rich_3	0.59	0.00	0.09	0.13	0.03	24.00	17.11	58.66	100.61
						Cu-rich_4	0.66	0.00	0.05	0.12	0.00	25.18	18.71	56.73	101.43
						Mean	**0.61**	**0.00**	**0.04**	**0.13**	**0.02**	**24.12**	**18.40**	**57.23**	**100.55**
					Cu	Cu_1	0.95	0.00	0.00	0.10	0.00	1.71	6.64	90.65	100.06
						Cu_2	0.59	0.00	0.00	0.18	0.01	2.45	8.55	88.25	100.02
						Cu_3	0.62	0.00	0.00	0.14	0.01	1.94	7.04	90.45	100.19
						Mean	**0.72**	**0.00**	**0.00**	**0.14**	**0.01**	**2.03**	**7.41**	**89.78**	**100.09**
				Slag	Glass	Glass_1	37.59	19.05	4.28	3.20	0.24	0.14	36.29	0.14	100.93
						Glass_2	36.98	18.96	4.25	3.17	0.25	0.16	37.41	0.09	101.28
						Glass_3	37.61	18.29	4.30	3.22	0.22	0.14	36.57	0.11	100.47
						Mean	**37.39**	**18.77**	**4.28**	**3.20**	**0.24**	**0.15**	**36.76**	**0.11**	**100.89**
					Olivine	Olivine_1	41.27	23.78	12.84	0.15	0.37	0.09	21.35	0.12	99.96
						Olivine_2	40.90	23.94	13.04	0.14	0.43	0.08	21.60	0.15	100.30
						Olivine_3	41.11	23.87	12.51	0.13	0.42	0.11	21.57	0.10	99.83
						Mean	**41.10**	**23.86**	**12.80**	**0.14**	**0.41**	**0.10**	**21.51**	**0.13**	**100.03**
					Spinel	Spinel_1	28.58	0.09	2.09	1.82	37.54	0.00	28.47	0.00	98.59
						Spinel_2	28.56	0.07	2.11	1.79	38.62	0.00	28.84	0.00	100.00
						Spinel_3	28.48	0.04	2.07	1.79	39.47	0.00	28.94	0.00	100.79
						Mean	**28.54**	**0.07**	**2.09**	**1.80**	**38.54**	**0.00**	**28.75**	**0.00**	**99.80**
29	1300	-6	-6	Matte	Cu-rich Glass	Cu-rich_1	0.03	0.00	0.00	0.10	0.12	19.97	6.65	74.43	101.31
						Cu-rich_2	0.05	0.00	0.02	0.11	0.07	19.36	6.18	73.96	99.75
						Cu-rich_3	0.02	0.00	0.00	0.06	0.09	19.47	6.47	74.26	100.37
						Mean	**0.03**	**0.00**	**0.01**	**0.09**	**0.10**	**19.60**	**6.43**	**74.22**	**100.48**
					Cu	Cu_1	0.32	0.00	0.00	0.23	0.01	0.06	0.75	99.71	101.07
						Cu_2	0.36	0.00	0.00	0.18	0.01	0.27	1.54	99.09	101.44
						Cu_3	0.94	0.00	0.00	0.18	0.02	0.09	0.77	98.73	100.75
						Mean	**0.54**	**0.00**	**0.00**	**0.20**	**0.01**	**0.14**	**1.02**	**99.18**	**101.08**
				Slag	Glass	Glass_1	36.46	15.83	5.89	3.91	0.11	0.20	38.20	0.08	100.67
						Glass_2	37.65	16.61	3.31	5.29	0.15	0.66	37.08	0.17	100.91
						Glass_3	36.93	16.22	4.74	4.89	0.14	0.61	37.92	0.12	101.57
						Mean	**37.01**	**16.22**	**4.64**	**4.70**	**0.13**	**0.49**	**37.73**	**0.13**	**101.05**
					Olivine	Olivine_1	38.47	17.18	15.16	0.13	0.45	0.04	30.01	0.09	101.53
						Olivine_2	37.90	16.90	15.32	0.14	0.56	0.02	29.29	0.03	100.16
						Olivine_3	37.90	16.89	14.90	0.12	0.49	0.00	30.23	0.05	100.57
						Mean	**38.09**	**16.99**	**15.12**	**0.13**	**0.50**	**0.02**	**29.85**	**0.06**	**100.76**
					Spinel	Spinel_1	26.69	0.12	2.95	2.56	33.85	0.02	34.57	0.05	100.82
						Spinel_2	28.35	0.27	2.54	2.91	31.21	0.00	34.60	0.03	99.90
						Spinel_3	27.84	0.15	2.22	1.78	35.80	0.00	33.43	0.04	101.28
						Mean	**27.63**	**0.18**	**2.57**	**2.42**	**33.62**	**0.01**	**34.20**	**0.04**	**100.67**

Run No	Temp (oC)	Log pO2	Log pS2	Phase	Subphase	Assay Point	% O	% Si	% Mg	%Al	%Cr	%S	% Fe	% Cu	Total
36	1300	-10	-4	Matte	Cu-rich Glass	Cu-rich_1	0.00	0.00	0.00	0.00	0.00	27.48	21.12	52.42	101.01
						Cu-rich_2	0.00	0.00	0.00	0.00	0.00	27.49	21.09	52.46	101.05
						Cu-rich_3	0.00	0.00	0.00	0.00	0.00	27.34	20.94	51.88	100.16
						Mean	**0.00**	**0.00**	**0.00**	**0.00**	**0.00**	**27.44**	**21.05**	**52.25**	**100.74**
					Fe-rich sulphide	Fe-rich_1	0.77	0.00	0.00	0.00	0.11	24.46	32.65	43.03	101.01
						Fe-rich_2	0.79	0.00	0.00	0.00	0.14	24.57	32.13	42.85	100.49
						Fe-rich_3	0.82	0.00	0.00	0.00	0.10	24.63	31.98	42.99	100.53
						Mean	**0.80**	**0.00**	**0.00**	**0.00**	**0.12**	**24.56**	**32.25**	**42.96**	**100.68**
				Slag	Olivine	Olivine_1	42.97	25.38	12.38	0.22	0.73	0.04	19.13	0.06	100.90
						Olivine_2	42.65	25.67	12.87	0.24	0.75	0.10	18.80	0.12	101.20
						Olivine_3	42.97	25.53	12.69	0.24	0.72	0.05	18.68	0.07	100.96
						Mean	**42.86**	**25.53**	**12.65**	**0.23**	**0.73**	**0.06**	**18.87**	**0.08**	**101.02**
					Glass	Glass_1	39.11	23.16	8.25	2.20	0.46	0.38	26.14	0.32	100.01
						Glass_2	39.19	22.95	8.22	2.24	0.49	0.41	26.19	0.27	99.97
						Glass_3	38.86	23.04	8.27	2.19	0.47	0.39	26.15	0.29	99.68
						Mean	**39.05**	**23.05**	**8.25**	**2.21**	**0.48**	**0.39**	**26.16**	**0.30**	**99.88**
					Spinel	Spinel_1	30.48	0.75	2.98	2.64	38.57	0.16	24.54	0.14	100.27
						Spinel_2	30.46	0.69	3.04	2.62	38.69	0.09	24.76	0.11	100.47
						Spinel_3	30.48	0.72	3.01	2.60	39.03	0.13	25.07	0.17	101.22
						Mean	**30.48**	**0.72**	**3.01**	**2.62**	**38.76**	**0.13**	**24.79**	**0.14**	**100.65**
25	1300	-8	-4	Matte	Cu-rich Glass	Cu-rich_1	1.13	0.00	0.00	0.15	0.01	25.17	12.27	61.62	100.35
						Cu-rich_2	1.79	0.00	0.06	0.15	0.01	25.40	12.18	61.96	101.55
						Cu-rich_3	1.75	0.00	0.06	0.12	0.01	25.22	11.69	62.71	101.57
						Mean	**1.56**	**0.00**	**0.04**	**0.14**	**0.01**	**25.26**	**12.05**	**62.10**	**101.16**
					Cu	Cu_1	0.89	0.00	0.00	0.26	0.00	0.08	1.57	96.89	99.69
						Cu_2	0.90	0.00	0.00	0.22	0.00	0.08	1.59	96.76	99.56
						Cu_3	0.71	0.00	0.00	0.19	0.01	0.07	1.63	96.99	99.60
						Mean	**0.83**	**0.00**	**0.00**	**0.23**	**0.00**	**0.08**	**1.60**	**96.88**	**99.61**
					Fe-rich sulphide	Fe-rich_1	13.26	0.10	0.04	0.12	0.16	15.87	36.08	35.77	101.39
						Fe-rich_2	13.57	0.29	0.02	0.16	0.15	12.16	38.28	34.42	99.05
						Fe-rich_3	12.79	0.22	0.06	0.15	0.18	14.44	34.81	38.99	101.65
						Mean	**13.21**	**0.20**	**0.04**	**0.14**	**0.16**	**14.16**	**36.39**	**36.39**	**100.69**
				Slag	Glass	Glass_1	35.40	15.29	7.28	2.25	0.10	0.26	39.87	0.20	100.66
						Glass_2	35.06	15.47	7.05	2.94	0.26	0.32	39.77	0.21	101.07
						Glass_3	34.38	14.49	7.70	2.20	0.24	0.35	40.03	0.09	99.47
						Mean	**34.95**	**15.08**	**7.34**	**2.46**	**0.20**	**0.31**	**39.89**	**0.17**	**100.40**
					Olivine	Olivine_1	36.61	15.16	15.86	0.16	0.77	0.02	32.28	0.07	100.94
						Olivine_2	36.71	16.12	15.78	0.12	0.81	0.08	32.22	0.03	101.86
						Olivine_3	35.89	15.98	14.20	0.18	0.92	0.11	32.86	0.06	100.20
						Mean	**36.40**	**15.75**	**15.28**	**0.15**	**0.84**	**0.07**	**32.45**	**0.05**	**101.00**
					Spinel	Spinel_1	27.59	0.13	2.22	0.86	39.86	0.00	30.45	0.00	101.10
						Spinel_2	28.53	0.09	2.27	0.92	39.52	0.02	28.39	0.01	99.74
						Spinel_3	28.45	0.14	2.00	0.37	40.38	0.00	28.32	0.03	99.69
						Mean	**28.19**	**0.12**	**2.16**	**0.71**	**39.92**	**0.01**	**29.05**	**0.01**	**100.18**
28	1300	-6	-4	Matte	Cu-rich Glass	Cu-rich_1	0.25	0.00	0.00	0.13	0.12	21.61	5.35	74.18	101.61
						Cu-rich_2	0.24	0.00	0.00	0.14	0.10	20.48	6.03	73.09	100.05
						Cu-rich_3	0.35	0.00	0.00	0.14	0.11	21.57	5.40	74.42	101.98
						Mean	**0.28**	**0.00**	**0.00**	**0.13**	**0.11**	**21.22**	**5.59**	**73.90**	**101.23**
				Slag	Olivine	Olivine_1	41.32	24.87	12.90	0.13	0.88	0.03	20.43	0.14	100.69
						Olivine_2	41.64	24.72	13.78	0.29	0.73	0.03	19.98	0.06	101.23
						Olivine_3	41.93	25.12	13.06	0.12	0.79	0.04	20.39	0.05	101.49
						Mean	**41.63**	**24.90**	**13.24**	**0.18**	**0.80**	**0.03**	**20.26**	**0.08**	**101.13**
					Glass	Glass_1	37.23	19.13	1.03	7.44	0.08	0.49	36.07	0.46	101.94
						Glass_2	37.14	19.47	1.45	7.13	0.25	0.30	35.14	0.31	101.19
						Glass_3	36.24	18.24	1.14	7.67	0.27	0.09	35.81	0.06	99.52
						Mean	**36.87**	**18.95**	**1.20**	**7.42**	**0.20**	**0.29**	**35.67**	**0.28**	**100.88**
					Spinel	Spinel_1	28.90	1.14	2.80	0.91	37.42	0.19	28.75	0.01	100.10
						Spinel_2	29.51	0.18	2.29	0.09	42.93	0.00	26.44	0.00	101.45
						Spinel_3	29.11	0.83	2.43	0.16	38.15	0.06	27.51	0.00	98.25
						Spinel_4	29.16	0.65	2.39	0.58	40.80	0.05	25.86	0.00	99.49
						Mean	**29.17**	**0.70**	**2.48**	**0.43**	**39.83**	**0.07**	**27.14**	**0.00**	**99.82**

Run No	Temp (oC)	Log pO2	Log pS2	Phase	Subphase	Assay Point	% O	% Si	% Mg	%Al	%Cr	%S	% Fe	% Cu	Total
						Fe-rich_1	0.64	0.00	0.07	0.00	0.19	25.10	34.40	39.12	99.51
					Fe-rich sulphide	Fe-rich_2	0.61	0.00	0.00	0.01	0.25	24.51	34.29	40.55	100.21
						Fe-rich_3	0.80	0.00	0.03	0.01	0.21	25.13	33.66	40.68	100.51
				Matte		**Mean**	**0.68**	**0.00**	**0.03**	**0.01**	**0.22**	**24.91**	**34.12**	**40.12**	**100.08**
						Cu-rich_1	0.00	0.00	0.00	0.00	0.00	26.65	20.76	51.80	99.21
					Cu-rich Glass	Cu-rich_2	0.00	0.00	0.00	0.00	0.00	26.61	21.40	52.20	100.21
						Cu-rich_3	0.00	0.00	0.00	0.00	0.00	26.81	22.46	51.36	100.64
						Mean	**0.00**	**0.00**	**0.00**	**0.00**	**0.00**	**26.69**	**21.54**	**51.79**	**100.02**
						Olivine_1	43.25	25.23	12.46	0.22	0.57	0.05	19.00	0.08	100.85
37	1300	-10	-2		Olivine	Olivine_2	43.22	25.17	12.41	0.20	0.58	0.09	19.14	0.07	100.89
						Olivine_3	43.35	25.37	12.53	0.24	0.62	0.07	19.23	0.04	101.45
						Mean	**43.27**	**25.26**	**12.47**	**0.22**	**0.59**	**0.07**	**19.12**	**0.06**	**101.06**
						Glass_1	41.64	23.13	2.35	7.21	0.51	0.50	25.32	0.20	100.86
					Glass	Glass_2	39.95	21.10	2.89	7.95	0.19	0.71	27.99	0.31	101.08
				Slag		Glass_3	40.73	21.48	2.64	7.47	0.27	0.64	27.53	0.27	101.03
						Mean	**40.78**	**21.90**	**2.62**	**7.54**	**0.32**	**0.62**	**26.95**	**0.26**	**100.99**
						Spinel_1	28.83	0.13	2.36	1.51	42.01	0.03	25.29	0.00	100.16
					Spinel	Spinel_2	29.51	0.13	2.53	2.01	40.82	0.03	24.49	0.01	99.52
						Spinel_3	29.47	0.12	2.41	1.84	41.58	0.02	24.78	0.00	100.23
						Mean	**29.27**	**0.13**	**2.43**	**1.79**	**41.47**	**0.03**	**24.85**	**0.00**	**99.97**
						Cu-rich_1	0.04	0.00	0.00	0.05	0.09	25.60	21.98	52.93	100.67
					Cu-rich Glass	Cu-rich_2	0.31	0.02	0.00	0.03	0.07	24.06	22.51	52.33	99.32
						Cu-rich_3	0.71	0.00	0.00	0.02	0.08	24.24	23.62	51.57	100.25
						Mean	**0.35**	**0.01**	**0.00**	**0.03**	**0.08**	**24.63**	**22.70**	**52.27**	**100.08**
				Matte		Fe-rich_1	1.17	0.00	0.30	0.06	0.24	22.65	33.63	40.18	98.23
					Fe-rich sulphide	Fe-rich_2	1.96	0.00	0.10	0.12	0.31	21.40	34.00	41.34	99.22
38	1300	-8	-2			Fe-rich_3	1.74	0.02	0.00	0.16	0.26	21.98	34.57	41.92	100.65
						Mean	**1.62**	**0.01**	**0.13**	**0.11**	**0.27**	**22.01**	**34.07**	**41.15**	**99.37**
						Glass_1	38.00	6.60	7.78	16.50	0.53	0.27	31.24	0.03	100.95
				Slag	Glass	Glass_2	38.09	4.38	8.41	16.77	0.56	0.67	30.79	0.63	100.30
						Glass_3	37.57	7.14	6.82	16.66	0.56	0.31	30.85	0.09	99.99
						Mean	**37.89**	**6.04**	**7.67**	**16.65**	**0.55**	**0.41**	**30.96**	**0.25**	**100.41**
						Cu-rich_1	0.12	0.00	0.06	0.12	0.03	27.77	20.82	51.62	100.53
					Cu-rich Glass	Cu-rich_2	0.34	0.01	0.04	0.13	0.00	27.98	20.57	51.48	100.53
						Cu-rich_3	0.56	0.00	0.03	0.15	0.05	27.63	20.66	51.64	100.72
						Mean	**0.34**	**0.00**	**0.04**	**0.13**	**0.03**	**27.79**	**20.68**	**51.58**	**100.59**
						Cu_1	0.54	0.00	0.16	0.00	0.02	8.19	8.44	84.15	101.51
					Cu	Cu_2	0.90	0.00	0.20	0.00	0.00	7.25	7.76	85.37	101.49
				Matte		Cu_3	0.89	0.00	0.21	0.00	0.03	6.55	8.06	84.35	100.09
						Mean	**0.78**	**0.00**	**0.19**	**0.00**	**0.02**	**7.33**	**8.09**	**84.63**	**101.03**
						Fe-rich_1	16.73	0.07	0.15	0.11	0.43	12.49	45.59	24.77	100.35
						Fe-rich_2	16.43	0.85	0.08	0.15	0.24	11.24	46.93	22.73	98.65
					Fe-rich sulphide	Fe-rich_3	18.66	0.37	0.24	0.17	1.52	10.22	45.51	25.31	101.99
						Fe-rich_4	18.15	0.82	0.15	0.18	0.31	11.83	46.57	24.09	102.09
27	1300	-6	-2			**Mean**	**17.49**	**0.53**	**0.16**	**0.15**	**0.62**	**11.44**	**46.15**	**24.23**	**100.77**
						Glass_1	40.32	22.13	1.97	7.32	0.54	0.31	28.43	0.15	101.17
					Glass	Glass_2	38.96	22.46	1.85	7.58	0.47	0.37	28.36	0.14	100.19
						Glass_3	39.77	21.95	1.92	7.64	0.52	0.33	29.02	0.16	101.33
						Mean	**39.68**	**22.18**	**1.91**	**7.51**	**0.51**	**0.34**	**28.60**	**0.15**	**100.90**
						Olivine_1	41.39	24.35	11.77	0.21	0.72	0.04	20.47	0.06	99.03
				Slag	Olivine	Olivine_2	41.26	24.58	11.63	0.22	0.67	0.03	20.68	0.05	99.14
						Olivine_3	41.29	24.43	12.14	0.21	0.65	0.05	21.88	0.05	100.71
						Mean	**41.32**	**24.46**	**11.85**	**0.22**	**0.68**	**0.04**	**21.01**	**0.05**	**99.62**
						Spinel_1	30.60	0.11	2.79	1.63	41.40	0.03	23.79	0.01	100.37
					Spinel	Spinel_2	30.48	0.10	2.88	1.75	40.77	0.03	23.92	0.01	99.94
						Spinel_3	31.09	0.13	2.97	1.67	40.93	0.03	24.13	0.00	100.96
						Mean	**30.73**	**0.12**	**2.88**	**1.69**	**41.03**	**0.03**	**23.95**	**0.01**	**100.42**

Run No	Temp (oC)	Log pO2	Log pS2	Phase	Subphase	Assay Point	% O	% Si	% Mg	%Al	%Cr	%S	% Fe	% Cu	Total
44	1400	-10	-6	Matte	Cu-rich Glass	Cu-rich_1	0.24	0.00	0.07	0.11	0.02	27.65	20.36	52.03	100.49
						Cu-rich_2	0.45	0.00	0.02	0.09	0.05	23.41	22.92	52.80	99.72
						Cu-rich_3	0.86	0.00	0.09	0.12	0.03	24.75	23.51	51.65	101.01
						Mean	**0.52**	**0.00**	**0.06**	**0.11**	**0.03**	**25.27**	**22.27**	**52.16**	**100.41**
					Fe-rich sulphide	Fe-rich_1	0.23	0.00	0.00	0.09	0.28	31.36	56.42	11.47	99.85
						Fe-rich_2	0.26	0.00	0.00	0.05	0.31	32.52	55.87	11.57	100.57
						Fe-rich_3	0.21	0.00	0.00	0.06	0.26	32.90	55.85	12.20	101.47
						Mean	**0.23**	**0.00**	**0.00**	**0.07**	**0.29**	**32.26**	**56.05**	**11.74**	**100.63**
					Spinel	Spinel_1	22.90	0.26	1.97	0.28	31.73	5.45	26.28	13.67	102.55
						Spinel_2	22.28	0.23	1.53	0.27	31.33	5.92	26.28	12.60	100.44
						Spinel_3	23.24	0.28	0.89	0.19	30.88	5.72	28.07	11.02	100.29
						Spinel_4	21.84	0.27	1.17	0.20	28.85	6.92	28.18	13.04	100.48
						Mean	**22.56**	**0.26**	**1.39**	**0.24**	**30.70**	**6.00**	**27.20**	**12.58**	**100.94**
				Slag	Glass	Glass_1	40.64	8.99	7.15	20.10	0.69	0.27	20.86	0.17	98.87
						Glass_2	40.73	8.85	7.02	20.13	0.67	0.33	21.10	0.10	98.92
						Glass_3	41.02	8.88	7.11	20.08	0.67	0.29	21.42	0.15	99.60
						Mean	**40.80**	**8.91**	**7.09**	**20.10**	**0.68**	**0.30**	**21.12**	**0.14**	**99.13**
43	1400	-8	-6	Matte	Cu-rich Glass	Cu-rich_1	0.20	0.02	0.00	0.12	0.01	25.64	22.13	51.66	99.78
						Cu-rich_2	0.26	0.00	0.04	0.13	0.04	27.54	22.31	51.85	102.18
						Cu-rich_3	0.00	0.00	0.07	0.09	0.01	26.67	25.14	48.47	100.45
						Mean	**0.15**	**0.01**	**0.04**	**0.11**	**0.02**	**26.62**	**23.20**	**50.66**	**100.80**
					Fe-rich sulphide	Fe-rich_1	0.19	0.05	0.04	0.09	0.83	30.90	60.28	8.65	101.04
						Fe-rich_2	0.74	0.03	0.07	0.05	0.75	31.09	59.31	9.36	101.39
						Fe-rich_3	0.90	0.06	0.10	0.06	0.78	31.33	59.00	8.93	101.17
						Mean	**0.61**	**0.05**	**0.07**	**0.07**	**0.79**	**31.11**	**59.53**	**8.98**	**101.20**
				Slag	Glass	Glass_1	38.05	21.59	7.57	2.32	0.68	0.31	30.43	0.02	100.96
						Glass_2	38.95	20.70	6.64	2.08	0.45	0.46	30.82	0.16	100.26
						Glass_3	39.08	20.59	6.99	2.50	0.49	0.45	31.07	0.27	101.44
						Mean	**38.69**	**20.96**	**7.06**	**2.30**	**0.54**	**0.41**	**30.77**	**0.15**	**100.89**
					Olivine	Olivine_1	39.25	18.02	24.14	0.16	0.27	0.05	18.19	0.16	100.23
						Olivine_2	38.11	18.82	25.90	0.10	0.25	0.07	18.31	0.15	101.71
						Olivine_3	40.43	17.58	22.69	0.15	0.31	0.02	19.56	0.12	100.86
						Mean	**39.26**	**18.14**	**24.25**	**0.14**	**0.28**	**0.04**	**18.68**	**0.14**	**100.93**
					Spinel	Spinel_1	32.34	0.99	5.52	0.26	38.11	0.00	23.93	0.04	101.18
						Spinel_2	32.61	2.03	5.46	0.68	38.29	0.00	21.18	0.04	100.28
						Spinel_3	33.49	1.06	5.03	0.04	40.65	0.02	19.54	0.00	99.82
						Mean	**32.81**	**1.36**	**5.33**	**0.33**	**39.02**	**0.01**	**21.55**	**0.03**	**100.43**
41	1400	-6	-6	Matte	Cu-rich Glass	Cu-rich_1	0.34	0.00	0.00	0.10	0.32	22.34	7.87	69.40	100.36
						Cu-rich_2	0.40	0.00	0.01	0.09	0.27	22.56	7.38	69.91	100.62
						Cu-rich_3	0.43	0.00	0.02	0.08	0.34	22.60	7.51	69.19	100.16
						Mean	**0.39**	**0.00**	**0.01**	**0.09**	**0.31**	**22.50**	**7.58**	**69.50**	**100.38**
					Cu	Cu_1	0.58	0.00	0.00	0.11	0.00	0.96	0.30	98.10	100.05
						Cu_2	0.50	0.00	0.00	0.19	0.00	0.71	0.40	98.68	100.48
						Cu_3	0.39	0.00	0.00	0.19	0.00	0.98	0.65	98.85	101.06
						Mean	**0.49**	**0.00**	**0.00**	**0.16**	**0.00**	**0.88**	**0.45**	**98.54**	**100.53**
				Slag	Glass	Glass_1	36.23	15.00	5.89	6.81	0.09	0.20	35.87	0.26	100.35
						Glass_2	36.55	14.98	6.00	7.08	0.07	0.18	34.62	0.21	99.68
						Glass_3	37.48	15.25	6.11	6.97	0.05	0.13	34.83	0.25	101.07
						Mean	**36.75**	**15.08**	**6.00**	**6.95**	**0.07**	**0.17**	**35.11**	**0.24**	**100.37**
					Olivine	Olivine_1	39.45	23.15	13.14	0.93	0.81	0.03	21.46	0.05	99.03
						Olivine_2	39.53	23.25	12.68	0.88	0.79	0.04	22.33	0.04	99.54
						Olivine_3	39.15	23.06	12.58	0.92	0.82	0.04	22.50	0.04	99.10
						Mean	**39.38**	**23.15**	**12.80**	**0.91**	**0.81**	**0.04**	**22.10**	**0.04**	**99.22**
					Spinel	Spinel_1	31.96	0.00	4.78	5.05	36.84	0.01	22.44	0.07	101.14
						Spinel_2	31.59	0.00	4.75	5.20	37.30	0.02	23.32	0.10	102.27
						Spinel_3	32.55	0.00	4.82	4.82	36.31	0.00	23.46	0.00	101.97
						Mean	**32.03**	**0.00**	**4.78**	**5.02**	**36.82**	**0.01**	**23.07**	**0.06**	**101.79**

Run No	Temp (oC)	Log pO2	Log pS2	Phase	Subphase	Assay Point	% O	% Si	% Mg	%Al	%Cr	%S	% Fe	% Cu	Total
45	1400	-10	-4	Matte	Cu-rich Glass	Cu-rich_1	0.12	0.03	0.06	0.09	0.00	25.76	20.80	53.97	100.81
						Cu-rich_2	0.39	0.00	0.00	0.12	0.00	26.01	21.94	53.37	101.83
						Cu-rich_3	0.52	0.05	0.05	0.11	0.03	24.87	21.65	52.91	100.19
						Cu-rich_4	0.27	0.02	0.02	0.08	0.00	26.13	20.18	52.58	99.28
						Mean	**0.32**	**0.02**	**0.03**	**0.10**	**0.01**	**25.69**	**21.14**	**53.21**	**100.52**
					Fe-rich sulphide	Fe-rich_1	0.32	0.01	0.02	0.10	0.96	33.52	54.96	11.68	101.56
						Fe-rich_2	0.30	0.00	0.00	0.00	0.94	33.45	55.73	11.81	102.23
						Fe-rich_3	0.28	0.00	0.03	0.15	0.89	33.70	54.63	11.75	101.45
						Mean	**0.30**	**0.00**	**0.02**	**0.08**	**0.93**	**33.56**	**55.11**	**11.74**	**101.75**
				Slag	Glass	Glass_1	40.27	8.74	6.25	20.62	0.60	0.30	21.25	0.01	98.04
						Glass_2	41.46	9.89	7.01	20.65	0.67	0.39	20.49	0.33	100.88
						Glass_3	42.34	9.73	6.94	20.51	0.66	0.34	20.42	0.25	101.18
						Mean	**41.36**	**9.45**	**6.73**	**20.59**	**0.64**	**0.34**	**20.72**	**0.19**	**100.03**
42	1400	-8	-4	Matte	Cu-rich Glass	Cu-rich_1	0.36	0.00	0.07	0.08	0.02	25.28	22.08	52.96	100.85
						Cu-rich_2	0.27	0.00	0.01	0.07	0.02	25.40	22.70	52.85	101.31
						Cu-rich_3	0.32	0.00	0.00	0.10	0.01	25.13	22.98	51.91	100.45
						Mean	**0.32**	**0.00**	**0.03**	**0.08**	**0.02**	**25.27**	**22.59**	**52.57**	**100.87**
					Fe-rich sulphide	Fe-rich_1	0.95	0.00	0.00	0.05	0.79	30.46	59.61	8.12	99.98
						Fe-rich_2	0.39	0.00	0.00	0.11	0.83	30.43	59.10	9.91	100.77
						Fe-rich_3	0.14	0.01	0.01	0.08	0.82	30.99	60.66	8.11	100.82
						Mean	**0.49**	**0.00**	**0.00**	**0.08**	**0.82**	**30.63**	**59.79**	**8.71**	**100.52**
				Slag	Glass	Glass_1	36.04	21.35	9.08	2.29	0.64	0.32	30.30	0.35	100.35
						Glass_2	37.87	21.11	6.42	2.32	0.72	0.35	31.94	0.23	100.96
						Glass_3	38.49	22.21	4.69	2.58	0.45	0.50	30.94	0.32	100.17
						Mean	**37.47**	**21.56**	**6.73**	**2.39**	**0.60**	**0.39**	**31.06**	**0.30**	**100.50**
					Olivine	Olivine_1	38.66	16.96	23.34	0.10	0.41	0.03	20.93	0.02	100.45
						Olivine_2	39.09	17.02	23.36	0.12	0.46	0.03	21.08	0.03	101.19
						Olivine_3	38.13	17.75	23.20	0.12	0.38	0.00	20.76	0.05	100.38
						Mean	**38.63**	**17.24**	**23.30**	**0.11**	**0.42**	**0.02**	**20.92**	**0.03**	**100.67**
					Spinel	Spinel_1	30.73	2.06	4.73	0.26	39.65	0.02	22.72	0.00	100.16
						Spinel_2	30.82	1.64	5.10	0.46	41.03	0.08	21.88	0.10	101.12
						Spinel_3	31.78	2.17	5.36	0.32	39.21	0.30	22.37	0.30	101.80
						Mean	**31.11**	**1.96**	**5.06**	**0.35**	**39.96**	**0.13**	**22.32**	**0.13**	**101.03**
40	1400	-6	-4	Matte	Cu-rich Glass	Cu-rich_1	0.41	0.00	0.00	0.09	0.00	22.00	6.85	70.78	100.12
						Cu-rich_2	0.48	0.02	0.00	0.20	0.00	21.62	7.07	71.55	100.94
						Cu-rich_3	0.32	0.00	0.00	0.09	0.02	22.43	6.49	70.26	99.60
						Cu-rich_4	0.38	0.00	0.00	0.10	0.00	22.09	7.34	71.38	101.29
						Mean	**0.40**	**0.01**	**0.00**	**0.12**	**0.00**	**22.04**	**6.94**	**70.99**	**100.49**
					Cu	Cu_1	0.12	0.00	0.00	0.09	0.00	0.01	0.40	99.21	99.83
						Cu_2	0.14	0.00	0.00	0.12	0.01	0.02	0.54	98.07	98.90
						Cu_3	0.10	0.00	0.00	0.14	0.01	0.02	0.53	98.75	99.56
						Mean	**0.12**	**0.00**	**0.00**	**0.12**	**0.01**	**0.02**	**0.49**	**98.68**	**99.43**
					Fe-rich sulphide	Fe-rich_1	1.38	0.01	0.00	0.11	0.77	21.75	40.76	35.85	100.64
						Fe-rich_2	1.95	0.00	0.51	0.18	0.76	20.19	41.48	35.11	100.18
						Fe-rich_3	1.69	0.00	0.15	0.09	0.74	19.67	41.80	37.37	101.51
						Mean	**1.67**	**0.00**	**0.22**	**0.13**	**0.76**	**20.54**	**41.35**	**36.11**	**100.78**
				Slag	Glass	Glass_1	37.18	15.37	6.44	6.69	0.07	0.23	34.95	0.35	101.27
						Glass_2	37.56	15.39	4.86	7.50	0.08	0.19	34.10	0.31	99.98
						Glass_3	36.47	15.51	5.99	7.12	0.09	0.17	35.51	0.21	101.07
						Mean	**37.07**	**15.42**	**5.76**	**7.10**	**0.08**	**0.20**	**34.85**	**0.29**	**100.77**
					Olivine	Olivine_1	37.81	0.23	7.86	25.64	7.28	0.00	22.27	0.00	101.09
						Olivine_2	37.16	0.14	7.89	25.79	7.82	0.04	22.29	0.00	101.14
						Olivine_3	37.36	0.15	7.74	24.39	8.22	0.00	22.00	0.00	99.85
						Mean	**37.44**	**0.18**	**7.83**	**25.28**	**7.77**	**0.01**	**22.19**	**0.00**	**100.69**
					Spinel	Spinel_1	31.75	0.12	4.09	3.48	38.42	0.02	23.64	0.03	101.54
						Spinel_2	31.60	0.08	4.00	3.26	38.94	0.00	23.42	0.04	101.34
						Spinel_3	31.47	0.23	3.56	2.83	41.22	0.00	22.33	0.01	101.64
						Spinel_4	31.46	0.11	3.51	2.55	42.31	0.04	21.75	0.03	101.76
						Mean	**31.57**	**0.14**	**3.79**	**3.03**	**40.22**	**0.01**	**22.78**	**0.03**	**101.57**

Run No	Temp (oC)	Log pO2	Log pS2	Phase	Subphase	Assay Point	% O	% Si	% Mg	%Al	%Cr	%S	% Fe	% Cu	Total
46	1400	-10	-2	Matte	Cu-rich Glass	Cu-rich_1	0.51	0.02	0.03	0.15	0.01	24.92	20.67	53.14	99.44
						Cu-rich_2	0.34	0.02	0.10	0.15	0.06	25.44	23.42	51.93	101.46
						Cu-rich_3	0.43	0.01	0.03	0.12	0.02	26.29	21.82	52.61	101.32
						Mean	**0.43**	**0.01**	**0.05**	**0.14**	**0.03**	**25.55**	**21.97**	**52.56**	**100.74**
					Fe-rich sulphide	Fe-rich_1	0.40	0.04	0.01	0.06	1.08	32.95	59.96	7.16	101.66
						Fe-rich_2	0.23	0.03	0.01	0.04	0.97	31.81	59.54	8.83	101.46
						Fe-rich_3	0.43	0.06	0.33	0.05	0.99	31.65	57.30	9.60	100.40
						Mean	**0.35**	**0.04**	**0.12**	**0.05**	**1.01**	**32.14**	**58.93**	**8.53**	**101.17**
					Spinel	Spinel_1	29.41	0.61	0.63	0.26	28.08	7.96	25.29	9.60	101.82
						Spinel_2	28.24	0.32	0.57	0.11	26.02	8.16	25.64	10.25	99.32
						Spinel_3	28.77	0.39	0.58	0.16	27.04	7.35	25.53	9.93	99.75
						Mean	**28.81**	**0.44**	**0.59**	**0.18**	**27.05**	**7.82**	**25.49**	**9.93**	**100.30**
				Slag	Glass	Glass_1	40.04	19.19	7.12	8.59	1.31	0.54	22.47	0.40	99.66
						Glass_2	40.29	19.35	6.93	8.82	1.18	0.41	23.43	0.26	100.67
						Glass_3	39.87	19.22	7.09	8.65	1.14	0.42	22.94	0.17	99.50
						Mean	**40.07**	**19.25**	**7.05**	**8.68**	**1.21**	**0.45**	**22.95**	**0.28**	**99.94**
39	1400	-8	-2	Matte	Cu-rich Glass	Cu-rich_1	0.51	0.01	0.00	0.08	0.61	25.40	24.30	49.00	99.91
						Cu-rich_2	0.40	0.00	0.03	0.09	0.69	26.00	23.51	49.57	100.30
						Cu-rich_3	0.58	0.00	0.03	0.10	0.68	25.19	22.31	51.71	100.60
						Mean	**0.50**	**0.00**	**0.02**	**0.09**	**0.66**	**25.53**	**23.37**	**50.09**	**100.27**
					Cu	Cu_1	0.04	0.00	0.00	0.13	0.03	13.53	13.11	74.70	101.52
						Cu_2	0.48	0.00	0.00	0.11	0.01	10.23	12.94	76.89	100.66
						Cu_3	0.68	0.00	0.00	0.15	0.00	11.66	11.10	77.02	100.61
						Mean	**0.40**	**0.00**	**0.00**	**0.13**	**0.01**	**11.81**	**12.38**	**76.20**	**100.93**
				Slag	Glass	Glass_1	38.00	7.93	7.67	17.94	0.54	0.28	27.62	0.20	100.18
						Glass_2	38.65	7.73	8.07	17.63	0.48	0.25	27.18	0.14	100.11
						Glass_3	38.56	7.72	7.83	17.58	0.51	0.29	27.15	0.23	99.87
						Mean	**38.40**	**7.79**	**7.86**	**17.71**	**0.51**	**0.27**	**27.31**	**0.19**	**100.05**
					Olivine	Olivine_1	38.75	8.62	7.44	19.51	1.62	0.31	21.96	0.18	98.40
						Olivine_2	39.31	8.45	7.94	19.24	1.45	0.49	22.27	0.17	99.32
						Olivine_3	39.71	8.86	7.46	18.89	1.53	0.49	21.94	0.19	99.06
						Mean	**39.26**	**8.64**	**7.61**	**19.21**	**1.53**	**0.43**	**22.06**	**0.18**	**98.93**
					Spinel	Spinel_1	32.92	1.92	6.23	0.26	36.47	0.02	23.12	0.00	100.95
						Spinel_2	31.74	1.84	6.54	0.46	38.41	0.08	22.47	0.10	101.64
						Spinel_3	32.46	1.87	6.67	0.32	35.98	0.30	22.69	0.12	100.41
						Mean	**32.37**	**1.88**	**6.48**	**0.35**	**36.96**	**0.13**	**22.76**	**0.07**	**101.00**
47	1400	-6	-2	Matte	Cu-rich Glass	Cu-rich_1	0.12	0.00	0.00	0.09	0.05	24.82	22.41	53.47	100.97
						Cu-rich_2	0.74	0.00	0.02	0.05	0.01	24.55	20.73	52.86	98.96
						Cu-rich_3	0.05	0.01	0.06	0.08	0.06	25.85	19.71	53.18	99.00
						Mean	**0.30**	**0.01**	**0.03**	**0.07**	**0.04**	**25.07**	**20.95**	**53.17**	**99.65**
					Fe-rich sulphide	Fe-rich_1	0.34	0.00	0.00	0.05	0.92	33.02	59.61	7.96	101.89
						Fe-rich_2	0.29	0.00	0.02	0.03	0.92	33.73	59.06	7.60	101.65
						Fe-rich_3	0.34	0.00	0.07	0.05	0.93	32.67	59.85	7.79	101.70
						Mean	**0.32**	**0.00**	**0.03**	**0.04**	**0.92**	**33.14**	**59.51**	**7.79**	**101.74**
					Spinel	Spinel_1	27.40	0.09	1.74	0.63	32.48	0.02	38.49	0.05	100.91
						Spinel_2	28.14	0.11	1.69	0.68	32.73	0.00	37.42	0.03	100.81
						Spinel_3	28.22	0.10	1.58	0.66	33.02	0.00	34.12	0.04	97.75
						Mean	**27.92**	**0.10**	**1.67**	**0.66**	**32.75**	**0.01**	**36.68**	**0.04**	**99.82**
				Slag	Glass	Glass_1	39.50	19.99	8.60	7.97	0.56	0.29	21.52	0.17	98.59
						Glass_2	39.94	19.86	8.68	7.84	0.59	0.46	21.47	0.14	98.98
						Glass_3	39.79	20.16	8.76	7.86	0.56	0.53	21.53	0.15	99.33
						Mean	**39.74**	**20.00**	**8.68**	**7.89**	**0.57**	**0.43**	**21.51**	**0.15**	**98.97**

Run No	Temp (oC)	Log pO2	Log pS2	Phase	Subphase	Assay Point	% O	% Si	% Mg	%Al	%Cr	%S	% Fe	% Cu	Total
52	1500	-10	-6	Matte	Cu-rich Glass	Cu-rich_1	0.37	0.01	0.05	0.08	0.01	25.14	24.23	50.07	99.96
						Cu-rich_2	0.28	0.00	0.08	0.06	0.04	25.24	24.27	49.13	99.09
						Cu-rich_3	0.38	0.00	0.04	0.05	0.02	27.17	22.13	51.96	101.74
						Mean	**0.34**	**0.00**	**0.06**	**0.06**	**0.02**	**25.85**	**23.54**	**50.39**	**100.26**
					Fe-rich sulphide	Fe-rich_1	0.28	0.00	0.06	0.12	0.87	33.30	56.95	10.63	102.20
						Fe-rich_2	0.80	0.01	0.08	0.10	0.88	29.66	56.44	13.68	101.65
						Fe-rich_3	0.24	0.05	0.00	0.11	0.87	33.17	55.27	11.02	100.72
						Mean	**0.44**	**0.02**	**0.04**	**0.11**	**0.87**	**32.04**	**56.22**	**11.77**	**101.52**
				Slag	Glass	Glass_1	41.23	17.32	6.95	10.26	0.49	0.43	23.86	0.37	100.91
						Glass_2	41.88	17.19	5.97	13.30	0.20	0.23	21.20	0.11	100.07
						Glass_3	41.87	17.17	6.04	12.73	0.25	0.32	22.07	0.40	100.83
						Mean	**41.66**	**17.23**	**6.32**	**12.10**	**0.31**	**0.33**	**22.38**	**0.29**	**100.60**
					Olivine	Olivine_1	40.85	0.14	9.11	33.52	0.57	0.00	15.39	0.00	99.57
						Olivine_2	40.85	0.15	9.00	34.02	0.33	0.00	15.25	0.00	99.60
						Olivine_3	40.78	0.15	9.61	33.40	0.56	0.00	14.99	0.00	99.50
						Mean	**40.83**	**0.15**	**9.24**	**33.65**	**0.49**	**0.00**	**15.21**	**0.00**	**99.56**
					Spinel	Spinel_1	32.65	0.14	4.84	5.09	40.26	0.01	18.48	0.00	101.47
						Spinel_2	32.40	0.15	4.83	4.25	42.31	0.01	18.43	0.00	102.38
						Spinel_3	32.83	0.16	4.89	6.24	38.49	0.01	18.09	0.08	100.79
						Mean	**32.63**	**0.15**	**4.85**	**5.19**	**40.36**	**0.01**	**18.33**	**0.03**	**101.54**
55	1500	-8	-6	Matte	Cu-rich Glass	Cu-rich_1	0.34	0.00	0.00	0.13	0.00	28.40	21.67	51.91	102.45
						Cu-rich_2	0.35	0.00	0.00	0.14	0.00	25.80	22.80	51.51	100.59
						Cu-rich_3	0.37	0.00	0.00	0.10	0.00	26.35	22.81	51.42	101.04
						Mean	**0.35**	**0.00**	**0.00**	**0.12**	**0.00**	**26.85**	**22.42**	**51.61**	**101.36**
					Fe-rich sulphide	Fe-rich_1	0.29	0.00	0.04	0.13	0.97	29.73	52.45	17.66	101.27
						Fe-rich_2	0.16	0.03	0.03	0.13	0.99	28.17	51.54	20.39	101.44
						Fe-rich_3	0.28	0.00	0.06	0.14	0.96	29.98	50.38	20.02	101.82
						Mean	**0.24**	**0.01**	**0.04**	**0.13**	**0.97**	**29.30**	**51.46**	**19.36**	**101.51**
				Slag	Glass	Glass_1	35.48	15.61	5.91	9.76	2.41	0.29	26.63	0.17	96.27
						Glass_2	37.87	16.23	6.20	10.11	2.43	0.30	26.45	0.18	99.75
						Glass_3	37.03	16.24	5.54	9.65	2.31	0.33	27.33	0.18	98.62
						Mean	**36.79**	**16.03**	**5.88**	**9.84**	**2.39**	**0.31**	**26.80**	**0.17**	**98.21**
					Olivine	Olivine_1	37.78	0.48	7.94	26.03	10.59	0.04	17.37	0.01	100.25
						Olivine_2	37.70	0.11	7.37	24.56	12.85	0.00	17.16	0.00	99.75
						Olivine_3	37.67	0.16	8.02	25.97	10.04	0.00	17.04	0.04	98.94
						Mean	**37.72**	**0.25**	**7.78**	**25.52**	**11.16**	**0.01**	**17.19**	**0.02**	**99.65**
					Spinel	Spinel_1	30.45	0.15	4.23	5.17	41.40	0.01	18.62	0.00	100.03
						Spinel_2	29.32	0.10	3.82	5.34	37.94	1.61	19.56	1.22	98.92
						Spinel_3	31.34	0.07	4.57	6.86	38.61	0.02	18.65	0.01	100.12
						Mean	**30.37**	**0.11**	**4.21**	**5.79**	**39.32**	**0.55**	**18.94**	**0.41**	**99.69**
50	1500	-6	-6	Matte	Cu-rich Glass	Cu-rich_1	0.72	0.00	0.00	0.20	0.02	19.70	0.47	77.69	98.80
						Cu-rich_2	0.58	0.00	0.00	0.19	0.03	19.80	0.69	77.70	98.99
						Cu-rich_3	1.12	0.00	0.01	0.14	0.02	19.43	0.47	77.22	98.43
						Mean	**0.81**	**0.00**	**0.00**	**0.18**	**0.03**	**19.64**	**0.54**	**77.54**	**98.74**
					Fe-rich sulphide	Fe-rich_1	1.35	0.00	0.01	0.11	0.93	15.15	52.23	30.84	100.62
						Fe-rich_2	0.79	0.00	0.03	0.13	0.92	14.50	51.48	32.53	100.38
						Fe-rich_3	0.94	0.00	0.02	0.11	0.93	14.74	50.96	32.67	100.39
						Mean	**1.03**	**0.00**	**0.02**	**0.12**	**0.93**	**14.80**	**51.56**	**32.01**	**100.46**
				Slag	Glass	Glass_1	36.70	4.81	11.07	14.57	0.11	0.08	29.55	1.84	98.72
						Glass_2	36.67	4.79	11.07	14.54	0.12	0.07	29.55	2.07	98.87
						Glass_3	36.26	4.85	10.94	14.47	0.16	0.10	30.10	1.08	97.96
						Mean	**36.54**	**4.81**	**11.02**	**14.53**	**0.13**	**0.08**	**29.74**	**1.66**	**98.52**
					Olivine	Olivine_1	35.75	6.94	26.49	0.15	7.93	0.03	21.96	0.10	99.35
						Olivine_2	36.55	7.14	28.19	0.15	5.68	0.00	21.46	0.08	99.25
						Olivine_3	35.24	6.65	25.60	0.12	8.54	0.00	21.88	0.12	98.14
						Mean	**35.84**	**6.91**	**26.76**	**0.14**	**7.39**	**0.01**	**21.76**	**0.10**	**98.91**
					Spinel	Spinel_1	31.43	0.19	5.06	4.31	39.38	0.01	19.74	0.01	100.14
						Spinel_2	31.47	0.22	5.18	4.36	39.62	0.01	19.93	0.01	100.81
						Spinel_3	31.58	0.20	5.21	4.41	39.88	0.02	19.83	0.02	101.15
						Mean	**31.49**	**0.20**	**5.15**	**4.36**	**39.63**	**0.01**	**19.83**	**0.01**	**100.70**

Run No	Temp (oC)	Log pO2	Log pS2	Phase	Subphase	Assay Point	% O	% Si	% Mg	%Al	%Cr	%S	% Fe	% Cu	Total
57	1500	-10	-4	Matte	Cu-rich Glass	Cu-rich_1	0.20	0.00	0.09	0.12	0.09	23.88	16.23	59.91	100.52
						Cu-rich_2	0.69	0.00	0.06	0.06	0.11	25.33	17.88	56.45	100.57
						Cu-rich_3	0.96	0.00	0.04	0.12	0.09	24.29	17.53	57.70	100.72
						Mean	**0.61**	**0.00**	**0.07**	**0.10**	**0.09**	**24.50**	**17.21**	**58.02**	**100.60**
					Fe-rich sulphide	Fe-rich_1	1.90	0.00	0.14	0.03	1.12	29.99	46.79	19.74	99.71
						Fe-rich_2	1.76	0.01	0.06	0.07	1.09	32.42	47.58	18.78	101.78
						Fe-rich_3	1.04	0.02	0.02	0.09	1.06	33.80	48.42	17.00	101.44
						Mean	**1.57**	**0.01**	**0.07**	**0.06**	**1.09**	**32.07**	**47.60**	**18.51**	**100.98**
					Spinel	Spinel_1	27.88	0.24	0.38	0.10	37.99	2.06	29.57	2.36	100.59
						Spinel_2	27.83	0.11	0.45	0.06	37.48	2.16	30.21	2.89	101.20
						Spinel_3	27.94	0.04	0.50	0.05	36.40	2.27	30.01	3.09	100.31
						Mean	**27.88**	**0.13**	**0.44**	**0.07**	**37.29**	**2.17**	**29.93**	**2.78**	**100.70**
				Slag	Glass	Glass_1	42.44	19.16	8.37	10.85	3.43	0.25	15.35	0.11	99.95
						Glass_2	42.58	19.26	8.48	10.82	3.44	0.23	15.33	0.15	100.28
						Glass_3	42.44	19.05	8.44	10.87	3.44	0.24	15.28	0.25	100.00
						Glass_4	43.49	19.65	8.65	11.19	3.39	0.29	15.20	0.08	101.95
						Mean	**42.74**	**19.28**	**8.49**	**10.93**	**3.42**	**0.25**	**15.29**	**0.15**	**100.54**
54	1500	-8	-4	Matte	Cu-rich Glass	Cu-rich_1	0.24	0.03	0.06	0.09	0.15	27.21	23.29	50.34	101.39
						Cu-rich_2	0.37	0.01	0.00	0.03	0.13	26.96	22.97	50.43	100.89
						Cu-rich_3	0.50	0.03	0.12	0.08	0.12	27.54	22.90	49.70	100.98
						Mean	**0.37**	**0.02**	**0.06**	**0.07**	**0.13**	**27.24**	**23.05**	**50.16**	**101.09**
					Fe-rich sulphide	Fe-rich_1	0.53	0.01	0.25	0.04	0.96	28.07	50.52	20.53	100.92
						Fe-rich_2	0.48	0.02	0.06	0.04	0.97	28.72	50.73	20.49	101.52
						Fe-rich_3	0.57	0.04	0.10	0.05	0.95	28.93	51.86	19.48	101.98
						Mean	**0.53**	**0.02**	**0.14**	**0.04**	**0.96**	**28.58**	**51.04**	**20.17**	**101.48**
				Slag	Glass	Glass_1	38.69	16.16	6.34	11.07	3.38	0.30	24.46	0.04	100.44
						Glass_2	38.26	16.04	6.60	11.32	3.36	0.49	24.30	0.92	101.29
						Glass_3	38.36	16.03	6.32	11.33	3.38	0.26	24.49	0.07	100.25
						Mean	**38.44**	**16.08**	**6.42**	**11.24**	**3.37**	**0.35**	**24.42**	**0.34**	**100.66**
49	1500	-6	-4	Matte	Cu-rich Glass	Cu-rich_1	0.80	0.00	0.00	0.15	0.00	20.39	0.62	77.59	99.55
						Cu-rich_2	1.47	0.00	0.00	0.14	0.00	20.37	0.68	76.76	99.42
						Cu-rich_3	0.67	0.00	0.00	0.16	0.00	20.22	0.40	78.61	100.05
						Mean	**0.98**	**0.00**	**0.00**	**0.15**	**0.00**	**20.32**	**0.57**	**77.65**	**99.67**
					Cu	Cu_1	0.63	0.00	0.00	0.23	0.05	0.21	0.09	97.40	98.61
						Cu_2	0.69	0.00	0.00	0.20	0.04	0.20	0.07	97.34	98.55
						Cu_3	0.67	0.00	0.00	0.19	0.06	0.19	0.08	97.48	98.68
						Mean	**0.66**	**0.00**	**0.00**	**0.21**	**0.05**	**0.20**	**0.08**	**97.41**	**98.61**
					Fe-rich sulphide	Fe-rich_1	18.26	0.08	0.00	0.13	0.93	7.93	27.35	45.12	99.79
						Fe-rich_2	18.93	0.06	0.00	0.15	0.92	7.76	29.78	43.51	101.10
						Fe-rich_3	20.37	0.20	0.00	0.13	0.94	6.38	28.37	43.43	99.82
						Mean	**19.19**	**0.11**	**0.00**	**0.13**	**0.93**	**7.36**	**28.50**	**44.02**	**100.24**
				Slag	Glass	Glass_1	38.70	15.29	4.63	10.78	0.00	0.09	30.35	1.60	101.44
						Glass_2	38.58	16.25	4.61	9.78	0.02	0.02	31.00	1.20	101.46
						Glass_3	40.26	15.32	3.53	15.52	0.03	0.04	24.19	2.16	101.04
						Mean	**39.18**	**15.62**	**4.26**	**12.03**	**0.02**	**0.05**	**28.51**	**1.65**	**101.31**
					Alumina-rich	Alumina_1	44.66	2.18	3.66	41.31	0.01	0.07	4.56	1.68	98.11
						Alumina_2	43.85	2.28	3.71	40.38	0.00	0.08	8.12	1.01	99.44
						Alumina_3	44.36	2.16	5.39	40.10	0.01	0.24	7.62	1.40	101.28
						Mean	**44.29**	**2.21**	**4.25**	**40.59**	**0.00**	**0.13**	**6.77**	**1.36**	**99.61**
					Olivine	Olivine_1	38.23	6.86	28.12	0.11	5.13	0.03	21.45	0.04	99.96
						Olivine_2	37.26	6.63	29.05	0.12	4.99	0.04	21.08	0.07	99.24
						Olivine_3	37.46	6.98	29.43	0.10	5.57	0.03	21.29	0.11	100.97
						Mean	**37.65**	**6.82**	**28.86**	**0.11**	**5.23**	**0.03**	**21.27**	**0.07**	**100.06**
					Spinel	Spinel_1	29.77	0.25	7.15	5.03	38.44	0.00	20.03	0.01	100.68
						Spinel_2	29.43	0.23	7.37	5.12	38.22	0.01	20.12	0.01	100.51
						Spinel_3	30.01	0.22	7.24	4.97	37.85	0.01	20.14	0.01	100.46
						Mean	**29.74**	**0.23**	**7.25**	**5.04**	**38.17**	**0.01**	**20.10**	**0.01**	**100.55**

Run No	Temp (oC)	Log pO2	Log pS2	Phase	Subphase	Assay Point	% O	% Si	% Mg	%Al	%Cr	%S	% Fe	% Cu	Total
56	1500	-10	-2	Matte	Cu-rich Glass	Cu-rich_1	0.37	0.00	0.00	0.14	0.13	25.98	15.36	58.44	100.42
						Cu-rich_2	0.33	0.00	0.02	0.03	0.07	26.42	17.34	55.97	100.18
						Cu-rich_3	0.33	0.00	0.00	0.12	0.00	25.80	15.59	59.04	100.87
						Mean	**0.34**	**0.00**	**0.01**	**0.10**	**0.07**	**26.06**	**16.10**	**57.82**	**100.49**
					Fe-rich sulphide	Fe-rich_1	1.53	0.00	0.02	0.07	0.86	34.67	59.70	4.41	101.26
						Fe-rich_2	1.39	0.02	0.01	0.09	0.87	30.72	59.89	8.44	101.43
						Fe-rich_3	1.31	0.03	0.00	0.09	0.86	32.90	60.28	5.73	101.19
						Mean	**1.41**	**0.01**	**0.01**	**0.08**	**0.86**	**32.76**	**59.96**	**6.19**	**101.29**
					Spinel	Spinel_1	28.09	0.10	0.21	0.06	39.45	3.30	28.39	1.09	100.68
						Spinel_2	26.80	0.15	0.25	0.08	40.97	1.32	28.86	1.76	100.20
						Spinel_3	26.92	0.09	0.26	0.02	41.94	2.43	27.97	1.38	101.02
						Spinel_4	24.07	0.19	0.16	0.08	41.70	3.43	28.21	1.52	99.35
						Mean	**26.47**	**0.13**	**0.22**	**0.06**	**41.02**	**2.62**	**28.36**	**1.44**	**100.31**
				Slag	Glass	Glass_1	40.25	18.11	7.78	10.45	7.38	0.19	14.88	0.05	99.09
						Glass_2	40.40	18.16	8.05	10.40	7.31	0.20	14.81	0.09	99.41
						Glass_3	40.84	18.31	8.04	10.48	7.37	0.19	15.12	0.04	100.39
						Mean	**40.50**	**18.19**	**7.96**	**10.44**	**7.36**	**0.19**	**14.94**	**0.06**	**99.63**
					Olivine	Olivine_1	41.44	22.09	7.08	11.33	1.29	0.26	14.08	0.02	97.58
						Olivine_2	42.26	23.19	7.79	10.42	1.32	0.24	14.46	0.01	99.68
						Olivine_3	42.33	24.23	5.02	13.04	1.03	0.18	14.76	0.00	100.58
						Mean	**42.01**	**23.17**	**6.63**	**11.60**	**1.21**	**0.23**	**14.43**	**0.01**	**99.28**
53	1500	-8	-2	Matte	Cu-rich Glass	Cu-rich_1	0.54	0.01	0.01	0.07	0.16	25.38	26.61	45.92	98.70
						Cu-rich_2	0.08	0.06	0.06	0.06	0.11	26.82	23.81	49.48	100.46
						Cu-rich_3	0.73	0.00	0.05	0.10	0.13	24.32	23.78	50.33	99.45
						Mean	**0.45**	**0.02**	**0.04**	**0.08**	**0.13**	**25.51**	**24.73**	**48.57**	**99.54**
					Fe-rich sulphide	Fe-rich_1	0.24	0.03	0.08	0.08	0.90	29.02	54.54	15.04	99.94
						Fe-rich_2	0.36	0.01	0.02	0.03	0.89	31.52	55.88	13.11	101.82
						Fe-rich_3	0.32	0.01	0.03	0.02	0.87	30.94	57.21	13.45	102.86
						Mean	**0.31**	**0.02**	**0.05**	**0.04**	**0.89**	**30.50**	**55.88**	**13.87**	**101.54**
					Spinel	Spinel_1	25.31	0.12	1.04	0.05	37.41	1.21	32.41	0.97	98.54
						Spinel_2	25.23	0.11	1.11	0.03	38.01	1.25	32.65	0.91	99.31
						Spinel_3	25.87	0.17	1.09	0.05	38.11	1.31	33.78	0.87	101.26
						Mean	**25.47**	**0.13**	**1.08**	**0.04**	**37.85**	**1.26**	**32.95**	**0.92**	**99.70**
				Slag	Glass	Glass_1	40.98	16.43	5.73	12.90	0.21	0.62	20.47	0.52	97.86
						Glass_2	41.13	16.69	5.74	13.16	0.24	0.22	21.55	0.10	98.82
						Glass_3	41.09	16.67	5.59	13.35	0.19	0.23	21.27	0.10	98.49
						Glass_4	41.12	16.76	5.97	12.55	0.29	0.21	21.82	0.30	99.01
						Mean	**41.08**	**16.64**	**5.76**	**12.99**	**0.23**	**0.32**	**21.28**	**0.25**	**98.55**
					Alumina-rich	Alumina_1	40.28	0.16	8.89	33.13	0.30	0.02	15.64	0.00	98.42
						Alumina_2	40.26	0.20	8.94	32.68	1.13	0.02	15.77	0.00	99.00
						Alumina_3	39.96	0.14	9.19	33.82	0.46	0.02	15.12	0.00	98.70
						Mean	**40.17**	**0.17**	**9.01**	**33.21**	**0.63**	**0.02**	**15.51**	**0.00**	**98.71**
					Spinel	Spinel_1	31.45	0.15	4.19	4.49	41.64	0.01	18.43	0.06	100.41
						Spinel_2	31.20	0.19	4.10	3.42	43.28	0.00	18.35	0.02	100.57
						Spinel_3	31.10	0.14	4.07	3.76	42.65	0.00	18.45	0.00	100.16
						Mean	**31.25**	**0.16**	**4.12**	**3.89**	**42.52**	**0.00**	**18.41**	**0.03**	**100.38**
48	1500	-6	-2	Matte	Cu-rich Glass	Cu-rich_1	0.66	0.00	0.00	0.21	0.67	20.37	0.39	77.16	99.46
						Cu-rich_2	1.21	0.00	0.00	0.15	0.71	20.00	0.78	76.08	98.93
						Cu-rich_3	0.96	0.00	0.00	0.26	0.69	19.81	0.50	75.92	98.14
						Mean	**0.94**	**0.00**	**0.00**	**0.21**	**0.69**	**20.06**	**0.56**	**76.39**	**98.84**
					Cu	Cu_1	0.67	0.00	0.00	0.24	0.00	0.30	0.08	96.77	98.06
						Cu_2	0.73	0.00	0.00	0.21	0.00	0.27	0.11	97.74	99.07
						Cu_3	0.69	0.00	0.00	0.22	0.00	0.28	0.09	96.85	98.14
						Mean	**0.70**	**0.00**	**0.00**	**0.23**	**0.00**	**0.29**	**0.09**	**97.12**	**98.42**
				Slag	Glass	Glass_1	37.00	15.87	5.46	11.10	0.08	0.07	29.78	0.96	100.32
						Glass_2	37.22	15.84	5.53	12.55	0.14	0.10	28.81	1.20	101.38
						Glass_3	37.10	14.98	4.15	12.06	0.09	0.05	30.46	2.05	100.94
						Mean	**37.11**	**15.56**	**5.05**	**11.91**	**0.10**	**0.08**	**29.68**	**1.40**	**100.88**
					Alumina-rich	Alumina_1	40.16	0.16	7.59	29.44	0.04	0.03	21.46	0.10	98.99
						Alumina_2	40.36	0.12	7.97	30.14	0.07	0.02	21.80	0.09	100.57
						Alumina_3	38.98	0.13	7.79	29.87	0.08	0.05	22.04	0.12	99.08
						Mean	**39.83**	**0.14**	**7.78**	**29.82**	**0.06**	**0.03**	**21.77**	**0.11**	**99.54**
					Olivine	Olivine_1	37.20	7.27	27.52	0.12	4.89	0.00	20.45	0.05	97.51
						Olivine_2	36.99	6.97	28.10	0.13	3.51	0.04	20.95	0.10	96.79
						Olivine_3	40.16	7.56	30.01	0.14	4.02	0.02	21.49	0.07	103.46
						Mean	**38.12**	**7.27**	**28.54**	**0.13**	**4.14**	**0.02**	**20.96**	**0.08**	**99.25**

Appendix C : Scanning Electron Micrographs

Micrograph No.1 : **34 Matte**

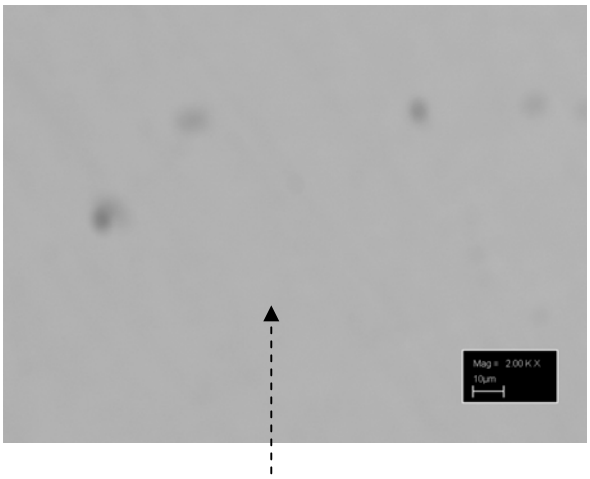

Cu- rich Glass(Matte)

Micrograph No.2 : **34 Slag**

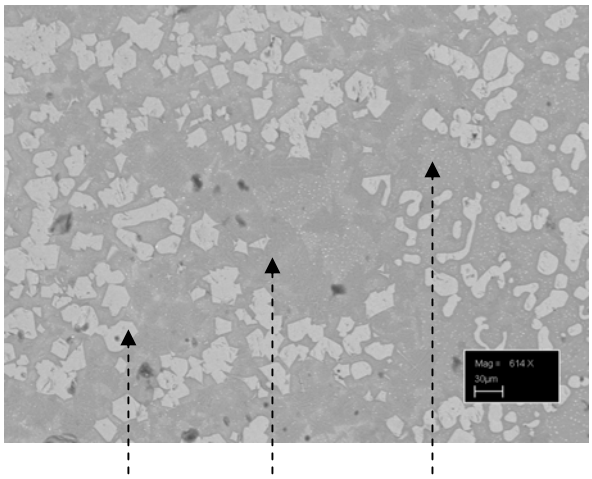

Spinel *Olivine* *Glass*

Micrograph No.3 : **32 Matte**

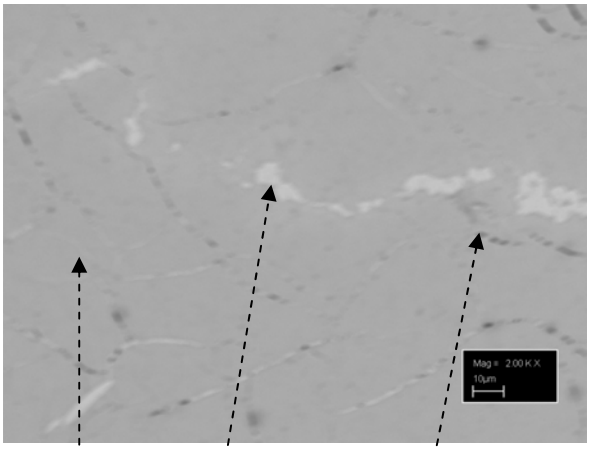

Cu-rich Glass *Cu* *Fe-rich sulphide (black spots)*

Micrograph No.4 : **32 Slag**

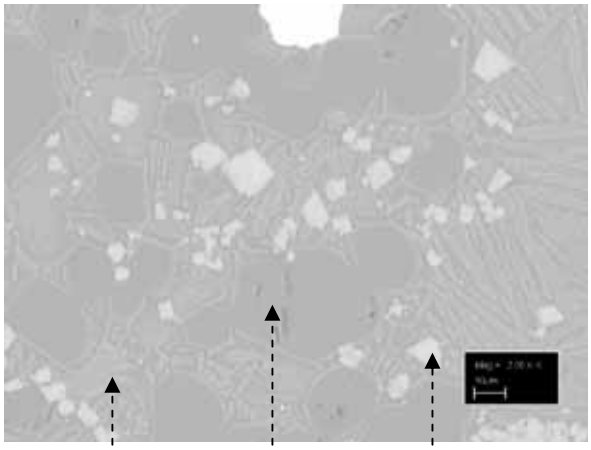

Glass *Olivine* *Spinel*

Micrograph No.5 : **29 Matte**

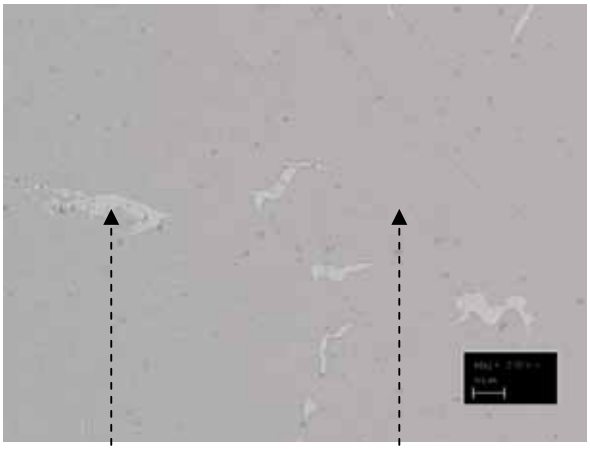

Cu *Cu-rich Glass*

Micrograph No.6 : **29 Slag**

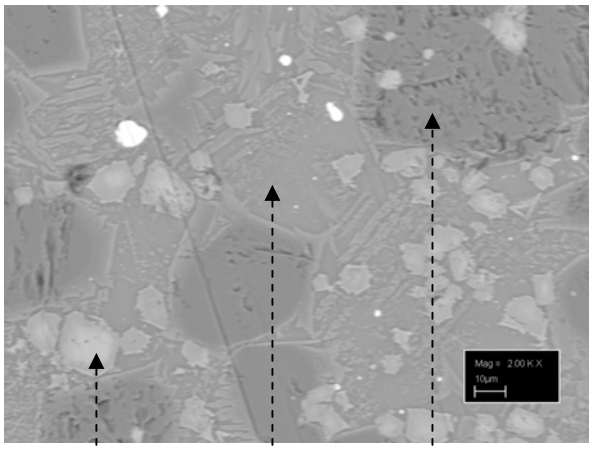

Spinel *Glass* *Olivine*

Micrograph No.7 : **36 Matte**

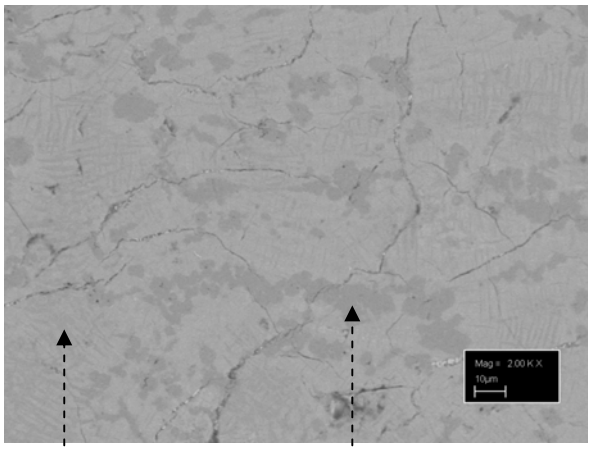

Micrograph No.8 : **36 Slag**

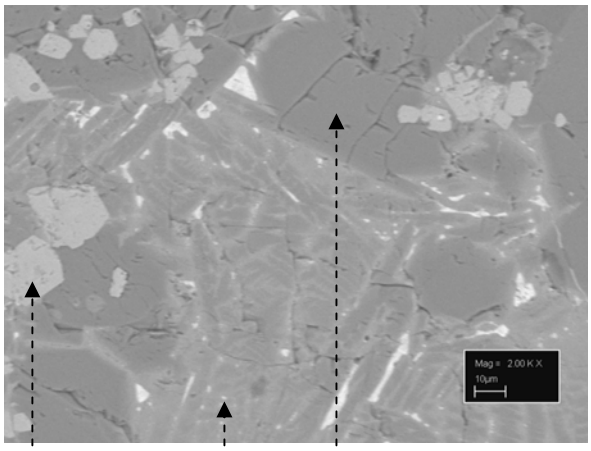

Micrograph No.9 : **25 Matte**

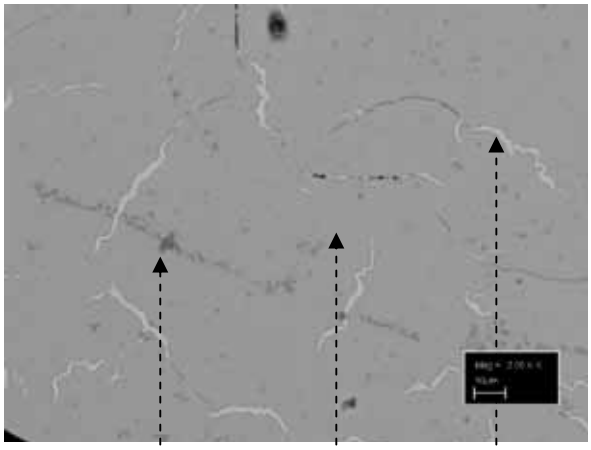

Micrograph No.10 : **25 Slag**

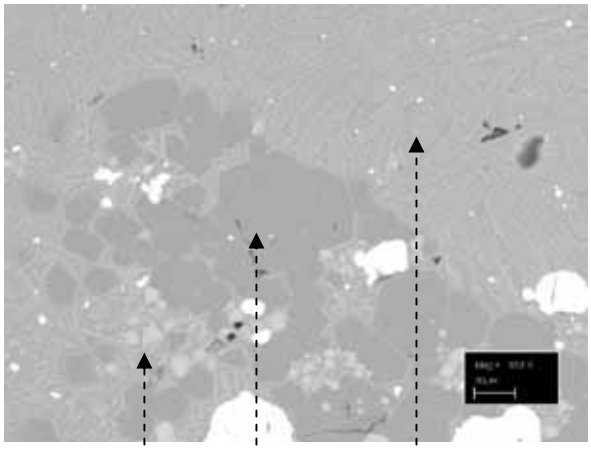

Micrograph No.11 : **28 Matte**

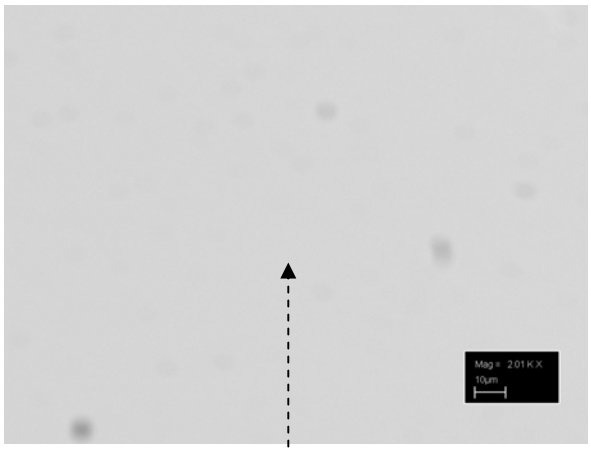

Micrograph No.12 : **28 Slag**

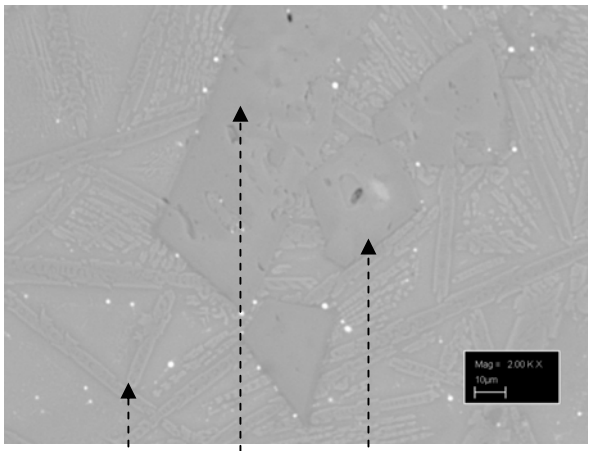

Micrograph No.13 : **37 Matte**

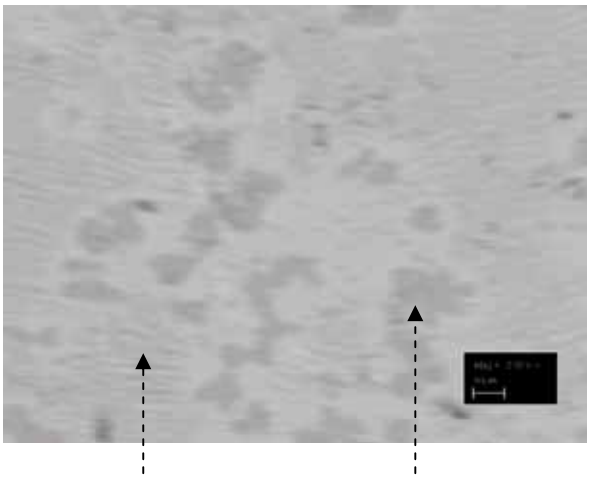

Cu-rich Glass *Fe-rich sulphide*

Micrograph No.14 : **37 Slag**

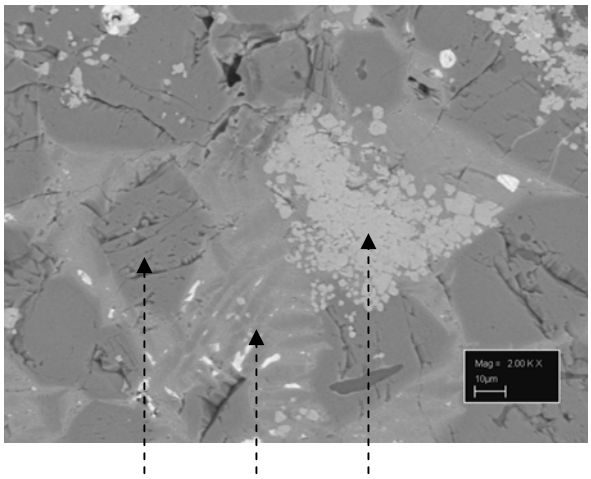

Olivine *Glass* *Spinel*

Micrograph No.15 : **38 Matte**

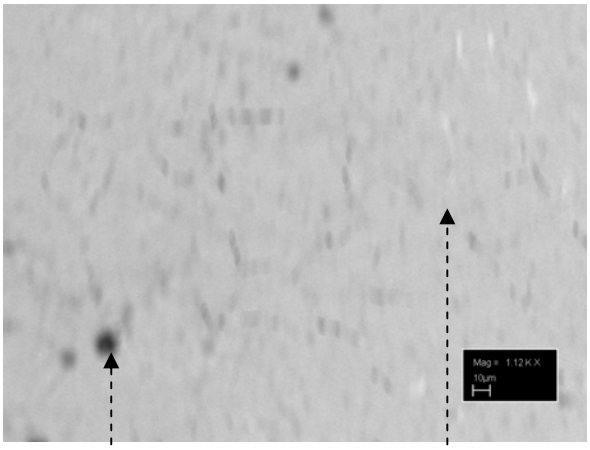

Fe-rich Sulphide *Cu-rich Glass*

Micrograph No.16 : **38 Slag**

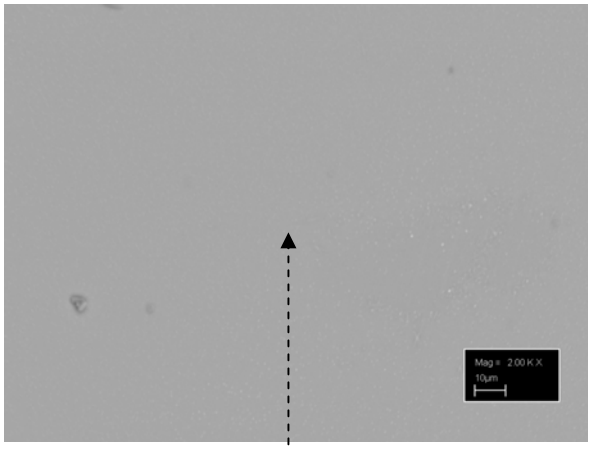

Glass

Micrograph No.17 : **27 Matte**

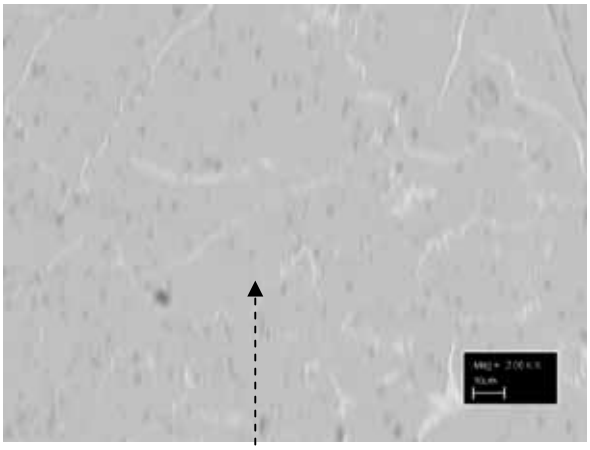

Cu-rich Glass

Micrograph No.18 : **27 Slag**

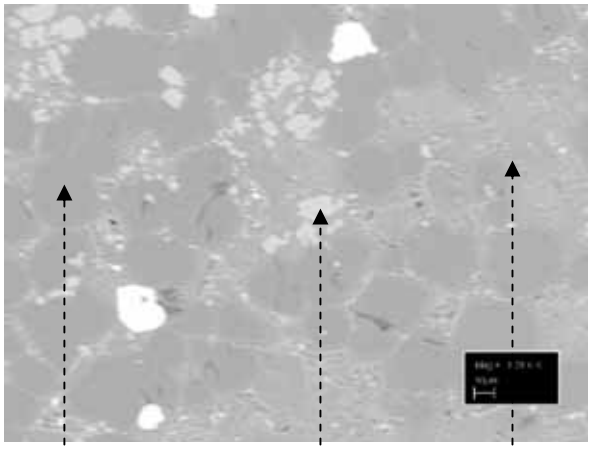

Olivine *Spinel* *Glass*

Micrograph No.19 : **44 Matte**

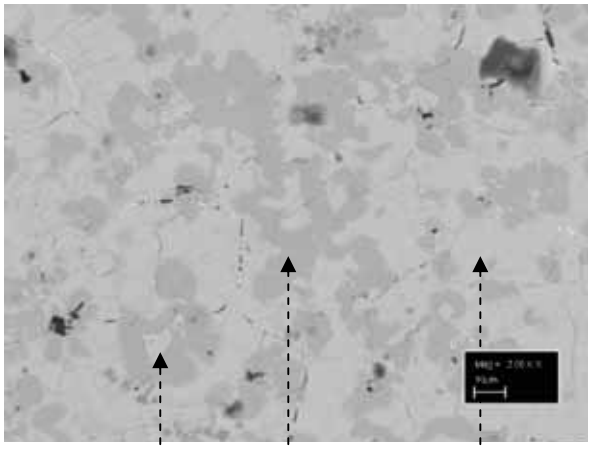

Micrograph No.20 : **44 Slag**

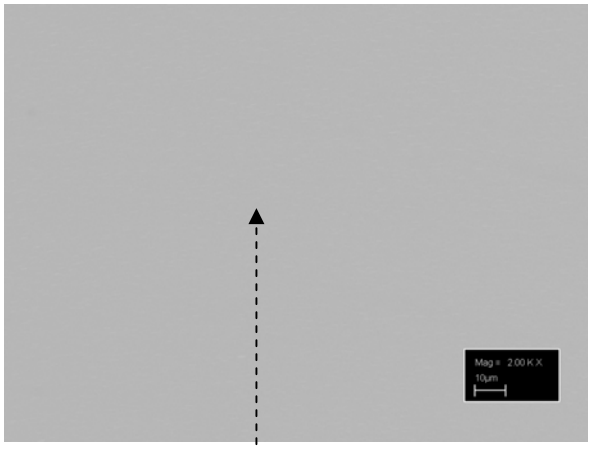

Micrograph No.21 : **43 Matte**

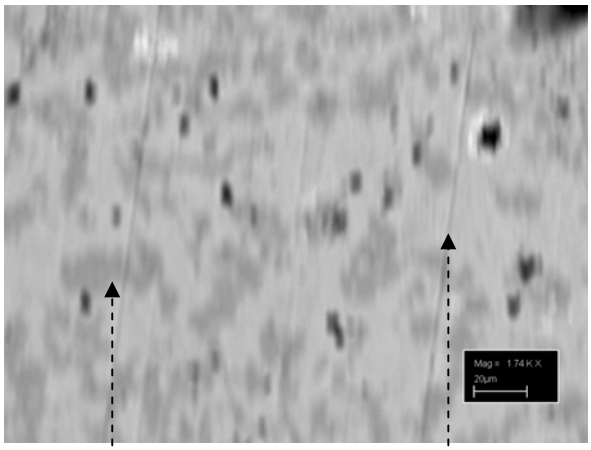

Micrograph No.22 : **43 Slag**

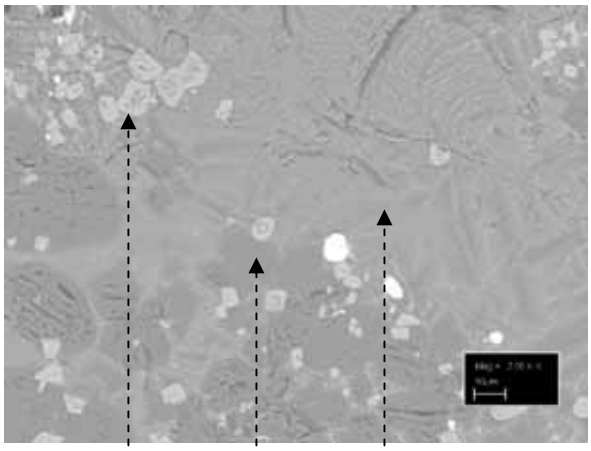

Micrograph No.23 : **41 Matte**

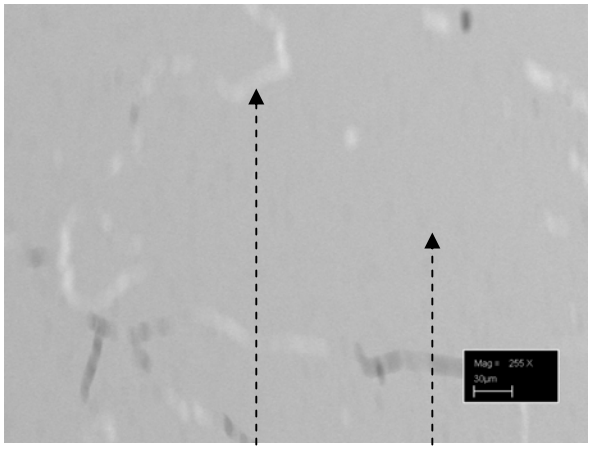

Micrograph No.24 : **41 Slag**

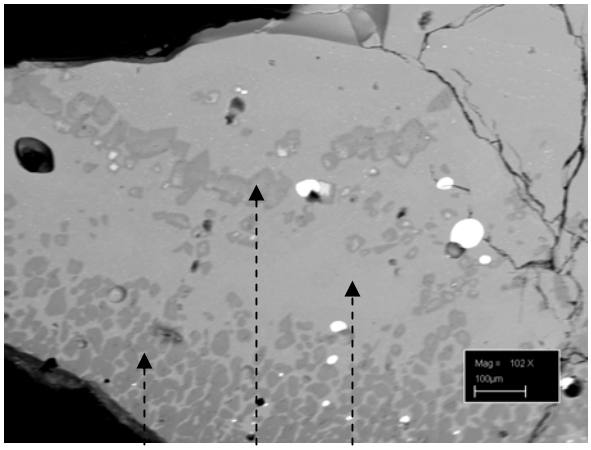

Micrograph No.25 : **45 Matte**

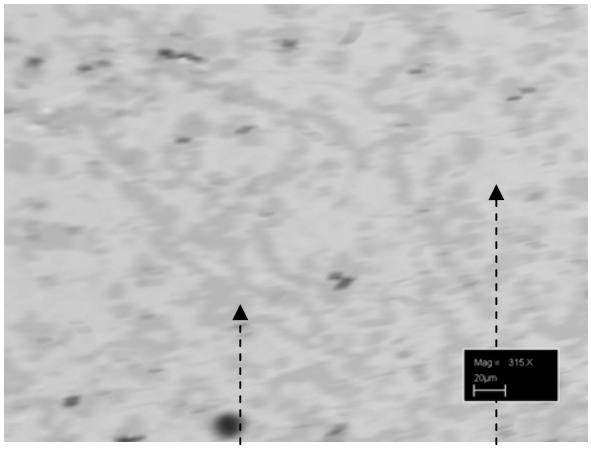

Micrograph No.26 : **45 Slag**

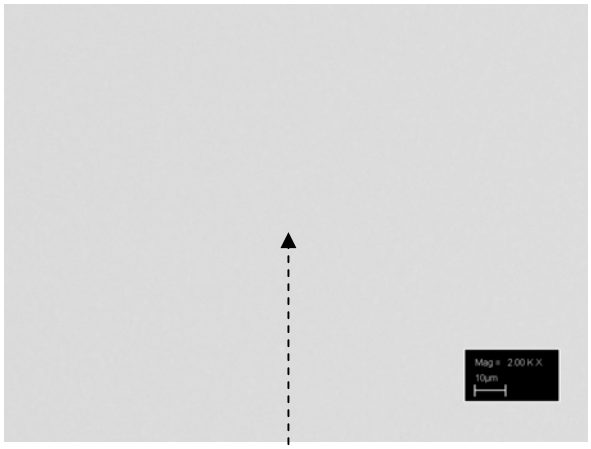

Micrograph No.27 : **42 Matte**

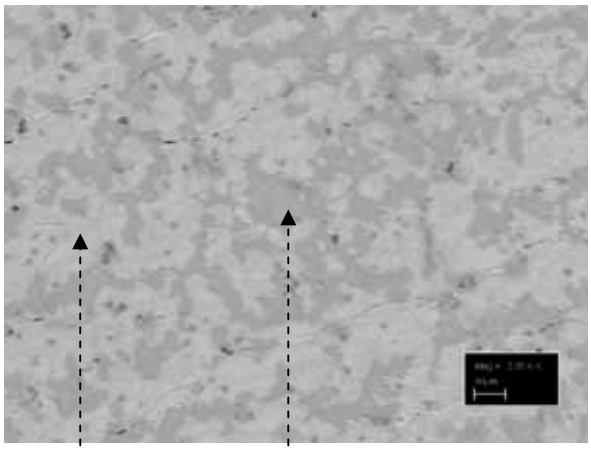

Micrograph No.28 : **42 Slag**

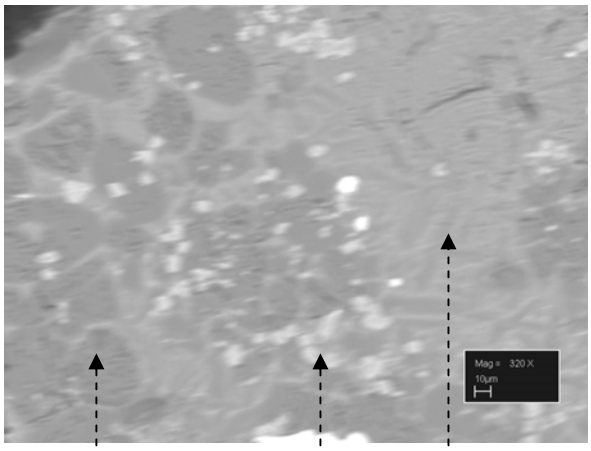

Micrograph No.29 : **40 Matte**

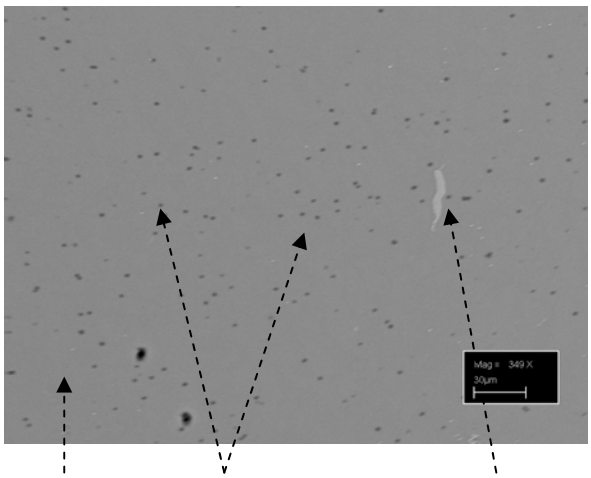

Micrograph No.30 : **40 Slag**

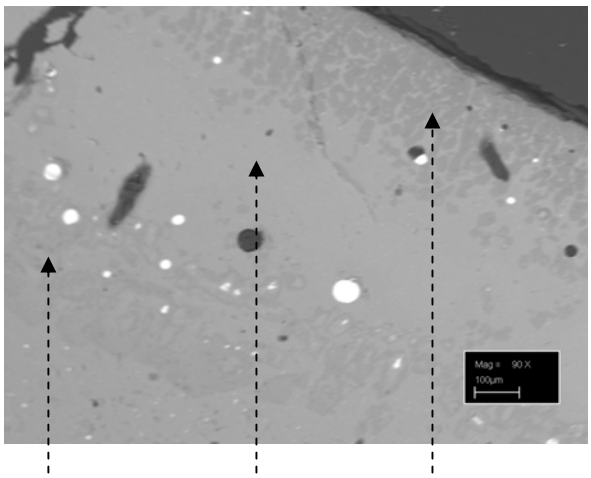

Micrograph No.31 : **46 Matte**

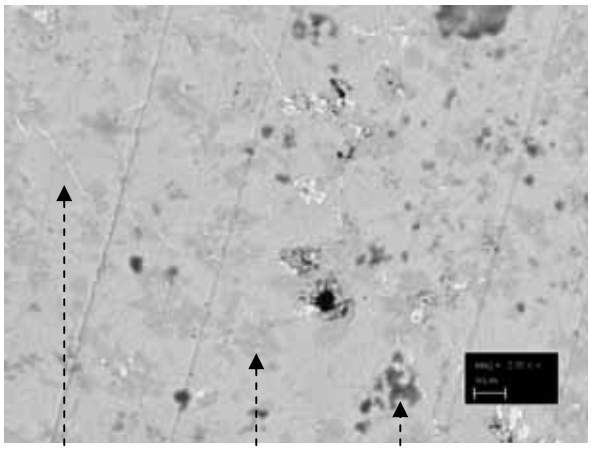

Cu-rich Glass *Fe-rich Sulphide* *Spinel*

Micrograph No.32 : **46 Slag**

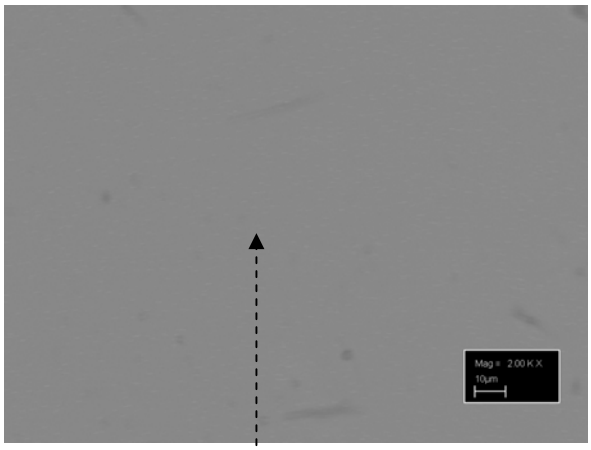

Glass

Micrograph No.33 : **39 Matte**

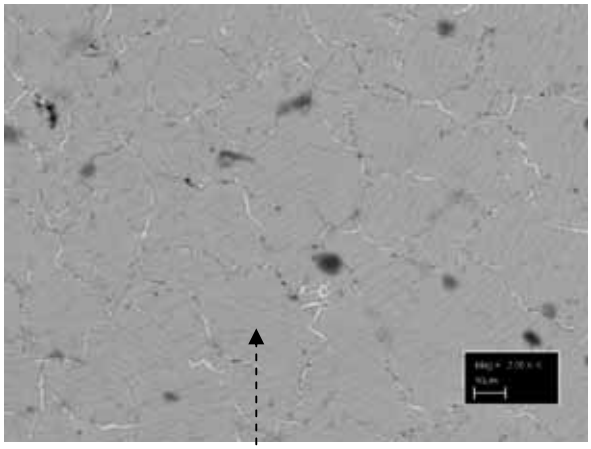

Cu-rich Glass

Micrograph No.34 : **39 Slag**

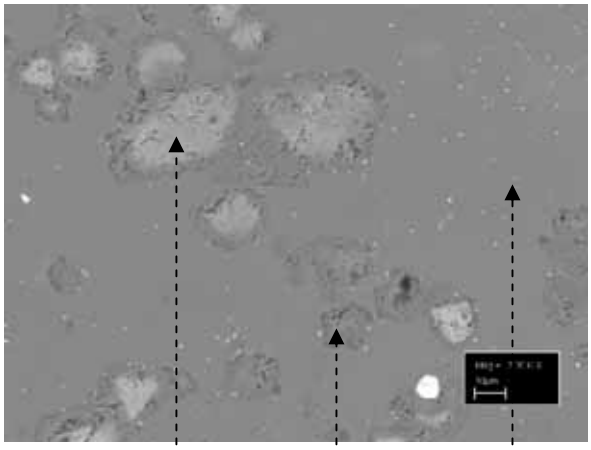

Spinel *Olivine* *Glass*

Micrograph No.35 : **47 Matte**

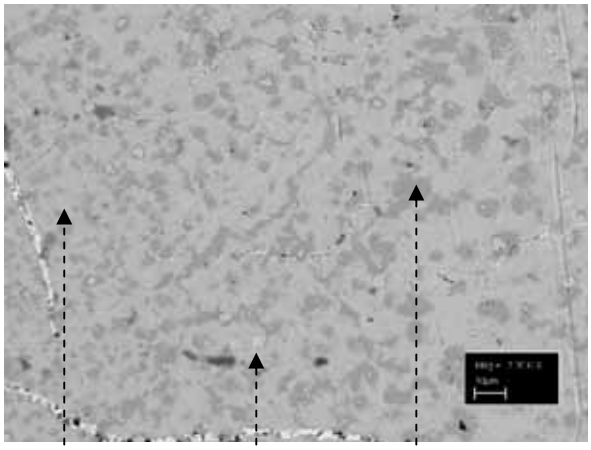

Cu-rich Glass *Spinel* *Fe-rich Sulphide*

Micrograph No.36 : **47 Slag**

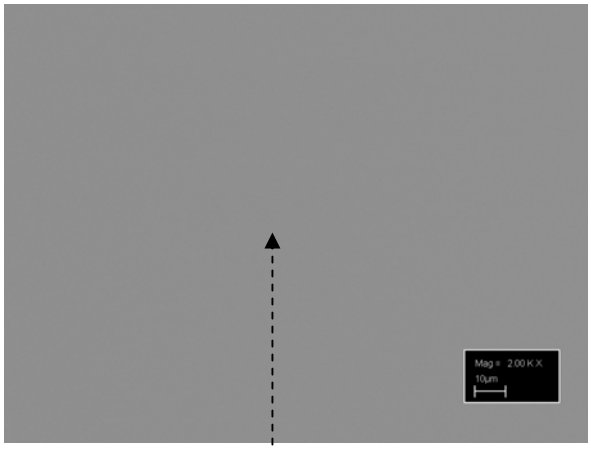

Glass

Micrograph No.37 : **52 Matte**

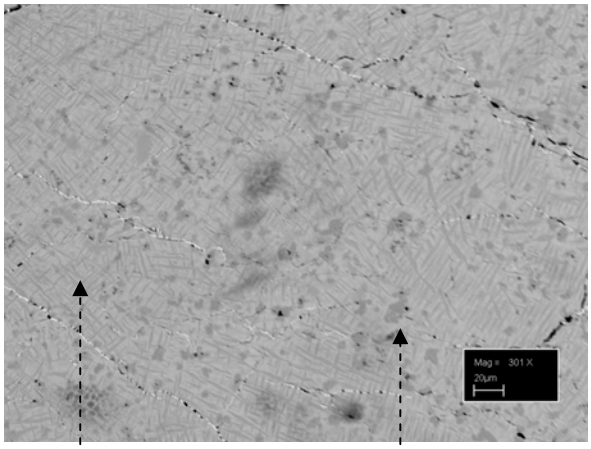

Micrograph No.38 : **52 Slag**

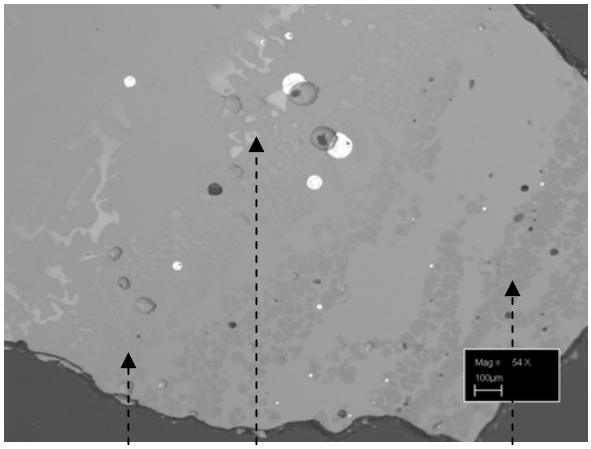

Micrograph No.39 : **55 Matte**

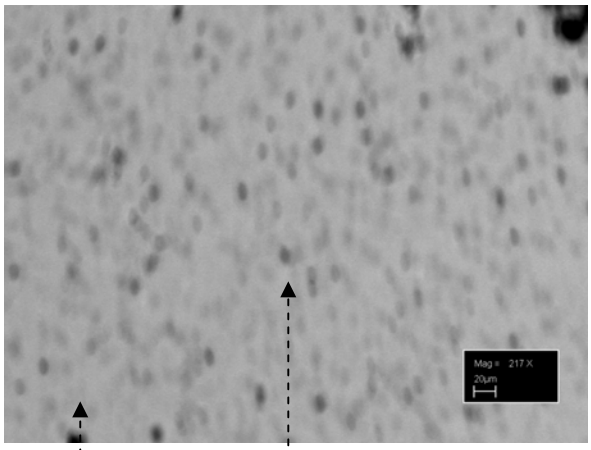

Micrograph No.40 : **55 Slag**

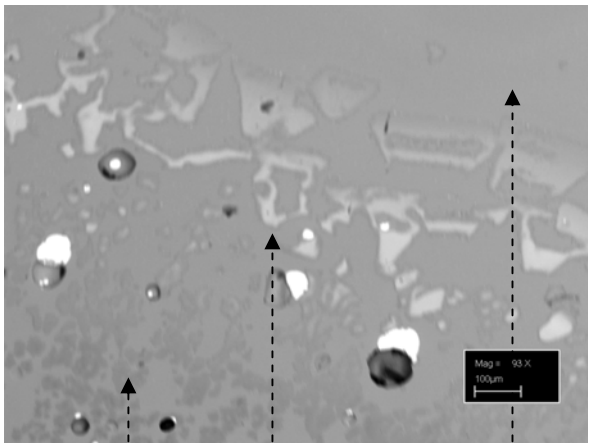

Micrograph No.41 : **50 Matte**

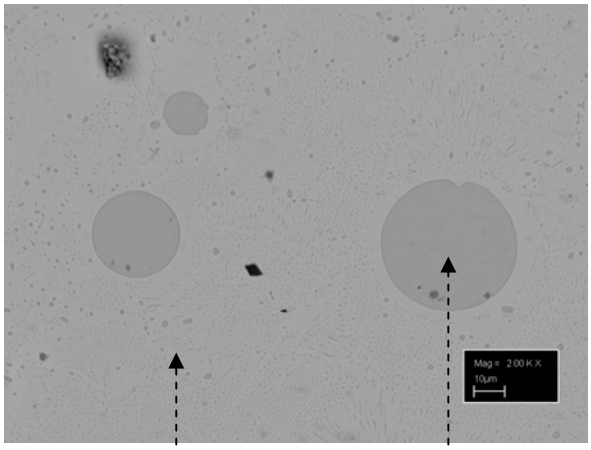

Micrograph No.42 : **50 Slag**

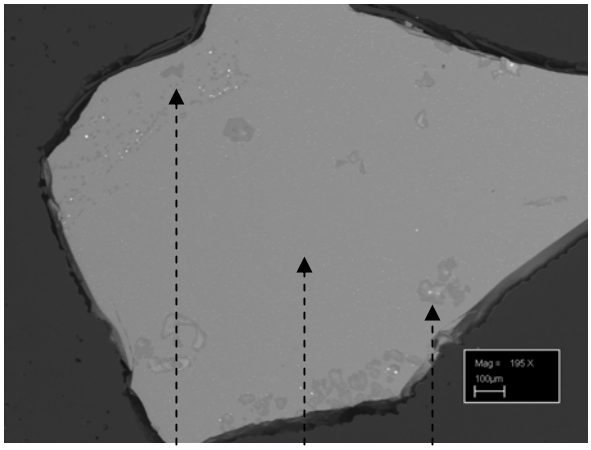

Micrograph No.43 : **57 Matte**

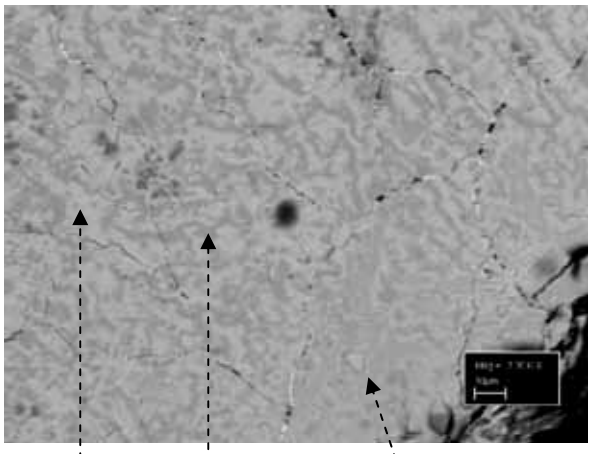

Cu-rich Glass *Fe-rich sulphide* *spinel*

Micrograph No.44 : **57 Slag**

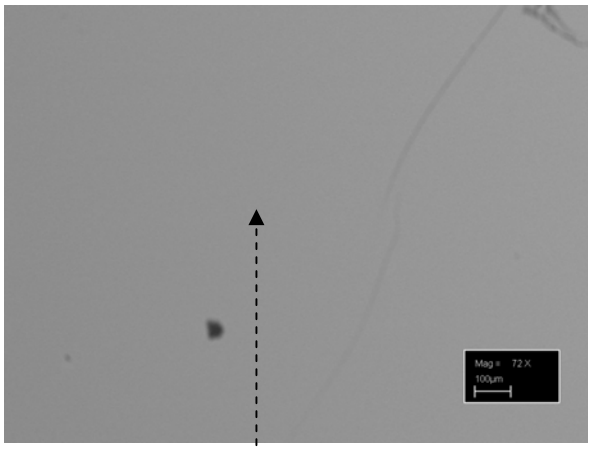

Glass

Micrograph No.45 : **54 Matte**

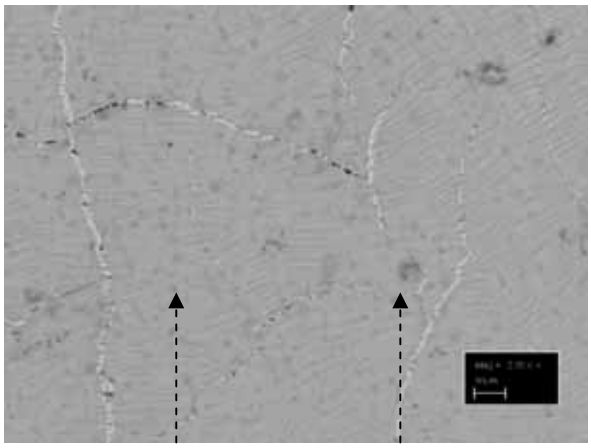

Cu-rich Glass *Fe-rich sulphide*

Micrograph No.46 : **54 Slag**

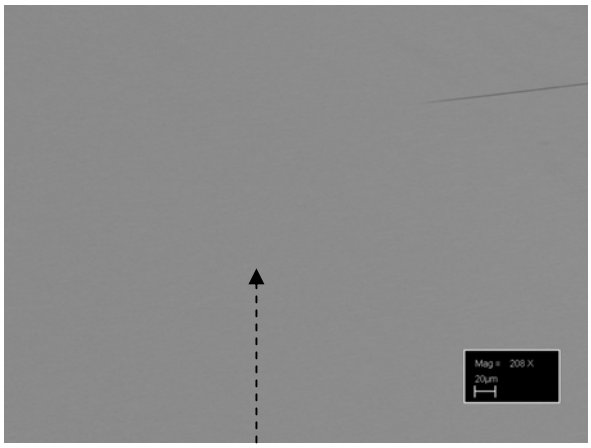

Glass

Micrograph No.47 : **49 Matte**

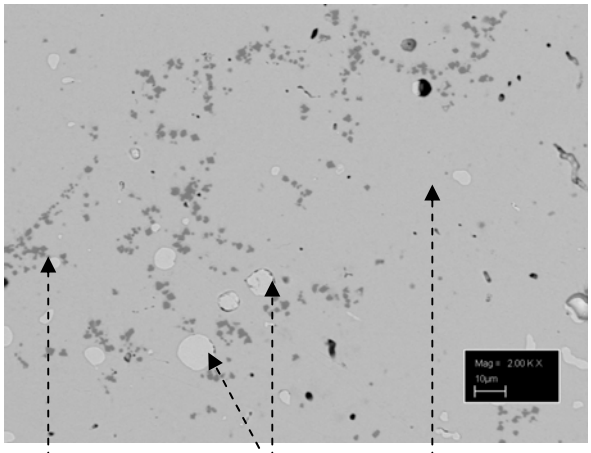

Fe-rich Sulphide *Cu* *Cu-rich Glass*

Micrograph No.48 : **49 Slag**

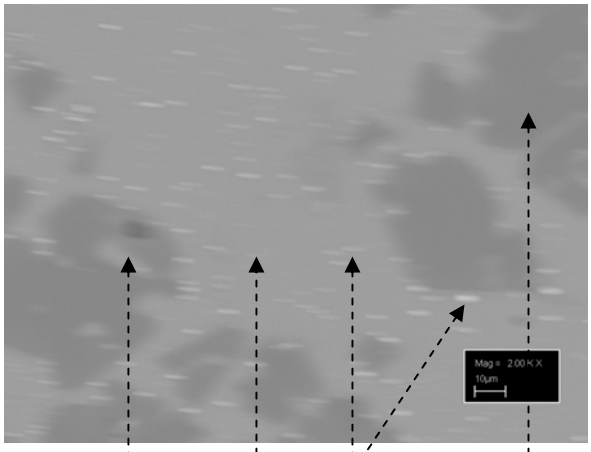

Mg-rich Spinel *Glass* *Alumina-rich (white spots)* *Olivine*

Micrograph No.49 : **56 Matte**

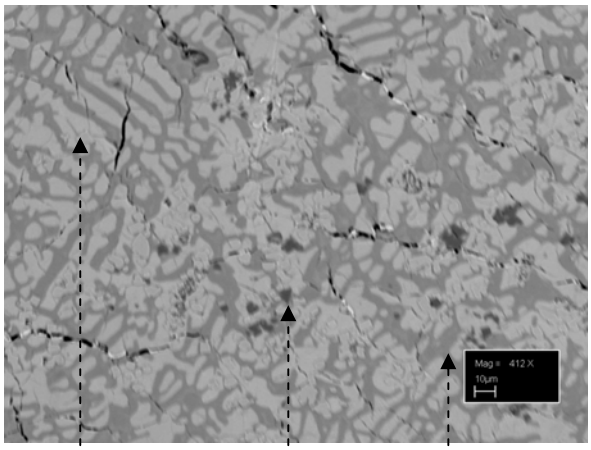

Micrograph No.50 : **56 Slag**

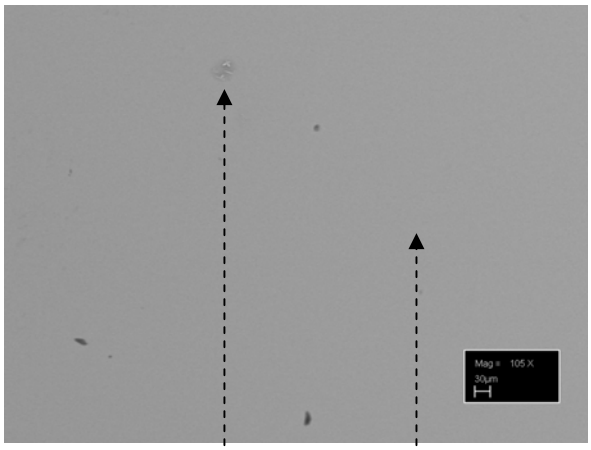

Micrograph No.51 : **53 Matte**

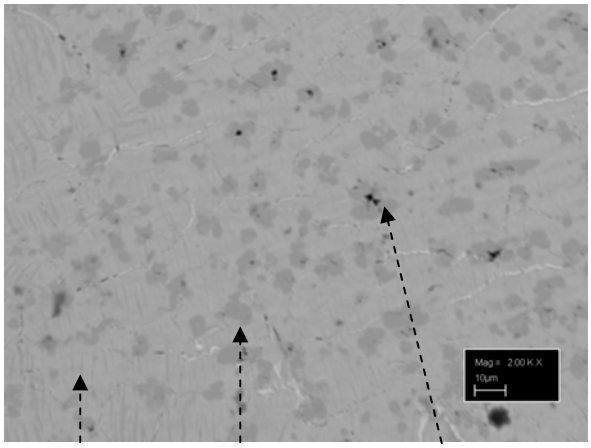

Micrograph No.52 : **53 Slag**

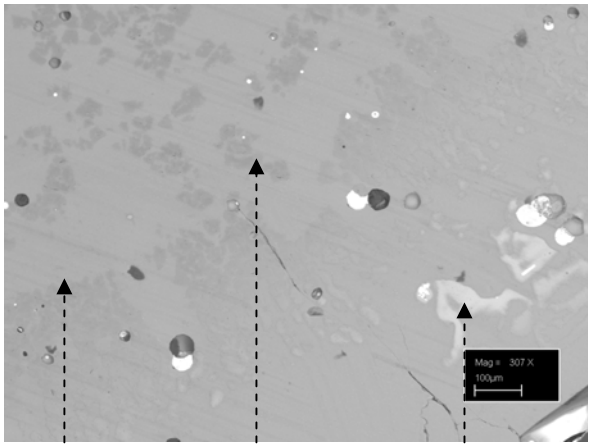

Micrograph No.53 : **48 Matte**

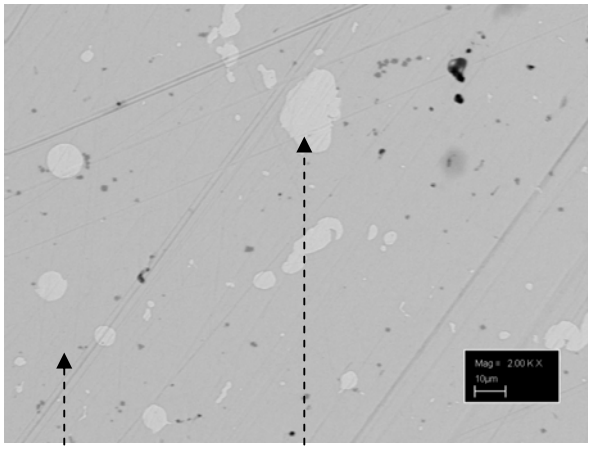

Micrograph No.54 : **48 Slag**

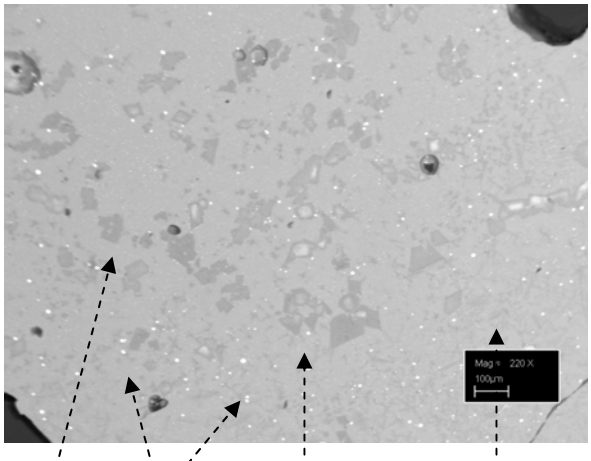

Appendix D: X-Ray Diffraction Profiles

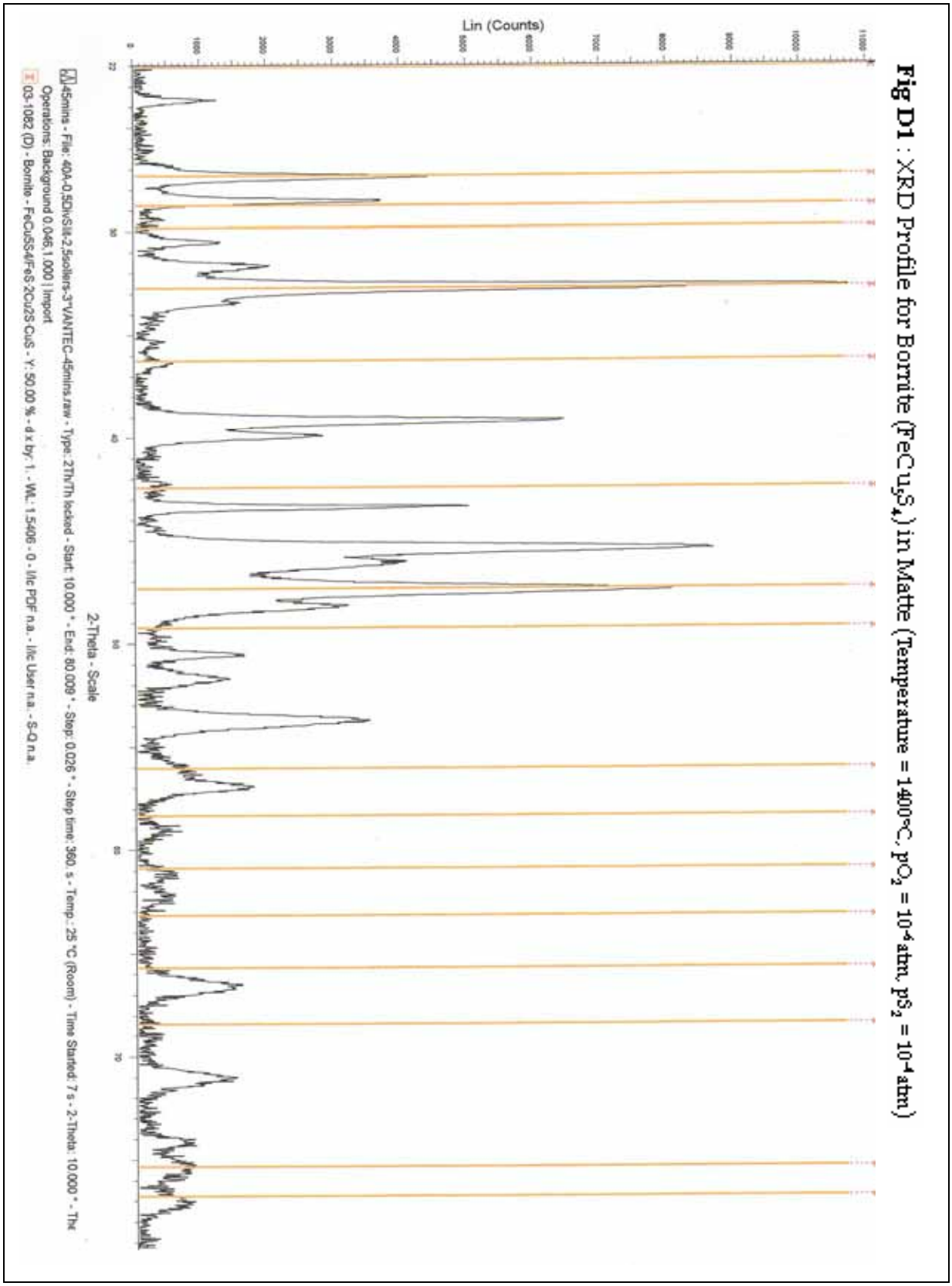

Fig D1 : XRD Profile for Bornite ($FeCu_2S_4$) in Matte (Temperature = 1400°C, $pO_2 = 10^{-4}$ atm, $pS_2 = 10^{-4}$ atm)

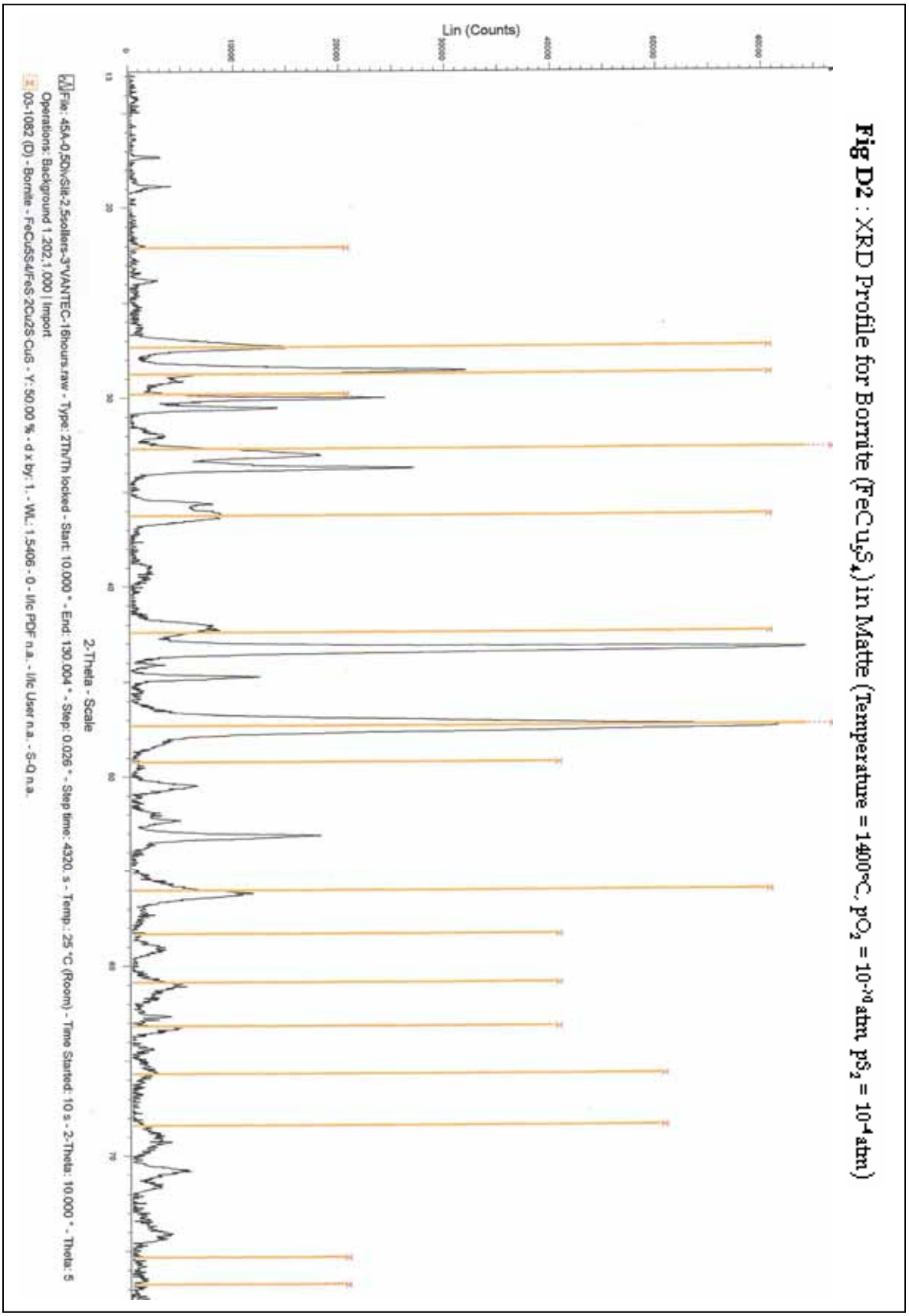

Fig D2 : XRD Profile for Bornite ($FeCu_5S_4$) in Matte (Temperature = 1400°C, $pO_2 = 10^{-20}$ atm, $pS_2 = 10^{-4}$ atm)

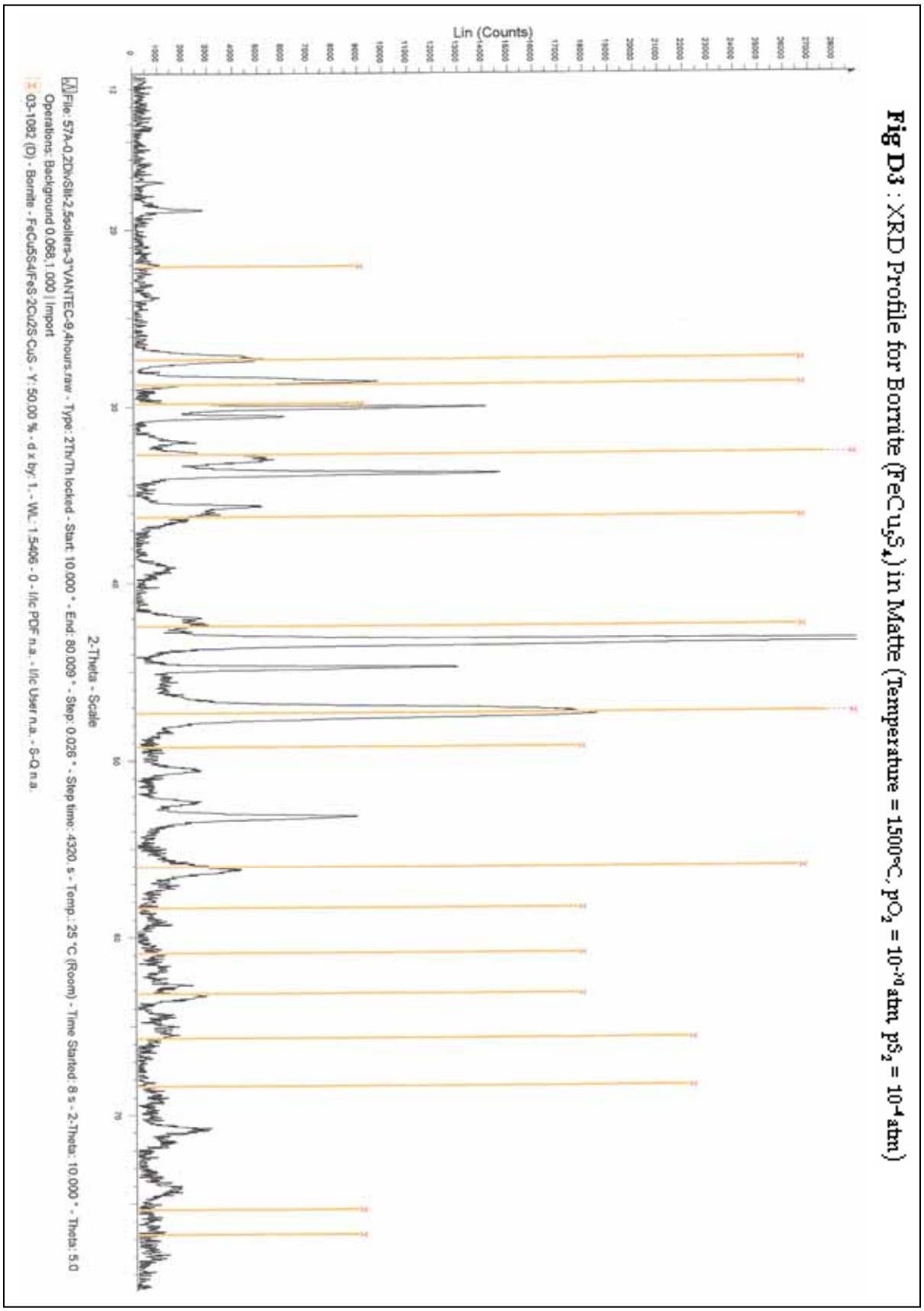

Fig D3 : XRD Profile for Bornite ($FeCu_5S_4$) in Matte (Temperature = 1500°C, $pO_2 = 10^{-10}$ atm, $pS_2 = 10^{-4}$ atm)

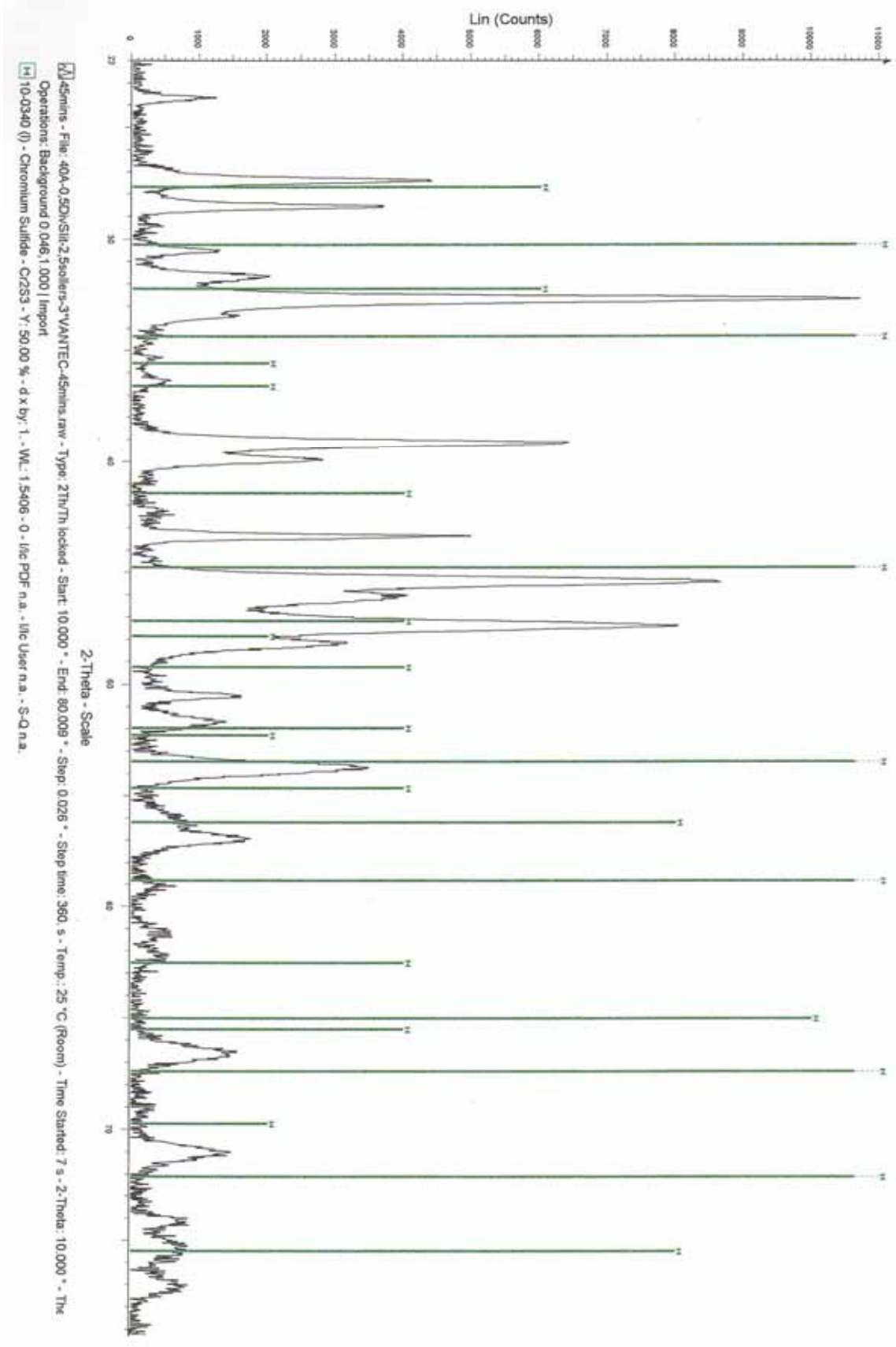

Fig D4 : XRD Profile for Cr_2S_3) in Matte (Temperature = 1400°C, pO_2 = 10^{-4} atm, pS_2 = 10^{-4} atm)

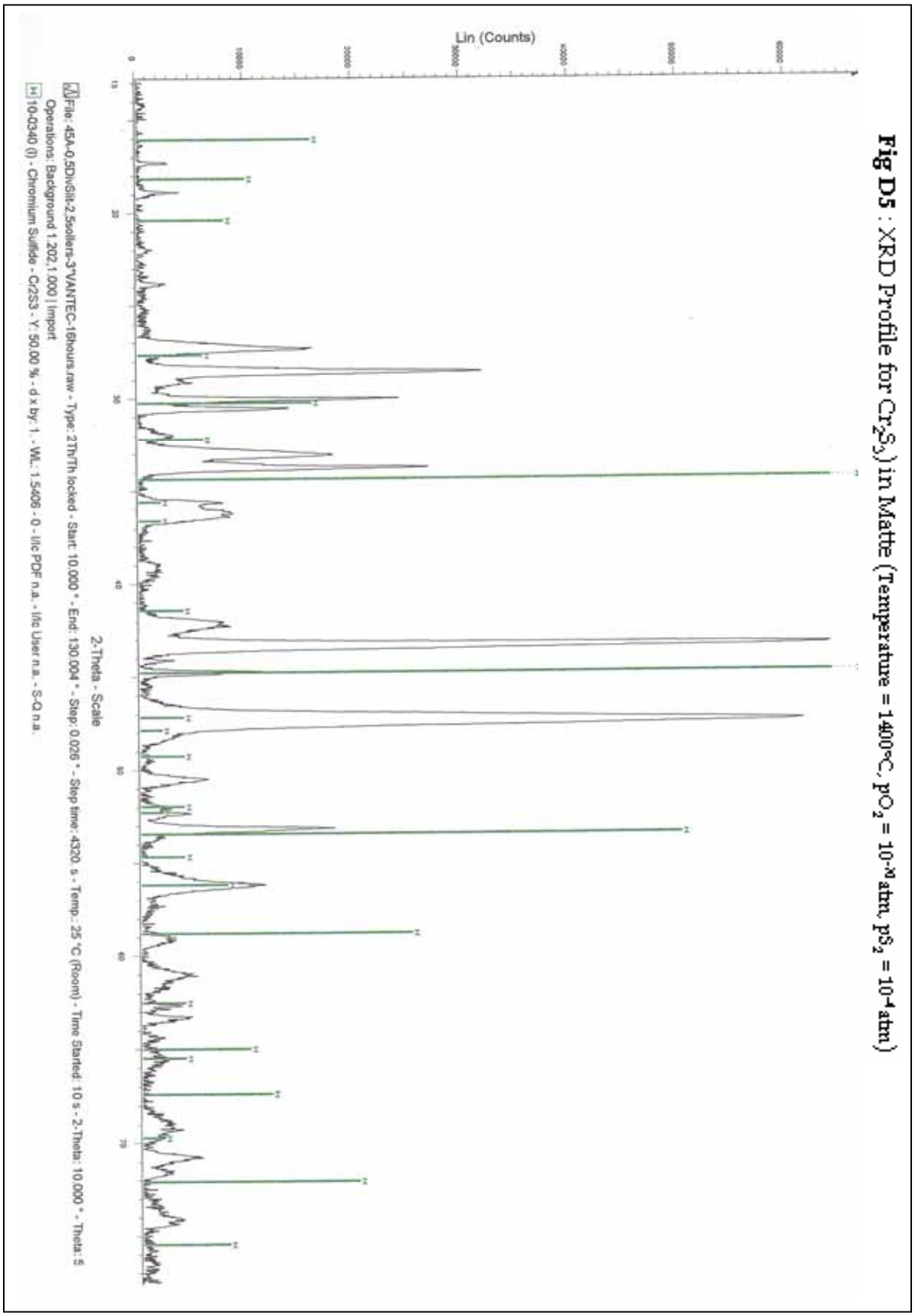

Fig D5 : XRD Profile for Cr_2S_3) in Matte (Temperature = 1400°C, pO_2 = 10^{-8} atm, pS_2 = 10^{-4} atm)

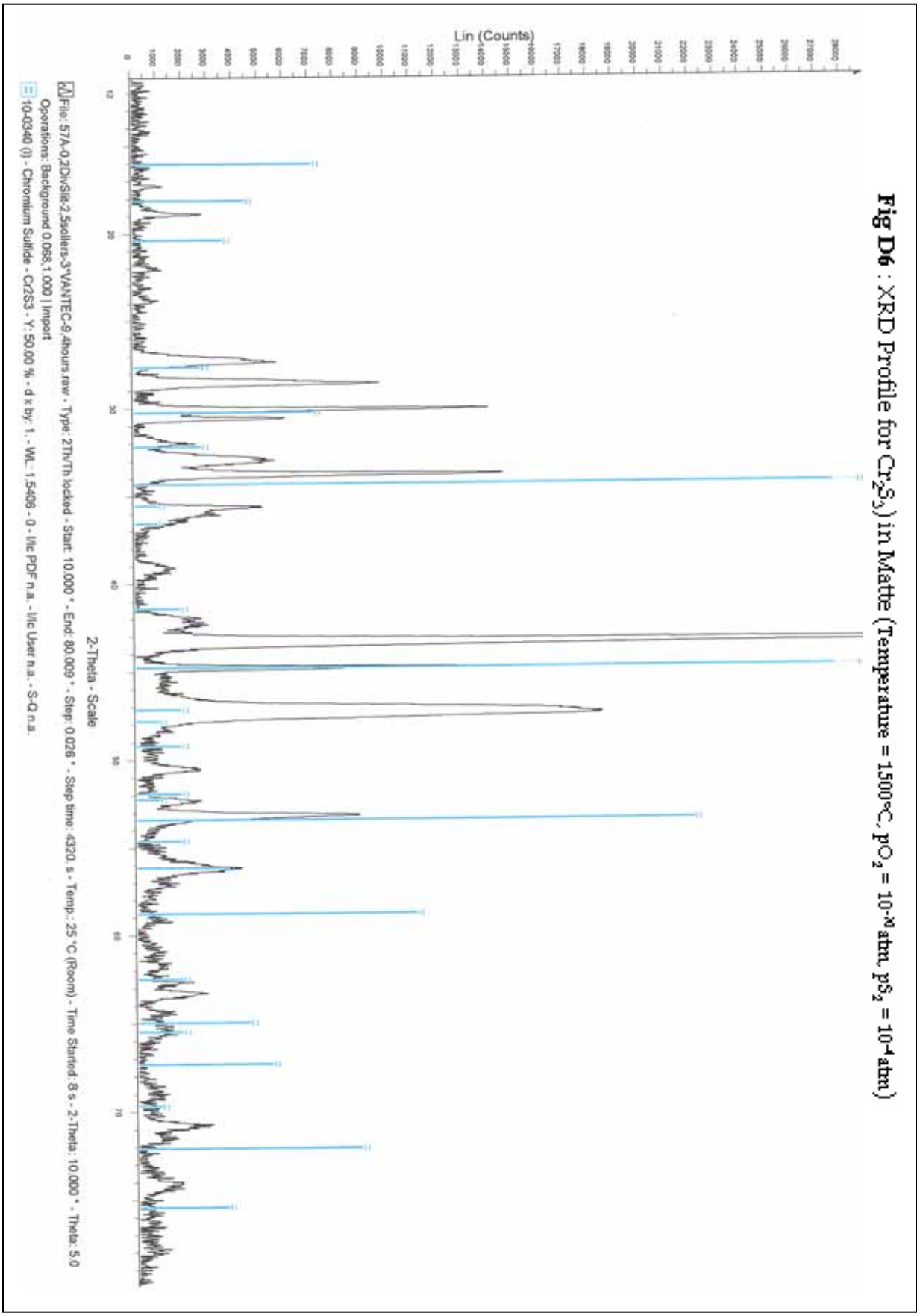

Fig D6 : XRD Profile for Cr_2S_3) in Matte (Temperature = 1500°C, pO_2 = 10^{-8} atm, pS_2 = 10^{-4} atm)

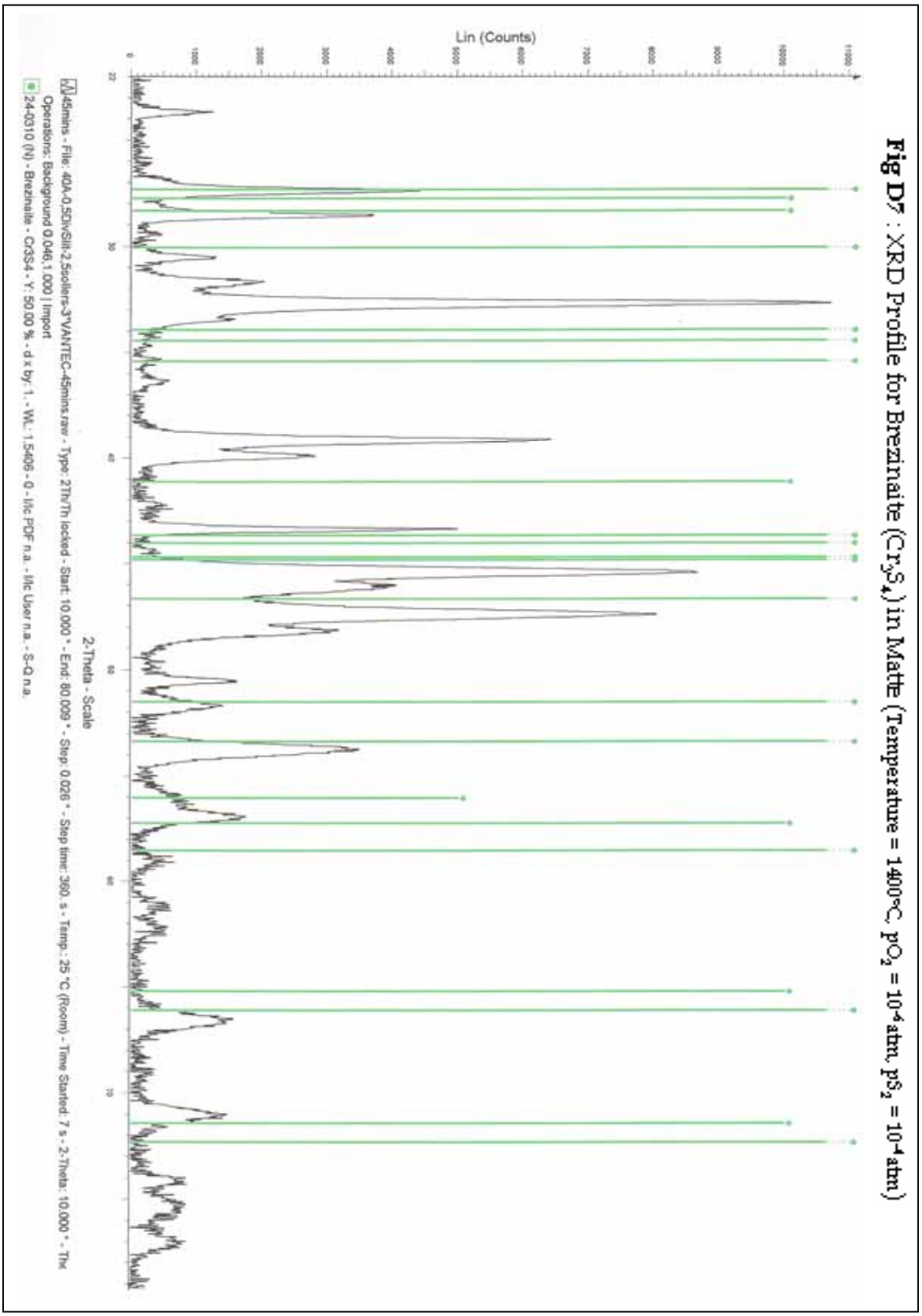

Fig D7 : XRD Profile for Brezinaite (Cr_3S_4) in Matte (Temperature = 1400°C, $pO_2 = 10^{-4}$ atm, $pS_2 = 10^{-4}$ atm)

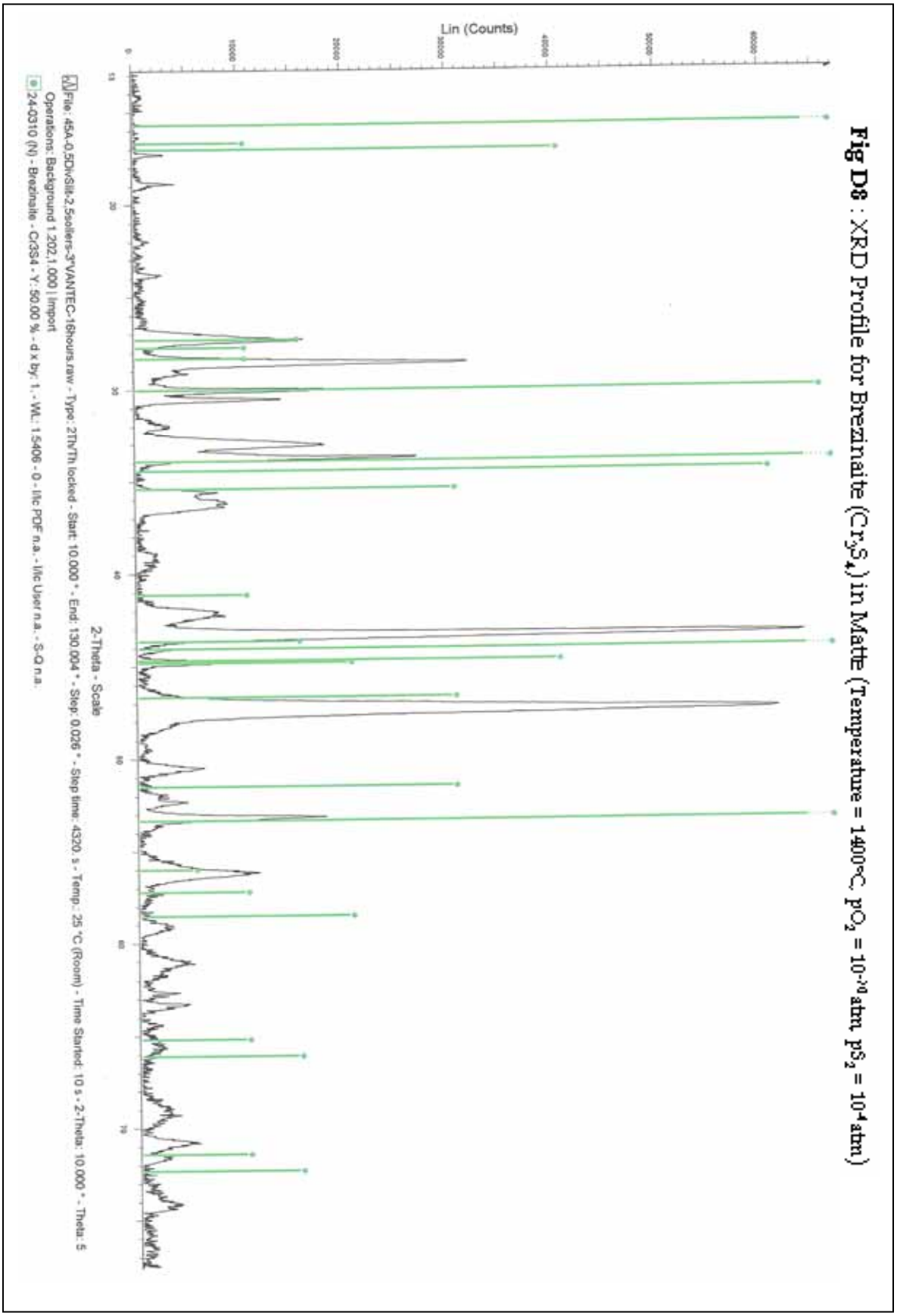

Fig D8 : XRD Profile for Brezinaite (Cr_3S_4) in Matte (Temperature = 1400°C, $pO_2 = 10^{-20}$ atm, $pS_2 = 10^{-4}$ atm)

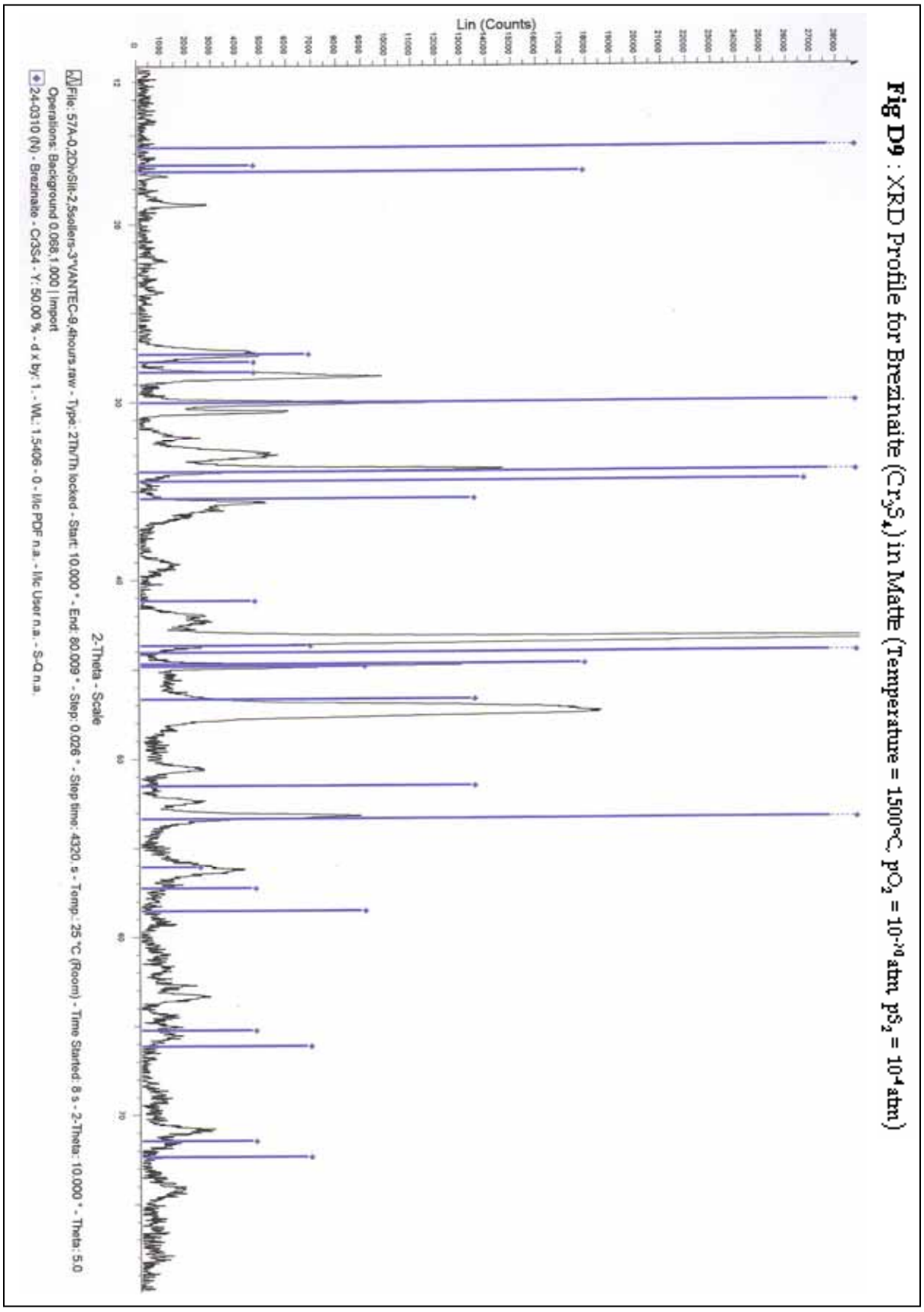

Fig D9 : XRD Profile for Brezinaite (Cr_3S_4) in Matte (Temperature = 1500°C, $pO_2 = 10^{-7.0}$ atm, $pS_2 = 10^{-4}$ atm)

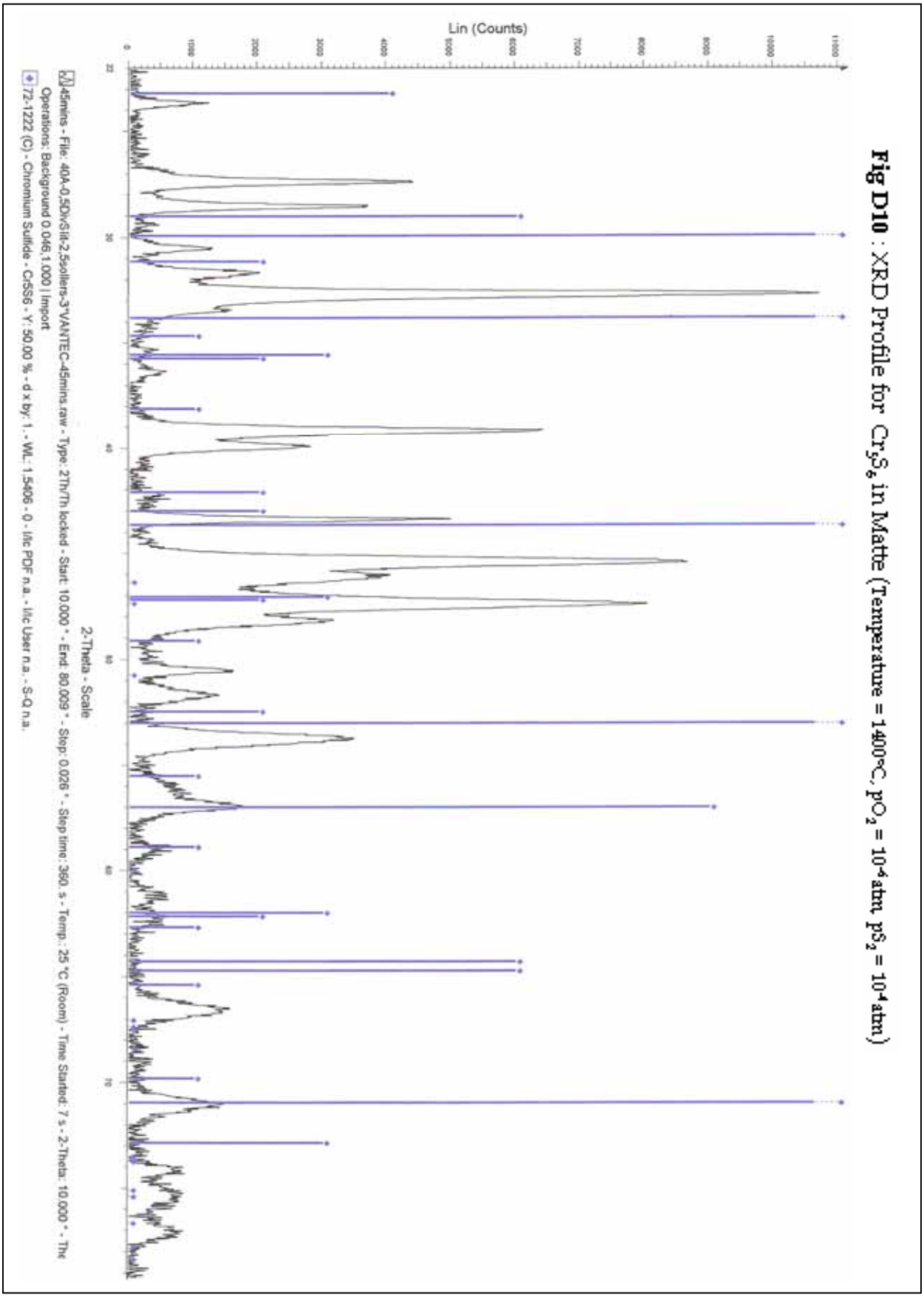

Fig D10 : XRD Profile for Cr_3S_6 in Matte (Temperature = 1400°C, pO_2 = 10^{-4} atm, pS_2 = 10^{-4} atm)

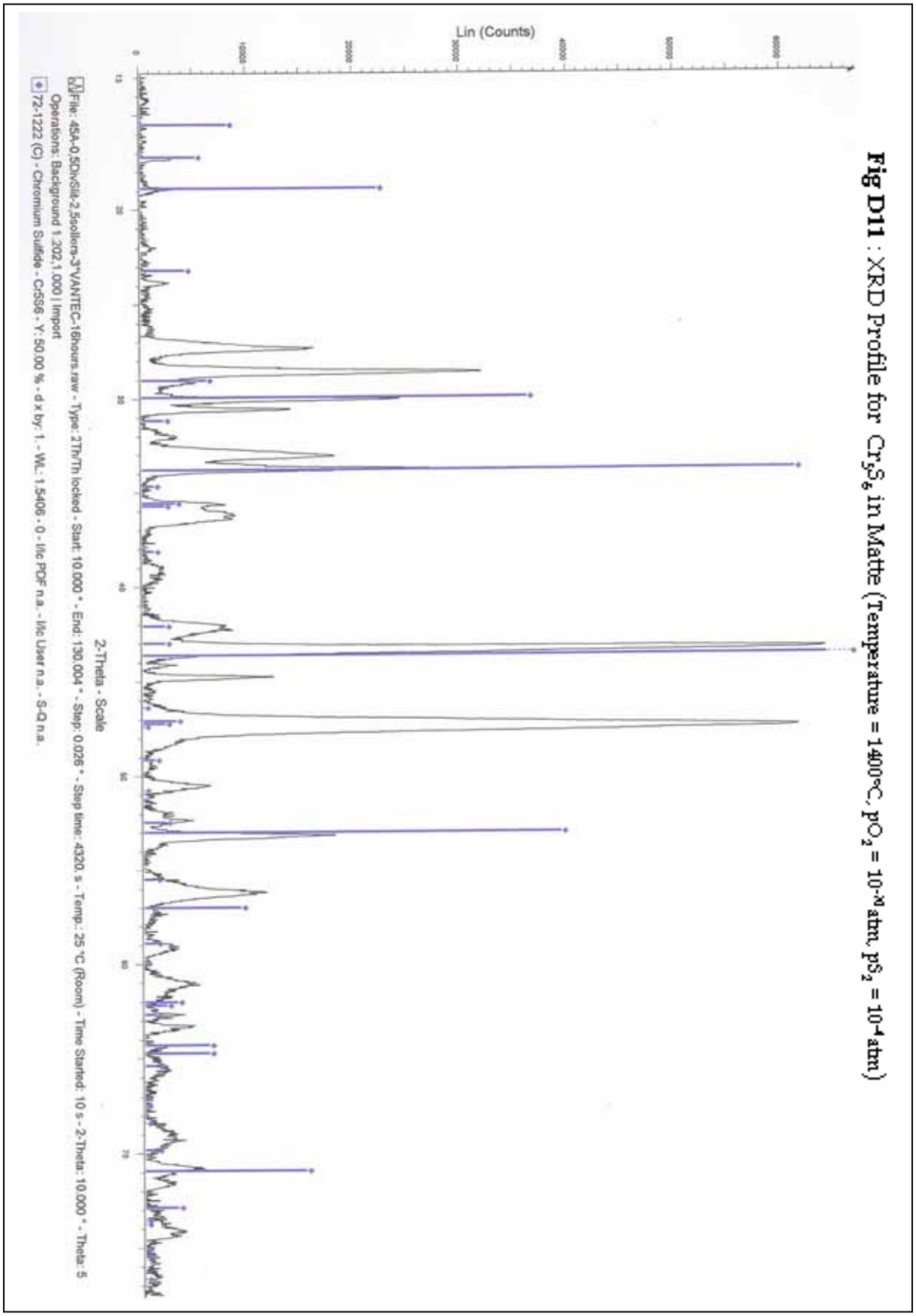

Fig D11 : XRD Profile for Cr_5S_6 in Matte (Temperature = 1400°C, $pO_2 = 10^{-8}$ atm, $pS_2 = 10^{-4}$ atm)

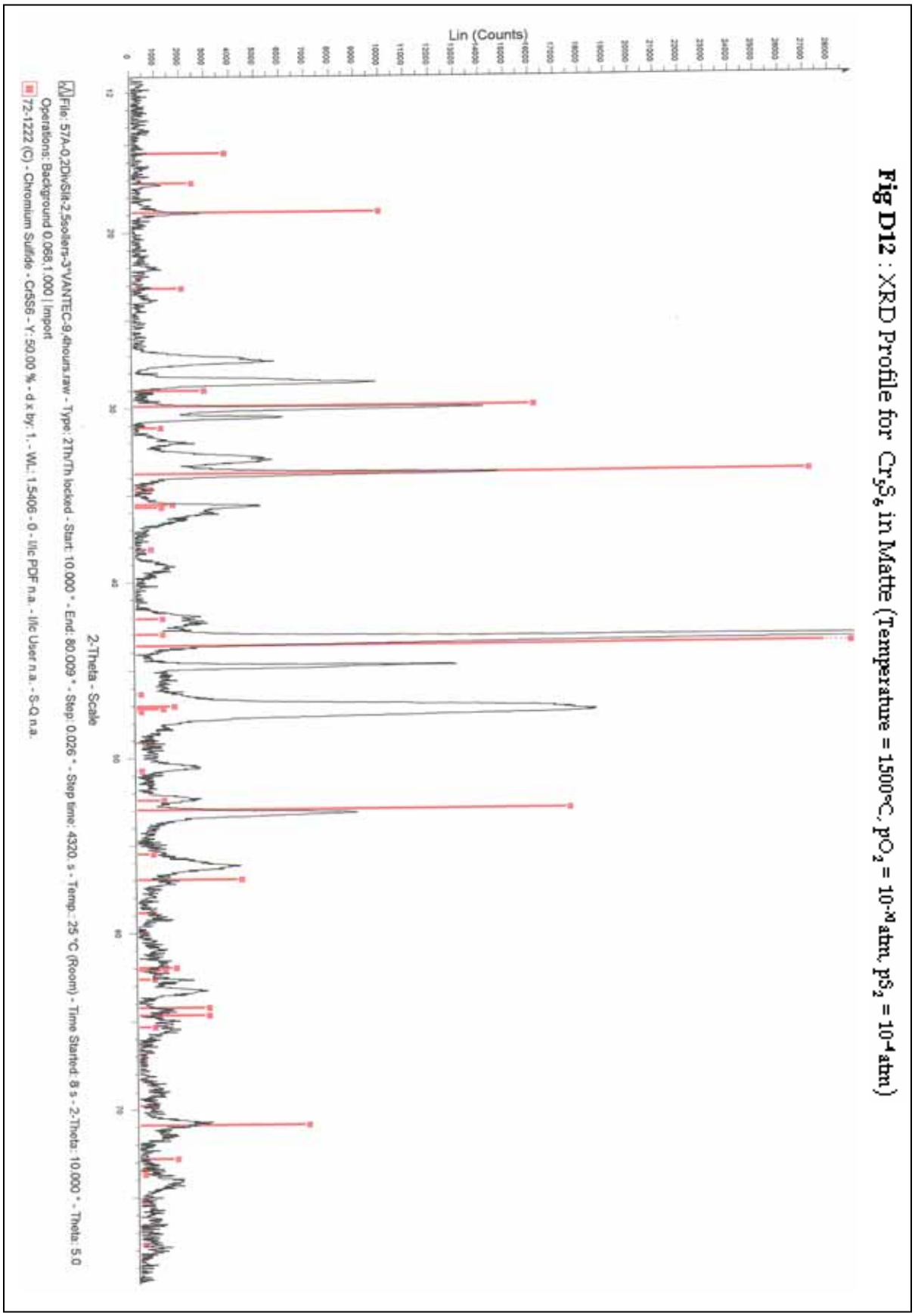

Fig D12 : XRD Profile for Cr_3S_6 in Matte (Temperature = 1500°C, $pO_2 = 10^{-8}$ atm, $pS_2 = 10^{-4}$ atm)

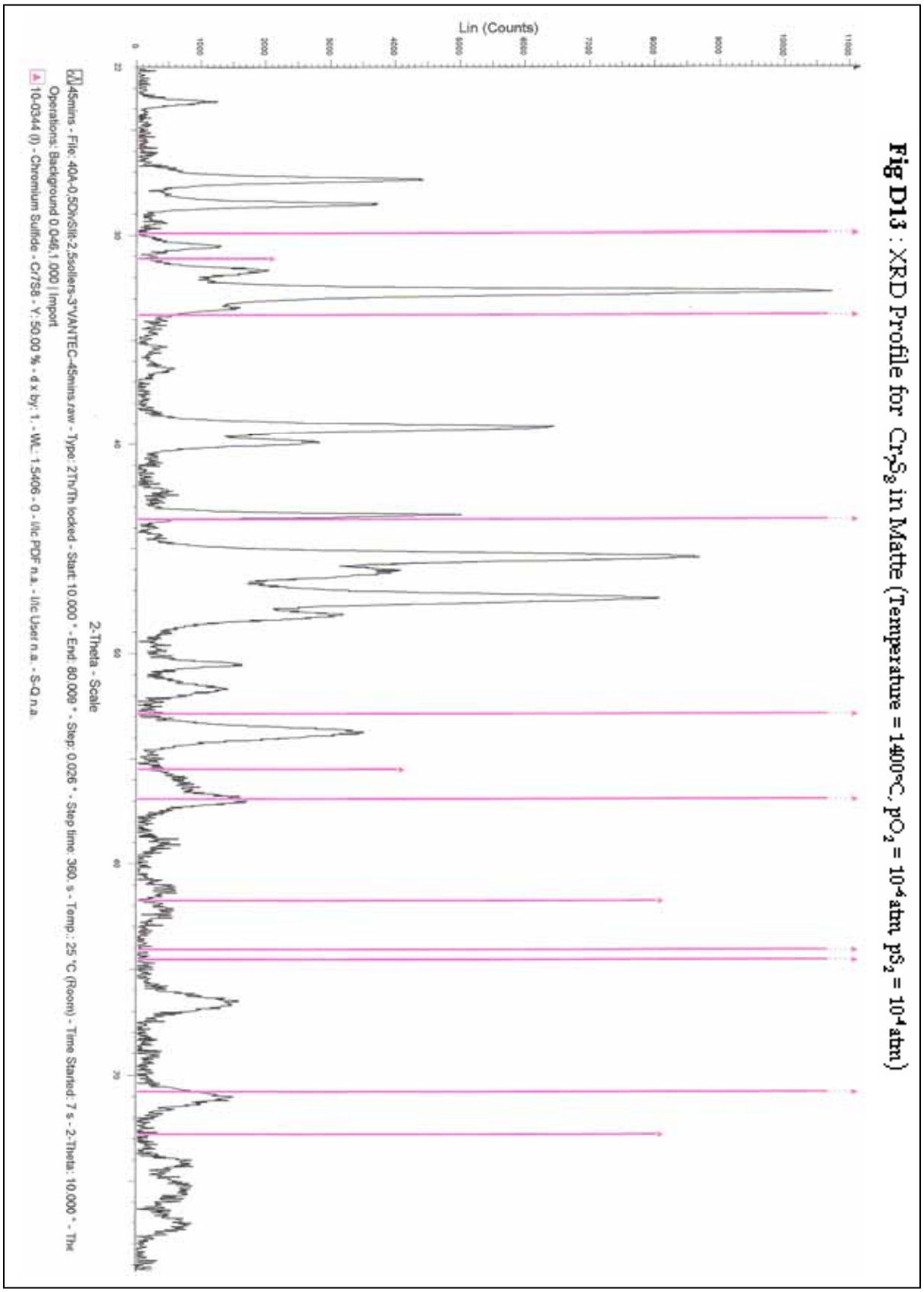

Fig D13 : XRD Profile for Cr_7S_8 in Matte (Temperature = 1400°C, $pO_2 = 10^{-4}$ atm, $pS_2 = 10^{-4}$ atm)

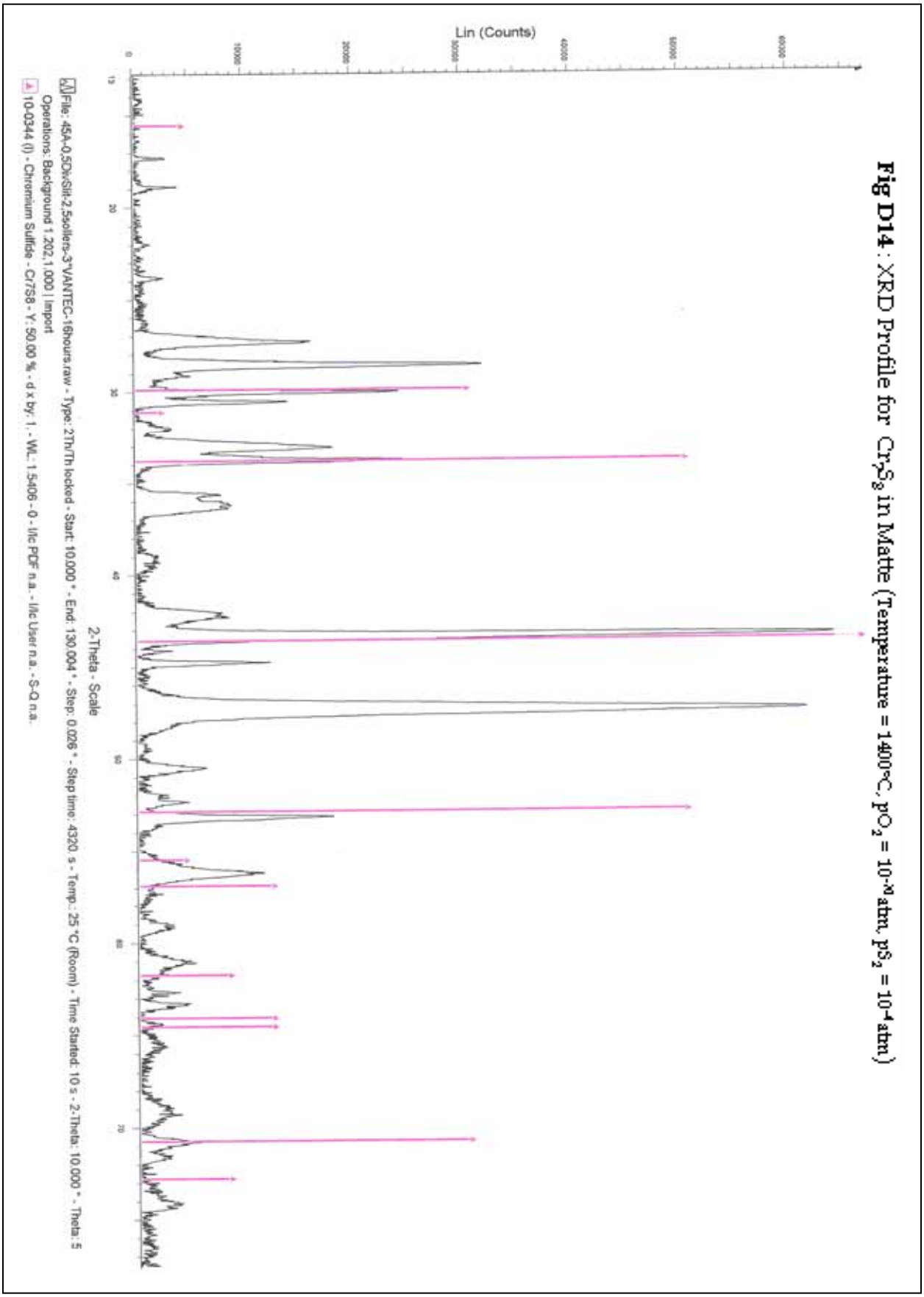

Fig D14 : XRD Profile for Cr_7S_8 in Matte (Temperature = 1400°C, $pO_2 = 10^{-9}$ atm, $pS_2 = 10^{-4}$ atm)

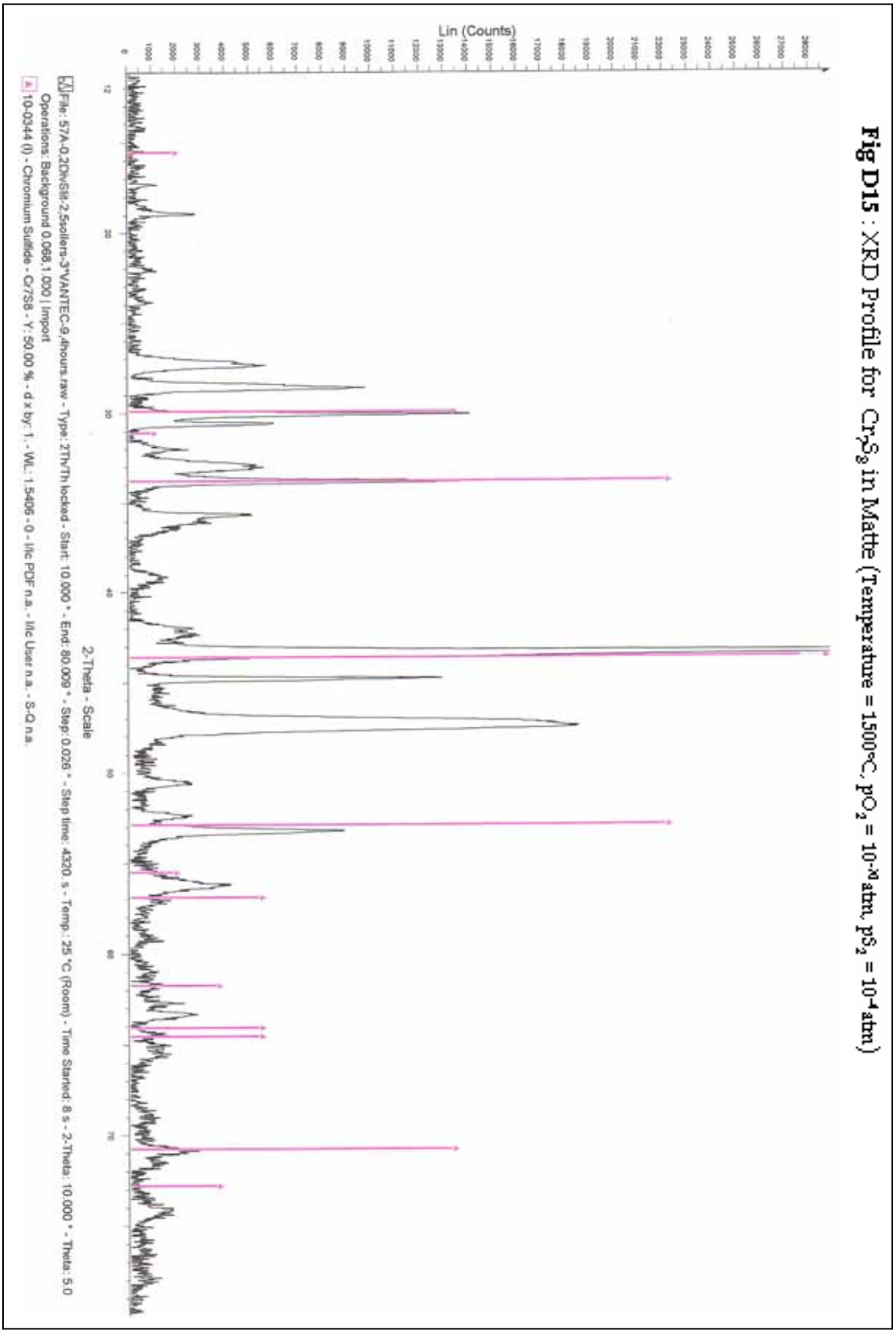

Fig D15 : XRD Profile for Cr_7S_8 in Matte (Temperature = 1500°C, $pO_2 = 10^{-8}$ atm, $pS_2 = 10^{-4}$ atm)

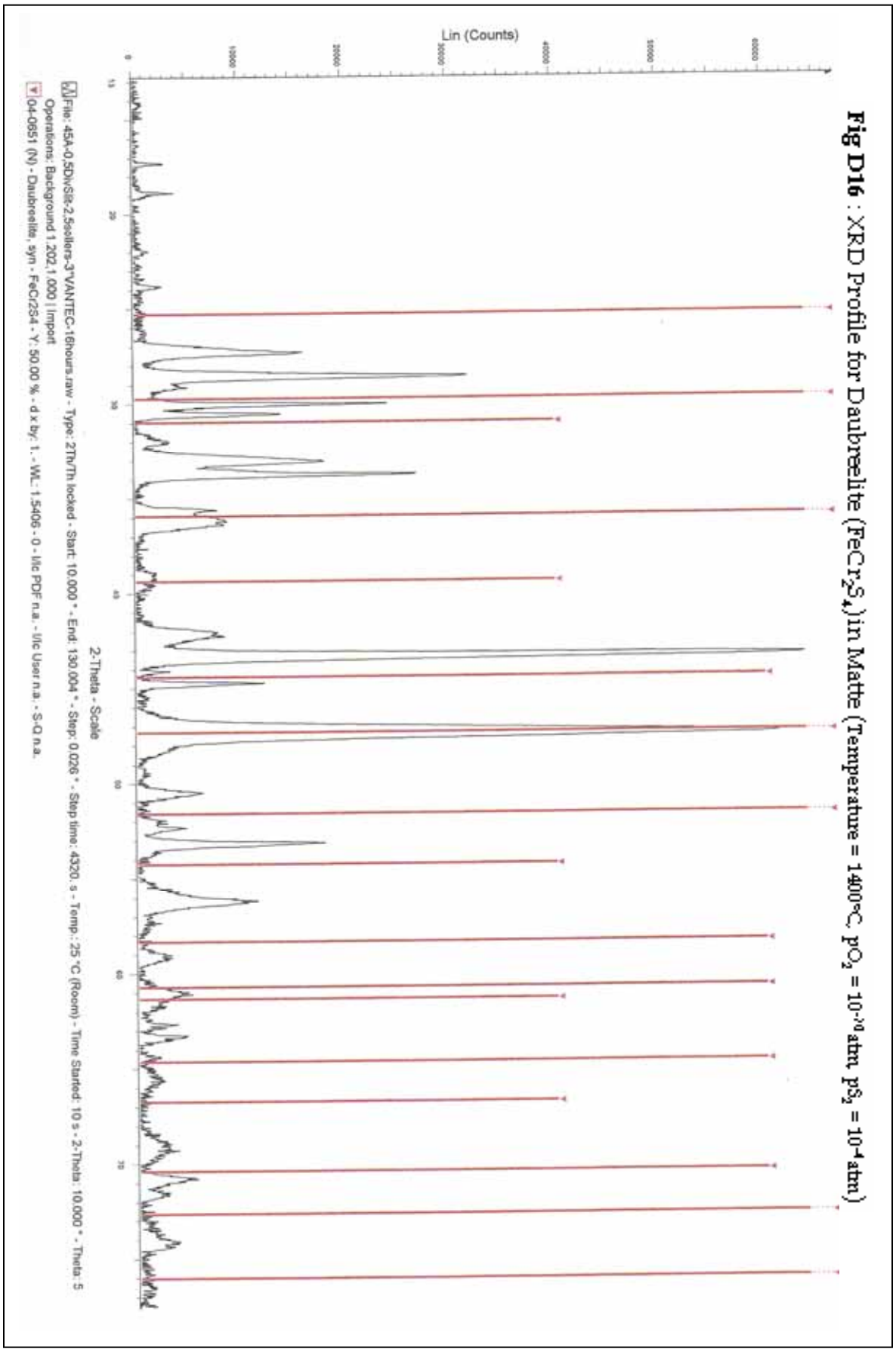

Fig D16 : XRD Profile for Daubreelite ($FeCr_2S_4$) in Matte (Temperature = 1400°C, $pO_2 = 10^{-9}$ atm, $pS_2 = 10^{-4}$ atm)

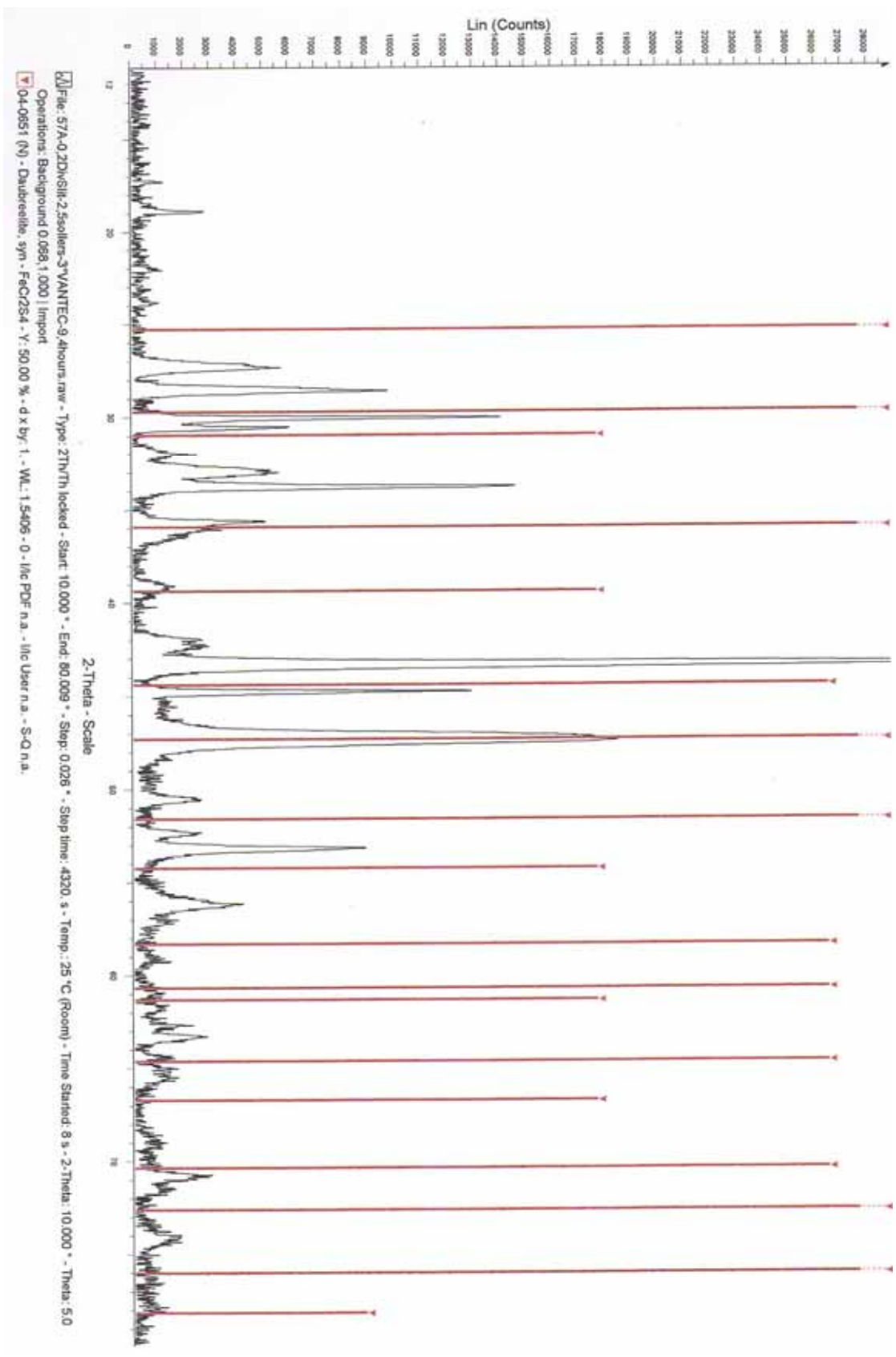

Fig D17 : XRD Profile for Daubreelite ($FeCr_2S_4$) in Matte (Temperature = 1500°C, $pO_2 = 10^{-7.9}$ atm, $pS_2 = 10^{-4}$ atm)

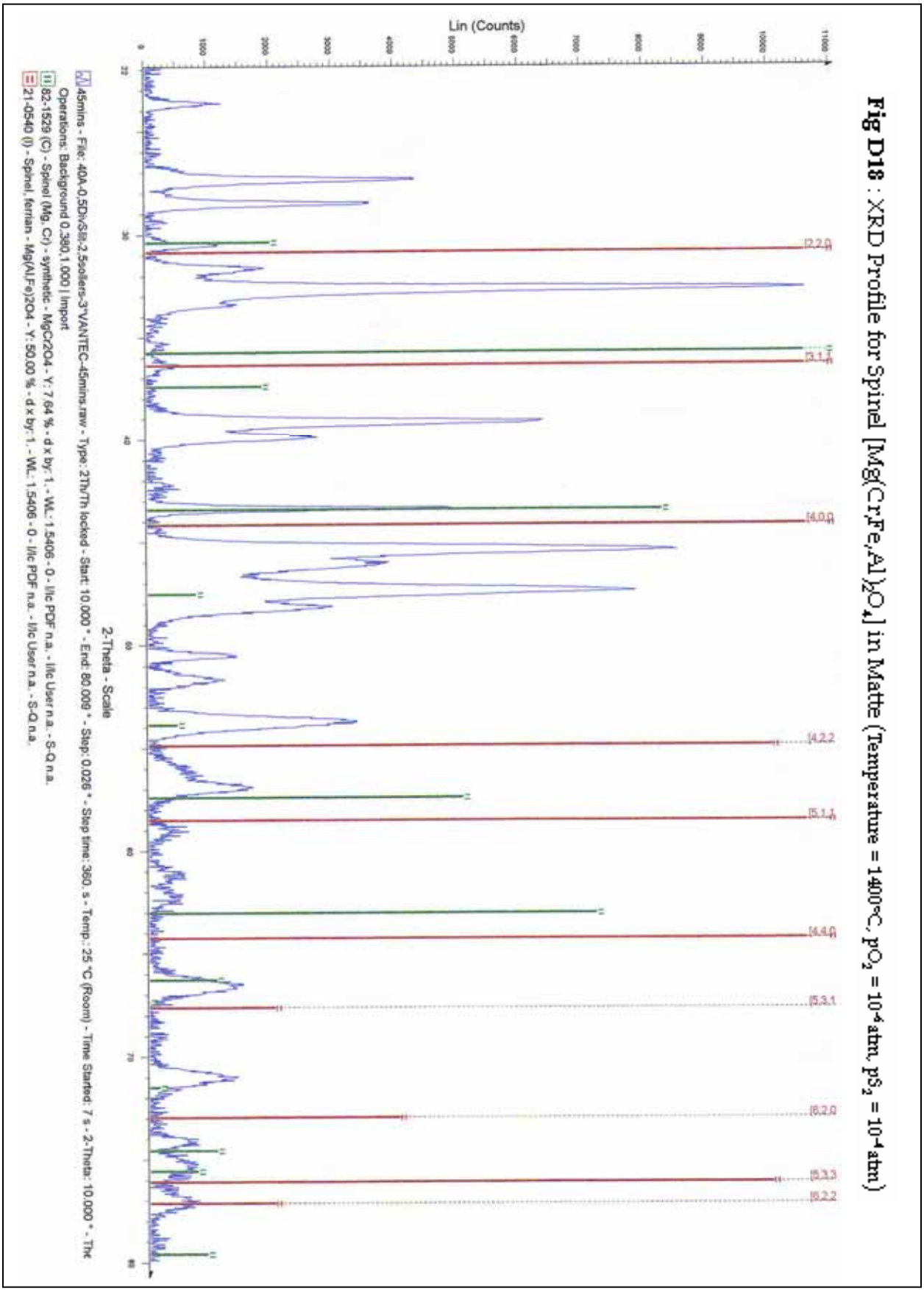

Fig D18 : XRD Profile for Spinel [$Mg(Cr,Fe,Al)_2O_4$] in Matte (Temperature = 1400°C, $pO_2 = 10^{-4}$ atm, $pS_2 = 10^{-4}$ atm)

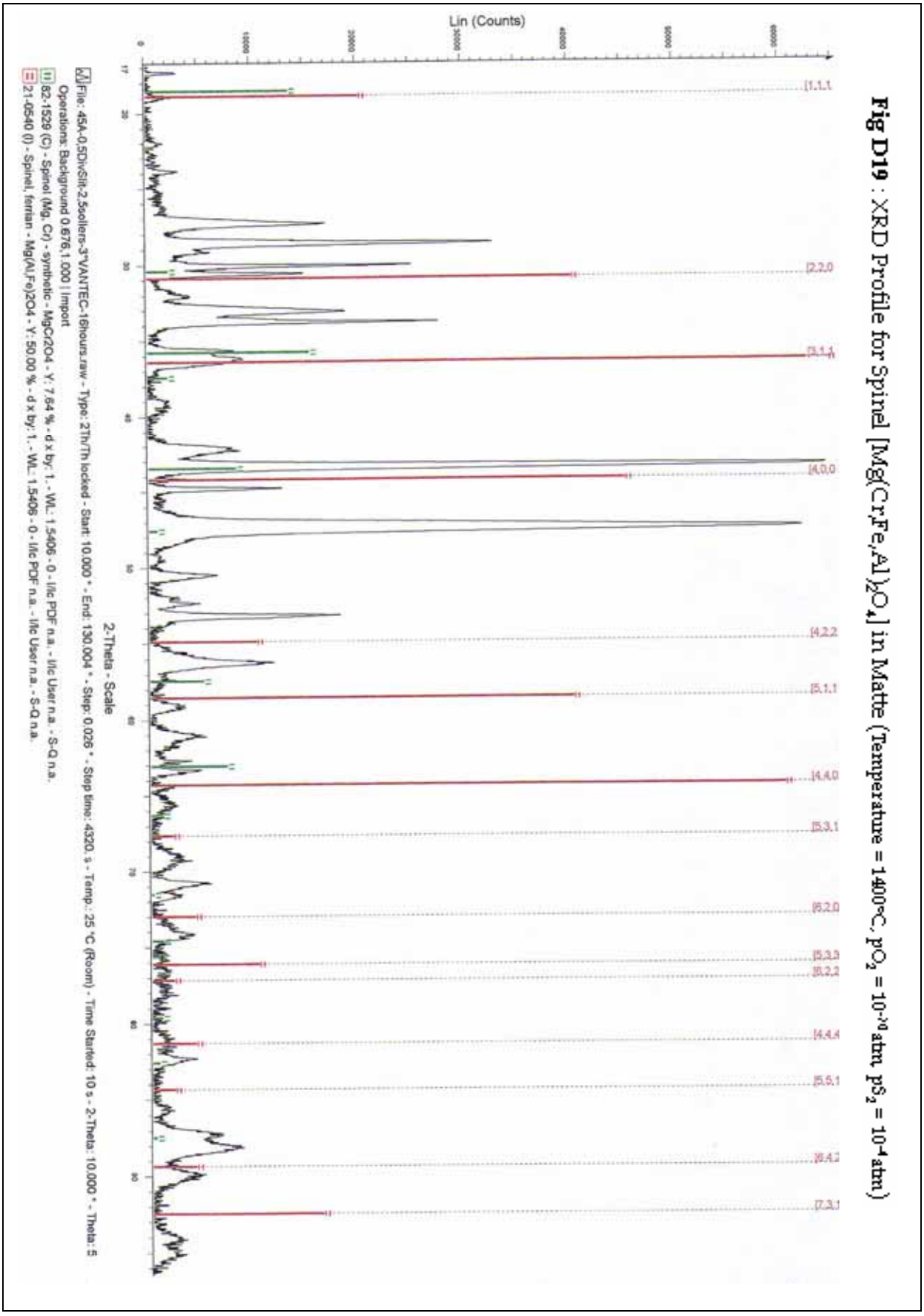

Fig D19 : XRD Profile for Spinel [$Mg(Cr,Fe,Al)_2O_4$] in Matte (Temperature = 1400°C, $pO_2 = 10^{-7.9}$ atm, $pS_2 = 10^{-4}$ atm)

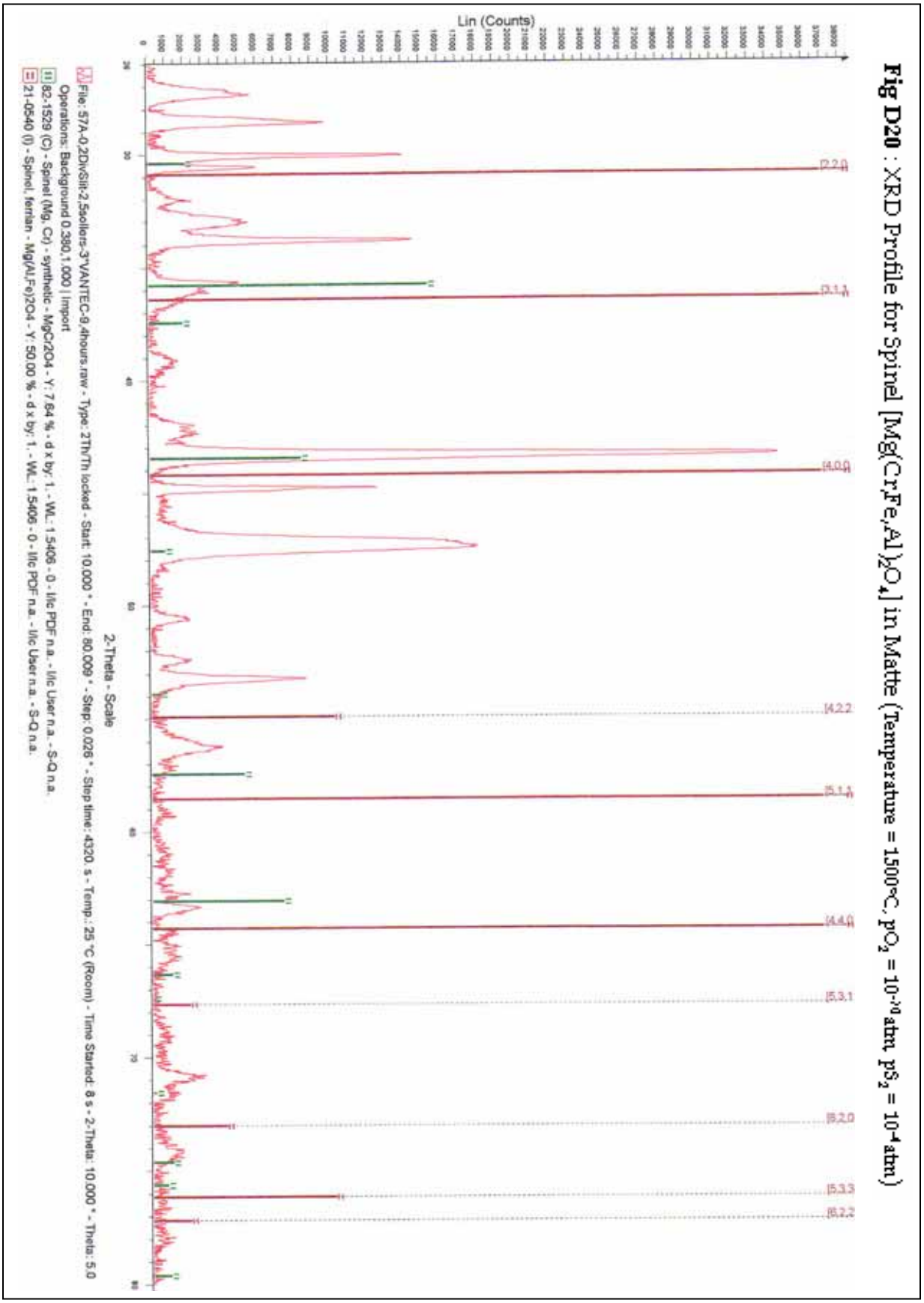

Fig D20 : XRD Profile for Spinel [$Mg(Cr,Fe,Al)_2O_4$] in Matte (Temperature = 1500°C, $pO_2 = 10^{-7.0}$ atm, $pS_2 = 10^{-4}$ atm)

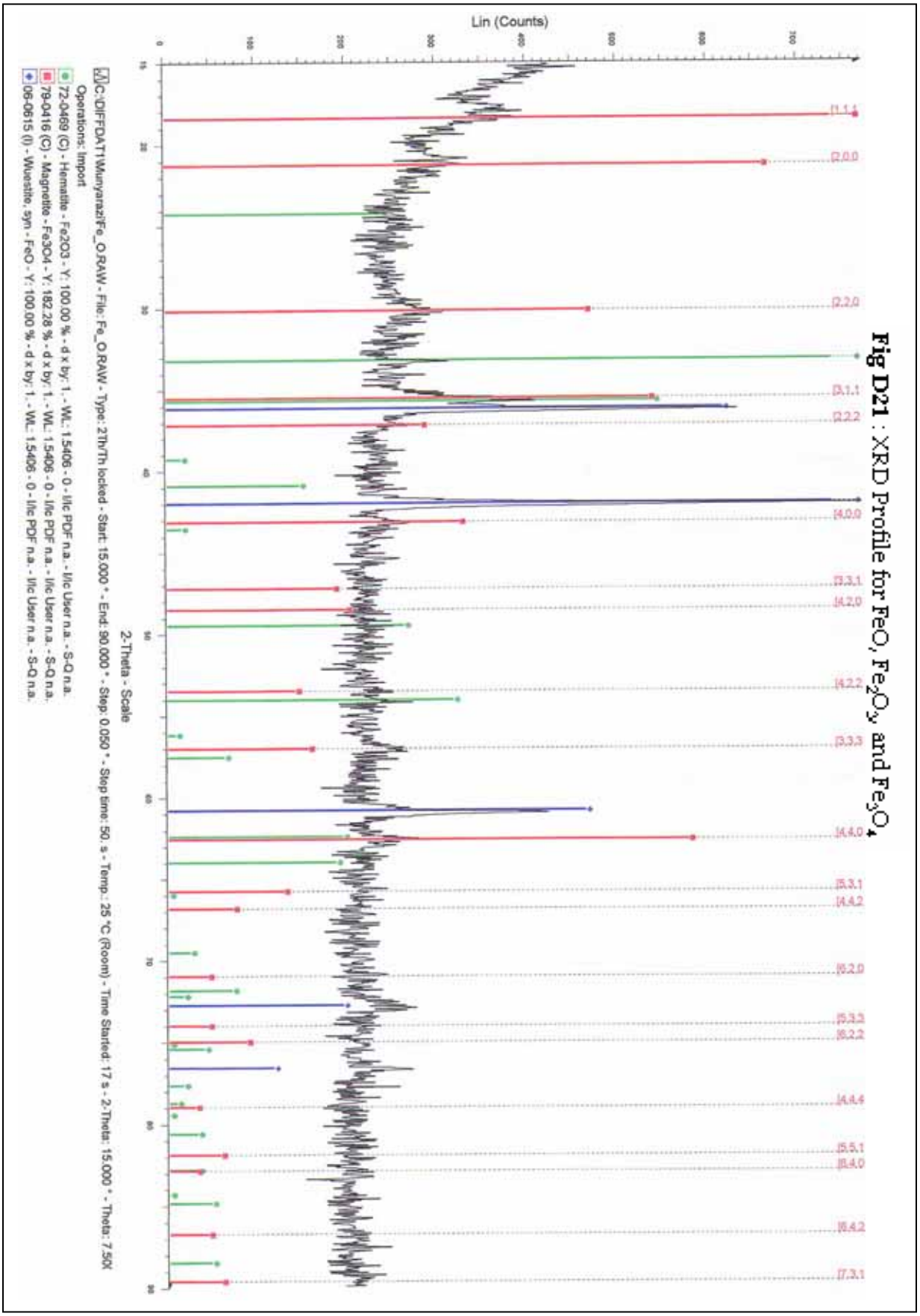

Fig D21 : XRD Profile for FeO, Fe_2O_3 and Fe_3O_4

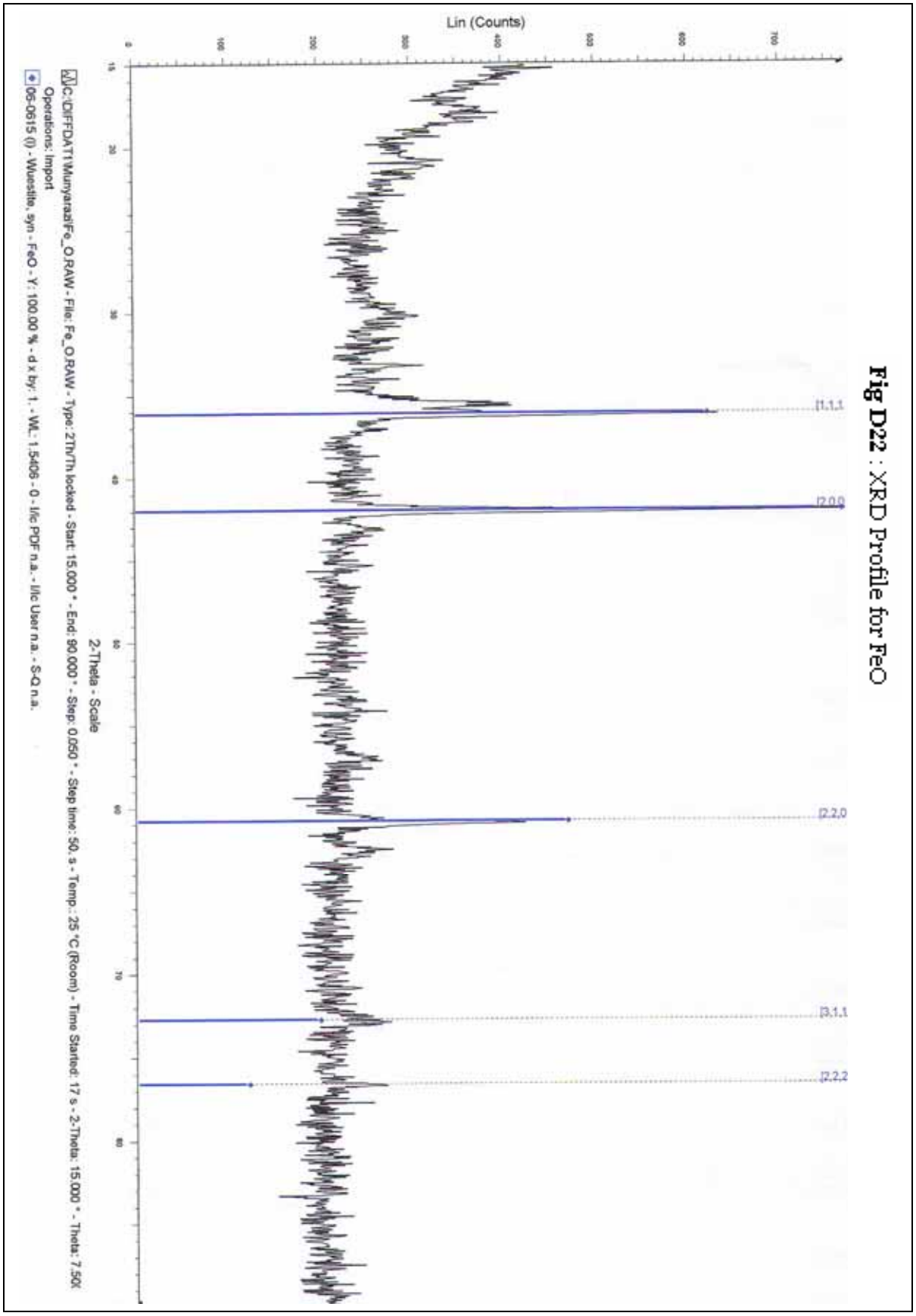

Fig D22 : XRD Profile for FeO